Utilizing Sedimentology and Geochronology to resolve the Architecture of Paralic Strata in Low-Accommodation Systems, McMurray Formation, Canada

by

Lucian Rinke-Hardekopf

M.Sc., RWTH Aachen University, 2015

B.Sc., University of Cologne, 2012

Thesis Submitted in Partial Fulfillment of the
Requirements for the Degree of
Doctor of Philosophy

in the
Department of Earth Sciences
Faculty of Science

SIMON FRASER UNIVERSITY

Fall 2021

Declaration of Committee

Name:	**Lucian Rinke-Hardekopf**
Degree:	**Doctor of Philosophy**
Title:	**Utilizing Sedimentology and Geochronology to resolve the Architecture of Paralic Strata in Low-Accommodation Systems, McMurray Formation, Canada**
Examining Committee:	**Chair: Dan Gibson** Professor, Earth Sciences
	Shahin E. Dashtgard Supervisor Professor, Earth Sciences
	James A. MacEachern Committee Member Professor, Earth Sciences
	Murray K. Gingras Committee Member Professor, Earth & Atmospheric Sciences University of Alberta
	Jeremy G. Venditti Examiner Professor, Geography
	M. Royhan Gani External Examiner Associate Professor, Earth, Environmental & Atmospheric Sciences Western Kentucky University

Abstract

A combined sedimentological-geochronological approach is employed to unravel the importance of paleoenvironments landward of the shoreline in understanding the stratigraphic architecture, and chronostratigraphy of the McMurray Formation in the Alberta Foreland Basin (referred to herein as the McMurray Depocenter; MDC), Canada. Presently, the McMurray Fm is subdivided based on the presence of regionally mappable mudstones, the bases of which are interpreted as flooding surfaces. However, the McMurray Fm comprises a wide range of paleoenvironments, and the Firebag Tributary in the northeastern MDC hosts a large volume of delta and coastal plain strata, including channels, mires, and interfluves. Facies characteristics, stratigraphic architecture, and geochronology of these deposits are explored and 3 main conclusions are derived.

First, petrographic trends in coals sitting at the top of the Lower McMurray formed following increasing rates (0.5-3 $mmyr^{-1}$) of sea-level rise during the Early Cretaceous. These coals outline the paleo-shoreline in the Firebag Tributary during Lower McMurray times. An ash-bed situated in this coal is dated at 121.39 ± 0.20 Ma, providing the first absolute age in the McMurray Fm. Second, the absolute age at the top of the Lower McMurray is used as a reference point to subdivide the McMurray Fm chronostratigraphically using detrital zircon (DZ). In a new stratigraphic approach to DZ geochronology, DZ samples from 5 stratigraphic intervals are combined to created novel grouped DZ samples. Grouped DZ samples showcase geographical provenance variability within depositional systems of the same stratigraphic interval, and are used calculate novel grouped maximum depositional ages. Third, detailed facies analysis and stratigraphic correlation of paralic strata in the Firebag Tributary allows for the identification of 2 progradational and 2 retrogradational phases of deposition. During Lower McMurray times the paleo-shoreline resided near the western edge of the Firebag Tributary, and mature paleosols underlying coals at its top indicate a potential maximum regressive surface. During the C2-B2 depositional units (DU), regression lead to paleo-shorelines close to the Alberta-Saskatchewan border. This is followed by a phase of progradation during the B1 DU, where paralic strata capping the unit lack evidence of base-level fall and demarcate major flooding. Progressive transgression ensued during deposition of the A2-A1 DUs. An ash-bed at the top of the B1 DU (115.07 ± 0.16 Ma) reveals that Lower McMurray to B1 DUs were deposited over ~1.6 Ma each, followed by ~0.8 Ma and ~0.4 Ma for the A2 and A1 DUs, respectively.

Keywords: stratigraphy of nearshore paleoenvironments; coal petrography and geochemistry; utility of ash beds in paralic coals for chronostratigraphy; detrital zircon maximum depositional ages; provenance variability; paleoshoreline migration

Dedication

I dedicate this thesis to my family and friends, all across the world.

Your love and support go beyond what I could ask for.

Acknowledgements

First and foremost, I would like to express my sincere gratitude to Dr. Shahin E. Dashtgard for his patience, encouragement, experience and mentorship in guiding me towards becoming the researcher I am. I could not have asked for a better supervisor throughout this journey. I would like to profound gratitude to Dr. James A. MacEachern for his expertise and time, as well as Dr. Murray K. Gingras for his insights and feedback. Discussions with all of you have shaped how I view sedimentology, and academic work in general.

I would also like to express my thanks to my internal examiner Dr. Jeremy G. Venditti and my external examiner Dr. M. Royhan Gani for taking the time to review my thesis, and sitting on my examining committee.

I would like thank past and present members of the ARISE Group, for their support, conversations, and feedback. In addition, I would like to express my gratitude to my fellow graduate students and friends, as well as the Graduate Student Society, who made my time at SFU an unforgettable and life changing experience. There is too many people I would love to thank personally, and frankly, I am too afraid to forget any individual person and believe you know who you are. I would also like to thank Susan Brook and the Thesis Support Group, who provide support and understanding when I needed it most. I am deeply appreciative of all your presences in my life, and acknowledge that I would not have been able to complete my PhD without you.

Finally, I would like to extend my thanks to the members of the McMurray Geology Consortium for sharing ideas during ours meetings in Calgary. Furthermore, I would like to thank sponsors of the McMurray Geology Consortium: BP plc, Cenovus Energy Inc., Husky Energy (now Cenovus Energy Inc.), Nexen CNOOC Ltd., and Woodside Energy Ltd., for funding this research.

Table of Contents

List of Tables

List of Figures

Chapter 1.

Introduction

The McMurray Formation of the Lower Cretaceous Mannville Group in the eastern Alberta Foreland Basin (AFB), Canada, (Fig. 1.1) hosts the Athabasca Oil Sands, which comprises roughly 1.5 x 10^{11} m^3 of in-place bitumen (Rahnama et al., 2013). Despite the vast economic importance of this resource, a regionally extensive sequence stratigraphic framework for the formation has not been developed, largely due to the erosion of stratigraphically important surfaces by channels and/or valley incision, as well as Pleistocene erosion of the most basinward marine facies. While extensive research has focused on the nature and distribution of regional shallow-marine parasequences (referred to herein as depositional units - DU) and the fluvial and fluvio-tidal channels that fed them (e.g., Ranger and Pemberton, 1997; Alberta Energy and Utilities Board, 2003; Hein and Cotterill, 2006; Hein et al., 2013; Château et al., 2019, 2020), far less attention has been given to the associated delta plain and coastal plain deposits (e.g., Rinke-Hardekopf et al., 2019). In this thesis, particular focus is placed on those sedimentary strata that accumulated in paralic depositional environments, which are defined as environments that are located landward of the paleo-shoreline, and are mainly freshwater but experience marine inundations. These paralic depositional environments hold valuable information pertaining to the regional base-level history, the trajectory of concomitant shorelines and by extension, the allostratigraphic architecture (e.g., Shanley and McCabe, 1994; Plint et al., 2001). In low-accommodation depositional settings such as the eastern AFB, cannibalization of stratigraphic units through channel-belt migration is common (e.g., Château et al., 2019), leading to a highly complex stratigraphy. Paralic strata can stabilize channel bank margins and promote preservation of deposits, including chronostratigraphically significant ash beds, by limiting erosion (e.g., Bohor and Triplehorn, 1993; Ainsworth et al., 2017; Dai et al., 2017). Furthermore, river systems feeding sediment into the basin can deliver detrital zircon, some of which exhibit a small lag-time between crystallization and deposition in the host strata (Saylor et al., 2012) and allow for approximation of depositional age (Dickinson and Gehrels, 2009). Therefore, sediment deposited landward of the paleo-shoreline provides an excellent opportunity to resolve the depositional history of nearshore depositional systems. This work showcases

the value of paralic deposits in resolving stratigraphic evolution and chronostratigraphic history of highly complex depositional systems with variable catchments, especially in basins largely devoid of other chronological information.

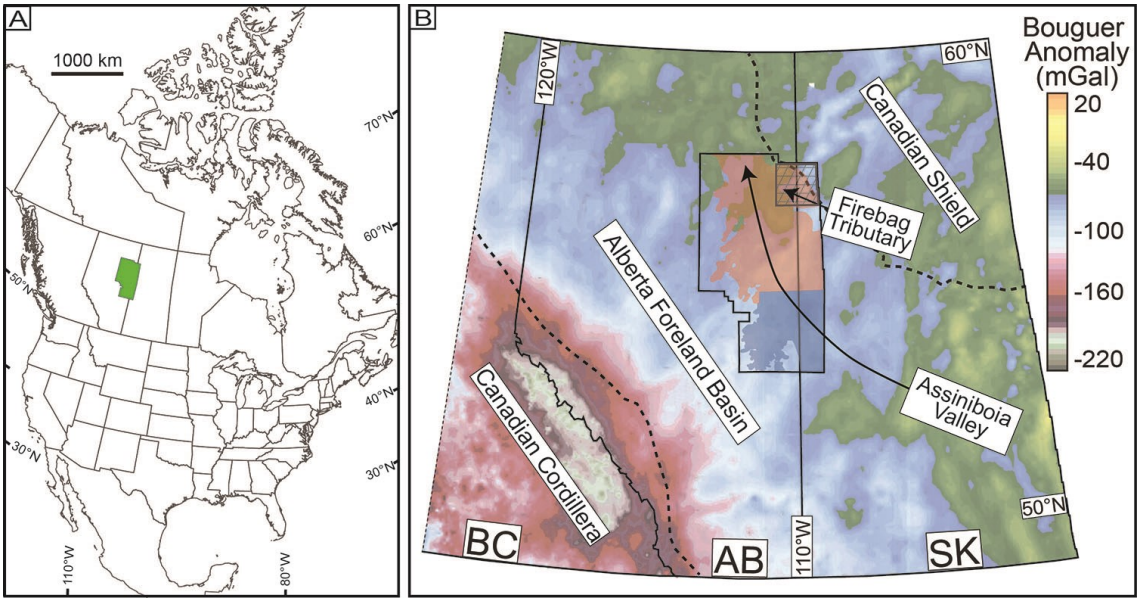

Figure 1.1. Study area location map
(A) Location of the McMurray Depocenter (green) in Alberta and Saskatchewan, Canada, including both the Athabasca and Cold Lake oil sands regions (adapted from Rinke-Hardekopf et al., 2021) **(B)** Bouguer gravity anomaly map of British Columbia (BC), Alberta (AB), and Saskatchewan (SK), Canada, showing the positions of the Canadian Cordillera, the Alberta Foreland Basin, and the Canadian Shield; black dashed lines demarcate the boundaries between them (adapted from Cant and Stockmal, 1989; Ross et al., 1994). Black arrows give the interpreted paleo-drainage direction for the Assiniboia Valley (Christopher, 1997; Horner et al., 2019) and Firebag Tributary (Rinke-Hardekopf et al., 2019). The black outlined polygon defines the approximate limit of the McMurray Depocenter (green polygon in A) and includes both the Athabasca oil sands (red overlay) and Cold Lake oil sands (blue overlay). The grey cross-hatched northeastern quadrant of the McMurray Depocenter is the study area (adapted from Rinke-Hardekopf et al., 2021)

Research undertaken as part of this thesis focusses on, but is not limited to, the northeastern quadrant of the McMurray Depocenter (MDC; Fig. 1.1B), which includes the Firebag Tributary (Ranger, 2006). Deposits in the Firebag Tributary are distinct from McMurray Formation strata found elsewhere in the basin in several ways. Firstly, McMurray Formation strata in the Firebag Tributary exhibit a higher proportion of paralic strata such as coals and paleosols (e.g., Hein et al., 2007; Rinke-Hardekopf et al., 2019). Secondly, they contain a higher proportion of sediment derived from the Canadian Shield (Benyon et al., 2014, 2016). As a result, strata of the Firebag Tributary have not been correlated reliably to other McMurray Formation deposits, the latter of which are

subdivided based on the presence/absence of marine mudstone at the bases of DUs (e.g., Ranger and Pemberton, 1997; Hein et al., 2006; Château et al., 2019).

The results of this thesis research demonstrate the possibilities of including paralic strata in stratigraphic analysis. Major contributions include: (1) relating detailed petrographic observations of a coal seam sitting at the top of the Lower McMurray to early Cretaceous relative sea-level rise; (2) proposing a novel stratigraphic approach for using maximum depositional ages to closely approximate true depositional ages in strata with rare syndepositional detrital zircon; (3) developing correlations between paralic strata and contemporaneous shallow-marine deposits to decipher shoreline trajectories within the McMurray Formation; and 4) utilizing volcanogenic zircon extracted from ash beds found in these paralic strata to develop a chronostratigraphic framework.

1.1. Overview

1.1.1. Tectono-Stratigraphic Evolution of the McMurray Depocenter

The MDC is located in northeastern Alberta and northwestern Saskatchewan, Canada, and encapsulates sedimentary successions deposited on the eastern margin of the Alberta Foreland Basin (AFB) and adjacent to the Canadian Shield (Fig. 1.1B). The AFB forms part of the fill of the Western Canada Sedimentary Basin (e.g., Porter et al., 1982; Poulton et al., 1994; Ross et al., 1994). The AFB tapers from SW to NE, and comprises over 6 km of Mesozoic through to Cenozoic strata at its western margin (Porter et al., 1982; Leckie and Smith, 1992; Poulton et al., 1994). Prior to arc accretion in the Middle Jurassic, the western margin of North America accumulated strata along a passive margin that may have been up to 20 km thick (Price, 1981; Leckie and Smith, 1992). In the MDC, the McMurray Formation directly overlies Devonian carbonates of the Beaverhill Lake Group (Carrigy, 1959; Schneider et al., 2013).

The AFB existed as an intracratonic foreland basin from the Jurassic to Early Eocene. It is situated between the Canadian Shield in the east and the ancestral Rocky Mountains in the west, and formed due to tectonic loading associated with oblique accretion of allochthonous terrains to the margin of the westward-moving North American Plate (Beaumont, 1981; Price, 1981; Monger et al., 1982; Porter et al., 1982; Leckie and Smith, 1992; Plint et al., 1993; Poulton et al., 1994; Monger and Price, 2002). Lithospheric

flexure associated with the ensuing orogenesis led to uplift and erosion, and created the paleotopography over which the McMurray Formation was deposited (Plint et al., 1993). The unconformable contact between Mesozoic and Paleozoic strata is known as the Sub-Cretaceous Unconformity (SCU; Jardine, 1974). Three orogen-parallel paleo-valleys formed on the SCU, and include (from west to east): Spirit River Valley, Edmonton Valley, and Assiniboia Valley, with the Assiniboia Valley containing the MDC (Fig. 1.1; Christopher, 1974; Leckie and Smith, 1992). Due to its position distal to the orogen, the MDC exhibits characteristics consistent with a low-accommodation setting (e.g., Leckie et al., 2004; Crerar and Arnott, 2007; Château et al., 2019).

The paleotopography on the SCU greatly impacted deposition of the McMurray Formation, especially during the early stages (e.g., Ranger and Pemberton, 1997). In addition, accommodation during deposition of the McMurray Formation was locally influenced by syndepositional subsidence associated with salt dissolution of the Devonian Prairie Evaporite Formation, as well as collapse of karsted limestones (e.g., Broughton, 2013b, 2014, 2016; Barton et al., 2017; Château et al., 2019; Rinke-Hardekopf et al., 2019).

1.1.2. Stratigraphy of the McMurray Formation

The McMurray Formation comprises a wide array of paralic through to shallow-marine sedimentary strata, including cross-stratified sand and mud, as well as paleosols and coal (e.g., Pemberton et al., 1982; Ranger and Pemberton, 1997). The McMurray Formation was deposited during a 3rd order transgression of the Boreal Sea, and is overlain by the Wabiskaw Member of the Clearwater Formation (Hein et al., 2013). This transgression is expressed in the McMurray Formation and forms the basis for its historical subdivision into lower (fluvial), middle (fluvio-tidal), and upper (shallow-marine) informal members (e.g., Carrigy, 1959; Pemberton et al., 1982; Mossop and Flach, 1983).

Presently, the most widely used stratigraphic framework for the McMurray Formation subdivides it into a series of progradational parasequences or parasequence sets, which are referred to herein as depositional units (DU). The McMurray Formation comprises 7 DUs, including (from bottom to top): Lower McMurray, C2, C1, B2, B1, A2, and A1 (Fig. 1.2; Château et al., 2020). The Lower McMurray is not formally defined, and occurs intermittently at the base of the McMurray Formation throughout the MDC, where

it largely comprises cross-stratified sand, coal, and paleosols (e.g., Pemberton et al., 1982; Broughton, 2014; Harris et al., 2016; Barton et al., 2017; Rinke-Hardekopf et al., 2019). The remaining DUs are up to 15 m in thick (Château et al., 2021) and are largely eroded along the main axis of the Assiniboia Valley through successive channel/valley incision (10–70 m deep) that potentially occurred during major base-level falls (Ranger and Pemberton, 1997; Alberta Energy and Utilities Board, 2003; Hein et al., 2006, 2013; Horner et al., 2018). Recently, several studies have shown that at least some channelized successions in the McMurray Formation are not likely to be incised valleys, but are more akin to contemporaneous channel-belts that fed the regional DUs further basinward (e.g., Baniak and Kingsmith, 2018; Château et al., 2020).

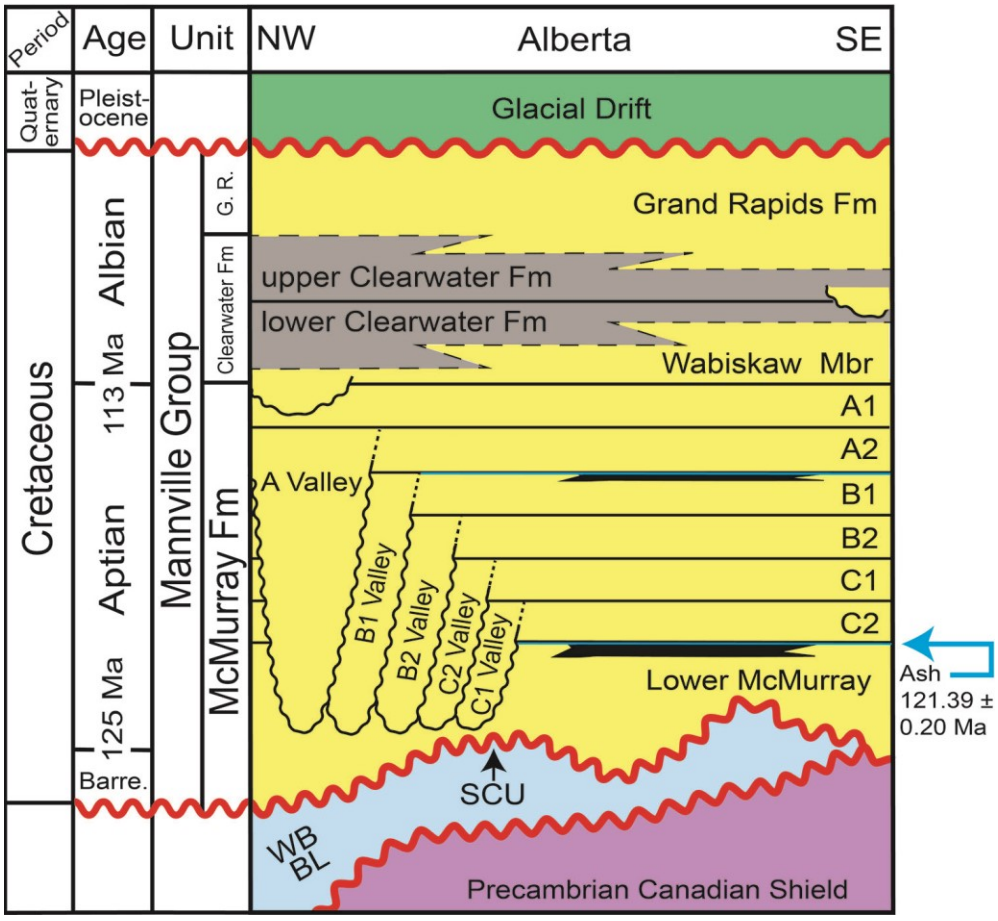

Figure 1.2. Stratigraphic framework for the Mannville Group in northeastern Alberta, Canada.

Clastic sediments (sand and sandstone (yellow), mudstone (grey), and coal (black)) unconformably overlie Devonian carbonates (blue) of the Woodbend (WB) and Beaverhill Lake (BL) groups and metamorphic rocks (purple) of the Precambrian Canadian Shield. The allostratigraphic framework of the Mannville Group includes multiple depositional units (bottom to top: Lower McMurray, C2, C1, B2, B1, A2, A1) and their associated paleo-valleys / channel belts (adapted from Rinke-

Hardekopf et al., 2021). Also included is the absolute age of an ash bed at the top the Lower McMurray (see Chapter 2; Rinke-Hardekopf et al., 2019).

1.2. Sequence Stratigraphy of Delta- and Coastal-Plain Deposits

Sequence stratigraphy was developed in the shallow-marine realm by interpreting shoreline trajectories observed in seismic imagery as a result of relative sea-level fluctuations (Posamentier and Vail, 1988; Van Wagoner et al., 1988). Once sedimentological criteria for these trajectories were established, the concepts were subsequently extended into the paralic realm by Shanley and McCabe (1991) and Wright and Marriot (1993) using coals and paleosols. Depositional environments on delta- and coastal-plains directly respond to changes in the groundwater table, and in paralic environments, the position of the groundwater table is hydrologically linked to the position of sea level (e.g., Diessel, 1992; Törnqvist, 1993). This hydrological connection forces a rise in the groundwater table when sea level increases and vice versa. Similar to relative sea-level in the shallow-marine realm, environments on delta- and coastal-plains can accumulate or erode sediment to the position of a hypothetical base-level, which is used herein as the collective term. Understanding how paralic environments react to fluctuations of base-level has allowed for correlation between shallow-marine and paralic sedimentary deposits (e.g., Shanley and McCabe, 1991; Diessel, 1992; Wright and Marriott, 1993; Banerjee et al., 1996; Bohacs and Suter, 1997; McCarthy and Plint, 1998; Kraus, 1999). In the McMurray Formation, paralic strata are often interpreted as part of the Lower McMurray, although they have been shown to occur at multiple stratigraphic levels (e.g., Flach and Mossop, 1985; Wightman and Pemberton, 1997).

Soils can form during phases of both low or falling base-level, and high or rising base-level (e.g., Wright and Marriott, 1993; Aitken and Flint, 1996; McCarthy and Plint, 1998; Kraus, 1999; Plint et al., 2001). In proximity to the shoreline, Wright and Marriott (1993) demonstrated that well-developed (i.e., mature) soils represent prolonged exposure during lowstand or highstand systems tracts (as well as the falling stage systems tract; Fig. 1.3), especially when base-level is low. Conversely, hydromorphic and weakly developed (i.e., immature) soils form during the transgressive systems tract, and are common to many paralic successions (Aitken and Flint, 1996). Consequently, paleosols can represent either subaerial unconformities or even flooding surfaces.

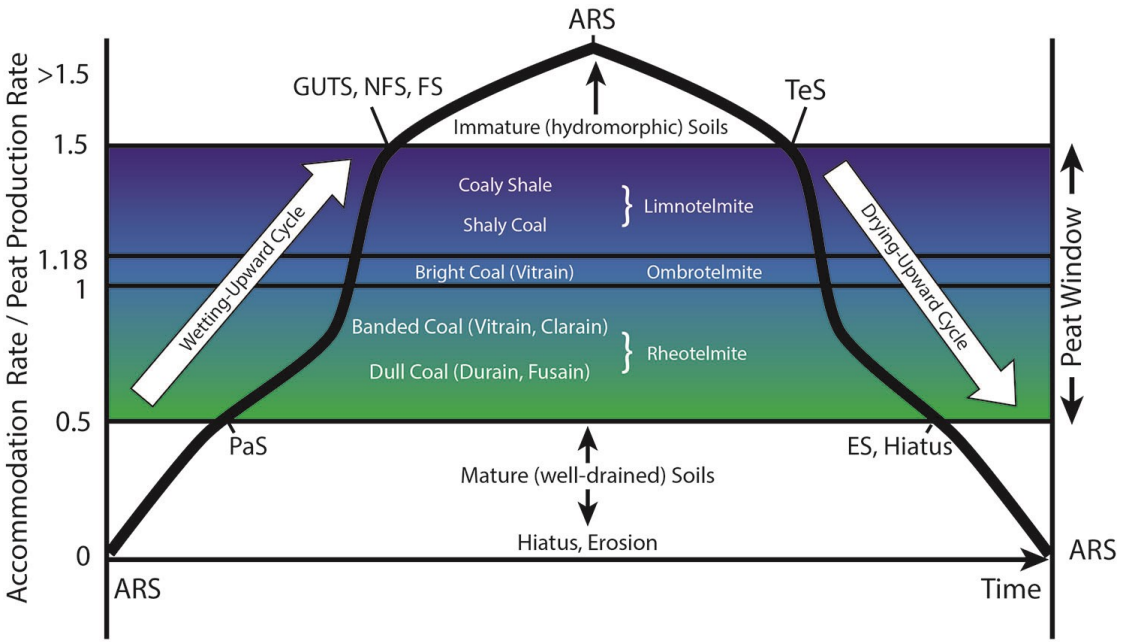

Figure 1.3. Diagram showing the relation between accommodation rate, peat production and coal lithotypes, as well as paleodepositional conditions.

Coal lithotype development under increasing base-level rise (wetting-upward cycles) is shown on the left half of the figure, and different coal lithotype successions during decreasing base-level rise (drying-upward cycles) are shown on the right side of the figure. Drying-upward cycles can have basal terrestrialization surfaces (TeS; peat development under falling base-level rise within a limnic environment) and can be capped by an erosional surface (ES) or hiatus at the top. Wetting-upward cycles can have a basal paludification surface (PaS; development of a mire over a paleosol) and be capped by a flooding surface (non-marine (NFS) or marine (FS) in origin), or a give-up transgressive surface (GUTS; non-hiatal shift to limnic deposition) at the top. During falling or negligible accommodation creation, soil formation can ensue (adapted from Rinke-Hardekopf et al., 2019).

1.3. Detrital Zircon Provenance and Maximum Depositional Ages

Detrital zircon (DZ) U-Pb geochronology has become an increasingly popular technique for investigating a wide range of questions pertaining to basin evolution (e.g., Gehrels et al., 2009; Gehrels and Pecha, 2014; Gehrels, 2014), sediment provenance (e.g., Moecher and Samson, 2006; Vermeesch, 2013; Benyon et al., 2014; Blum and Pecha, 2014), and timing of deposition (e.g., Dickinson and Gehrels, 2009; Coutts et al., 2019). Sediment provenance is assessed by grouping zircon grains into DZ populations based on their age, which are interpreted to relate to probable source regions (Gehrels, 2000; Andersen, 2005). In the McMurray Formation, DZ samples were used to show that the Assiniboia Valley was likely fed by a continental-scale drainage system (Fig. 1.4; Blum

and Pecha, 2014), with smaller tributaries deriving sediment from the Canadian Cordillera and the Canadian Shield (Benyon et al., 2014, 2016).

The youngest DZ population is typically used to calculate maximum depositional ages (MDA), and a variety of methods exist for obtaining them (e.g., Dickinson and Gehrels, 2009; Barbeau et al., 2009; Ross et al., 2017; Coutts et al., 2019; Herriott et al., 2019; Copeland, 2020; Sharman and Malkowski, 2020). Popular methods include using youngest single grains, statistical methods, or weighted means derived from a subset the youngest grains (Dickinson and Gehrels, 2009; Johnstone et al., 2019; Vermeesch, 2020).

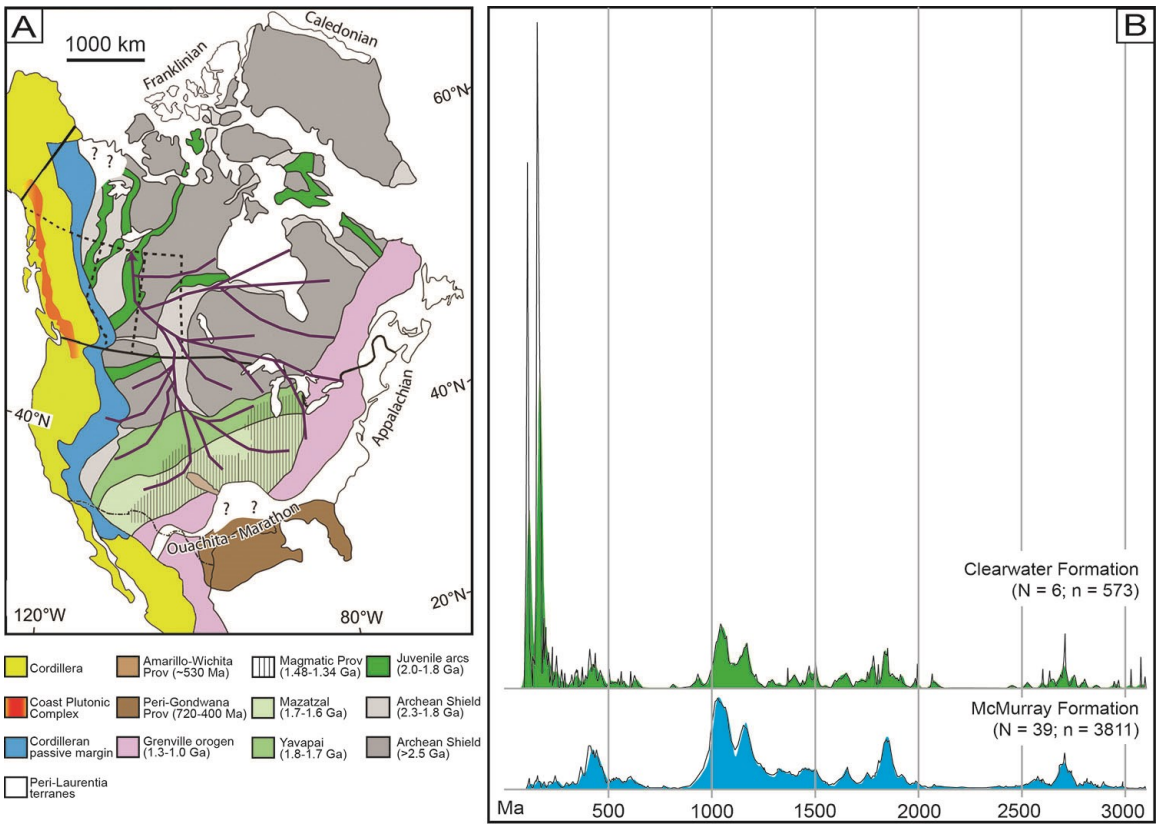

Figure 1.4. Tectonic provinces of North America and provenance of sediment reconstructed using DZ.

(A) Sediment source regions in North America (adapted from: Monger et al., 1982; Gehrels and Pecha, 2014), and an interpreted reconstruction of the Early Cretaceous drainage network (solid, thick purple lines) that may have formed the sediment sources for the McMurray Fm in the Assiniboia Valley (Blum and Pecha, 2014). I note that the map, as presented by Blum and Pecha (2014), only shows the distribution of igneous and metamorphic basement strata **(B)** Normalized kernel density estimates (blue and green shaded areas), as well as normalized probability density plots (black lines) of all DZ samples used in this study of the McMurray Formation (N = 37 DZ samples; n = 3811 dated DZ grains) and the Clearwater Formation (N = 6 DZ samples; n = 573 dated DZ grains). The kernel density estimate plot was created with a fixed 10 Ma bandwidth. Figure taken from Rinke-Hardekopf et al. (2021).

1.4. Study Area

Research presented in this thesis investigates deposits of the McMurray Formation in both the Athabasca and Cold Lake oil sands regions, referred to collectively herein as the MDC (Fig. 1.4). The MDC covers an area exceeding 60,000 km^2 between townships (T) 50 and 100 and ranges (R) 23 west (W) of the 3rd meridian (23W3) and 20W4M (Fig. 1.5). Townships are defined through the Dominion Land Survey system (DLS), which subdivides western Canada into 6 x 6 mile (~10 x 10 km) blocks. Within the MDC, McMurray Formation sediments were deposited in numerous paleotopographic lows on an unconformable surface - the Sub-Cretaceous Unconformity (SCU), which truncates underlying Devonian-aged carbonates of the Beaverhill Lake Group. The most notable paleotopographic low is the southeast-to-northwest-trending “Assiniboia Valley”, which is also commonly referred to as the “main fairway” (Fig. 1.5A; Christopher, 1974). In addition, several smaller off-axis paleo-drainage systems have been identified, including the Grouse-, Sparrow-, Pelican-, and Ells paleo-valleys in the western MDC. Another off-axis paleo-drainage, the Firebag Tributary, is identified in the northeastern quadrant of the MDC (Fig. 1.5A).

The Firebag Tributary is the primary study area of this dissertation. There, McMurray Formation strata exhibit thicknesses between ~30 and 120 m (where they have not been eroded by Pleistocene-aged glaciation; Fig. 1.5C). The Firebag Tributary is situated directly west of the Canadian Shield and covers ~10,000 km^2 of NE Alberta and NW Saskatchewan, between townships T90 and T100 and ranges R23W3 and R6W4 meridian (Fig. 1.4).

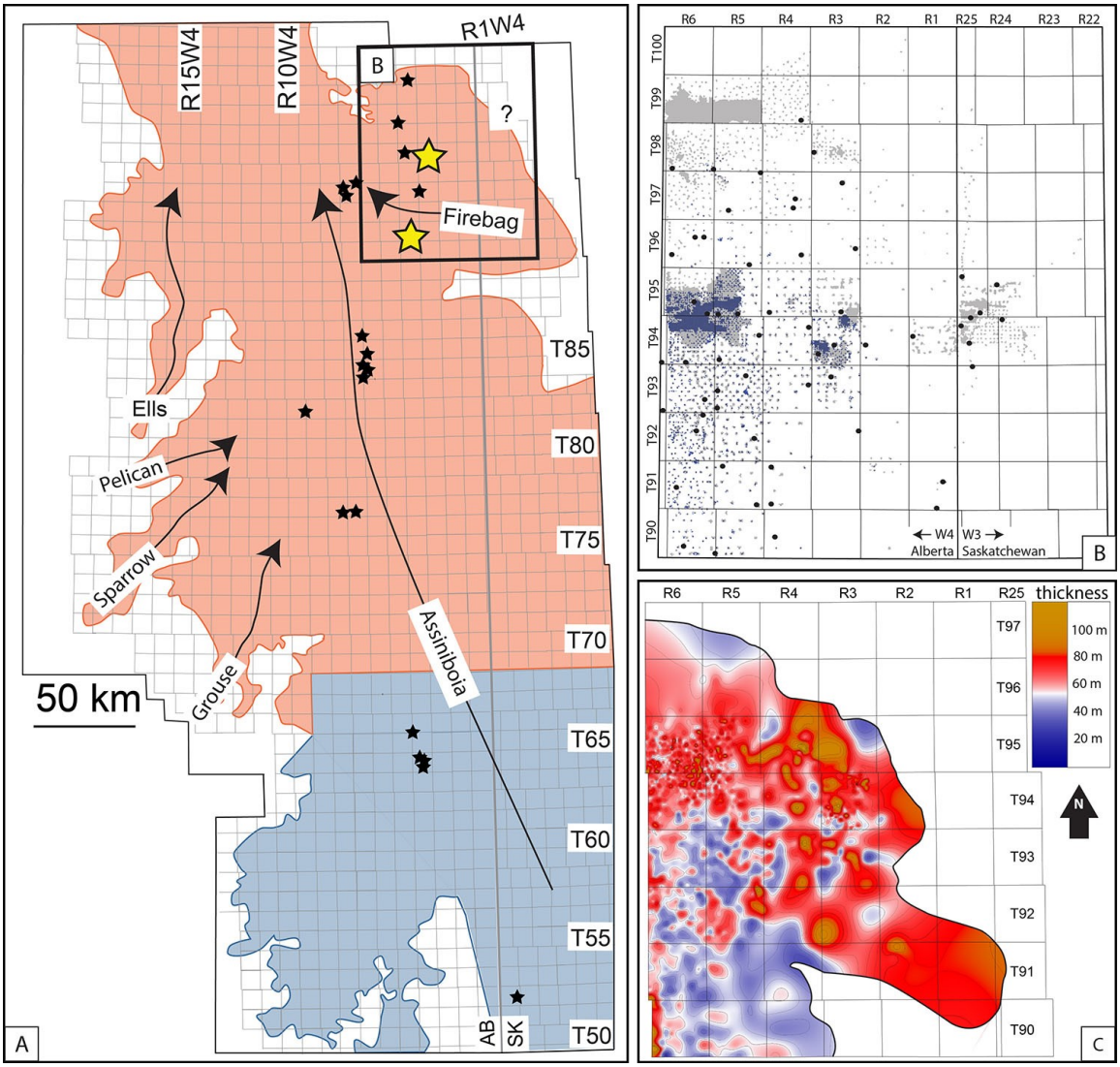

Figure 1.5. Data used in this thesis.
(A) The extent of the McMurray Depocenter, including both the Athabasca (red overlay) and Cold Lake (blue overlay) oil sands regions (location given in Fig. 1.1A). The grey grid defines (T)ownships and (R)anges (W)est of the 3rd and 4th Meridian; this boundary is also the border between Alberta and Saskatchewan. Paleotopographic lows on the SCU are interpreted as paleo-valleys, and the axes of these valley is defined by the bock lines. The locations from which detrital zircon samples were taken are shown with black stars, and the locations of ash samples derived from coal beds in core are defined by yellow stars (adapted from Christopher, 1974; Hein et al., 2006; Broughton, 2013a; Château et al., 2019; Rinke-Hardekopf et al., 2019, 2021). The location of the main study area (i.e., the Firebag Tributary; B) is defined by the bold black outline. **(B)** The main study including all studied cores (black circles), and all available well logs (grey dots); those wells that preserve the top of the McMurray Formation are highlighted in blue. **(C)** Thickness of the McMurray Formation in the Firebag Tributary. The outline of the thickness isopach is a 10 km radius around wells that preserve the top and base of the McMurray Formation, and hence, can be used to define the isopach thickness of the McMurray Fm.

1.5. Objectives and Thesis Organization

The main objective of this thesis is to demonstrate how paralic sedimentary strata in stratigraphically complex nearshore depositional environments, and detrital zircon U-Pb geochronology can be utilized in resolving and refining stratigraphic architecture in time and space, as well as in assessing provenance variability. This thesis is divided into 5 chapters, and includes: an introduction (Chapter 1); three chapters (Chapters 2–4), that each relate to the three projects that form the body of the thesis (two of which are published in peer-reviewed journals, and one which is in review); and a conclusions chapter (Chapter 5).

Chapter 2 focusses on the evolution of the coal seam at the top of the Lower McMurray during the earliest transgression of the Boreal Sea in the Early Cretaceous. Detailed petrographic observations of this coal seam allowed the identification of several internal wetting-upward and drying-upward cycles, as well as stratigraphically significant surfaces, which directly record regional base-level changes. A discrete, arcuate-shaped distribution of this coal seam is identified and interpreted to preserve the shape of the paleo-shoreline. The thickness of the coal seam is utilized to estimate the rate of Early Cretaceous relative sea-level rise during initial southward transgression of the Boreal Sea. Lastly, an ash-bed within the coal seam was sampled and dated using chemical abrasion thermal ionization mass-spectrometry (CA-TIMS). The age derived from zircon in the ash-bed provides the first absolute geochronological age for the McMurray Formation. This work is published as Rinke-Hardekopf et al. (2019).

In Chapter 3, the age of the aforementioned ash-bed is used as a chronological reference point to attempt chronostratigraphic subdivision of the McMurray and Clearwater formations using maximum depositional ages (MDAs) derived from detrital zircon (DZ). Stratigraphic correlation is used to subdivide a total of 43 DZ samples into five stratigraphic intervals. For each of the five stratigraphic intervals, all associated DZ samples are combined to create novel, grouped DZ samples. Grouped DZ samples are then compared to individual DZ samples by means of their population proportions and multi-dimensional scaling to understand geographical provenance variability. Grouped DZ samples are used to calculate novel grouped MDAs (gMDAs). Grouped MDAs enable reasonable estimations of true depositional ages for depositional units, and demonstrate the value of gMDAs in approximating depositional age when syn-depositional DZ are accessory

components of the DZ population (i.e. <5%). This work is published as Rinke-Hardekopf et al. (2021).

In Chapter 4, detailed facies analysis (sedimentology, ichnology) is used to understand stratigraphic relations between paralic and shallow-marine strata within the Firebag Tributary. Correlation of the bases of regionally distributed marine mudstones with the tops of coals and gleyed paleosols is highlighted. This correlation not only allows for an extension of the stratigraphic framework of the McMurray into coastal settings, but also showcases the trajectory of the shorelines found in the McMurray Formation. As well, the age of an ash bed situated within the coal seam at the top of the B1 depositional unit has also been determined. The age of the ash-bed at the top of the B1 DU is a high-certainty maximum depositional age that is interpreted to correspond to the true depositional age. Together with the previously dated ash bed (see Chapter 2), these absolute ages are used to discuss depositional rates of the McMurray Formation. This work is currently in review as Rinke-Hardekopf et al. (*in review*).

1.6. Data and Methods

This thesis includes a variety of data sources, including: descriptions and lithologs of cored intervals, photographed core intervals, well logs, coal petrographic descriptions, ash and sulphur content of coal seams, detrital zircon (DZ) samples, and bentonitic claystone (ash) geochronology samples. Core lithologs and photographs, well-logs, as well as ash-derived absolute ages are referred to in all chapters. Coal petrography, and the ash and sulphur content of coal seams are referred to in Chapter 2. DZ analyses are presented in Chapter 4. For detailed methodologies related to each research project, refer to the methods section in the respective chapter.

In the Firebag Tributary, detailed sedimentological and ichnological facies descriptions were completed on 60 cored intervas (Fig. 1.5B) and data were recorded using AppleCORE (donated to Simon Fraser University by Dr. Mike Ranger). Detailed core descriptions were supplemented by descriptions derived from 348 photographed cored intervals. Approximately 68,750 wells penetrate the top of the McMurray Formation in the MDC (determined using GeoScout, donated to Simon Fraser University by GeoLOGIC), and 4,763 of those are located within the Firebag Tributary (Fig. 1.5C). Correlations made based on observations in core and were extended throughout the

Firebag Tributary (Fig. 1.5B), as well as locations elsewhere in the MDC using available well logs. Individual well-logs contain some or all of the following curves: gamma ray, caliper, photo-electric effect, neutron and density porosity, and resistivity. In addition, well-logs were used to map the thickness of the McMurray Formation throughout the Firebag Tributary, and thickness maps were created in Petrel 2015 (donated to Simon Fraser University by Schlumberger).

Ash-bed samples were taken from two cores in the Firebag Tributary (Fig. 1.5A) for chemical-abrasion thermal ionization mass-spectrometry (CA-TIMS after Mattinson, 2005), and processed at the Isotope Geology Laboratory of Boise State University, Idaho, USA. In Chapter 2, the age derived from zircon in an ash-bed contained in a coal seam towards the top of the Lower McMurray in the core from 1AA/09-05-091-04W4 is presented. In Chapter 4, similar data are presented from an ash-bed contained in a coal seam towards the top of the B1 DU in well 1AA/02-03-095-03W4.

Petrographic descriptions and ash and sulphur content of coals are used in Chapter 2, and include data from 6 different cored locations. Petrographic descriptions of coals are derived from 4 wells: 1AA/09-05-091-04W4, 1AA/14-35-092-06W4, 1AA/10-24-093-04W4, and 1AA/10-11-093-06W4. Ash- and sulphur-content data are derived from coal in two wells: 1AA/12-20-098-05W4 and 1AA/05-29-098-05W4. Together, these data are used to interpret wetting-upward and/or drying-upward cycles in coal seams located at the top of the Lower McMurray.

Provenance analysis and maximum depositional ages are presented in Chapter 3, and include data from 43 DZ samples (Fig. 1.5A). Of these 43 DZ samples, 39 were derived from literature sources (Benyon et al., 2014, 2016; Blum and Pecha, 2014). Additionally, 4 new DZ samples were taken from 3 cored intervals, including 2 from well 1AA/10-24-093-04W4, and 1 from wells 1AA/13-01-052-27W3 and 1AA/10-17-095-04-W4. These DZ samples were analyzed at the Centre for Applied Basin Studies at the University of Calgary, Alberta, Canada, using a Agilent 7700 quadrupole ICP-MS (Matthews and Guest, 2016). Between 68 and 262 individual grains were recovered and analyzed in the 4 new samples. DZ provenance is assessed by pairwise statistical comparison of DZ samples using the Kuiper V_{max} statistic and visualized as 2D MDS plots (Vermeesch, 2013, 2018a), as well as DZ age-population proportions comparisons, all calculated with detritalPy (Sharman et al., 2018). MDAs are calculated based on several

popular methods, including the youngest single grain (Dickinson and Gehrels, 2009), the maximum likelihood algorithm (Vermeesch, 2020), weighted means derived from a subset of 2+ or 3+ youngest grains overlapping in their 1σ or 2σ uncertainty (Dickinson and Gehrels, 2009), and lastly, the youngest 3 grains overlapping at 2σ uncertainty (Ross et al., 2017).

Chapter 2.

Transgression of the McMurray Sub-Basin during Lower McMurray Times

A version of this chapter has been published as: L. Rinke-Hardekopf, S. E. Dashtgard and J. A. MacEachern, 2019: Earliest Cretaceous Transgression of North America Recorded in Thick Coals: McMurray Sub-Basin, Canada: International Journal of Coal Geology, v. 204, p.18-33, doi: 10.1016/j.coal.2019.01.011.

2.1. Abstract

Strata of the Lower Cretaceous McMurray Formation in the McMurray Sub-Basin (MSB) of Alberta and Saskatchewan, Canada, comprise marginal marine, tidal-fluvial, fluvial and interfluve deposits. In the Firebag Tributary located in the northeastern portion of the sub-basin, a thick coal seam (up to >20 m) forms a semi-continuous bed at the top of the lowermost McMurray Fm deposits (herein referred to as Lower McMurray). In coastal plain settings, peat-forming mires are highly sensitive archives of base-level. I investigate the stratigraphic significance of coals in the Firebag Tributary by analyzing coal petrography (4 cores), coal geochemistry (2 cores), and coal distribution in ~4500 wells. Additionally, I record the first absolute age for the McMurray Fm through the dating of an ash layer within the coal seam.

The petrographic character and distribution of coals in the northeastern part of the MSB suggest a complex history of base-level rise at the end of Lower McMurray deposition. Wetting-upward character coal seams record initial transgression of the Boreal Sea during a 4^{th} order sea level rise (Milankovitch-scale) within lowstand to early transgressive systems tract conditions. Sea-level rise during Lower McMurray times was estimated based on temperate climate peat formation rates, as well as peat-to-coal compaction factors, and probably occurred on a scale of 0.5-3 mm a^{-1}. Seam-internal wetting-upward cycles suggest that base-level rise was punctuated. Locally, compound and drying-upward character coals represent zones of high accommodation, wherein peat accumulation in mires was influenced by phases of syn-depositional subsidence and karst collapse. The thickest coals in the study area form an arc on a coastal plain as the Boreal

Sea inundated east- to southeastward into the Firebag Tributary. Within the arc of thick coals, a north-south decrease in coal thickness is interpreted to reflect the general southward inundation of the Boreal Sea across the MSB. Exceptionally thick coals (>10 m) likely formed where basement processes (e.g., karsting in Devonian carbonates) provided preferential groundwater pathways.

Chemical abrasion thermal ionization mass spectrometry dating of 5 sharply faceted zircons recovered from an ash bed within the coal provides the first absolute age (121.39 ± 0.2 Ma – Aptian) to the southward transgression of the Boreal Sea. I hypothesize that initial inundation of the MSB was related to tectonic activity in the Canadian Cordillera and the onset of magmatic flow in the western Coast Plutonic Complex.

2.2. Introduction

The Firebag Tributary in the northeastern quadrant of the Athabasca Oil Sands Region of Alberta, Canada (Fig. 2.1) hosts sediments of the Lower Cretaceous McMurray Formation, which were deposited during transgression of the Boreal Sea (Hein and Cotterill, 2006). These deposits encompass shallow-marine, tidal-fluvial, fluvial and interfluve deposits that accumulated on the Sub-Cretaceous Unconformity (SCU; Pemberton et al., 1982; Ranger and Pemberton, 1997). The top of the lowermost deposits of the McMurray Fm (commonly informally referred to as Lower McMurray; e.g., Carrigy, 1959; Pemberton et al., 1982; Ranger and Pemberton, 1997; Hein et al., 2013) largely comprise fluvial sands, which are commonly capped by a coal horizon overlying a single paleosol. Locally, the coal and paleosol succession cumulatively exceeds 10 m in thickness. The precursors to these coals, peat-forming mires, are highly sensitive archives of water table fluctuations during the accumulation of a mire, and these changes are preserved in the composition of the peat (and the resulting coal) (e.g., Diessel, 1992). Herein, stratigraphic correlations, isopach mapping, as well as petrological and geochemical analyses of Lower McMurray coals are used to investigate the stratigraphic significance and allogenic forces that drove Lower McMurray coal accumulation.

Within mires, peat accumulates in two distinctive domains, known as the upper acrotelm (active plant production, and aerobic decay of plants by micro-organisms) and the lower inert catotelm (peat preservation due to significantly decreased aerobic decay of organic matter) (Ingram, 1978; Clymo, 1984). While the acrotelm exhibits significant

hydraulic conductivity, the catotelm shows negligible hydraulic conductivity due to organic matter compaction. The boundary between the acrotelm and catotelm forms the long-term water table, which is used to approximate mire base-level (Diessel, 1992; Banerjee et al., 1996; Bohacs and Suter, 1997). Mires require a continuously rising water table (in relationship to the sedimentation surface) to create the accommodation space necessary for peat accumulation (Diessel, 1992; Jerrett et al., 2011b). The position of the water table is controlled by both (1) subsidence – tectonic or sediment compaction, and (2) water supply – primarily derived from rainfall (ombrotrophic mires can form when water table is "domed" over regional water table by sponge-like water retention of plants) or by regional groundwater (rheotrophic mire) (von Bubnoff, 1937; Clymo, 1984; Winston, 1994; Diessel et al., 2000; Wadsworth et al., 2002; van Asselen et al., 2010; Jerrett et al., 2011c). Additionally, Clymo (1984) showcased that upward expulsion of water during peat compaction can partially maintain water table levels within the mire. Von Bubnoff (1937) estimated that 90% of known coals formed where peats accumulated on coastal plains, which contrasts the distribution of modern mires; these are also widely distributed throughout the continent interior in the northern hemisphere (Gore, 1982). In paralic environments, the regional groundwater table is hydrologically connected with sea level (e.g., Diessel, 1992; Törnqvist, 1993; Bohacs and Suter, 1997), and coal seams are widely recognized to be overlain by marginal marine strata during transgression, or to overlie marine strata during regression (Shanley and McCabe, 1991; Diessel, 1992; Flint et al., 1995; Banerjee et al., 1996; Bohacs and Suter, 1997; Diessel et al., 2000; Wadsworth et al., 2002, 2003; Davies et al., 2006; Jerrett, et al., 2011a; Chalmers et al., 2013; Deschamps et al., 2017; Omodeo-Salé et al., 2017).

The Firebag Tributary in the McMurray Sub-Basin (MSB) of Alberta, Canada (Fig. 2.1) provides an excellent opportunity to study the stratigraphic significance and allogenic forces driving the deposition of coals. While the Lower McMurray has been treated largely as a lithostratigraphic entity, a combination of stratigraphic correlation, 3D modelling and petrographic observations are used herein to resolve coal-seam evolution within a sequence stratigraphic framework. Furthermore, I present the first absolute age date of the McMurray Formation, based on zircons extracted from an *in situ* ash layer within the coal. This date provides an age for resolving some of the earliest relative sea-level fluctuations in the Western Canada Sedimentary Basin during the southward transgression of the Boreal Sea in the Lower Cretaceous.

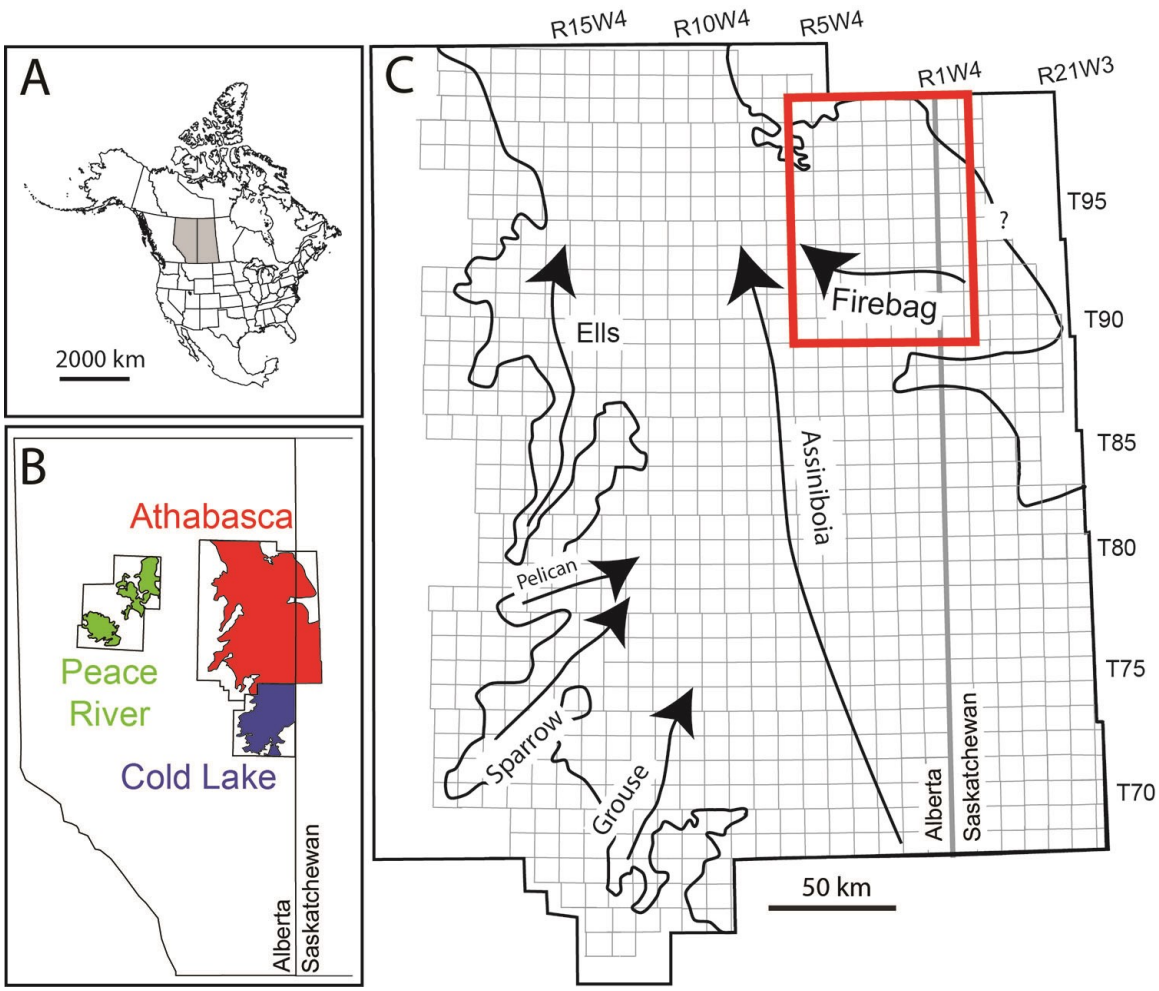

Figure 2.1. Overview of the study area
(A) The provinces of Alberta (light grey) and Saskatchewan (dark grey), in Canada. **(B)** Location of McMurray Sub-Basin (MSB) in the Athabasca oil sands region (red), as well as the extent of bituminous sands in the Peace River (green) and Cold Lake (blue) oil sands deposits of Alberta and Saskatchewan. **(C)** Outline of the MSB (thick black line) and the main paleotopographic lows on the Sub-Cretaceous Unconformity (commonly referred to as paleovalleys). The outline of MSB is defined where the thickness of the McMurray Fm and time-equivalent strata (e.g., Dina Fm in Saskatchewan) is less than 30 m. The red rectangle highlights the study area. The question mark along the eastern margin of MSB denotes uncertainty regarding the position of the original depositional edge of the basin, owing to Pleistocene glacial erosion of McMurray Fm strata. The grey grid represents the subdivision of Alberta into Township and Range blocks: 6 mile (10 km) by 6 mile blocks. (Maps adapted from: Christopher, 1997; Ranger and Pemberton, 1997; Broughton, 2013b; Hein et al., 2013; Hein and Dolby, 2018).

2.2.1. Sequence Stratigraphy of Coals

Peat accumulation in mires is dependent on accommodation space (A) and net primary productivity of plants (PP) (Clymo, 1984; Shanley and McCabe, 1991; Diessel, 1992; Bohacs and Suter, 1997). Accommodation space refers to the space between a theoretical depositional surface and base-level (Banerjee et al., 1996; Diessel et al., 2000;

Omodeo-Salé et al., 2017). Primary productivity of plants in mires is relatively constant in individual climate zones (Diessel, 2007 and references therein). By extension, peat accumulation is primarily driven by base-level change. Mires form when rates of base-level rise are close to peat production rates (Diessel, 2007) and specifically at A/PP ratios between 0.5 and 1.5. Mires thrive at A/PP ratios between 1–1.18 (Fig. 2.2; Diessel et al., 2000). When base-level rise outpaces a mire's capacity to build up organic matter, limnotelmatic (A/PP = 1.18–1.5) and eventually limnic (A/PP > 1.5) conditions develop (Fig. 2.2). Base-level fall generally leads to termination of peat formation in mires (Jerrett et al., 2011c). Coals can exhibit either a (1) wetting-upward character through accelerating base-level rise (increasing A/PP ratio), typical of late lowstand systems tracts (LST) and transgressive systems tracts (TST), or (2) a drying-upward character (decreasing A/PP ratio) through declining base-level rise, typical of the highstand systems tracts (HST) (Banerjee et al., 1996; Diessel et al., 2000; Holz et al., 2002; Davies et al., 2006; Chalmers et al., 2013). Mires are typically abundant during late LST, early TST, and middle HST, when rates of base-level rise are closest to those of peat production (Diessel, 2007). Wetting-upward and drying-upward characteristics are preserved in the petrological composition of the resulting coal.

Wetting-upward cycles in coals are defined petrographically as successions of terrigenous sediments and durain-dominated coals overlain by clarain- and vitrain-dominated coals as well as coaly shales (Fig. 2.2; e.g., Wadsworth et al., 2002; Diessel, 2007; Jerrett et al., 2011c). Mires that "wet upwards" shift landward relative to the shoreline and display an increasing ash content upward as more allochthonous material enters the mire during limnotelmatic and limnic conditions (Holz et al., 2002). Drying-upward cycles in coals show the opposite succession in terms of coal petrography, with fusain, terrigenous sediment and/or durains (all formed during increased subaerial exposure) overlying clarain-, vitrain- and shale-dominated coals. The ash contents in drying-upwards coals decrease upwards, reflecting dropping relative sea level and the basinward shift of mires (Fig. 2.2; Bohacs and Suter, 1997; Diessel, 2007; Jerrett et al., 2011a). However, the overall accommodation conditions have a direct influence on the resulting coal lithotypes, as demonstrated by studies of high- (e.g., Wadsworth et al., 2003) and low-accommodation settings (e.g., Chalmers et al., 2013) (Fig. 2.2). A low-accommodation regime is prone to forming highly oxidized lithotypes like durains and fusains, whereas high-accommodation settings favor shaley coals and coaly shales (Fig. 2.2C, D).

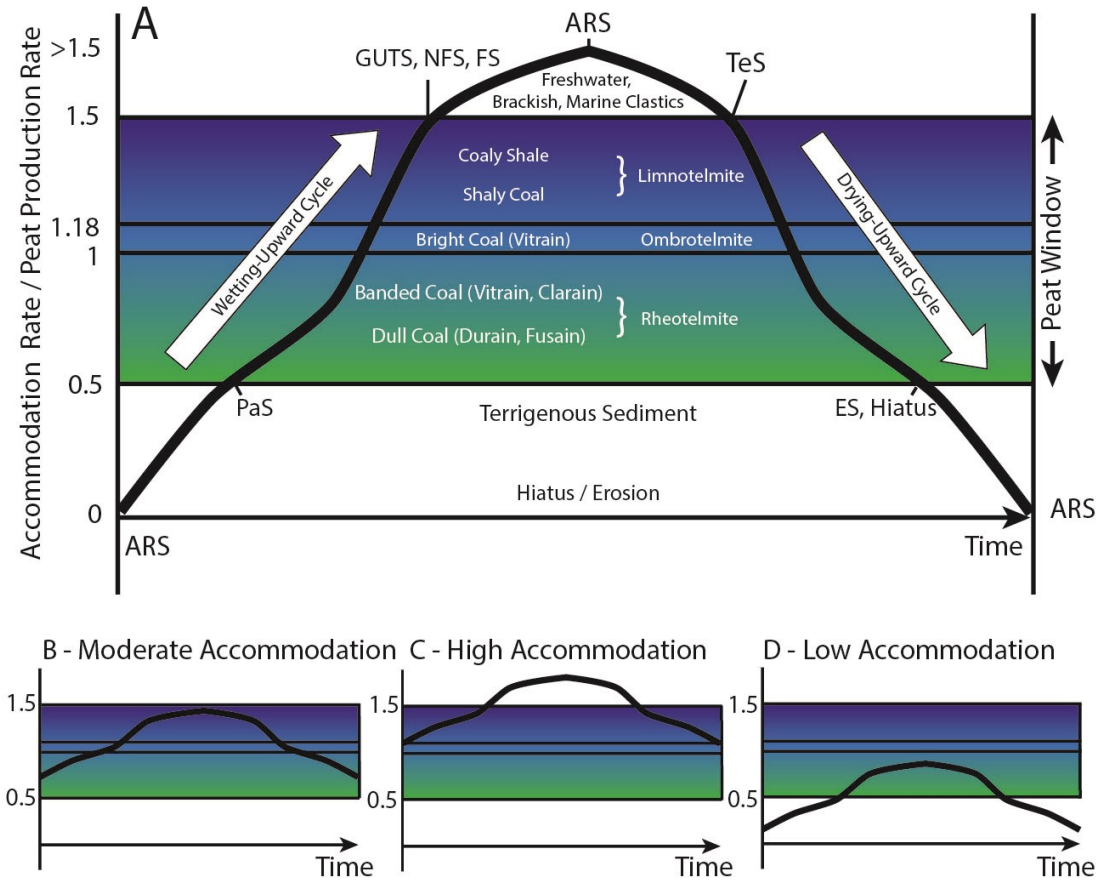

Figure 2.2. Relationship between coal petrography and base-level
(A) Schematic diagram of the relationship between accommodation rate, peat production and coal lithotypes, and associated paleoenvironmental conditions. The left limb indicates coal lithotype development under increasing base-level rise (wetting-upward cycles) and the right limb indicates the development of different coal lithotypes during decreasing base-level rise (drying-upward cycles). Drying-upward cycles are bound at their bases by terrestrialization surfaces (TeS; peat development under falling base-level rise within a limnic environment) and an erosional surface (ES) or hiatus at the top. Wetting-upward cycles are bound at the base by a paludification surface (PaS; development of a mire over a paleosol), and a flooding surface (non-marine (NFS), or marine (FS) in origin), or a give-up transgressive surface (GUTS; non-hiatal shift to limnic deposition) at the top. **(B–D)** Schematic graphs showing the same wetting-drying cycles under different accommodation regimes (adapted from Wadsworth et al., 2002; and Jerrett et al., 2011c).

Petrographic trends in coal seams are bound by stratigraphically significant surfaces (Fig. 2.2; Diessel et al., 2000; Wadsworth et al., 2002, 2003). Accommodation reversal surfaces (ARS) are defined by shifts from wetting-upward to drying-upward cycles or *vice versa* (Davies et al., 2006). An ARS situated between a wetting-upward and drying-upward succession is a flooding surface (potentially a maximum flooding surface). An ARS situated between a drying-upward and wetting-upward succession defines a regressive surface that may correspond to a sequence boundary (Davies et al., 2006). A paludification surface (PaS) defines the base of a coal (mire) that develops on a paleosol

(soil) during base-level rise (Fig. 2.2). A terrestrialization surface (TeS) defines the base of a mire that develops in a limnic environment during declining rates of base-level rise (typically non-hiatal), and can be equivalent to a maximum flooding surface (Diessel et al., 2000). Wetting-upward sequences can also be capped by a give-up transgressive surface (GUTS), or by a non-marine or marine flooding surface. All three of these surfaces reflect the mire's inability to keep up with base-level rise. While a GUTS is demarcated by a non-hiatal transition from limnotelmatic to clastic sedimentation, non-marine and marine flooding surfaces exhibit an erosional shift from mire formation to clastic sedimentation. Drying-upward surfaces can also be terminated by erosional surfaces that may correspond to subaerial unconformities (Diessel et al., 2000; Diessel, 2007).

2.2.2. Geology of the McMurray Formation

The McMurray Fm is the basal unit of the Lower Cretaceous Mannville Group (Fig. 2.3). It overlies the Sub-Cretaceous Unconformity (SCU) and is capped by the Wabiskaw Member (Mbr) of the Clearwater Fm. The McMurray Fm forms part of a 3rd order stratigraphic sequence and consists of several internal systems tracts (Hein et al., 2013). The SCU erosionally truncates carbonates of the Devonian Beaverhill Lake Group (Carrigy, 1959). Subsidence, collapse and brecciation of Devonian carbonates occur locally, and have been attributed to dissolution (up to 200 m below the SCU) of the Devonian Prairie Evaporite Fm (Ranger and Pemberton, 1997). Karsting has been recognized directly below the SCU, creating numerous paleo-sinkholes and other karst features (e.g., Broughton, 2013b; Barton et al., 2017)

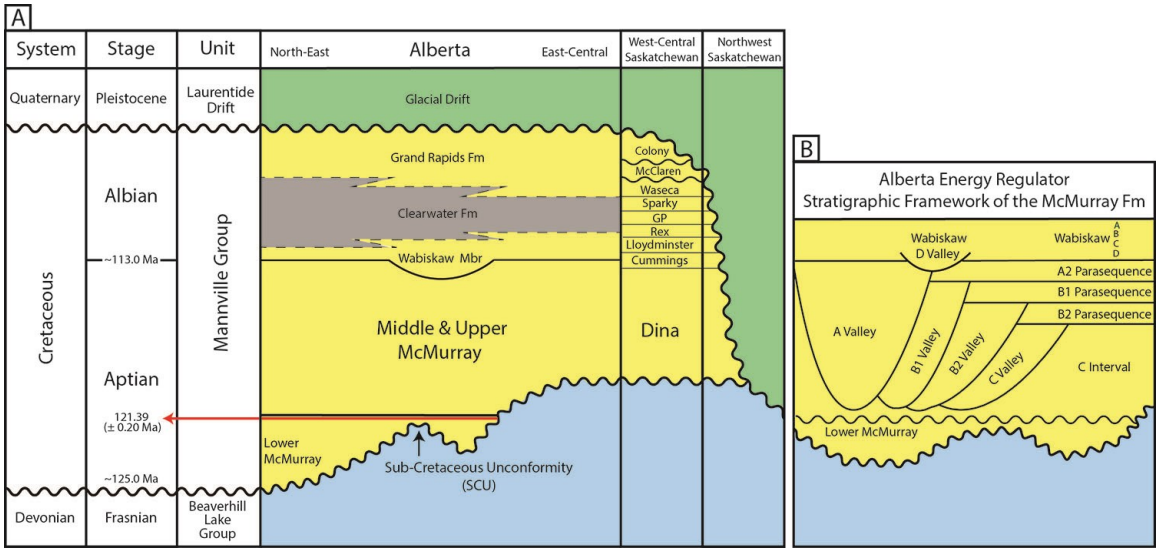

Figure 2.3. Chronostratigraphic chart of the Mannville Group in the Firebag Tributary of Alberta and time-equivalent strata in west-central and northwestern Saskatchewan (numerical ages taken from Cohen et al., 2013).

(A) Siliciclastic sediments (yellow for sandstone and gray for mudstone/shale) overlie Devonian carbonates (blue) of the Beaverhill Lake Group (adapted from Hein et al., 2013). The Sub-Cretaceous Unconformity (SCU) and Lower McMurray are also shown. An in situ date (red arrow) from the top of the Lower McMurray Fm is shown, based on data presented herein. Towards the northeast, Pleistocene glacial erosion removed the Mannville Group (Mossop and Flach, 1983). **(B)** Stratigraphic framework of the McMurray Formation in Alberta (adapted from Hein and Cotterill, 2006; and Hein et al., 2013)

Carrigy (1959) proposed the first lithostratigraphic characterization of the McMurray Fm, subdividing it into lower, middle and upper members. While the lower member largely preserves terrestrial strata, the overlying middle and upper members record increasing marine influence (e.g., Mossop and Flach, 1983; Ranger and Pemberton, 1997). The fluvial interpretation of the Lower McMurray was based initially on sedimentological observations, including cross-stratified sands, pedogenically altered muds, and the presence of coals (Carrigy, 1959; Mossop and Flach, 1983; Keith et al., 1988; Harris et al., 2016). Deposition of the Lower McMurray in a terrestrial setting was confirmed locally through identification of continental trace fossils such as *Naktodemasis* and *Taenidium* (Harris et al., 2016). Following its initial lithostratigraphic subdivision, multiple stratigraphic frameworks were developed for the McMurray Fm. The most prominent stratigraphic model interprets the McMurray Fm as a series of parasequences deposited during sea level rise, which were partially eroded by valley incisions during intermittent sea level falls (Fig. 2.3B; Hein et al., 2013). However, in the Hein et al. (2013) stratigraphic framework, the Lower McMurray remains a lithostratigraphic unit comprising

terrestrial deposits at the base of the succession, due to difficulties in correlation of the terrestrial deposits to equivalent strata elsewhere in the basin. Terrestrial systems commonly exhibit slow response times to base-level change and rarely show significant shifts in lithological character (Diessel et al., 2000). Consequently, sea level changes observed within strata elsewhere in the basin are difficult to correlate to the strata of the Lower McMurray. Coal accumulations are an exception to this rule (Wadsworth et al., 2003) and provide a high-resolution archive of base-level changes.

2.2.3. Study Area – Firebag Tributary

The Firebag Tributary is located at the northeastern margin of the MSB. Paleo-drainage in the Firebag Tributary is interpreted to have been from east to west, debouching into the northwestward flowing Assiniboia Valley (Fig. 2.1; Christopher, 1997; Hein et al., 2007). The study area extends over approximately 10,000 km^2 from Township 06, Range 99 West of the 4th Meridian in the northwest (06-099W4) to 24-90W3 in the southeast (Fig. 2.1). Erosional truncation of McMurray Fm strata is at a maximum in the northeast and extends as far south as the Firebag Tributary (Fig. 2.3A; Andriashek and Atkinson, 2007; Hein et al., 2013).

The McMurray Fm in the Firebag Tributary exhibits a high proportion of terrestrial strata, which are commonly interpreted as either Lower McMurray Fm in Alberta (Hein et al., 2007), or the equivalent Dina Fm in Saskatchewan (Fig. 2.1; Christopher, 1997). Specifically, the Firebag Tributary hosts significant coal deposits, which are uncommon elsewhere in the MSB (Hein et al., 2007) and provide unique insights into the early transgression of the Boreal Sea.

2.2.4. Data and Methods

Stratigraphic Mapping and 3D Modelling

Twenty cross-sections were created in GeoScout, using 419 of the 4,500 publicly available well logs (Fig. 2.4). The cross-sections were used to correlate the Lower McMurray across the study area, and to act as control points for interpreting the other 4,100 well logs. All interpreted well logs subsequently were used to map the extent of the SCU, base and top of the coal-bearing strata, top of the Lower McMurray (Top LM), and top of the “B1 parasequence” (Fig. 2.3B; *cf*. Hein et al., 2013). The top of the B1

parasequence was chosen as a datum, because it provides the most laterally persistent and least diachronous (relative to the age of the coal) surface, and shows minimal post-depositional deformation. I base this interpretation on the consistent thickness of strata between the top of B1 and the top of the McMurray Formation. Limited deformation of the surface post-dated coal deposition and pre-dated creation of the datum. Three cross-sections — two depositional dip-oriented (A–A', B–B'), and one depositional strike-oriented (C–C') — incorporating 34 wells (Fig. 2.4) were chosen to highlight the relationship of coals to the SCU and the top of the Lower McMurray. Notably, cross-section B–B' is hung from the top of the Lower McMurray, as the top of the B1 parasequence is commonly absent. Locally, wells were hung on reference elevations where the top of the Lower McMurray is also not preserved.

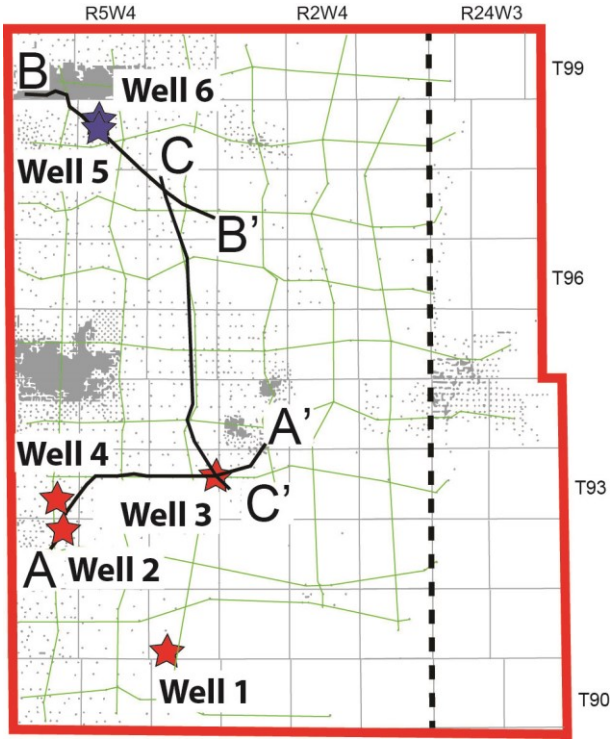

Figure 2.4. Outline of the study area and the data used in this study.
Grey dots mark the approximately 4,500 well logs that were used for 3D modelling. The four wells with core log descriptions are indicated by red stars, and the two wells with geochemical data are indicated by blue stars. The locations of cross-sections A–A', B–B' (Fig. 2.5) and C-C' (Fig. 2.6) are shown. Green lines give the location of cross-sections used as guidelines for picking stratigraphic tops in wells.

The SCU was picked on well logs based on an upwards decrease in photoelectric (Pe) values to below 2.3, an upwards increase in density porosity (on a sandstone density scale), and an upwards convergence of the neutron- and density-porosity (ND) readings,

also on a sandstone density scale. Together, these three geophysical readings mark a shift upwards from carbonate to clastic lithologies, and the contact is easily identifiable throughout the entire study area. Coal strata are located above the SCU, and were discerned based on their high ND log response, which commonly exceeds 50% porosity. Coal strata can be laterally traced up to 10s of km. Where coal is preserved, the top of the Lower McMurray is demarcated by a sharp decrease upwards in ND readings (sand-on-coal contact), and/or a decrease in gamma-ray response (sand over a shale-rich deposit). Where coal strata are absent, the top of Lower McMurray is not certain, and the contact commonly displays a 10–20% increase in porosity on ND logs from below to above the contact. This is interpreted to record valley incision by high-energy fluvial channels near the end of Lower McMurray time. Additionally, sediments overlying the top of the Lower McMurray commonly exhibit increasing-upward gamma-ray signatures and diverging ND log readings, reflecting tidal-fluvial point bars in the increasingly marine influenced McMurray C interval. Lastly, throughout large portions of the study area, the top of the B1 parasequence is demarcated by a pronounced increase in resistivity (commonly to > 100 ohm meters), located between 2–10 m below the top of the McMurray Fm. The top of B1 is laterally continuous across the study area, except where it has been removed by glacial erosion. Diamict, deposited during Pleistocene deglaciation, is identified on logs by variable and high ND readings as well as uniform resistivity readings.

Mapping and 3D modelling of coals were completed using all 4,500 well logs. Tops were picked in GeoScout using interpreted cross-sections as a guide for identifying surfaces (Fig. 2.4); these tops were subsequently exported to Petrel. As coals are not laterally continuous, zero thicknesses were assigned to wells without coals to improve the accuracy of Petrel interpolation algorithms. This was done in Python by creating a top and base of coal seams in wells with no coal, and equating their depth to the SCU at that location. Thereby, a zero thickness for the coal is created for a specific well (regardless of Lower McMurray thickness, which was picked separately). Importantly, zero isopachs were only added where overlying tops (Lower McMurray, B1) are not removed by glacial erosion, because one could not be sure of non-deposition vs. erosion of the coal. The list of tops exported from GeoScout and modified in Python were then imported into Petrel 2016. Petrel 2016 was used to create isochore points and model isopach surfaces using convergent interpolation. The isochore points algorithm adds thickness points every 50 m between wells and improves the quality of successive mapping done with the convergent

interpolation algorithm. Notably, isochore point creation can, on occasion, produce negative thicknesses; in such cases, the values were equated to zero. Adding zero isopachs for wells in Python and creating isochore points between wells ensured that isopach overestimation was limited when running the convergent interpolation algorithm. Convergent interpolation is a control point-oriented algorithm, which uses the previously created grid of isochore points to create a high-resolution surface. Convergent interpolation honors areas with high data-density (wells) and interpolates where data-density is sparse. Isopach maps were used to highlight depositional trends of coal deposits, as well as their relationships to SCU paleotopography. Additionally, I mapped the areas where Pleistocene glaciation eroded part of the McMurray Fm.

Macroscopic Descriptions and Geochemistry

Detailed petrographic, sedimentologic and ichnologic descriptions were done for four subsurface cores containing thick coal sequences (red stars, Fig. 2.4): 1AA/09-05-091-04W4 (Well 1); 1AA/14-35-092-06W4 (Well 2); 1AA/10-24-093-04W4 (Well 3); and 1AA/10-11-093-06W4 (Well 4). Core observations were summarized in combined coal petrographic, sedimentologic and ichnologic core logs. Coal lithotypes were logged to determine intra-seam wetting- and drying-upward cycles, as well as the overall character of the seam. Additionally, the contacts between coals and with underlying and overlying clastic sediments were analyzed to determine the character of mire initiation and termination, respectively. Sedimentologic and ichnologic observations were used to interpret depositional environments, as well as to determine whether syn-depositional subsidence or tectonism impacted coal accumulation.

Macroscopic observations were compared to previously acquired coal geochemical data (e.g., ash content, sulphur content) for 2 cored coal intervals (blue stars, Fig. 2.4). These wells are: 1AA/12-20-098-05W4 (Well 5); and 1AA/05-29-098-05W4 (Well 6). Similar to the coal petrography approach, changing ash and sulphur contents within coal seams were used to interpret drying- or wetting-upward cycles, and to identify stratigraphically significant surfaces.

Chemical Abrasion Thermal Ionization Mass-Spectrometry

Bentonitic claystone beds (ash layers) between 1 and 3 cm in thickness occur in coals in wells 1, 2 and 3 (Fig. 2.4). The yellowish-white, 3 cm thick claystone bed in Well

1 (1AA/09-0-5-091-04W4) is located at a depth of 201.35 m below the Kelly Bushing, and occurs in a clarain; this ash bed was sampled for zircons. Uranium-Lead (U-Pb) ratios were obtained on single zircon grains through chemical abrasion isotope dilution thermal ionization mass spectrometry (CA-TIMS; modified after Mattinson, 2005) at the Isotope Geology Laboratory at Boise State University, Idaho, USA. CA-TIMS U-Pb dates and uncertainties were calculated using standard algorithms (Schmitz and Schoene, 2007), EARTHTIME ET535 tracer solution (Condon et al., 2015), and standard U-decay constants (Jaffey et al., 1971). $^{206}Pb/^{238}U$ ratios and dates were corrected for initial ^{230}Th disequilibrium, using $D_{Th/U} = 0.20 \pm 0.05$ (1σ) (Crowley et al., 2007).

2.3. Results

2.3.1. Stratigraphy and Distribution of Coal Strata in the Firebag Tributary

Cross-sections A–A', B–B' (Fig. 2.5) and C–C' (Fig. 2.6) depict coals between 1 and 23 m in thickness that form a semi-continuous bed at the top of the Lower McMurray. Coals commonly exhibit either single seams, as seen in the SW extent of cross-section A–A', or multiple (up to 3) sub-seams (center and NE; Fig. 2.5A). Coal seam splits overlie distinctive paleotopographic lows along the SCU (e.g., 1AA/10-24-093-04W4; Fig. 2.5A). Coals are not continuously distributed at the top of the Lower McMurray (e.g., cross-section C–C'; Fig. 2.6), and in zones where coals are absent, well logs show thick sand packages of variable thickness situated in stratigraphic positions where the coals would be expected (e.g., 1AA/02-15-095-04W4; Fig. 2.6). Where the coal-seam is split, cross-sections A–A' and C–C' show that surrounding wells commonly lack coals (e.g. 1AA/12-25-093-04W4; Fig. 2.6). The relationship between paleotopography on the SCU, the variable distribution of coals, and the location of coal seam splits becomes more apparent when observing trends throughout the entirety of the study area (Fig. 2.7).

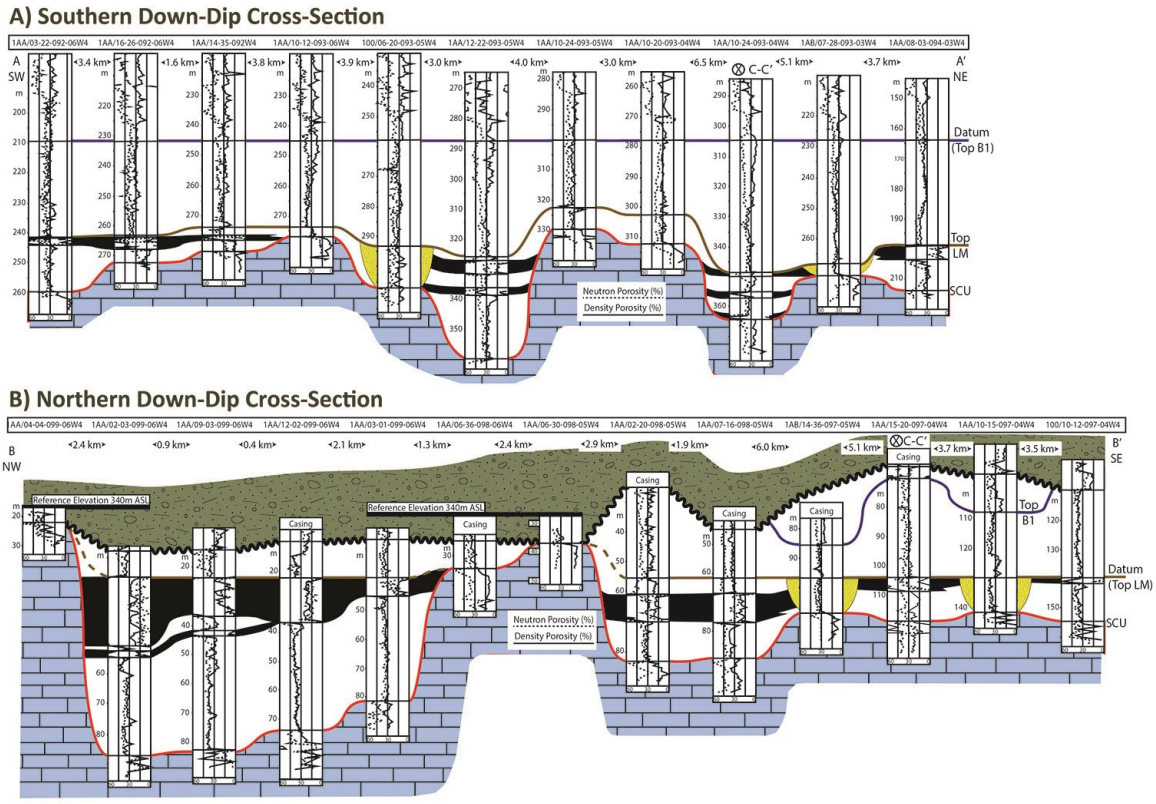

Figure 2.5. Regional dip-parallel cross-sections in the study area, where all coal occurrences are mapped.

These cross-sections display neutron-density porosity logs (depth in m), which are best suited to highlighting coal intervals (black). Channels are shown in yellow. The locations of the cross-sections are shown in Fig. 2.4. The intersection with cross-section C–C' is noted in both cross-sections. **(A)** Cross-section A–A' runs through the southern portion of the study area. Coals are up to ~6 m thick and locally, coal seams are separated by intervening clastic deposits. Three surfaces are indicated: SCU (red line), top of Lower McMurray (green line), and top of the B1 parasequence (blue line), which is used as the datum. **(B)** Cross section B–B' describes a NW to SE transect that exhibits coals ranging from 2 - 23 m in thickness and that are split locally. Three surfaces are indicated: SCU (red line), top of Lower McMurray (green line) and erosional contact with Quaternary glacial deposits (wavy black line). The top of the Lower McMurray is used as a datum, because the overlying strata are commonly removed. Where the top of the Lower McMurray is removed, wells are hung on local reference elevations.

SCU paleotopography is determined by mapping the isopach from the SCU to the top of B1 parasequence, wherein the upper surface is deemed to be effectively horizontal. Correspondingly, thick strata reflect paleotopographic lows and thin strata reflect paleotopographic highs on the surface. SCU paleotopography (Fig. 2.7A) exhibits pronounced structural lows (isopach > 60 m; cold colors) in the central study area (e.g., 95-04W4), and potentially in the NE (e.g., 97-02W4) and SE corners (e.g., 91-01W4). Additionally, the NW corner (98—06-05W4, Fig. 2.7A) of the study area shows very deep local depressions along the SCU, and many of the thickest coals align with these

paleotopographic lows (Fig. 2.7B). Numerous zones with thick coals, however, do not align with paleotopographic lows along the SCU (e.g., 91-04W4). Figure 7C does not appear to show a correlation between coal thicknesses < 5 m and SCU paleotopography (linear regression has a fit of $R^2 = 0.08$). That said, coals thicker than 5 m are more prevalent in paleotopographic lows along the SCU (linear regression has a fit of $R^2 = 0.16$). Wells that do not preserve the top of the B1 are excluded from Figure 2.7C. As such, multiple wells preserving thick coals, specifically in the northern portion of the study area are not included, and hence, correlation between > 5 m thick coals and thicker SCU-B1 isopachs may be stronger than indicated (Fig. 2.7C).

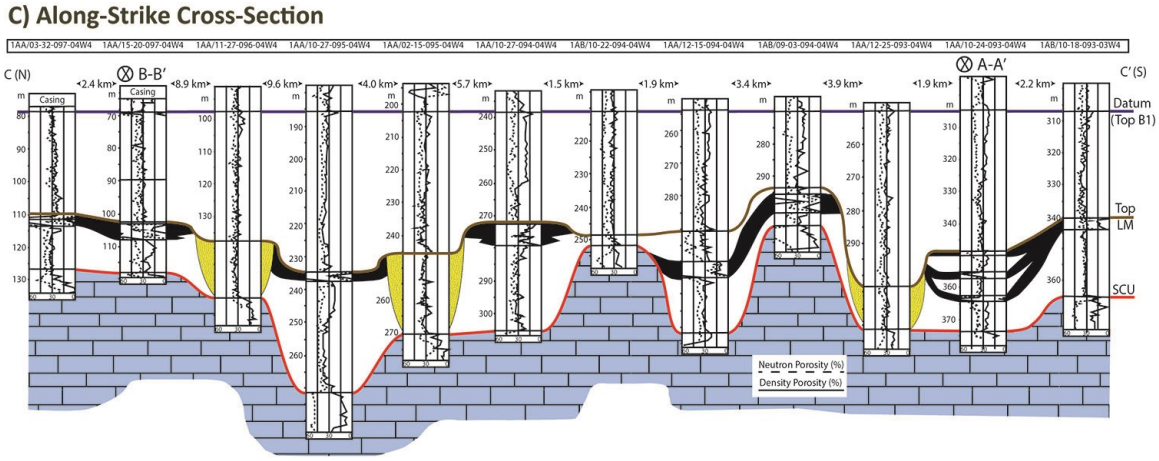

Figure 2.6. Regional along-strike cross-section C–C' in the study area, where all coal occurrences are mapped.

This cross-section displays neutron-density porosity logs (depth in m), which are best suited to highlight coal intervals. Channels are shown in yellow. The location of the cross-section is shown in Fig. 2.4. The intersections with cross-section A-A' and B-B' are noted on the cross section. Cross-section C–C' runs from the north to the south of the Firebag Tributary (along strike), where coals range from 0 – 7 m thick and are locally separated by intervening clastic deposits. Three surfaces are indicated: SCU (red line), top of Lower McMurray (green line) and the top of the B1 parasequence (blue line), which was used as the datum.

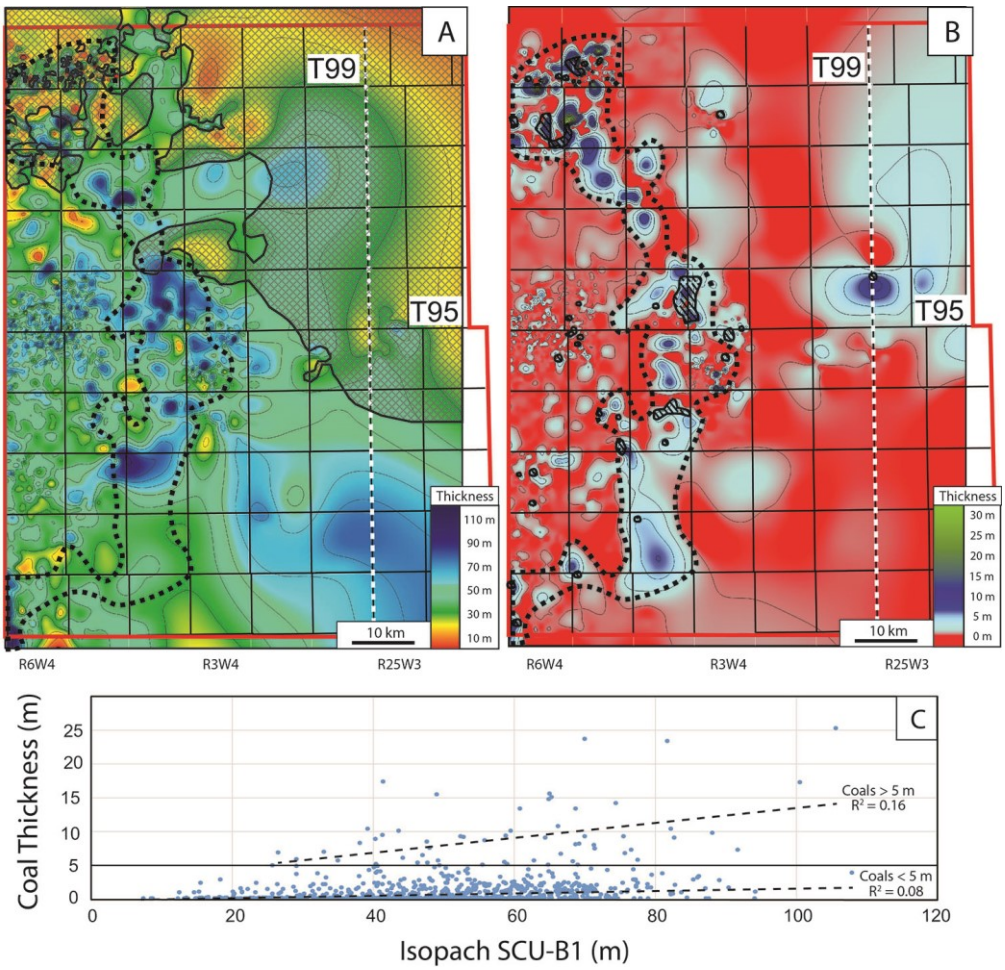

Figure 2.7. Isopach maps of the study area. The black dashed line outlines the area where net coal thicknesses exceed 5m. The white dashed line is the Alberta – Saskatchewan border.

(A) Isopach map of SCU to the top of the B1 paraserquence. Cold colors (blues and greens) refer to thick sediment packages (interpreted as paleotopographic lows on the SCU), and hot colors (reds and yellows) refer to thin sediment packages (interpreted as paleotopographic highs on the SCU). The area outlined by grey cross-hatching refers to zones where Pleistocene glaciation has eroded McMurray Fm strata (SCU to Pleistocene deposits isopach < 30 m). **(B)** Isopach map of net coal thickness (excluding intra-seam clastics) in the study area. Light blue colors refer to coals <5 m thick, and dark blues and greens refer to coals between 6 and 32 m thick. The area of thick coal deposition forms an arcuate shape. Black hatch-marked areas refer to zones where the coal seam is split into 2 or 3 sub-seams. **(C)** Plot of net coal thickness versus SCU to B1 parasequence isopachs for all wells in the study area that preserve coal and the top of B1 (1049 wells). Two linear regression lines (dashed lines) are added for coals above and below 5 m in thickness. Coals thinner than 5 m do not appear to follow a trend towards specific isopach thicknesses (R^2 = 0.08); however, coals thicker than 5 m appear to trend towards thicker isopachs (R^2 = 0.16).

Isopach mapping of coal seams further reveals that the thickest coals form a distinctive, approximately 5–20 km wide arcuate shape that is convex towards the east. This arc of thickened coal runs from northwest (99-06W4) to southwest (92-06W4) in the study area, and within this arc, thicknesses decrease from north to south. Notably, the

thickness trend may be understated, owing to glacial erosion of the McMurray Fm interval (and by extension, its coals) in the northern part of the study area (e.g., 98-04W4 and 98-05W4; Fig. 2.7A).

2.3.2. Coal Seam Cyclicity – Description and Interpretation

Detailed petrographic and sedimentologic observations of coals in the Firebag Tributary reveal coal seams with multiple wetting-upward, drying-upward, or compound (drying- and wetting-upward) cycles. Well 1 displays 4 wetting-upward cycles, and the seam was initiated through paludification above a thick, rooted, yellowish-grey paleosol (PaS, 205.4; Fig. 2.8). Lithotype successions in all 4 wetting-upward cycles (W1–4) of the coal seam in Well 1 are manifested as terrigenous sediments and/or durains, overlain by clarains or vitrains, and finally by shaley coals. A shift of lithotype successions within individual wetting-upward cycles is observed locally. The lowermost wetting-upward cycle in Well 1, W1 (Fig. 2.8), is characterized by terrigenous sediments overlain by durain and, subsequently, clarain. The second (W2) and third (W3) wetting-upward cycles are characterized by durain overlain by clarain and then vitrain. Finally, the uppermost wetting-upward cycle W4 is characterized by durain directly overlain by shaley coal. Correspondingly, W1 to W4 record an upwards increase of the A/PP ratio within the mire. Throughout the coal seam in Well 1, the amount of macroscopically visible pyrite and pyritized wood increases upwards. The surface at the top of W4 is defined by a sharp, non-hiatal shift to clastic deposition (GUTS, 199.25 m; Well 1, Fig. 2.8), and overlying clastics comprise cemented heterolithics displaying the trace fossil *Naktodemasis* as well as common carbonaceous debris.

Well 2 (Fig. 2.8) displays 1 wetting-upward cycle, and the coal seam was also initiated through paludification on a thick, rooted, yellowish-grey paleosol. The single wetting-upward cycle (W1) in Well 2 is marked by terrigenous sediments successively overlain by durain, clarain and finally shaley coal. W1 is capped by erosional non-marine flooding surface (276.6 m; Well 2, Fig. 2.8), which in turn, is overlain by cross-stratified sands.

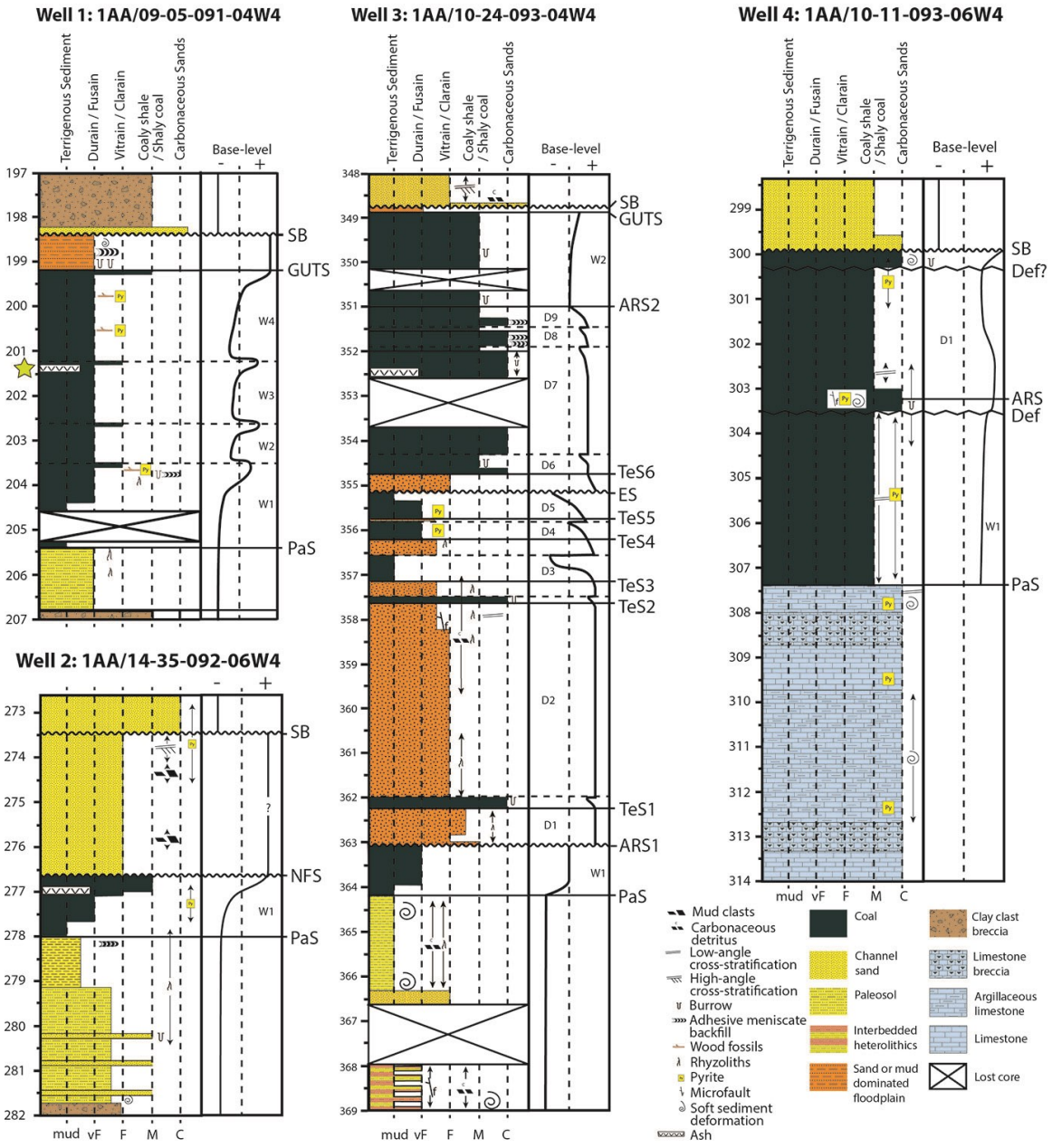

Figure 2.8 Combined facies (lithology, sedimentary structures, grain size, bioturbartion and accessories) and coal petrographical logs (lithotypes) for 4 wells.

Each well includes an interpreted base-level curve, with wetting-upward (W) and drying-upward (D) cycles identified, as well as stratigraphically significant surfaces (ARS: accommodation reversal surface; PaS: paludification surface; TeS: terrestrialization surface; GUTS: give-up transgressive surface; NFS: non-marine flooding surface; SB: sequence boundary at top of the Lower McMurray). The locations of these wells are given in Fig. 2.4. Well 1 includes the location of the ash sampled for zircons (yellow star).

Coals in wells 3 through 6 record multiple drying-upward cycles, or compound seams. Wells 3 and 4 (Fig. 2.8) record erratic A/PP shifts (i.e., coaly shales over durain)

and lithotypes common to high A/PP ratios (e.g., shaley coals, coaly shales, and carbonaceous sands). The coal seam in Well 3 overlies mud- and sand-rich deposits exhibiting soft-sediment deformation (e.g., convolute bedding and micro-faults) and common root traces. This coal was initiated through paludification (PaS at 364.2 m, Well 3, Fig. 2.8) above the yellowish-grey paleosol. The overlying wetting-upward cycle W1 is demarcated by terrigenous sediment overlain by durain, and capped by ARS1 (also a non-marine flooding surface) at 363.1 m (Well 3; Fig. 2.8). ARS1 demarcates a shift from a wetting-upward to drying-upward character within the seam, and is overlain by 9 consecutive drying-upward cycles D1-D9 (363.1 – 351 m, Well 3; Fig. 2.8). The lowermost drying-upward cycles (D1, D2) are characterized by rooted sandstones overlain by organic-rich sands (363.1 – 357.5 m, Well 3; Fig. 2.8), reflecting a major increase in the A/PP ratio. Above this, three successive drying-upward cycles D3-D5 (357.5 m – 355.15 m, Well 3, Fig. 2.8) occur, demarcated by thinner, rooted sands (<0.3 m) capped by terrigenous sediment and durain, and reflecting a decrease in the A/PP ratio. Following erosion at 355.15 m, the uppermost 4 drying-upward cycles (D6 to D9) are characterized by rooted sandstones overlain by carbonaceous sands and coaly shales as well as carbonaceous sands capped by coaly shales (355.15 – 351 m, Well 3, Fig. 2.8). Carbonaceous sands display common *Naktodemasis* and other unidentified burrows. This reflects a major shift in the mire to lithotypes associated to high A/PP ratios. The lowermost drying-upward cycles (D1 to D5) all contain internal TeS (TeS 1-5, Well 3; Fig. 2.8), reflecting mire initiation in freshwater environments. Drying-upward cycle D6 displays the final terrestrialization before limnotelmatic conditions that persist in D7 to D9. Following D9, a second accommodation reversal surface (ARS2 at 351 m, Well 3; Fig. 2.8) demarcates a shift from a drying-upward to wetting-upward character of the seam. The wetting-upward cycle W2 overlying ARS2 is characterized by a shaley coal, which becomes increasingly shale-rich upward. W2 is capped by a non-hiatal shift to heterolithic deposits (GUTS at 348.8 m, Well 3; Fig. 2.8), which are, in turn, overlain by cross-stratified sands.

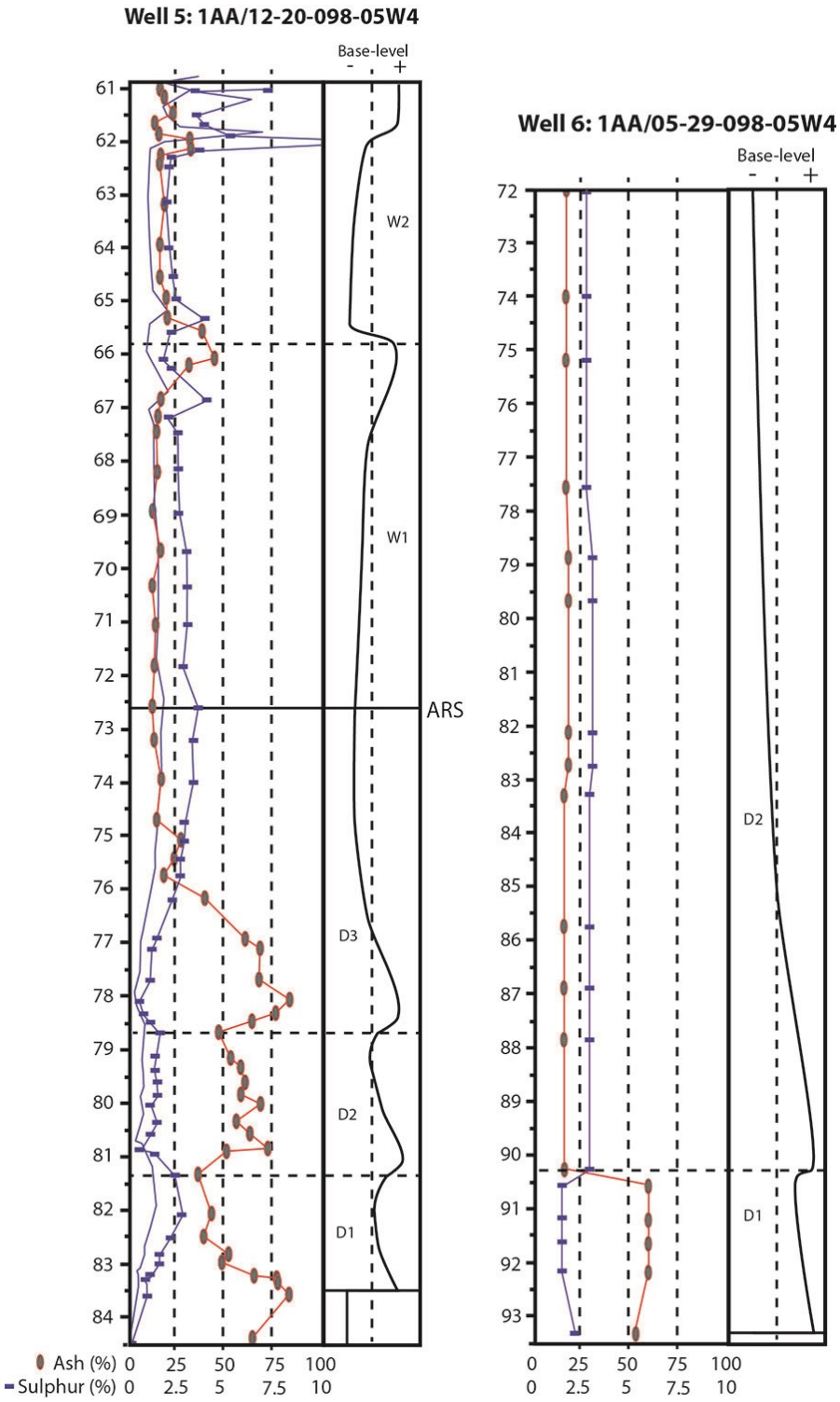

Figure 2.9. Geochemical plot of the the ash and sulphur content for 2 wells.
Each well includes an interpreted base-level curve, with wetting-upward (W) and drying-upward (D) cycles, as well as stratigraphically significant surfaces (ARS: accommodation reversal surface; PaS: paludification surface). The locations of these wells are given in Fig. 2.4.

Well 4 also displays a compound coal seam that directly overlies the SCU (307. 4 m, Well 4; Fig. 2.8). The SCU overlies highly brecciated carbonates and argillaceous limestones exhibiting convolute bedding. The argillaceous limestones are very light colored and form a paleosol; hence, coals in Well 4 initiate through paludification above the SCU (307.4m, Well 4; Fig. 2.8). The lowermost wetting-upward cycle W1 between 307.4 m and 303.2 m is characterized by a shaley coal that is overlain by coaly shale and carbonaceous sands (Well 4; Fig. 2.8), indicating limnotelmatic conditions. In contrast to all other coals, clastic-rich lithotypes in W1 exhibit inclined bedding, the angle of which decreases upward across the interval 307.5 to 303.5 m (apparent dip in core: 25° to ~0°, Well 4; Fig. 2.8). W1 is capped by an ARS at 303.2 m, where a shift to a drying-upward character is observed. Furthermore, a pyritized micro-fracture and soft-sediment deformation occur at the depth of the ARS (Well 4; Fig. 2.8). The overlying drying-upward cycle D1 is characterized carbonaceous sands capped by slightly inclined (<5° apparent dip in core) coaly shales (303.2 – 300.3 m, Well 4, Fig. 2.8). The coal seam in Well 4 is capped by an carbonaceous sand that displays soft-sediment deformation and rare burrows, which is erosively overlain by cross-stratified sands at 299.9 m (Well 4; Fig. 2.8).

Wells 5 and 6 (Fig. 2.9) show very thick coal seams of 21.5 and 23.0 m, respectively. These record a drying-upward character seam and a compound coal seam. Upwards from the base of the coal in Well 5 at 84.5 m, three drying-upward cycles (D1 to D3) are recorded between 84.5 m and 72.6 m (Fig. 2.9). The drying-upward cycles display decreasing ash contents (from >75% to < 25%) and slightly increasing sulphur contents (0 to 4%). These drying-upward cycles are capped by an ARS at 72.6 m, which demarcates a change in the geochemical characteristics. The ARS is overlain by two wetting-upward cycles (W1 and W2) that exhibit an increase in ash contents towards the top (15 to 50%), coupled with a marked increase in sulphur contents (2.5% to 14 %). W1 and W2 exhibit a total thickness of 11.5 m. In contrast to that of Well 5, the coal of Well 6 displays two drying-upward cycles D1 and D2, which are characterized by decreasing and generally low ash values (Well 5; Fig. 2.9) and constant sulphur values. Notably, data in Well 6, and to a lesser extent Well 5, are significantly less dense (0.1-2.5m between ash/sulphur measurements) than continuous petrographic logs (Fig. 2.8).

2.3.3. Absolute Age from CA-TIMS

From the sampled ash bed in Well 1, five sharply faceted zircon grains were manually recovered from the ash layer. These zircons are approximately 100 µm long and 20–40 µm in the other dimensions. CA-TIMS dating of these zircons exhibits a tight $^{206}Pb/^{238}U$ cluster of highly precise ages ranging between 120.99 Ma and 121.54 Ma (error ± 0.31-0.8 Ma; Fig. 2.10B). A weighted mean age for these grains was calculate using Isoplot (Ludwig, 2012), yielding 121.39 ± 0.20 Ma (mean standard weighted deviation = 0.6, probability of fit = 0.65). Additionally, the quality of these data was tested by calculating the probability of concordance in Isoplot, utilizing the $^{206}Pb/^{238}U$ and $^{207}Pb/^{235}U$ ratios, as well as their respective 2σ errors. Probability of concordance yielded 76%, which is well beyond the lowermost cutoff of 1% suggested by Matthews and Guest (2016).

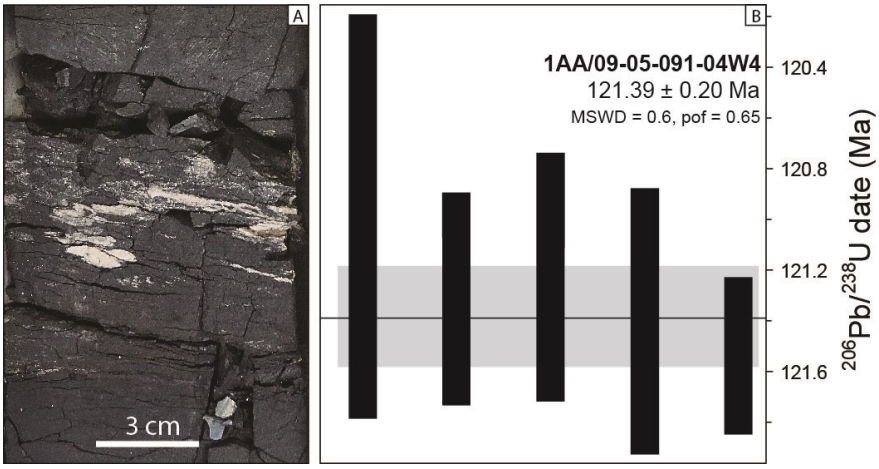

Figure 2.10. Ash bed in the LM coal seam of well 1AA/09-05-091-04W4
(A) Yellowish-white bentonitic claystone band within a clarain (201.35 m, Well 1). This claystone was sampled for zircons. **(B)** Ages of single zircon grains that were dated with CA-TIMS and show a highly precise cluster of $^{206}Pb/^{238}U$ ages. Isoplot 4.15 (Ludwig, 2013) was used to calculate a weighted mean average age of the dated grains. This produced a calculated age of 121.39 ± 0.20 Ma (mean standard weighted deviation (MSWD) = 0.6, probability of fit (pof) = 0.65).

2.4. Discussion

2.4.1. Processes Impacting Regional Coal Distribution in the Lower McMurray

Coal in the McMurray Fm of the Firebag Tributary form a semi-continuous bed at the top of the Lower McMurray (Figs 2.5 and 2.6). Mire initiation through paludification and non-hiatal drowning of mires by fresh- or saline waters (GUTS in wells 1 and 3, Fig. 2.8;

and >10 % sulphur in Well 5, Fig. 2.9) towards the top of the Lower McMurray showcases the transgressive nature of the Lower McMurray coal seam. The semi-continuous distribution of the coal and its transgressive character are consistent with peat-accumulation within a low- to moderate-accommodation regime (e.g., Diessel, 2007; Chalmers et al., 2013). Where the top of the coal seam is not preserved, the contact with the overlying McMurray C interval (Fig. 2.3B) is commonly disconformable, due to non-deposition of coal or its erosion by fluvial and tidal-fluvial channels.

The arc of thick coals in the Firebag Tributary is interpreted to reflect mire formation on a shore-parallel coastal plain, as the Boreal Sea inundated the Firebag Tributary from WNW to ESE (Fig. 2.11B). The transgressive coal seam could have provided a tabular (albeit diachronous) coal distribution, as base-level began to rise in increasingly landward positions. The lack of thick coal accumulations outside of the arc suggests that mires were restricted to a particular time and space where base-level rise provided a zone of optimal A/PP ratios for their formation. Diessel (1992) described similar narrow belts of coals parallel to the coastlines on delta plains in the Upper Cretaceous Ferron Sandstone of Utah, USA, and the Lower Cretaceous Fahler Mbr in NW Alberta, Canada. The lack of evidence for a shoreline protuberance in the Firebag Tributary suggests that a coastal plain interpretation is more probable (Fig. 2.12). Zones where coals are absent within the arc are interpreted to reflect westward-flowing fluvial (locally tidally affected) channels in the Firebag Tributary (Fig. 2.12B), which debouched into the Assiniboia Valley (e.g., Hein et al., 2007). Within the arc of thick coals, a north-south decrease in coal thickness is evident (Fig. 2.11A). Many authors have shown that transgression of North America by the Boreal Sea occurred from north to south (e.g., Leckie and Smith, 1992; Wightman and Pemberton, 1997). As base-level rose, zones of favorable A/PP ratios migrated south, likely leading to a diachroneity in mire initiation and, by extension, slightly thicker coals in the northern part of the study area. While the north-south trend observed in the arc falls in line with such an inundation direction of the Boreal Sea, it is noteworthy that many coals in the north also coincide with paleotopographic lows along the SCU (see below).

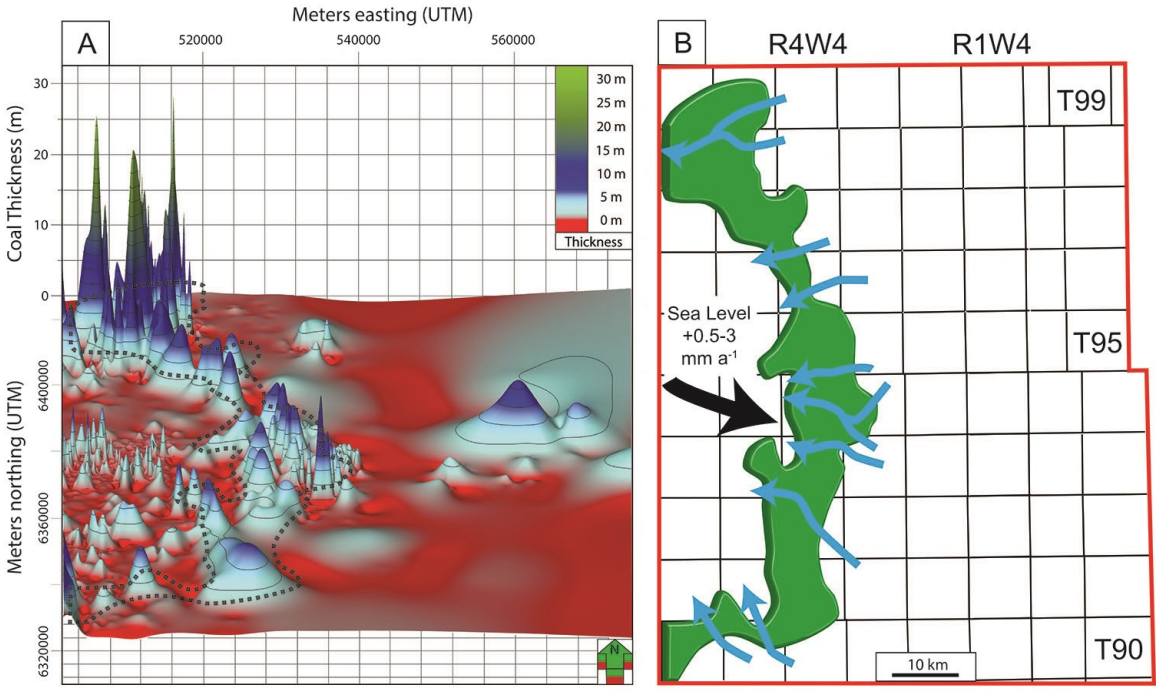

Figure 2.11. Coal thickness distributions in the study area, with the arcuate-shaped distribution of coals outlined.

(A) Oblique, 3D view of the coal isopach and the main distribution trend. This map is the same as that shown in Figure 2.7B, with 1000-fold vertical exaggeration. This shows the distinctive north-south decrease in coal thickness. **(B)** Outline of the study area overlain with the Dominion Land Survey (DLS) grid. The green area gives the location of the arcuate-shaped coal trend. The blue arrows represent zones within this trend characterized by thin (<1 m) or absent coals, interpreted to reflect rivers that likely flowed contemporaneously with coal accumulation. The black arrow indicates the interpreted direction of inundation of the Boreal Sea from the WNW into the Firebag Tributary. A calculated rate of sea-level rise for the Boreal Sea during Lower McMurray time is included (sea level rise: 0.5 – 3 mm a^{-1}).

2.4.2. Processes Impacting Coal-Internal Cyclicity

Internally, coals at the top of the Lower McMurray exhibit wetting-upward, drying-upward and compound (wetting- and drying upward) characters. Drying-upward and compound coals are associated with paleotopographic lows along the SCU, and commonly record highly variable (short-term) rates of base-level change (e.g., 1AA/10-24-093-04W4; Figs. 2.5A and 2.8). Conversely, wetting-upward coals comprise lithotype successions recording continuous base-level shifts and lack obvious internal hiatal surfaces; therefore, they are interpreted to record long-term base-level rise (Fig. 2.12B-1). Wetting-upward coals exhibit up to 4 cycles (Well 1; Fig. 2.8), the lithotype successions of which indicate successively higher rates of base-level rise. Similar wetting-upward cycles in coals have been shown in other successions of Lower Cretaceous strata of the Western Canada Sedimentary Basin, and particularly in the Mannville Grp. These coals

were interpreted to represent paralic rheotrophic mires that formed and evolved in low-accommodation settings and preserved regional base-level rises (e.g., Chalmers et al., 2013; Deschamps et al., 2017; Omodeo-Salé et al., 2017). Increasing rates of base-level rise are typical of late LST / early TST mire accumulation (e.g., Diessel, 2007), and suggest that the coals in the MSB formed during initial southward transgression of the Boreal Sea (Fig. 2.12B). This is further corroborated by the non-hiatal drowning or erosion of mires towards to end of Lower McMurray times (Fig. 2.12D). Nevertheless, it is noted that wetting-upward cycles have also been attributed to long-term climatic change and higher effective precipitation (precipitation over evapo-transpiration) in temperate regions, as well as mire-internal decreasing hydraulic conductivity (Clymo, 1984; Winston, 1994). While 4 consecutive wetting-upward cycles are recorded in Well 1, primary productivity capacity in other mires located further basinward (northward) was likely outpaced by accommodation creation, thereby terminating peat production before the end of Lower McMurray time (e.g., Well 2; Figs. 2.8 and 2.12C-2). However, due to the lack of correlatability between coal-internal wetting-upward cycles, it is also possible that variability in local mire hydraulics produced the differences in the number of wetting-upward cycles encountered.

Drying-upward cycles can preserve the record of decreasing rates of accommodation creation (where paralic mires are rheotrophic; e.g., Wadsworth et al., 2002; Jerrett et al., 2011b) and/or autogenic processes (e.g., water expulsion during auto-compaction, or natural long-term mire development; Clymo, 1984; Winston, 1994). Compound character coals in the Holocene mires of NW Europe have been linked to multiple stages of peat formation in the geologic record (Banerjee et al., 1996; Wadsworth et al., 2002; Chalmers et al., 2013; Davies et al., 2006; Omodeo-Salé et al., 2017), as well as to climate-induced shifts (increasing rainfall) from rheotrophic to ombrotrophic conditions (e.g., Hughes and Barber, 2003). In the MSB, thick drying-upward and compound coal seams (up to >20 m) are developed in local high-accommodation zones in the NW and central portions of the study area; zones that align with paleotopographic lows on the SCU (Fig. 2.12B). Drying-upward and compound coals commonly display lithotype successions indicative of sudden changes in A/PP ratios, as well as coal seam splits with multiple seam-internal TeS coupled with clastic-rich lithotypes (Wells 3 and 4; Fig. 2.8). Coal-seam splits and internal clastic intervals in the coals also coincide with deformation structures in the seams as well as in the Lower McMurray strata underlying

them (e.g., dipping coal seams, Well 4; Fig. 2.8, Fig. 2.12B-3). Together, these observations are interpreted to represent syn-depositional subsidence during coal formation rather than rapid base-level fluctuations. Syn-depositional subsidence and karst collapse have been acknowledged as one of the main drivers of base-level change in both the MSB (Broughton, 2014; Barton et al., 2017), in other coal deposits of the Mannville Grp (Broughton, 1977; Wadsworth et al., 2002, 2003; Chalmers et al., 2013), and in the Carboniferous coal seams of Kentucky (Greb et al., 1999). Drying-upward character coals are interpreted to reflect mires in 'keep up' mode (Diessel et al., 2000), reflecting punctuated but overall high rates of base-level rise (A/PP = >1.18; Fig. 2.12B) associated with syn-depositional subsidence. During phases of active karsting and collapse, the basement underlying the mires subsided, leading to major accommodation space creation (water table rise) and inducing rapid build-up of organic matter in the mires to prevent drowning (drying-upward cycles). Coal seam splitting occurred when mires were incapable of building up organics at a rate sufficient to match or exceed the subsidence rate, possibly resulting from karst collapse in the underlying Devonian carbonates. In contrast to the purely drying-upward coals, thick compound coal seams (e.g., Well 5, Fig. 2.9) show that mire development was driven by both regional base-level changes and phases of active subsidence. In these seams, ARS's are interpreted to reflect the onset of syn-depositional activity when transitioning from wetting- to drying-upward coal characteristics (Well 3; Fig. 2.8), or termination of syn-depositional activity when transitioning from drying- to wetting-upward coal character (e.g., Well 3; Fig. 2.8 or Well 5; Fig. 2.9, Fig. 2.12C). Banerjee et al. (1996) first described the occurrence of transgressive-regressive coal seam splitting in the Mannville Grp of central Alberta during the main TST, as a function of the rate base-level rise exceeding the capacity of the mire to form organic matter (Diessel, 2007). I argue that coal seam splitting (as well as drying-upward and compound coals) in the Firebag Tributary mainly relates to punctuated syn-depositional subsidence or karst collapse and represent deviations from the otherwise continuous wetting-upward character of the coal-seam, rather than to multiple coal formation events or autogenic processes. Additionally, I hypothesize that syn-depositional karsting may have provided preferential conduits for groundwater flow (Fig. 2.12B-2), which created accommodation space for peat accumulation. Highly overthickened (>20 m) coals likely developed in cenote environments (e.g., 98-06W4; Fig. 2.7B), which have been reported in the MSB (Hein and Dolby, 2018). Comparable karst-related Tertiary brown coals are also developed in

Central Europe, where coal seams locally exceed 100 m in thickness on a highly irregular surface (Diessel, 1992).

In contrast to the drying-upward coal seams, the compound coal seams also record thick wetting-upward cycles, interpreted to be characteristic of mires responding to regional (long term) base-level rise. For example, the compound coal seam in Well 5 depicts 2 wetting-upward cycles with a cumulative thickness of 11.5 m that overlie a seam-internal ARS (Fig. 2.9), which is significantly thicker than the approximately 6 m wetting-upward coal seam observed in Well 1 (Fig. 2.8). Uncertainty regarding the north-south distribution trend remains; while this trend likely reflects transgression of the Boreal Sea towards the south, the magnitude of thickness variability likely also reflects local effects associated with syn-depositional basement activity.

2.4.3. Timing and Rate of Sea Level Rise at the End of Lower McMurray Deposition

The duration of coal seam formation is estimated by incorporating average peat accumulation rates and compaction factors. Dependent on the climate zone, peat typically accumulates at a rate of 0.1–6 mm a^{-1} (Bohacs and Suter, 1997; Diessel, 2007). I regard a rate of 1–2 mm a^{-1} to be typical for temperate climates (cf. Diessel, 2007). A compaction factor of 5–10 for sub-bituminous coals is applied (e.g., Ryer and Langer, 1980; Nadon, 1998; Diessel et al., 2000). Using these assumptions, I calculate that full coal seams of wetting-upward coals, in the Firebag Tributary were deposited (excluding depositional hiatuses) over thousands to tens of thousands of years (i.e., on Milankovitch and sub-Milankovitch time scales), as part of a 4^{th} order relative sea level rise. Individual wetting-upward cycles represent 5^{th} order and higher base-level fluctuations (associated to relative sea level and, possibly, climate variability).

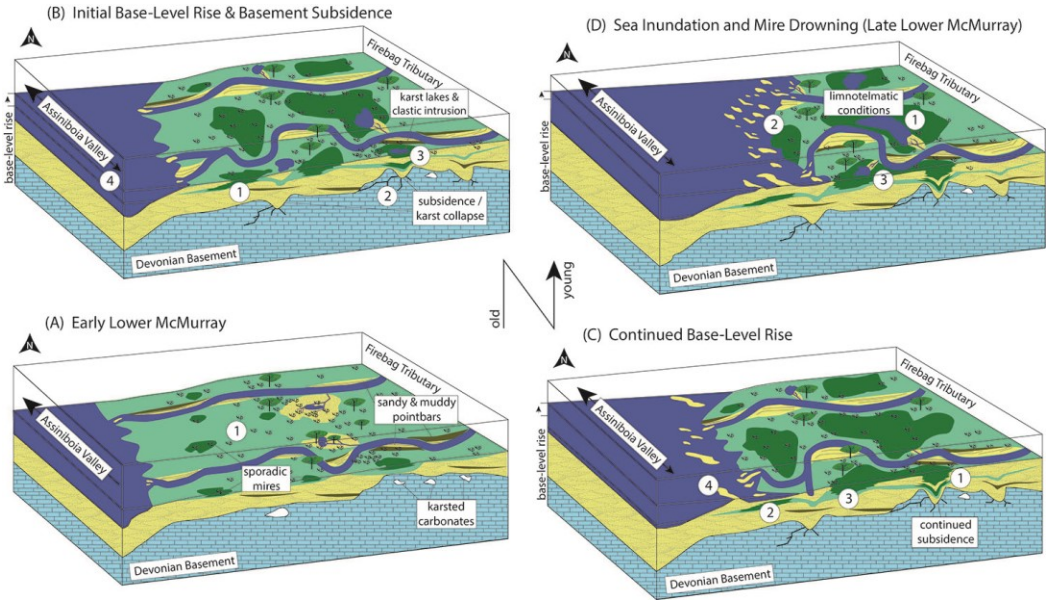

Figure 2.12. Schematic block diagrams depicting four stages of peat accumulation in mires on the coastal plain of the Firebag Tributary. Colors are as follow: mires (in cross-section peat) in dark green, interfluve soils in light green, sands (intra-channel bars, part of pointbars, crevasse splays, mouth bars, tidal bars) in yellow, mud (part of pointbars) in brown. Basement rocks are Devonian carbonates (blue) of the Beaverhill Lake Group.

(A) Coastal plain of the Firebag Tributary during early Lower McMurray times with 2 fluvial channels meandering alongside sporadically distributed mires and through widespread soils (1 indicates interfluve soil formation). The 2 fluvial channels debouche into SE-NW flowing Assiniboia Valley; primary flow direction within Assiniboia Valley is indicated (the large arrow indicates NW directed fluvial discharge). **(B)** Initial base-level rise leads to widespread mires on the coastal plain with a wetting-upward character (1). Locally, tectonic activity in the basement causes non-favorable conditions within mires with A/PP ratios over 1.18. Basement processes create preferential groundwater conduits along fractures (2) and local coal seam splitting where mires drown (3). A second smaller arrow is added to indicate the direction of potential tidal flow-modulation in the Assiniboia Valley due to base-level rise shifting the tidal limit to the SE (4). **(C)** Continued base-level rise produces multiple wetting-upward cycles (3), and fluvial channels are restricted in their ability to meander. Basinward mires may drown before the end of Lower McMurray base-level rise where A/PP ratios exceed 1.5 (2). Accommodation reversal surface may form and mires can produce wetting-upward cycles in areas where syn-depositional tectonic activity has ceased (1). Flooded low-relief areas may allow the formation of tidal bars (4). **(D)** Rate of base-level rise outpaces the capacity of mires to build up organic matter, and widespread mire drowning ensues through clastic inundation (1), limnic conditions, or sea inundation in basinward positions with sulphur-rich coals (2). Fluvial channels are no longer restricted in their flow and locally erode into the accumulated peats (3).

Time frames required to form coals of significant thicknesses, as found in the Firebag Tributary, also give an insight into relative sea level change during Lower McMurray time. I interpret that the wetting-upward coal seam in Well 1 (Fig. 2.8) records a continuous, full archive of relative sea level rise during the Lower McMurray. As no hiatal surfaces were identified within the coal seam, the A/PP ratio remained between 0.5 and

1.5, and base-level rise approximated the rate of peat production (1–2 mm a^{-1}). Lithotype successions in Well 1 exhibit an increase in the rate of base-level rise and reflect a shift from rheotelmatic (A/PP = 0.5-1.0) to limnotelmatic conditions (A/PP = 1.18-1.5) toward the top of the seam. By extension, I hypothesize that the rate of relative sea level rise (rate of sea level rise = rate of peat production * A/PP) during Lower McMurray time increased from approximately 0.5-1 mm a^{-1} at the base to 1.5-3 mm a^{-1} at the top of the seam in Well 1.

2.4.4. Implications of Ash-Derived Aptian Age for the Chronostratigraphy of the Western Canada Sedimentary Basin

The tight cluster of highly precise ages derived from sharply faceted zircons reflects volcanic aeolian deposition of ash (Fig. 2.10) contemporaneous with deposition of the Lower McMurray at 121.39 (± 0.20) Ma. This date is the first absolute age for the McMurray Fm, and places the Lower McMurray firmly in the early Aptian. The onset of magmatic flow in the western Coast Plutonic Complex in southern and central British Columbia, Canada, is known to have occurred after an extensive period of tectonic quiescence (Friedman and Armstrong, 1995; Gehrels et al., 2009), making the Canadian Cordillera a likely source of this volcanic material. As this ash layer is encased by significant thicknesses of coal, I hypothesize that the earliest transgression recorded in coals of the MSB is directly related to tectonic activity in the Canadian Cordillera. Furthermore, this absolute age is also derived from the stratigraphically lowermost unit of Assiniboia Valley in the Western Canada Sedimentary Basin (Fig. 2.3), and therefore provides the earliest onset of relative sea-level rise in the Cretaceous.

2.5. Conclusions

The petrographic character and distribution of coals in the northeastern part of the McMurray Sub-Basin suggests a complex history of base-level rise at the end of Lower McMurray deposition and during initial transgression of the Boreal Sea. Transgression occurred during a 4th order relative sea level rise (Milankovitch-scale), and internal wetting-upward successions represent 5th and higher order cyclicity (sub-Milankovitch scale). Locally, compound and drying-upward character coals represent zones of high accommodation, wherein peat accumulation was influenced by syn-depositional subsidence and karst collapse in underlying Devonian carbonates. Overall, an arc of thick

coals formed on a coastal plain as the Boreal Sea inundated east- to southeast into the Firebag Tributary. The north-south decrease in coal thickness is interpreted to reflect the general southward inundation of the Boreal Sea across the MSB. Exceptionally thick coals (>10 m) likely formed where basement processes (i.e., karsting in Devonian carbonates) provided preferential groundwater pathways and created additional accommodation space.

CA-TIMS dating of 5 sharply faceted zircons collected from a volcanic ash within the coal yield the first absolute age (121.39 ± 0.2 Ma) for the McMurray Fm, and places the Lower McMurray in the early Aptian. This age suggests that initial marine inundation of the MSB was related to tectonic activity in the Canadian Cordillera.

Chapter 3.

Geochronological Subdivision of Marginal Marine Strata based on Combining Detrital Zircon Samples

A version of this chapter has been published as: L. Rinke-Hardekopf, S. E. Dashtgard, C. Huang, H. D. Gibson, 2021: Application of grouped detrital zircon analyses to determine provenance and closely approximate true depositional age: Early Cretaceous McMurray-Clearwater succession, Canada: Geoscience Frontiers, v. 12 (2), p.877-892, doi: 10.1016/j.gsf.2020.11.016.

3.1. Abstract

In the Lower Cretaceous McMurray-Clearwater succession of the intracontinental Alberta Foreland Basin, Canada, detrital zircon U-Pb geochronology samples (referred to herein as DZ samples) have been used to interpret the strata as representing a paleo-continental-scale drainage system. However, the majority of DZ samples are relatively small (n≈90–100), and syndepositional DZ (i.e., crystallization age <5Ma older than depositional age) are rare. This has forced a reliance on dinocysts with long stratigraphic ranges to chronostratigraphically subdivide the McMurray-Clearwater succession rather than employing maximum depositional ages (MDAs) derived from DZ samples. Herein, 43 DZ samples (taken from 20 subsurface cores) are assigned to 1 of 5 stratigraphic intervals, and in each stratigraphic interval all associated DZ samples are combined to produce a grouped DZ sample. Analysis and comparison of individual and grouped DZ samples are used to (1) assess variability in provenance through time and space, and (2) assess the accuracy of chronostratigraphically subdividing the succession using MDAs.

Along the main paleo-drainage axis, a comparison of dissimilarity between DZ samples from the same stratigraphic interval, as well as between stratigraphic intervals, reveals increasing average dissimilarity between individual DZ samples and their respective grouped DZ sample with increasing spatial separation of samples. These data indicate that in the McMurray Depocenter some sediment is sourced from local tributaries, leading to geographical provenance variability.

Calculated MDAs for all 43 DZ samples and grouped MDAs (gMDAs) for the 5 grouped DZ samples are compared to an ash-derived absolute age and existing biostratigraphy. In the McMurray Formation, comparison of MDAs to gMDAs shows that in basins with rare syndepositional DZ, the gMDA method improved depositional age estimates by transforming low-confidence MDAs (e.g., youngest single grains) into high-confidence (multi-grain) gMDAs. In the Clearwater Formation where syndepositional DZ are plentiful (i.e., >5% of the total DZ population), calculating maximum likelihood ages from grouped DZ samples avoids negatively biased (i.e., too young) MDAs. I suggest grouped DZ samples and the gMDA method be used in systems with multiple DZ samples from a well-defined stratigraphic interval as a means of assessing variability in provenance within a depositional system and for improving estimates of depositional ages using DZ.

3.2. Introduction

Detrital zircon (DZ) U-Pb geochronology analysis of clastic sedimentary successions has rapidly evolved into a fundamental analytical technique for resolving questions related to basin evolution (e.g., Ross et al., 2005; Cawood et al., 2012; Gehrels, 2014; Bhattacharya et al., 2016; Quinn et al., 2016; Sickmann et al., 2016; Matthews et al., 2017; Huang et al., 2019; Schwartz et al., 2019), sedimentary provenance (e.g., Moecher and Samson, 2006; Jacobson et al., 2011; Vermeesch, 2013, 2018; Benyon et al., 2014, 2016; Blum and Pecha, 2014; Finzel, 2014; Sharman et al., 2015; Sundell and Saylor, 2017; Coutts et al., 2020) and the timing of sediment deposition (e.g., Dickinson and Gehrels, 2009; Matthews and Guest, 2016; Daniels et al., 2018; Englert et al., 2018; Coutts et al., 2019; Kent et al., 2019; Vermeesch, 2020). Sediment provenance is interpreted from age groupings of zircon in DZ populations, and these age populations are assigned to probable paleo-source regions (Gehrels, 2000; Andersen, 2005). The youngest grains in DZ samples are commonly used to calculate maximum depositional ages (MDAs; e.g., Dickinson and Gehrels, 2009; Spencer et al., 2016; Coutts et al., 2019; Herriott et al., 2019; Sharman and Malkowski, 2020; Vermeesch, 2020).

In the McMurray-Clearwater succession of the intracontinental Alberta Foreland Basin, Canada, multiple studies have employed DZ U-Pb geochronology to interpret the strata as the deposits of a continental-scale drainage system that flowed northward through the McMurray Depocenter and debouched into the Boreal Sea (Fig. 3.1; Benyon et al., 2014, 2016; Blum and Pecha, 2014). These DZ U-Pb geochronology studies, as

well as most others, typically comprise DZ U-Pb geochronology samples (herein referred to as DZ samples) with 50–150 dated grains. Appropriate DZ sample sizes have been a topic of discussion for decades (Dodson et al., 1988; Vermeesch, 2004; Andersen, 2005). Multiple recent studies highlight the importance of high-n (300–1000 grains) DZ samples (Pullen et al., 2014; Englert et al., 2018; Daniels et al., 2018; Coutts et al., 2019; Huang et al., 2019) that allow for accurate and precise characterization of DZ population proportions (i.e., provenance), and enable the identification of accessory (≤5%) and potentially locally derived DZ populations (Andersen, 2005; Pullen et al., 2014).

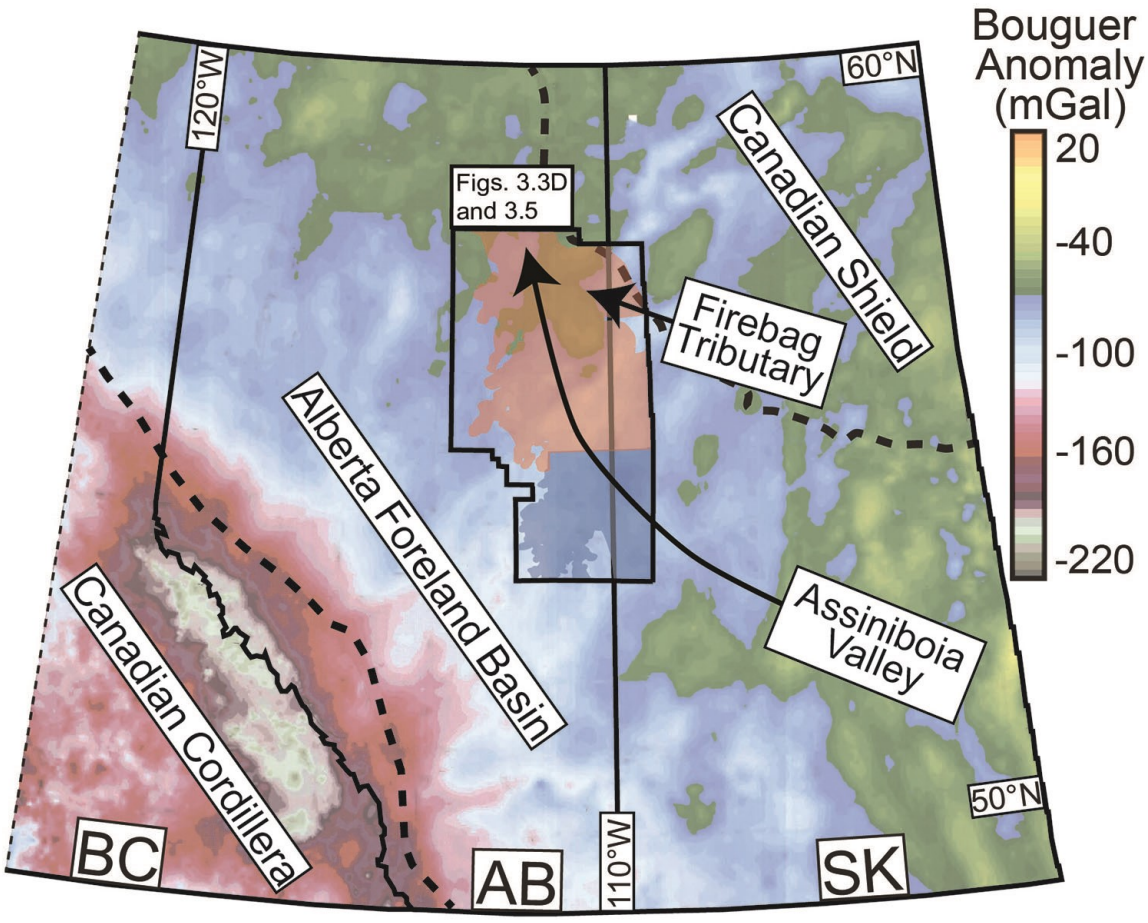

Figure 3.1. Bouguer gravity anomaly map of British Columbia (BC), Alberta (AB), and Saskatchewan (SK), Canada, showing the positions of the Canadian Cordillera, the Alberta Foreland Basin, and the Canadian Shield.

The thick black dashed lines mark the boundaries between them (adapted from Cant and Stockmal, 1989; Ross et al., 1994). Also included is an interpreted drainage direction (black arrow) for the Assiniboia Valley (Christopher, 1997; Horner et al., 2019), and the Firebag Tributary (Rinke-Hardekopf et al., 2019). The study area (black polygon) encompasses most of the McMurray Depocenter and is subdivided into the Athabasca oil sands (red overlay) and Cold Lake oil sands (blue overlay).

In basins rich with syndepositional DZ (i.e., crystallization age <5 Ma older than depositional age), MDAs have been successfully employed to approximate true depositional ages (TDAs) (e.g., Dickinson and Gehrels, 2009; Daniels et al., 2018; Englert et al., 2018; Huang et al., 2019). In the McMurray Depocenter, the absence of an adjacent volcanic arc, as well as obstruction of eastward-flowing rivers from the North American Cordillera resulted in a limited accessory DZ population that is broadly coeval with deposition of the McMurray Formation (Benyon et al., 2016). Calculated MDAs are largely predepositional in these basin settings due to both the significant influx of zircon from older sources and scarcity of syndepositional zircon (Moecher and Samson, 2006; Cawood et al., 2012; Pullen et al., 2014). Consequently, chronostratigraphic subdivision of the McMurray-Clearwater succession continues to be derived from low precision biostratigraphy, rather than DZ MDAs (Hein et al., 2013; Hein and Dolby, 2018). In the McMurray Depocenter, chronostratigraphic subdivision of strata and comprehensive characterization of provenance via DZ analysis requires an approach that provides the advantages of high-n DZ samples in accurately representing provenance and addressing local heterogeneities.

Herein, basin-wide correlations of stratigraphically significant surfaces are used to associate 43 new and previously published DZ samples (from 20 core locations) into 1 of 5 stratigraphic intervals. Individual DZ samples in a stratigraphic interval are combined to generate a high-n “grouped” DZ sample, with one grouped DZ sample per stratigraphic interval. I analyze individual and grouped DZ samples to (1) assess variability in provenance across the basin in time and space using multi-dimensional scaling and DZ population proportion comparison; and, (2) attempt chronostratigraphic subdivision of the succession by calculating MDAs for both individual and grouped DZ samples. Calculated MDAs are compared to igneous zircon from an ash-bed within the McMurray Formation and to established biostratigraphy of the McMurray-Clearwater succession. These comparisons enable us to explore the accuracy of MDAs in the McMurray-Clearwater succession and to assess heterogeneity in sediment provenance within and between intervals. I propose grouped DZ analysis and MDAs derived from grouped DZ samples (gMDAs) as a relatively novel method that should be used in sedimentary strata with multiple DZ samples from a well-defined stratigraphic interval to assess variability in provenance within a depositional system and to improve estimates of depositional ages using DZ.

3.3. Geology and Geochronology of the McMurray and Clearwater Formations

3.3.1. Stratigraphy

The Lower Cretaceous Mannville Group in the McMurray Depocenter, Canada, was deposited during a 3rd order transgression of the Boreal Sea and comprises the McMurray and Clearwater formations (Fig. 3.2A; Hein et al., 2013). Transgression is expressed as a shift from fluvial, to fluvio-tidal, to marginal-marine clastic sedimentary strata upwards through the McMurray Formation, and then marine clastic strata in the Clearwater Formation (e.g., Pemberton et al., 1982; Mossop and Flach, 1983; Ranger and Pemberton, 1997; Hubbard et al., 2011; Timmer et al., 2016; La Croix et al., 2019; Weleschuk and Dashtgard, 2019). Strata of the McMurray Formation range in thickness between ~30 m and ~90 m, and can locally exceed 130 m (Hein et al., 2013). McMurray Formation strata are locally overthickened due to syndepositional salt dissolution in the underlying Devonian Prairie Evaporite Formation (Broughton, 2014; Hauck et al., 2018; Château et al., 2019). Strata of the Clearwater Formation range in thickness between 30 m and 120 m in the Cold Lake region (McCrimmon and Arnott, 2002; Wellner et al., 2018).

The most widely applied (largely allo-)stratigraphic model of the McMurray Formation subdivides it into a series of depositional units that comprise from bottom to top: Lower McMurray, C2, C1, B2, B1, A2 and A1 (Ranger and Pemberton, 1997; Alberta Energy and Utilities Board, 2003; Hein and Cotterill, 2006; Hein et al., 2013; Horner et al., 2018; Château et al., 2019, 2020). While the Lower McMurray is not formally recognized, it is identified in a wide range of studies at the base of the McMurray Formation (e.g., Pemberton et al., 1982; Hein et al., 2006, 2013; Harris et al., 2016; Rinke-Hardekopf et al., 2019). Depositional units are separated by stratigraphically important surfaces and are partially eroded by deeply (~10–70 m) incised channels (Figs. 3.2 and 3.3). Channels have been interpreted as valleys that were cut during forced regression, and were subsequently filled during sea level rise (Fig. 3.2A; Ranger and Pemberton, 1997; Hein and Cotterill, 2006; Hubbard et al., 2011; Labrecque et al., 2011; Hein et al., 2013; Horner et al., 2018). However, both Château et al. (2019, 2020) and Weleschuk and Dashtgard (2019) have recently argued that the valleys are more akin to channels, and at least some channels were contemporaneously with the regionally extensive depositional units.

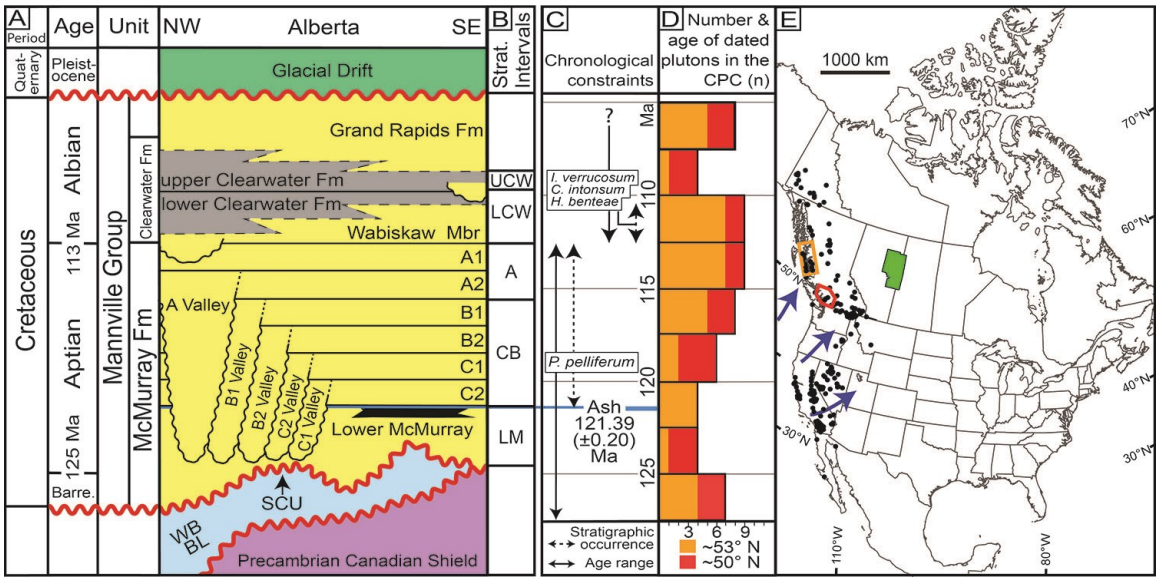

Figure 3.2. Overview of the Lower Cretaceous Mannville Group with focus on location and timing constraints.

(A) Allostratigraphic framework for the Mannville Group in northeastern Alberta, Canada (Château et al., 2020; Hein et al., 2013; Wellner et al., 2018). Clastic sediments (sandstone (yellow), mudstone (grey), coal (black)) unconformably overlie Devonian carbonates of the Woodbend (W.B.) and Beaverhill Lake (B.L.) groups (blue) and metamorphic rocks of the Precambrian Canadian Shield (purple). **(B)** The 5 stratigraphic intervals defined in this study include the Lower McMurray (LM), CB Interval (CB), A Interval (A), lower Clearwater Formation (LCW), and upper Clearwater Formation (UCW). **(C)** Published age constraints for the McMurray and Clearwater Formations include an ash-derived absolute age at the top of the Lower McMurray (blue line, Rinke-Hardekopf et al., 2019), and dinocysts (dashed arrows indicate their distribution in the strata and solid arrows indicate the age ranges of each dinocyst species) (Hein and Dolby, 2018). **(D)** Grouped histogram of dated plutons in the Coast Plutonic Complex (CPC) of the Canadian Cordillera, binned into 2.5 Ma intervals. Plutons in southern British Columbia (red oval in E) are shown in red (~50°N, Friedman and Armstrong, 1995) and those from west-central British Columbia (orange box in E) are shown in orange (~53°N, Gehrels et al., 2009). **(E)** Volcanic and intrusive rocks in Canada and the USA dated between 130 and 97 Ma (black dots; Gastil et al., 1978; Christiansen et al., 1994; Canadian Geochronology Database, 2013; Laskowski et al., 2013). Blue arrows indicate Cretaceous paleo-wind patterns (Elder, 1988; Hay and Floegel, 2012). The study area is defined by the green polygon.

The Lower McMurray comprises mainly terrestrial strata. The unit is situated on the Sub-Cretaceous Unconformity, and occurs along the axis of the main Assiniboia Valley (Fig. 3.3C; e.g., Broughton, 2014; Barton et al., 2017), as well as in the Firebag Tributary (Fig. 3.3A; Rinke-Hardekopf et al., 2019). The top of the Lower McMurray is located at the top of a paleosol and/or coal seam. It is readily identified on well logs via changes in neutron-density porosity or gamma-ray properties between an underlying coal / paleosol and an overlying sandstone and mudstone (Fig. 3.3A).

Individual valleys of the subsequent CB and A intervals are identified as single or multiple, variably-bioturbated and generally muddying-upwards inclined heterolithic strata

with increasing-upwards gamma ray signatures; these are interpreted as fluvio-tidal point-bars (Fig. 3.3B; e.g., Hein and Cotterill, 2006; La Croix et al., 2019; Baniak and Kingsmith, 2018). Valleys are commonly capped by depositional units which consist of single or multiple regressive parasequences with generally sandying upward (decreasing gamma ray) signatures, and depositional units are subdivided by regionally extensive flooding surfaces identified on well logs by their high gamma ray (>100 API) signatures (Fig. 3.3; Château et al., 2019).

The McMurray Formation is transgressively overlain by the Wabiskaw Member of the Clearwater Formation (Figs. 3.2A and 3.3C; Keith et al., 1988). The Clearwater Formation is subdivided into 4 to 13 depositional bodies (McCrimmon and Arnott, 2002; Feldman et al., 2008); however, based on core-, well-log, and 3D seismic data, Wellner et al. (2018) subdivided the Clearwater Formation in the Cold Lake Region into two genetic units that are separated by a regional subaerial unconformity. The lower Clearwater Formation includes the Wabiskaw Member, the base of which is identified by a few metres thick, bioturbated, glauconitic sandstone with an increase upwards in photo-electric log readings from ~2 to ~2.3–2.5 (Fig. 3.3). The glauconitic sandstone is overlain by fluvio-deltaic bioturbated interbedded sand and mudstone of the lower Clearwater Formation (e.g., Ranger and Pemberton, 1997; Hein et al., 2013; Hein and Dolby, 2018; Wellner et al., 2018). These are overlain by stacked channel systems with consistently low gamma ray (<60 API) and high resistivity (>10 Ωm) associated with the upper Clearwater Formation (Fig. 3.3C).

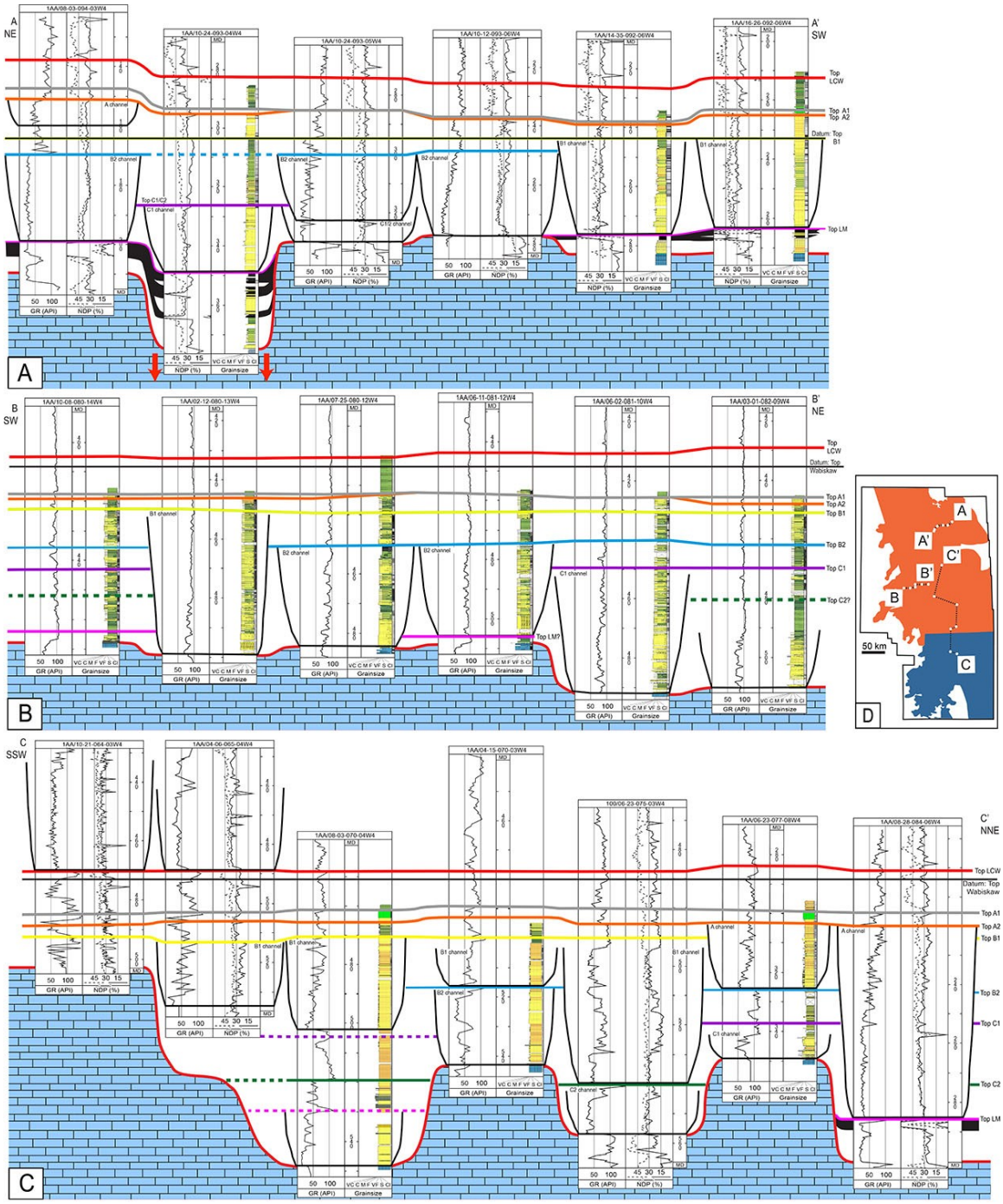

Figure 3.3. **Cross sections of the McMurray and Clearwater formations showing the regional correlation of depositional units, and their associated channels in black (Top LM: magenta; Top C2: dark green; Top C1: dark blue; Top B2: light blue; Top B1: yellow; Top A2: orange; Top A1: grey; lower Clearwater Formation: red; upper Clearwater Formation at top). For each well along the section, a combination of the gamma ray log (GR), neutron-density porosity log (NDP), and core strip-logs (where available) are included.**

(A) Cross-section of the Firebag Tributary in the northeastern extent of the McMurray Sub-Basin. Note the coals (black) at the top of the Lower McMurray Formation (adapted from: Rinke-Hardekopf et al., 2019). Datum is the top of the B1 depositional unit. Syndepositional collapse is indicated by the red arrows. **(B)** Cross-section of the Sparrow Paleovalley in the western extent of the McMurray Depocenter (adapted from: Château et al., 2019). Datum is the top of the Wabiskaw Member of the Clearwater Formation. **(C)** Cross-section showing correlation of the McMurray-Clearwater succession between the Cold Lake and Athabasca Oil Sands regions. The top of the Wabiskaw Member of the Clearwater Formation is used as the datum, and the cross-section is adapted from Wellner et al. (2018) and Horner et al. (2019). **(D)** Locations of cross-sections A–A', B–B', C–C', as well as locations of wells used in the cross sections (white dots).

3.3.2. Chronostratigraphic Constraints

Mannville Group chronostratigraphy is largely based on biostratigraphy, and specifically palynology (Fig. 3.2C). The McMurray Formation is inferred to be Aptian based on a paucity of Neocomian (Berriasian, Valanginian and Hauterivian) flora and the presence of the dinocyst *Pseudoceratium pelliferum* (Hein and Dolby, 2018). The last appearance datum age of *P. pelliferum* in the Boreal Sea is debated, and ranges between the latest Barremian and late Aptian (Stovert et al., 1996; Heimhofer et al., 2007). The onset of deposition of the Wabiskaw Member (lower Clearwater Formation) is interpreted as late Aptian to middle Albian based on the first appearance of 3 dinocysts: *Impagidinium verrucosum*, *Cyclonephelium intonsum*, and *Hapsocysta benteae* (Fig. 3.2C; Hein and Dolby, 2018).

Until recently, *in situ* datable materials (e.g., zircon in ash beds) have not been identified in the McMurray-Clearwater succession likely due to the dominance of fluvial through marginal-marine deposits. Rinke-Hardekopf et al. (2019) documented the first absolute age in the McMurray Formation from an ash bed situated within a coal seam at the top of the Lower McMurray (Fig. 3.2C; chemical abrasion thermal ionization mass spectrometry of 5 zircon, 2σ weighed mean average: 121.39 ± 0.20 Ma). This age provides a precise geochronological constraint for the uppermost depositional units of the McMurray Formation.

The source of the ash at the top of the Lower McMurray is hypothesized to be the Coast Plutonic Complex of southern and central British Columbia, Canada. The Coast Plutonic Complex was volcanically active from the Barremian through the Albian during which time the Sierra Nevada and Idaho batholiths were experiencing magmatic lulls (Figs. 3.2D–E; Elder, 1988; Friedman and Armstrong, 1995; DeCelles, 2004; Decelles et al., 2009; Gehrels et al., 2009; Laskowski et al., 2013). During the Cretaceous,

paleoclimate modelling predicts that westerly wind-patterns (wind from west to east) persisted in the northwestern U.S.A. and southwestern Canada. The paleo-winds are interpreted to have been less consistent and weaker than today due to greenhouse climatic conditions in the Early Cretaceous (Bush, 1997; Hay and Floegel, 2012), but they appear to have been sufficient to transport ash from the Coast Plutonic Complex eastward to the Alberta Foreland Basin.

3.3.3. Provenance

Based on DZ U-Pb geochronology, the McMurray Formation is interpreted as the deposit of a continental-scale drainage system with a myriad of sources across North America, although source areas changed through time (Fig. 3.4; Benyon et al., 2014, 2016; Blum and Pecha, 2014). River systems attributed with depositing the Lower McMurray are hypothesized to have had their headwaters in the Canadian Shield (Benyon et al., 2016). River systems that sourced the overlying McMurray Formation (C2 to A1 depositional units) are hypothesized to have drained either eastern North America, all of North America, or the SW USA (Benyon et al., 2014). Multiple smaller tributaries (Fig. 3.1; e.g., Firebag Tributary, Rinke-Hardekopf et al., 2019) also appear to have drained into that system along the SE to NW main trunk valley of the McMurray Formation (Assiniboia Valley; Christopher, 1997).

In the overlying Clearwater Formation, there is a significant increase in the proportion of syndepositional DZ sourced from the North American Cordillera (Fig. 3.4; Benyon et al., 2014; Blum and Pecha, 2014). This increase is attributed to both drowning of paleo-highlands west of the Assiniboia Valley that acted as a physical barrier to easterly flowing rivers, and to elevated volcanic activity in the Cordilleran arcs of northwestern USA and southwestern Canada (Fig. 3.2C; Decelles et al., 2009; Blum and Pecha, 2014; Horner et al., 2019).

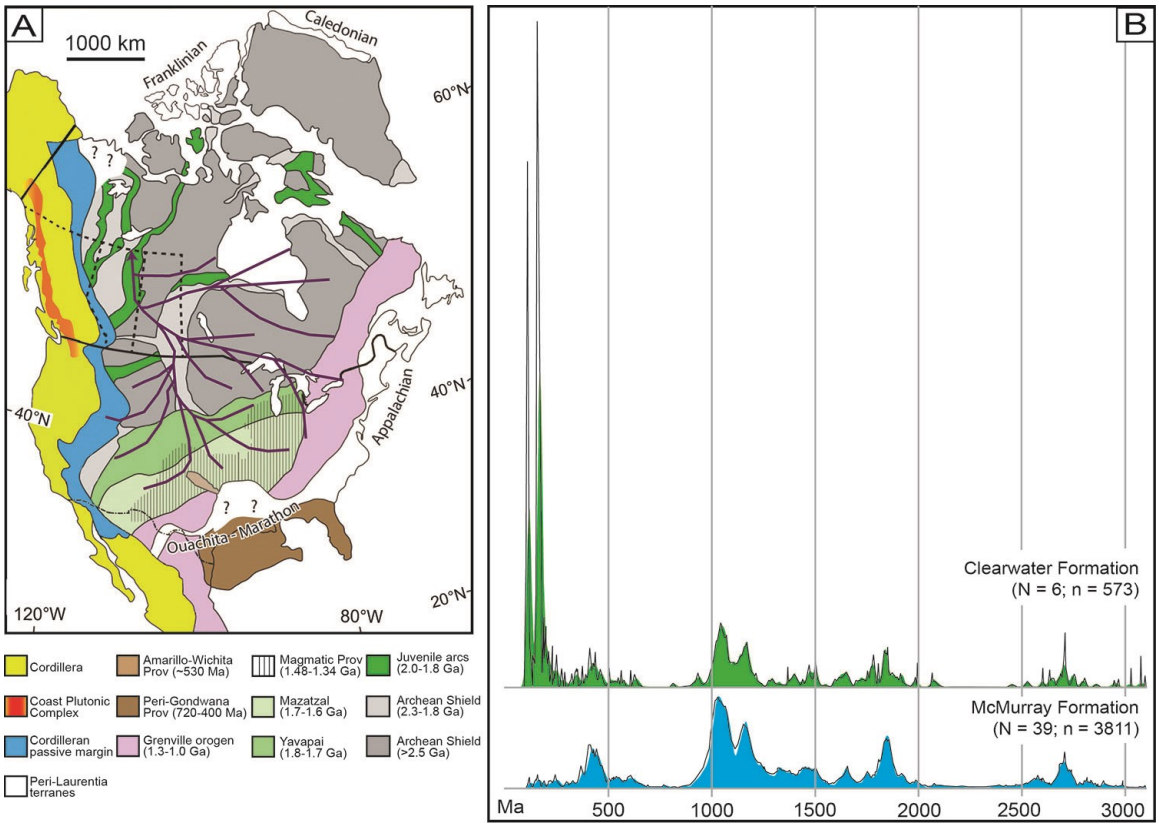

Figure 3.4. Provenance of the McMurray Depocenter interpreted with DZ geochronology

(A) Sediment source regions in North America (adapted from: Monger et al., 1982; Gehrels and Pecha, 2014), and a hypothesized reconstruction of the Early Cretaceous drainage network (solid, thick purple lines) that potentially flowed through the Assiniboia Valley (Blum and Pecha, 2014). **(B)** Normalized kernel density estimates (blue and green shaded areas) and normalized probability density plots (black line) of all DZ samples in the McMurray Formation (N = 39 DZ samples; n = 3811 dated DZ grains) and the Clearwater Formation (N = 6 DZ samples; n = 573 dated DZ grains). Plots were created with detritalPy, and the kernel density estimate plot was created with a fixed 10 Ma bandwidth.

3.3.4. Study Area

The McMurray Depocenter covers over 60,000 km^2. It encompasses the Athabasca and Cold Lake oil sands regions (Fig. 3.5; red and blue, respectively), and ranges from ~53 to 58 °N latitude and ~110 to 113 °W longitutde. Detrital zircon samples analyzed in this study are derived from 20 subsurface core locations in the McMurray Depocenter and each core location is given in both latitude-longitude coordinates and unique well identifiers (Table 3.1; Fig. 3.5).

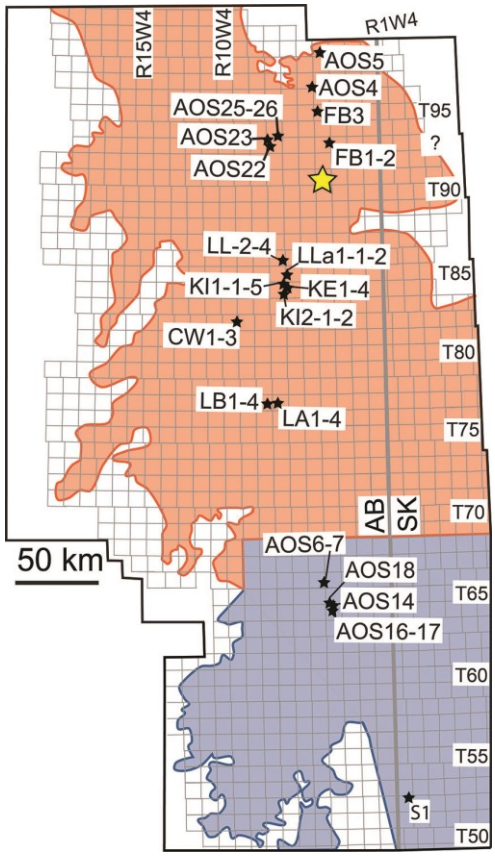

Figure 3.5. Close up of the study area.
The grey grid is the Dominion Land Survery system, which subdivides western Canada into townships: 6 mile (~10 km) by 6 mile blocks. Well locations are marked by black stars and locations are given as unique well identifiers (UWI; Table 3.1). The yellow star marks the core from which an absolute age was determined for the top of the Lower McMurray (Rinke-Hardekopf et al., 2019).

3.4. Data and methods

3.4.1. Determining Stratigraphic Intervals of DZ Samples

Determining the stratigraphic position of DZ samples relies on published core- and well-log interpretations of the McMurray Formation (Château et al., 2019; Rinke-Hardekopf et al., 2019; Weleschuk and Dashtgard, 2019; Horner et al., 2018, 2019; Martin et al., 2019; Château et al., 2020), and of the Clearwater Formation (Fig. 3.3; Wellner et al., 2018). According to GeoScout, the study area contains ~68,750 wells that penetrate the top of the McMurray Formation. Of these, ~380 core logs and ~20,500 well logs have been interpreted in the aforementioned studies, and these datasets are used to determine the stratigraphic positions of DZ samples.

Herein, the McMurray-Clearwater succession is subdivided into 5 intervals (Fig. 3.2B; Table 3.1). These intervals include: (1) the Lower McMurray; (2) the CB Interval, which includes the C2, C1, B2, and B1 depositional units and C2,C1, B2, and B1 valleys; (3) the A Interval, which includes the A2 and A1 depositional units and the A valley; (4) the lower Clearwater Formation; and, (5) the upper Clearwater Formation (Figs. 3.2B and 3.3).

3.4.2. Detrital Zircon Analytical Procedures and Data

Detrital zircon samples used in this study include 4 new DZ samples and 39 literature-derived DZ samples. For each new DZ sample, I collected ~5–10 kg of fine- to medium-grained sandstone. Laser ablation inductively coupled plasma mass spectrometry (LA-ICP-MS), U-Th-Pb dating of DZ samples was conducted at the Centre for Applied Basin Studies, at the University of Calgary, Canada, and the new DZ data are provided in *Supplementary Material A* (along with ablation sequence, reference materials, and data reduction). Detrital zircon grains were ablated using an ASI Resochron™ 193 nm excimer laser ablation system, including a Laurin Technic M-50™ dual volume chamber. Isotope signal intensities are analyzed using an Agilent 7700 quadrupole ICP-MS (Matthews and Guest, 2016). The Geo- and Thermochronology Lab at the University of Calgary used a probability of concordance <1% as a cut-off for each zircon grain. Details regarding the analytical procedures can be found in Matthews and Guest (2016). The four new samples include FB1 (n = 68), FB2 (n= 230) and S1 (n = 262), all of which are derived from the Lower McMurray, and FB3 (n = 75), which is derived from the CB Interval.

The 39 literature-derived DZ samples include 12 DZ samples from Blum and Pecha (2014), 9 DZ samples from Benyon et al. (2014), and 18 DZ samples from Benyon et al. (2016; Table 3.1). All 39 DZ samples were analyzed in the Arizona LaserChron Center (analytical details can be found in: Gehrels et al., 2008). These studies base concordance of grains on the ratio of ($^{206}Pb/^{238}U$)/($^{206}Pb/^{207}Pb$) ages, and in dates older than 500 Ma, grains are discarded at >20% discordance. Younger grains are not discarded due to high uncertainty of the $^{206}Pb/^{207}Pb$ age. While both laboratories from which data was derived follow standard guidelines for U-Pb geochronology (Horstwood et al., 2016), potential bias may have been introduced due to comparison of inter-laboratory data. These uncertainties are generally within the scale of analytical uncertainty (Košler et al., 2013), and are not considered to significantly impact the analysis presented. DZ grains

used for gMDA calculations do not appear biased towards samples analyzed in specific laboratories.

Of the 43 DZ samples, there are 10 samples from the Lower McMurray (grouped n = 1,227), 13 DZ samples from the CB Interval (grouped n = 1,249), 14 samples from the A Interval (grouped n = 1,335), 4 DZ samples from the lower Clearwater Formation (grouped n = 379), and 2 DZ samples from the upper Clearwater Formation (grouped n = 194). I combine all grains from DZ samples within a stratigraphic interval to produce a single grouped DZ sample. For example, the grouped DZ sample for the A Interval contains 14 DZ samples located within the A2 and A1 depositional units and the A Valley, and these samples are derived from subsurface cores along an ~200 km transect of Assiniboia Valley (Table 3.1; Fig. 3.5).

Table 3.1. Sample IDs, locations, unique well identifiers (UWIs), latitude, longitude, sample depths, stratigraphic interval

(LM: Lower McMurray, CB: CB interval, A: A interval, LCW: lower Clearwater Formation, UCW: upper Clearwater Formation), and depositional unit, as well as source for new DZ samples and literature-derived DZ samples (1: Benyon et al. (2016); 2: Benyon et al. (2014); 3: Blum and Pecha (2014)). In the literature source column, sample names in brackets refer to the names of DZ samples in the source literature.

Sample ID	Location	UWI	Lat.	Lon.	Sample depth	Strat. Interval	Dep. Unit	Source
AOS 17	Cold Lake	1AA/12-27-64-4-W4	54.56726	-110.53194	493 – 495m	LM	LM	3
AOS 22	Athabasca	1AA/06-17-93-7W4	57.06681	-111.09502	261.5 – 262.5m	LM	LM	3
AOS 5	Athabasca	1AA/01-09-099-04W4	57.57102	-110.58053	-	pers. comm. M Blum: LM	-	3
AOS 7	Cold Lake	1AA/14-12-065-05W4	54.61657	-110.62612	-	pers. comm. M Blum: LM	-	3
FB1	Athabasca	1AA/10-24-093-04W4	57.08369	-110.49908	344.3 – 346.6m	LM	LM	New
FB2	Athabasca	1AA/10-24-093-04W4	57.08369	-110.49908	358.2 – 361.1m	LM	LM	New
KI1-1	Athabasca	1AB/06-34-084-07W4	56.32269	-111.02364	~313m	LM	LM	2 (Sample 8)
KI2-1	Athabasca	1AA/02-11-084-07W4	56.26144	-110.98824	~355.5m	LM	LM	2 (Sample 1)
LA-1	Athabasca	100/10-20-77-7W4	55.68715	-111.05795	~347m	LM	LM	1
S1	Cold Lake	1AA/13-01-052-27W3	53.46623	-109.86095	580.3 – 578.5m	LM	LM	New

Sample ID	Location	UWI	Lat.	Lon.	Sample depth	Strat. Interval	Dep. Unit	Source
AOS 23	Athabasca	1AA/03-30-093-07W4	57.09200	-111.12295	221-223m	CB	C1/2 Valley	3
CW-1	Athabasca	1AA/13-24-082-10W4	56.12792	-111.43557	~493m	CB	B1 Valley	1
FB3	Athabasca	1AA/10-17-095-04-W4	57.24457	-110.61218	259.2 – 262.3m	CB	B1 Valley	New
KE-1	Athabasca	1AA/08-19-084-06W4	56.29465	-110.93251	~277m	CB	C1/2 Valley	1
KE-2	Athabasca	1AA/08-19-084-06W4	56.29465	-110.93251	~263m	CB	B1 Valley	1
KI1-2	Athabasca	1AB/06-34-084-07W4	56.32269	-111.02364	~293m	CB	C1/2 Valley	2 (Sample 2)
KI1-3	Athabasca	1AB/06-34-084-07W4	56.32269	-111.02364	~271m	CB	B1 Valley	2 (Sample 4)
LA-2	Athabasca	100/10-20-77-7W4	55.68715	-111.05795	~341m	CB	B1 Valley	1
LA-3	Athabasca	100/10-20-77-7W4	55.68715	-111.05795	~336m	CB	B1 Valley	1
LB-1	Athabasca	1AB/08-14-077-08W4	55.66910	-111.12303	~360m	CB	B2 Valley	1
LB-2	Athabasca	1AB/08-14-077-08W4	55.66910	-111.12303	~342m	CB	B2 DU	1
LB-3	Athabasca	1AB/08-14-077-08W4	55.66910	-111.12303	~333m	CB	B1 Valley	1
LLa1-1	Athabasca	1AA/06-18-085-06W4	56.36934	-110.94432	~250m	CB	C1/2 Valley	2 (Sample 5)
AOS 25	Athabasca	1AA/14-03-094-07W4	57.13128	-111.04437	207 – 209m	A	A Valley	3
AOS 26	Athabasca	1AA/14-03-094-07W4	57.13128	-111.04437	223 – 225m	A	A Valley	3
AOS 4	Athabasca	1AA/15-01-097-05W4	57.39391	-110.66677	-	pers. comm. M Blum: A	-	3
CW-2	Athabasca	1AA/13-24-082-10W4	56.12792	-111.43557	~436m	A	A Valley	1
CW-3	Athabasca	1AA/13-24-082-10W4	56.12792	-111.43557	~464m	A	A Valley	1
KE-3	Athabasca	1AA/08-19-084-06W4	56.29465	-110.93251	~244m	A	A Valley	1
KI1-4	Athabasca	1AB/06-34-084-07W4	56.32269	-111.02364	~249.5m	A	A Valley	2 (Sample 7)
KI2-2	Athabasca	1AA/02-11-084-07W4	56.26144	-110.98824	~288m	A	A Valley	2 (Sample 3)
LA-4	Athabasca	100/10-20-077-07W4	55.68715	-111.05795	~326m	A	A Valley	1
LB-4	Athabasca	1AB/08-14-077-08W4	55.66910	-111.12303	~312m	A	A2 DU	1

Sample ID	Location	UWI	Lat.	Lon.	Sample depth	Strat. Interval	Dep. Unit	Source
LL-2	Athabasca	1AA/02-13-086-07W4	56.45157	-110.96308	~220m	A	A Valley	1
LL-3	Athabasca	1AA/02-13-086-07W4	56.45157	-110.96308	~210m	A	A Valley	1
LL-4	Athabasca	1AA/02-13-086-07W4	56.45157	-110.96308	~174m	A	A2 DU	1
LLa1-2	Athabasca	1AA/06-18-085-06W4	56.36934	-110.94432	~191m	A	A Valley	2 (Sample 6)
AOS 6	Cold Lake	1AA/14-12-065-05-W4	54.61657	-110.62612	486-488m	LCW	LCW	3
AOS 14	Cold Lake	1AA/08-33-064-04W4	54.57753	-110.53630	476-479m	LCW	LCW	3
KE-4	Athabasca	1AA/08-19-084-06W4	56.29465	-110.93251	~200m	LCW	LCW	1
KI1-5	Athabasca	1AB/06-34-084-07W4	56.32269	-111.02364	~213m	LCW	LCW	2 (Sample 9)
AOS 16	Cold Lake	1AA/12-27-064-04W4	54.56726	-110.53194	481-483m	UCW	UCW	3
AOS 18	Cold Lake	1AA/09-04-065-04W4	54.59574	-110.53602	459-461m	UCW	UCW	3

3.4.3. Multi-Dimensional Scaling

Multi-dimensional scaling (MDS) plots visualize provenance-variability between DZ samples by utilizing various statistical methods to quantify dissimilarity between these DZ samples (Vermeesch, 2013, 2018a; Sharman et al., 2018; Saylor and Sundell, 2016). Multi-dimensional scaling plots are used herein to analyze the variability of provenance within (1) a single stratigraphic interval, as well as (2) between the 5 stratigraphic intervals of the McMurray-Clearwater succession. Multi-dimensional scaling plots are generated with detritalPy (Sharman et al., 2018) using the Kuiper statistic (V_{max}) to create a dissimilarity metric for MDS, as well as to create Shepard plots to assess goodness of fit. For this study, the Kuiper statistic is preferred over the Kolmogorov-Smirnov statistic because of the proportional heterogeneity in the front and tail-end of DZ distributions encountered between the McMurray and Clearwater formations (Vermeesch, 2018a); the McMurray Formation is dominated by old DZ (>800 Ma) and the Clearwater Formation is dominated by young DZ (<250 Ma; Fig. 3.4B). High Kuiper statistic values reflect samples that are more dissimilar and low Kuiper statistic values indicate that samples are less dissimilar. Shepard plots showcase the relationship between calculated dissimilarities metrics and plotted distances in the resulting MDS plot. An MDS plot with a “good fit” will

exhibit a linear relationship in the Shepard plot, meaning distances displayed on the MDS plot consistently scale to the dissimilarity metric. The outcomes of statistical comparisons (Kolmogorov-Smirnov and Kuiper statistic) and proportions of DZ populations within both individual and grouped DZ samples are provided in *Supplementary Material B*.

3.4.4. DZ Population Proportion Analysis

DetritalPy (Sharman et al., 2018) was also used to calculate the proportion of specific DZ populations within individual and grouped DZ samples. Detrital zircon population age bins reflect the main igneous and metamorphic sources across North America, and these have been interpreted previously as the sources of DZ in the Mannville Group (Fig. 3.4; Benyon et al., 2014, 2016; Blum and Pecha, 2014). Igneous and metamorphic sources include: (1) the North American Cordillera (<250 Ma), (2) the Appalachian Orogen (300–750 Ma) (3) the Grenville Orogen (800–1300 Ma), (4) Mid-continent sources (1300–1500 Ma), (5) Yavapai-Mazatzal sources (1600–1800 Ma), (6) the Trans-Hudson Province (1800–2000 Ma), and (7) the Superior and Wyoming Provinces of the Canadian Shield (>2.5 Ga; Table 3.2). I calculate the average proportions of DZ derived from these 7 source regions in each grouped DZ sample. I also calculate a standard deviation of the proportion of a particular source amongst all non-grouped DZ samples of a stratigraphic interval, and the average proportion of DZ from those sources in the grouped DZ sample for the same stratigraphic interval. Lastly, I note the maximum and minimum DZ population proportions in individual DZ samples per stratigraphic interval (Table 3.2).

3.4.5. Maximum Depositional Age (MDA) and Grouped MDA (gMDA) Calculations

The youngest dated DZ grains in a DZ sample are commonly used to interpret the MDA, and numerous calculation methods exist to obtain MDAs (e.g., Ludwig and Mundil, 2002; Barbeau et al., 2009; Dickinson and Gehrels, 2009; Ludwig, 2012; Chen et al., 2016; Zhang et al., 2016; Ross et al., 2017; Coutts et al., 2019; Johnstone et al., 2019; Herriott et al., 2019; Copeland, 2020; Sharman and Malkowski, 2020; Vermeesch, 2020). Previous authors have used (1) the youngest single grain (e.g., Dickinson and Gehrels, 2009), (2) statistical methods (e.g., Johnstone et al., 2019; Vermeesch, 2020), and/or most frequently (3) calculated weighted means derived from a subset of the youngest DZ whose

ages overlap within uncertainty (e.g., Dickinson and Gehrels, 2009). These various methodologies have drawbacks and advantages (see Coutts et al., 2019, for a thorough review). While youngest single grains may be affected by lead loss or matrix effects (Spencer et al., 2016; Herriott et al., 2019), Coutts et al. (2019) showcased both negative and positive bias in all MDA calculation methods given increasing DZ sample size. Vermeesch (2020) argues that it is theoretically impossible for any of these methods to converge at a correct solution with increasing DZ sample size, and hence, proposed the "maximum likelihood age" as a statistically sound approach to address these biases based on maximum likelihood estimates originally developed for fission track thermochronology (Galbraith and Laslett, 1993; Galbraith, 2005). This method fits a Gaussian curve over the youngest zircon population, the center of which provides the best depositional age.

In this study, I calculate MDAs using: (1) youngest single grain (YSG); (2) the weighted mean of the youngest cluster of 2 or more grains whose uncertainties overlap at 1σ (YGC1σ); (3) the youngest cluster of 3 or more grains whose uncertainties overlap at 2σ (YGC2σ) (Dickinson and Gehrels, 2009); (4) the weighted mean average of the youngest 3 grains (Y3Zo) within 2σ uncertainty (Ross et al., 2017; Huang et al., 2019); and (5) the maximum likelihood age algorithm (MLA; Vermeesch, 2020). These 5 methods are chosen as they include the most widely applied MDA calculation methodologies (YSG, YGC1σ, YGC2σ), methods shown to be reasonably accurate (e.g., Y3Zo; Ross et al., 2017; Coutts et al., 2019), and the newly proposed MLA approach (Vermeesch, 2020; to avoid confusion the MLA approach is herein treated as an equivalent calculation method to derive an MDA or a gMDA). As all dates used in the MDA calculations are Mesozoic, only the $^{206}Pb/^{238}U$ dates are used (Spencer et al., 2016); MLA utilizes the $^{238}U/^{206}Pb$ and the $^{207}Pb/^{206}Pb$ ratios. I calculate MDAs for all individual DZ samples (MDAs) and grouped MDAs (gMDAs) for grouped DZ samples. MDAs and gMDAs for all methods are calculated with Isoplot 4.15 and IsoplotR (Ludwig, 2012; Vermeesch, 2018b). DZ grains are used with their respective 2σ errors (including analytical and systematic uncertainty); MLA uses the errors of the aforementioned ratios. MDAs and gMDAs are only included where Isoplot 4.15 calculates a probability of fit that is ≥0.05 for weighted means. All calculated MDAs and gMDAs can be found in *Supplementary Material C.*

The ability of MDAs and gMDAs to approximate TDAs is tested by comparing these values to the ID-TIMS zircon age at the top of the Lower McMurray and to biostratigraphic designations; each calculated age is defined as either "syndepositional" or

“predepositional”. The gMDAs and MDAs from the Lower McMurray are classified as syndepositional if they are between the ash age (121.39 Ma ± 0.20 Ma; Rinke-Hardekopf et al., 2019) at the top of the Lower McMurray, and the Barremian (129.4 Ma), which is the palynologically defined lower limit of the Lower McMurray (Heimhofer et al., 2007; Hein and Dolby, 2018). For McMurray Formation strata overlying the Lower McMurray (CB Interval and A Interval), syndepositional ages are those between the ash age (lower limit) and the end of the Aptian (113 Ma; upper limit), the latter of which is the palynologically defined end of the McMurray Formation deposition. In the Clearwater Formation, ages are classified as syndepositional if they are Albian or younger (Fig. 3.2C, Hein and Dolby, 2018).

3.5. Results

3.5.1. Grouped and Individual DZ Samples

The 10 DZ samples in the Lower McMurray are distributed along a depositional transect (straight line between the 2 most distal DZ sample locations) of 459 km (Fig. 3.6A). In the MDS plot of DZ samples from the Lower McMurray, populations are distributed evenly around the grouped sample with a mean Kuiper statistic of 0.25 (max: 0.38, min: 0.15, standard deviation: 0.08) between individual DZ samples and the grouped DZ sample (Fig. 3.7A). The linear relation expressed in the Shepard plot for the Lower McMurray indicates a good fit (i.e., distances plotted in the MDS plot adequately reflect calculated dissimilarity metrics; Fig. 3.7B). In the Lower McMurray, DZ population proportion variability is largely observed in DZ populations derived from the Grenville Orogen (g-avg: 40%, max: 59%, min: 18%, stdev: 13%), the Trans-Hudson region (g-avg: 14%, max: 40%, min: 3%, stdev: 14%), and the Appalachian Orogen (g-avg: 13%, max: 28%, min: 4%, stdev: 8%; Fig. 3.6B, Table 3.2)

The 13 DZ samples in the CB Interval are distributed along a depositional transect of 178 km (Fig. 3.6C). In the respective MDS plot, DZ samples are also evenly distributed around the grouped DZ sample (with exception of FB3) with a mean Kuiper statistic of 0.17 (max Kuiper statistic: 0.54, min Kuiper statistic: 0.10, standard deviation: 0.12) between individual DZ samples and the grouped DZ sample (Fig. 3.7C). However, the Shepard plot for the CB interval does not show a linear relation, and by extension is a poor fit (Fig. 3.7D). In the CB Interval, DZ population proportion variability is largely observed

in DZ populations derived from the Grenville Orogen (g-avg: 46%, max: 62%, min: 23%, stdev: 10%), the Trans-Hudson region (g-avg: 9%, max: 37%, min: 2%, stdev: 9%), and the Canadian Shield (g-avg: 12%, max: 36%, min: 4%, stdev: 9%; Fig. 3.6D, Table 3.2).

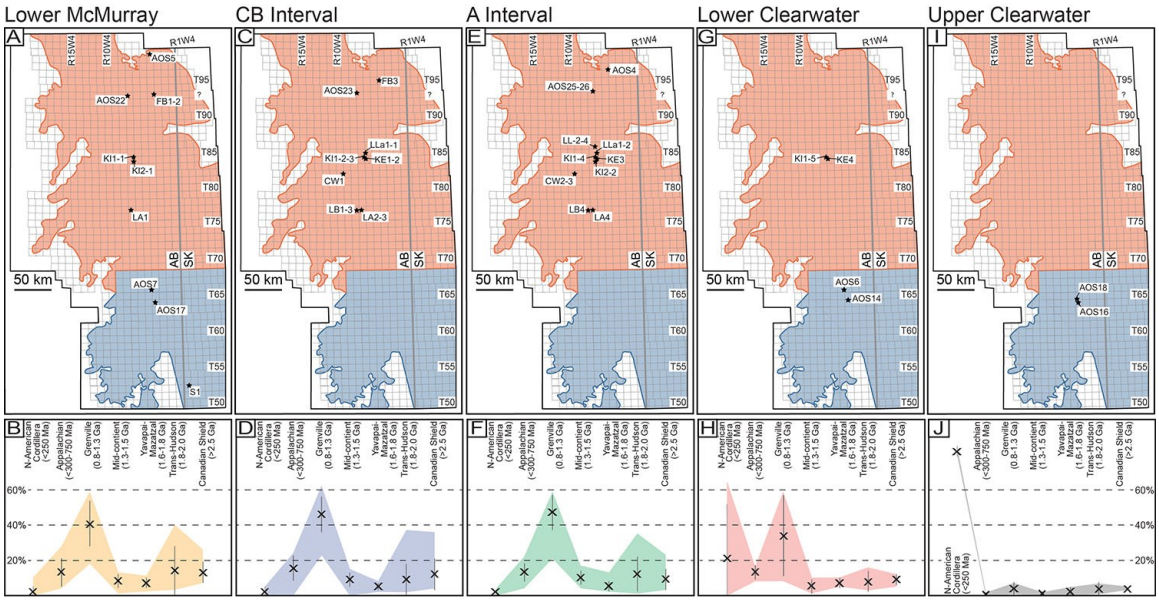

Figure 3.6. DZ samples in the 5 stratigraphic intervals.
(A, C, E, G, I) Distribution of wells (black stars) from which DZ samples are derived for each of the 5 stratigraphic intervals. **(B, D, F, H, J)** Plots highlighting the proportions of DZ populations in each stratigraphic interval that were derived from various North American source terranes defined in Blum and Pecha (2014) and Benyon et al. (2014, 2016). The X's in each column of each plot mark the proportion of DZ age populations in the grouped DZ samples, and the grey bars give the standard deviation of that population across all individual DZ samples (g-avg, stdev; Table 3.2). Shaded areas demarcate the range in proportions of age clusters in individual DZ population in each stratigraphic interval (max and min, Table 3.2). All data displayed in this figure is available in *Supplementary Material C*.

The 14 DZ samples from the A Interval are distributed along a depositional transect of 194 km (Fig. 3.6E). DZ samples are evenly distributed around the grouped DZ sample (except for AOS4) with a mean Kuiper statistic of 0.20 (max Kuiper statistic: 0.44 (AOS4), min Kuiper statistic: 0.10, standard deviation: 0.08) between individual DZ samples and the respective grouped DZ sample (Fig. 3.7E). The linear relation expressed in the Shepard plot for the A Interval indicates a good fit (Fig. 3.7F). In the A Interval, DZ population proportion variability is largely observed in DZ populations derived from the Grenville Orogen (g-avg: 47%, max: 59%, min: 21%, stdev: 10%) and the Trans-Hudson region (g-avg: 12%, max: 35%, min: 1%, stdev: 10%; Fig. 3.6F, Table 3.2).

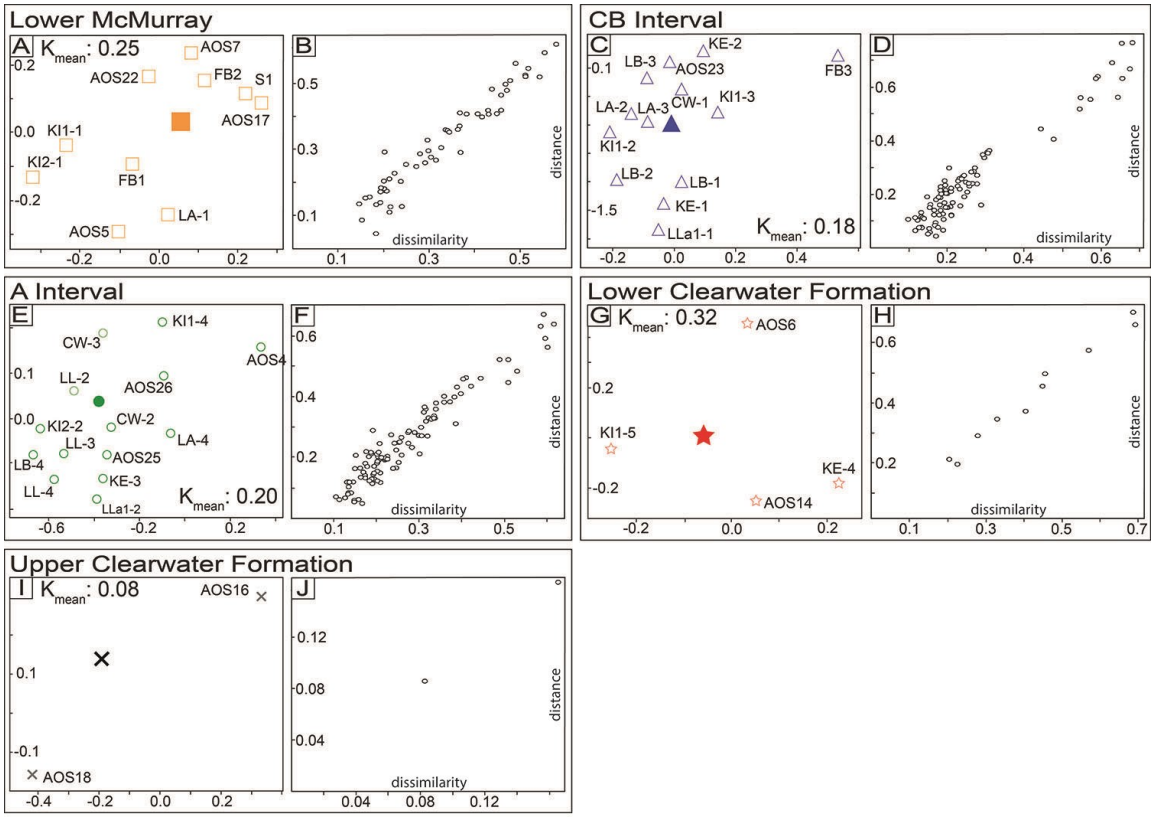

Figure 3.7. MDS plots for the 5 stratigraphic intervals.
(A, C, E, G, I) Metric Kuiper's statistic MDS plot highlighting dissimilarities of individual DZ samples (open symbols) to the grouped DZ sample (filled symbols) in each stratigraphic interval. Also indicated is the mean Kuiper statistic (K_{mean}) between individual DZ samples and the grouped DZ sample. **(B, D, F, H, J)** Shepard plots for A, C, E, G, and I, which highlight the relation between respective Kuiper V_{max} dissimilarity tables (*Supplementary Materials B*) and plotted distances in the MDS plots. A "good fit" of the MDS plot will result in a linear relation between distance and dissimilarity metric, as dissimilarity is an adequately represented by distance in the respective MDS plot.

The 4 DZ samples in the lower Clearwater Formation are distributed along a depositional transect of 191 km (Fig. 3.6G). DZ samples are distributed around the grouped DZ sample in the MDS plot with a mean Kuiper statistic of 0.32 (Fig. 3.7G). The linear relation expressed in the Shepard plot for the lower Clearwater Formation indicates a good fit (Fig. 3.7H). In the lower Clearwater Formation, DZ population proportion variability is largely observed in DZ populations derived from the Cordillera (g-avg: 21%, max: 65%, min: 0%, stdev: 31%), and the Grenville Orogen (g-avg: 34%, max: 59%, min: 8%, stdev: 23%; Fig. 3.6H, Table 3.2).

Table 3.2. Average proportions that DZ populations (given with their respective age range) constitute in the grouped DZ sample (g-avg) of each stratigraphic interval (LM: Lower McMurray, CB: CB interval, A: A interval, LCW: lower Clearwater Formation, UCW: upper Clearwater Formation).

I also give the standard deviation (stdev) of DZ populations from individual DZ samples to the average in the grouped DZ sample. Lastly, I add the maximum (max) and minimum (min) proportions that DZ populations constitute in all individual DZ samples for a stratigraphic interval. Detailed data can be found in *Supplementary Material B.*

		Cordillera <250 Ma	Appalachian 300-750 Ma	Grenville 800-1300 Ma	Mid-Continent 1300-1500 Ma	Yavapai-Mazatzal 1600-1800 Ma	Trans-Hudson 1800-2000 Ma	Canadian Shield >2500 Ma
LM	g-avg	2%	13%	40%	8%	7%	14%	13%
	stdev	3%	8%	13%	4%	3%	14%	6%
	max	10%	28%	59%	13%	11%	40%	26%
	min	0%	4%	18%	1%	2%	3%	7%
CB	g-avg	2%	15%	46%	9%	5%	9%	12%
	stdev	1%	7%	10%	4%	2%	9%	9%
	max	5%	24%	62%	15%	8%	37%	36%
	min	0%	0%	23%	0%	2%	2%	4%
A	g-avg	2%	13%	47%	10%	5%	12%	9%
	stdev	1%	5%	10%	4%	3%	10%	6%
	max	4%	22%	59%	17%	13%	35%	23%
	min	0%	4%	21%	4%	2%	1%	3%
LCW	g-avg	21%	13%	34%	5%	7%	8%	9%
	stdev	31%	4%	23%	4%	3%	6%	3%
	max	65%	16%	59%	10%	10%	16%	12%
	min	0%	8%	8%	1%	5%	3%	5%
UCW	g-avg	82%	1%	4%	1%	2%	4%	4%
	stdev	n/a	n/a	n/a	n/a	n/a	n/a	n/a
	max	84%	1%	7%	2%	5%	7%	5%
	min	80%	1%	1%	0%	0%	1%	4%

The 2 DZ samples in the upper Clearwater Formation are located at a distance of only 3 km from one another (Fig. 3.6I). The linear relation expressed in the Shepard plot for the upper Clearwater Formation indicates a good fit (Fig. 3.7I); lack of individual samples must however be taken into account. In contrast to the lower Clearwater Formation, the 2 DZ samples are very similar (mean Kuiper statistic: 0.08) and display no notable variability in the DZ population proportion analysis (Fig. 3.6J).

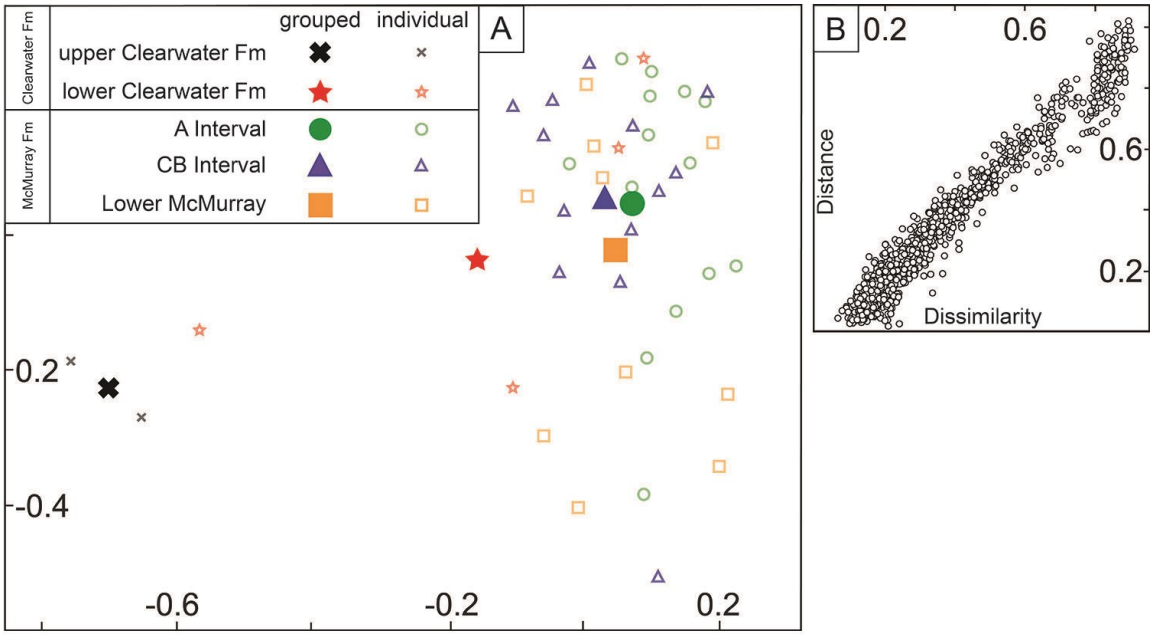

Figure 3.8. MDS plot including all individual and grouped DZ samples.
(A) Metric Kuiper's statistic MDS plot highlighting the dissimilarities between all grouped DZ samples for stratigraphic intervals (full circles), as well as all individual DZ samples (open circles) that they comprise (LM: Lower McMurray, CB: CB interval, A: A interval, LCW: lower Clearwater Formation, UCW: upper Clearwater Formation). **(B)** Shepard plot highlighting the relation between plotted distances in (A) and dissimilarities (data available for download in *Supplementary Materials B*).

In the MDS plot of all DZ samples from all stratigraphic intervals of the McMurray Formation, individual DZ samples overlap regardless of their stratigraphic interval. The Shepard plot for these data exhibits a clear linear relation between plotted distance and calculated Kuiper statistic, indicating a good fit (Fig. 3.8B). Grouped DZ samples of the McMurray Formation are very similar; they have Kuiper statistics of 0.07–0.09 (Fig. 3.8) and show little variability in DZ population proportions (Table 3.2, Fig. 3.6). The grouped DZ sample of the lower Clearwater Formation is located between the grouped DZ samples of the McMurray Formation and the upper Clearwater Formation. Dissimilarity between the grouped DZ sample of the lower Clearwater Formation and the McMurray Formation (mean Kuiper statistic: 0.22) is significantly lower than to the upper Clearwater Formation (mean Kuiper statistic: 0.63). Dissimilarity between Clearwater Formation DZ samples and McMurray Formation DZ samples is associated with a stepwise increase in the youngest, Cordilleran-derived DZ population from 2% in the McMurray Formation to 21% in lower Clearwater Formation, and 82% in the upper Clearwater Formation (Table 3.2). This is accompanied by a stepwise decrease in all older DZ populations. In particular, Grenville

Orogen derived DZ grains decrease from ~45% in the McMurray Formation, to 34% in the lower Clearwater Formation, and to 4% in the upper Clearwater Formation (Table 3.2).

3.5.2. MDA and gMDAs

Of the 1,227 DZ ages from the Lower McMurray, 4 grains (0.33% of 1,227 DZ) are syndepositional within 2σ uncertainty (Fig. 3.9A). MDAs calculated from individual DZ samples of the Lower McMurray yield 3 syndepositional MDAs using YSG (FB1, FB2, AOS7), 3 syndepositional MDAs using MLA (FB1, FB2, AOS7; note: the MLA algorithm reverts to YSG when only 1 syndepositional grain is available), and only 1 syndepositional MDA using multi-grain methods (FB2, YGC1σ/MLA: 121.8 ± 2.4 Ma, 2 grains; Fig. 3.9A). The gMDAs derived from the grouped DZ sample that includes all samples from the Lower McMurray yield a syndepositional depositional age of 121.9 ± 2.6 Ma using the YGC1σ and Y3Zo methods (based on 3 grains), and 123.5 ± 1.9 Ma / 123.5 ± 2.2 Ma when employing the MLA and YGC2σ methods (4 grains; Fig. 3.9B, C).

In the CB Interval, only 3 grains (0.24% of 1,249 DZ) are syndepositional within 2σ uncertainty and these grains are in the samples AOS23, KE-1, and LLa1-1 (Fig. 93.A); the youngest YSG MDA belongs to KE-1 (117.6 ± 17.6 Ma). Multi-grain MDA calculations for individual DZ samples all return predepositional ages, with the youngest grain cluster (YGC1σ) MDA for all samples in the CB interval being 155.6 ± 7.1 Ma (LB-1, 2 grains; Fig. 3.9A). The gMDAs calculated for the grouped DZ sample for the CB interval yield syndepositional ages of 124.9 ± 3.5 Ma (MLA), and 126.4 ± 4.8 Ma (YGC1σ, Y3Zo, YGC2σ; Fig. 3.9C).

Of the 1,335 DZ in the A interval, 6 grains (0.45%) are syndepositional within 2σ uncertainty, and MDA calculations produce 7 syndepositional MDAs derived from 4 individual samples (AOS 4, KI1-4, KI2-2, LB-4, Fig. 3.9A); the youngest YSG age is found in sample KI1-4 (116.2 ± 4.5 Ma). Calculated multi-grain MDAs for individual samples (YGC1σ/Y3Zo/YGC2σ; result from MLA is similar) produce only one syndepositional MDA within 2σ uncertainty (AOS4: 123.6 ± 5.8 Ma); however, this age is older than the ash at the top of the Lower McMurray (121.39 Ma ± 0.20). In contrast, gMDAs for the A interval yield ages of 116.8 ± 4.2 Ma (YGC1σ; 2 grains), 118.6 ± 1.7 Ma (MLA), 118.8 ± 3.5 Ma (Y3Zo, 3 grains), and 119.2 ± 3.4 Ma (YGC2σ, 5 grains; Figs. 3.7B-C).

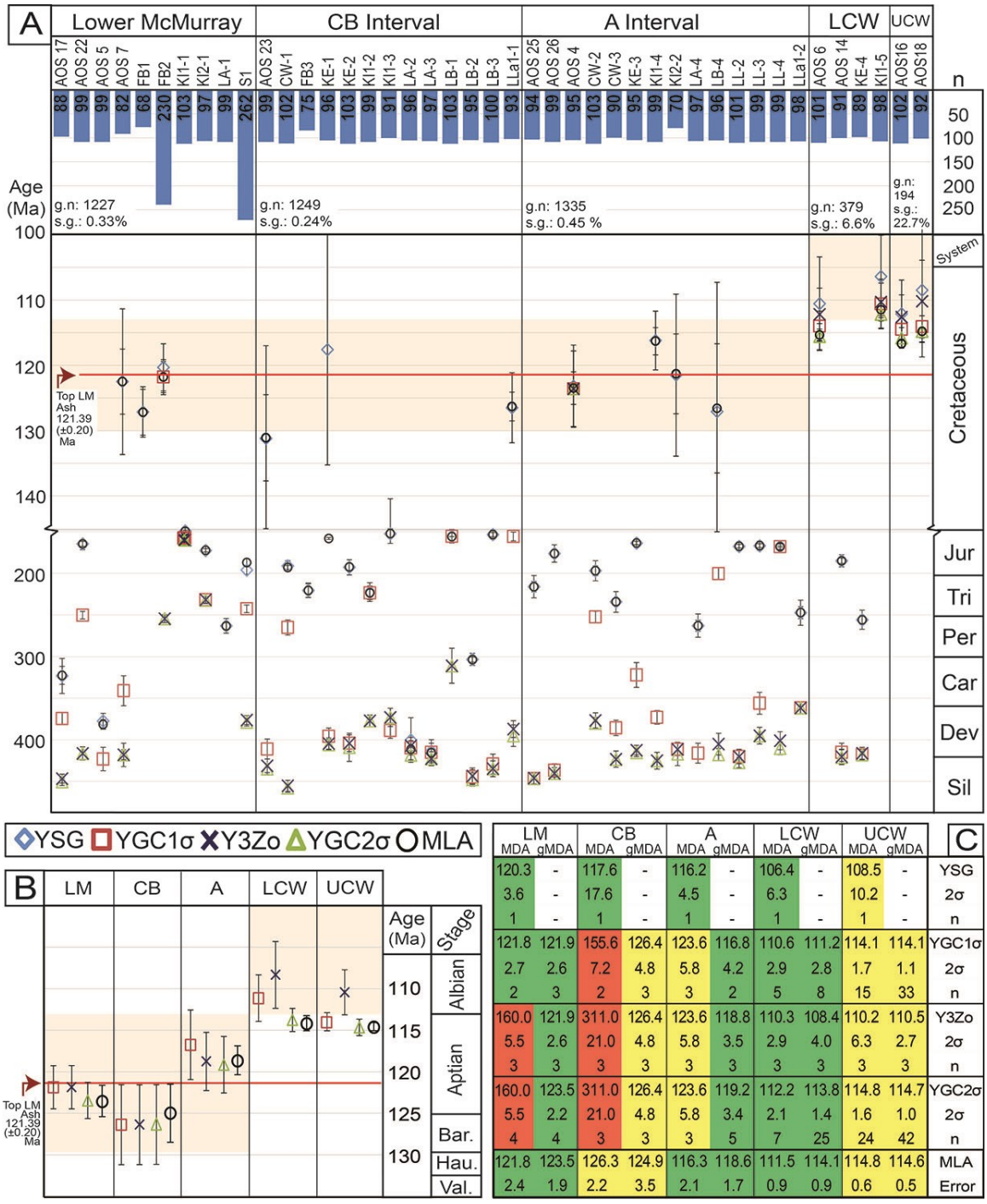

	LM MDA	LM gMDA	CB MDA	CB gMDA	A MDA	A gMDA	LCW MDA	LCW gMDA	UCW MDA	UCW gMDA	C
	120.3	-	117.6	-	116.2	-	106.4	-	108.5	-	YSG
	3.6	-	17.6	-	4.5	-	6.3	-	10.2	-	2σ
	1	-	1	-	1	-	1	-	1	-	n
	121.8	121.9	155.6	126.4	123.6	116.8	110.6	111.2	114.1	114.1	YGC1σ
	2.7	2.6	7.2	4.8	5.8	4.2	2.9	2.8	1.7	1.1	2σ
	2	3	2	3	3	2	5	8	15	33	n
	160.0	121.9	311.0	126.4	123.6	118.8	110.3	108.4	110.2	110.5	Y3Zo
	5.5	2.6	21.0	4.8	5.8	3.5	2.9	4.0	6.3	2.7	2σ
	3	3	3	3	3	3	3	3	3	3	n
	160.0	123.5	311.0	126.4	123.6	119.2	112.2	113.8	114.8	114.7	YGC2σ
	5.5	2.2	21.0	4.8	5.8	3.4	2.1	1.4	1.6	1.0	2σ
	4	4	3	3	3	5	7	25	24	42	n
	121.8	123.5	126.3	124.9	116.3	118.6	111.5	114.1	114.8	114.6	MLA
	2.4	1.9	2.2	3.5	2.1	1.7	0.9	0.9	0.6	0.5	Error

Figure 3.9. MDA calculation for individual and grouped DZ samples in the McMurray and Clearwater formations.

(A) Calculated MDAs using YSG, YGC1σ, Y3Zo, YGC2σ, MLA methods. Sample name (row 2) and number of zircon (blue bars and number in bold, row 3) are shown for each sample. Samples are grouped by stratigraphic intervals (row 1). Row 3 also includes the total (grouped) number of concordant zircon ages per interval (g.n) and the percentage of syndepositional grains (s. g.). The age of the ash at the top of the Lower McMurray (red line, thickness includes to age uncertainty), and biostratigraphic constraints (orange shaded areas) (Fig. 3.2) are depicted. The symbol legend for MDAs is shown below. The Y-axis contains both numerical age (Ma) and chronostratigraphic

systems (Jur: Jurassic, Tri: Triassic, Per: Permian, Car: Carboniferous, Dev: Devonian, Sil: Silurian); note the scale change at the Cretaceous-Jurassic boundary. **(B)** Calculated gMDAs for each stratigraphic interval (LM: Lower McMurray, CB: CB interval, A: A interval, LCW: lower Clearwater Formation, UCW: upper Clearwater Formation) using multi-grain MDA techniques. (Acronyms: Bar.: Barremian, 129.4-125 Ma; Hau.: Hauterivian 132.9-129.4 Ma; Val.: Valaginian 139.8–132.9 Ma). **(C)** Table of the youngest calculated depositional ages for each stratigraphic interval using the 5 MDA calculation techniques, for both individual DZ samples (MDAs) and all DZ in an interval (gMDAs). Highlighting is added to compare MDAs and gMDAs relative to the ash-derived absolute age, as well as biostratigraphic age constraints. Green highlighting indicates a syndepositional MDA or gMDA, yellow indicates the MDA or gMDA is syndepositional within its 2σ uncertainty and red indicates a MDA or gMDA that is predepositional. All MDAs and gMDAs for individual samples and stratigraphic intervals are provided in *Supplementary Material B*.

Of the 379 DZ in the lower Clearwater Formation, 25 grains (6.6%) are syndepositional within 2σ uncertainty, and both MDAs and gMDAs return syndepositional ages using multi-grain MDA calculation techniques. Ten syndepositional MDAs are calculated, with all 10 coming from 2 DZ samples (AOS 6, KI1-5). For individual DZ samples, the youngest grain cluster (Y3Zo) of all samples in the lower Clearwater Formation is 110.3 ± 2.9 Ma (KI1-5, 3 grains; Fig. 3.9A); the MLA of sample KI1-5 yields an age of 111.5 ± 0.9 Ma. The gMDAs for the lower Clearwater Formation yield ages of 111.2 ± 2.8 Ma (YGC1σ, 8 grains), 108.4 ± 4.0 Ma (Y3Zo, 3 grains), 113.8 ± 1.4 Ma (YGC2σ, 25 grains), and 114.1 ± 0.9 Ma (MLA) respectively (Figs. 3.7C-B).

Of the 194 DZ in the upper Clearwater Formation, 44 grains (22.7%) are syndepositional within 2σ uncertainty. For individual DZ samples, the Y3Zo MDA yields an age of 110.2 ± 6.3 Ma (AOS 18, 3 grains; Figs. 7A, C); the MLA of sample AOS 18 yields an age of 114.8 ± 0.6 Ma. The gMDAs for the upper Clearwater Formation yield ages of 114.1 ± 0.9 Ma (MLA) / 114.1 ± 1.1 Ma (YGC1σ, 33 grains), 110.5 ± 2.7 Ma (Y3Zo, 3 grains) and 114.7 ± 1.0 Ma (YGC2σ, 42 grains; Fig. 3.9C).

3.6. Discussion

3.6.1. Mitigating Provenance Variability with Grouped DZ Samples

Combining individual DZ samples into a grouped DZ sample for a well-defined stratigraphic interval not only enables conversion of moderate-n DZ samples (n ≈ 100) into high-n DZ samples (n ≈ 400 – 1300), but it also enables us to investigate provenance variability in time and space. Individual DZ samples derived from individual stratigraphic intervals of the McMurray Formation exhibit significant variability in the DZ population

composition. I relate these findings to (1) DZ sample size and to (2) the geographical distribution of DZ samples within a stratigraphic interval.

First, while individual DZ population proportions in DZ samples of the Lower McMurray exhibit major variability (up to ~41%; Fig. 3.6B; Table 3.2), individual DZ samples with the most grains (i.e., S1: n = 261, Kuiper statistic = 0.20, and FB2: n = 230, Kuiper statistic = 0.15; Fig. 3.7A) are among the most similar to the Lower McMurray grouped DZ sample. Conversely, DZ samples with least number of grains (e.g., KI2-1: n = 80; LA-1: n = 82) are frequently the most dissimilar to the grouped DZ sample (KI2-1: Kuiper statistic = 0.38; LA-1: Kuiper statistic = 0.31; Fig. 3.7A). These findings are not surprising, and recently several authors have noted the need for high-n DZ samples to accurately and precisely interpret provenance and calculate MDAs (Pullen et al., 2014; Coutts et al., 2019).

Second, variability in the proportion of specific age populations across DZ samples derived from the same stratigraphic interval is controlled by geographical distribution (separation) of the samples. In the McMurray Formation, the average dissimilarity between DZ samples increases (Lower McMurray > A Interval > CB Interval) with increasing geographical separation of DZ samples within each stratigraphic interval (Fig. 3.6 and 3.7). The Lower McMurray has the greatest spatial separation (maximum distance between DZ samples is 459 km) and the largest average dissimilarity (0.25) between individual DZ samples and its grouped DZ sample (Figs. 3.6A and 3.7A). In contrast, the CB Interval has the smallest geographical distribution of DZ samples (maximum distance between DZ samples is 178 km) of the three McMurray Formation intervals, and has the lowest average dissimilarity (0.18) between individual DZ samples and the grouped DZ sample (Figs. 3.6C and 7C). I interpret this correlation to reflect sediment input from various smaller tributaries entering the SE to NW drainage system in the Assiniboia Valley. Smaller tributaries could include the westward flowing Firebag Tributary (Rinke-Hardekopf et al., 2019) or smaller tributaries from the Cordillera in the central portions of the McMurray Depocenter (Benyon et al., 2016). Based on this, I suggest that for large areas such as the McMurray Depocenter, grouped DZ samples provide a more complete record of provenance for the depositional system and the time of deposition. This finding agrees with Jacobson et al. (2011) who showcased along-strike variability in provenance within schist bodies of a forearc basin in the southwestern U.S.A., and with Sickmann et al. (2016) who showed admixing of two individual river catchments in deep-sea systems of central California. In

order to more precisely characterize provenance sources and mixing in paleo-depositional systems across space, future studies should use regionally distributed, high-n DZ samples.

3.6.2. Syndepositional DZ Populations and Sample Sizes

In the 3 stratigraphic intervals of the McMurray Formation (Lower McMurray, CB, and A Intervals), 0.37% of DZ ages overlap with the biostratigraphic age of the McMurray Formation (Fig. 3.9A), and this amount of syndepositional DZ is comparable to the percentage of syndepositional DZ in modern and Holocene sediment samples globally (~0.4%; Sharman and Malkowski, 2020).

Dodson et al. (1988) provides the following equation (Eq. 1) for determining the probability of encountering a particular DZ population given a number of DZ dated and assuming an equal distribution of DZ throughout the sedimentary body:

$$P = (1 - f)^n \quad \text{[Eq. 1]}$$

where, *P* is the probability of missing a particular DZ population, *f* is the proportion that the particular DZ population constitutes of a DZ sample, and *n* is the total number of analyzed DZ grains. Given 0.37% syndepositional DZ in the McMurray Formation and using Equation 1, the theoretical minimum number of zircon needed to derive a syndepositional MDA using the Y3Zo or YGC2σ methods is 810; however, a sample with 810 grains has only a 63.5% probability of containing 3 syndepositional grains suggesting a larger sample size is needed. To have a 95% probability of encountering at least 3 syndepositional DZ in sedimentary strata similar to the McMurray Formation, 2,420 DZ must be analyzed.

In the Clearwater Formation, proportions of syndepositional zircon are significantly higher (lower Clearwater Formation: 6.6%, and upper Clearwater Formation: 22.7%, Fig. 3.10A), and both the lower Clearwater Formation and upper Clearwater Formation return syndepositional MDAs from most DZ samples within 2σ uncertainty (Fig. 3.9). For a 95% probability of encountering at least 3 syndepositional DZ in strata of the Clearwater Formation, Eq. 1 indicates that sample sizes of 132 grains (lower Clearwater) and 35 grains (upper Clearwater) are sufficient.

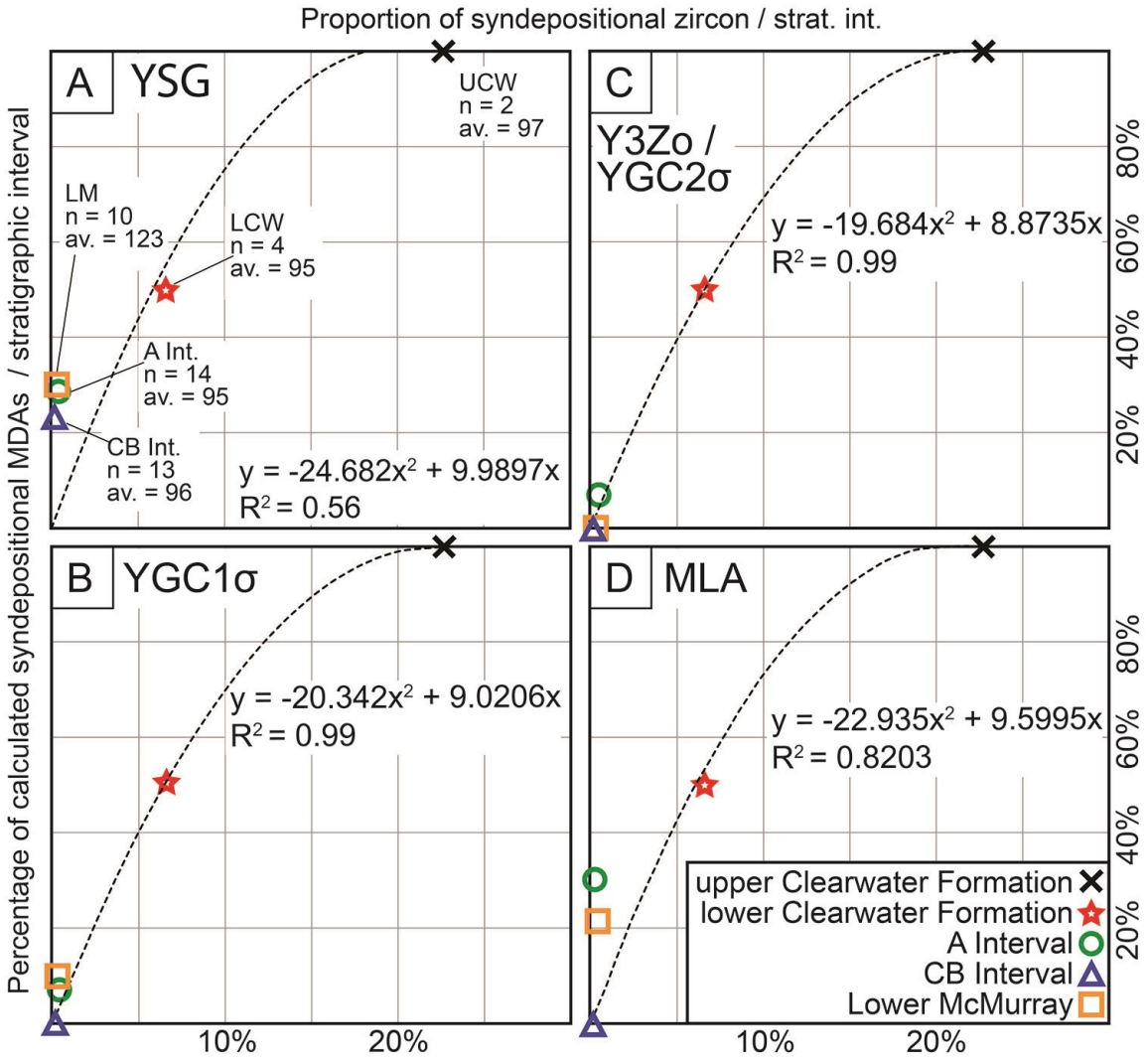

Figure 3.10. Likelihood of calculating a syndepositional MDA given a proportion of syndepositional zircon.

(A-D) Percentage of DZ samples (n = number of samples in each stratigraphic interval; row 2, Fig. 3.4) that return syndepositional MDAs using 5 different methods: (A) YSG, (B) YGC1σ, and (C) Y3Zo / YGC2σ (combined here, as results are identical), (D) MLA. The percentage of syndepositional MDAs (calculated using the 5 methods) are determined for each stratigraphic interval and are plotted *vs* the percentage of syndepositional zircon in each stratigraphic interval. The second order polynomial regression line with formula and R^2 values are given for each relation.

For the Lower Mannville Group in the McMurray Depocenter, the relation between the proportion of syndepositional zircon to the probability of calculating a syndepositional MDA from a DZ sample with ~100 DZ is shown in Figure 3.10. If the proportion of syndepositional zircon is 1%, syndepositional MDAs are only derived in ~9% of DZ samples using the YSG method, 9% using YGC1σ, and 8.5% using Y3Zo/ YGC2σ. To achieve a 95% probability of calculating a syndepositional MDA, ~16% syndepositional zircon are required (YSG), and this increases to 17.5% for MDAs calculated using grain

clusters (YGC1σ/Y3Zo/YGC2σ). I note that the relation expressed by the MLA (Fig. 3.10D) is quite similar to that of YSG (Fig. 3.10A) as MLA reverts to YSG when there is a low percentage of syndepositional zircon. However, Vermeesch (2020) notes that MLA converges towards the likeliest TDA with increasing DZ sample size, and by extension, with increasing the percentage of syndepositional DZ.

I caution that these values will change with the number of grains analyzed per DZ sample, with catchment sizes in source regions, and with distances to active volcanic arcs (Sharman and Malkowski, 2020). Our estimates also assume an equal distribution of DZ throughout a basin, the validity of which is unlikely (see section 5.1). However, in basins where DZ data exists, similar regressions to those employed herein, in combination with probabilistic calculations of missing a DZ population, can allow for a more informed decision when taking DZ samples for the purpose of MDA calculations.

3.6.3. gMDAs vs MDAs

In the McMurray and Clearwater formations, gMDAs provide improved accuracy over MDAs derived from individual samples, especially given adequate stratigraphic control, and are therefore more chronostratigraphically significant. In the McMurray Formation where syndepositional DZ are accessory, the youngest single grains from several individual DZ samples are grouped in gMDAs and calculated multi-grain ages can be closer to TDA (i.e., gMDAs are often younger than MDAs). In the Clearwater Formation where syndepositional DZ are more prevalent, gMDAs can help address potential negative bias in calculated MDAs (i.e., MDAs younger than TDA; Fig. 3.9C).

In the McMurray-Clearwater example described herein, the accuracy of gMDAs relative to MDAs for approximating TDAs is well expressed. The gMDAs in the Lower McMurray closely approximate the TDA (ash: 121.39 ± 0.20 Ma *vs* gMDA: YGC1σ/Y3Zo gMDA: 121.9 ± 2.6 Ma, 3 grains, MLA: 123.5 ± 1.9 Ma). In the A Interval, only gMDA estimates yield a multi-grain age younger than that of the ash at the top of the Lower McMurray (YGC1σ: 116.8 ± 4.2 Ma; Y3Zo: 118.8 ± 3.5 Ma; MLA: 118.6 ± 1.7 Ma; YGC2σ: 119.2 ± 3.4 Ma), while in contrast only 1 individual DZ samples yields a multi-grain MDA that overlaps with the ash age within uncertainty (AOS4, YGC1σ: 123.6 ± 5.8 Ma, MLA: 123.5 ± 2.5 Ma; Fig. 3.9C). The gMDAs for the lower Clearwater Formation (e.g., Y3Zo: 108.4 ± 4.0 Ma) and upper Clearwater Formation (e.g., Y3Zo: 110.5 ± 2.7 Ma) post-date

the biostratigraphically defined onset of deposition (113 Ma). In contrast, gMDAs calculated with the MLA algorithm yield ages of 114.1 ± 0.9 Ma for the lower Clearwater Formation, as well as 114.6 ± 0.5 Ma for the upper Clearwater Formation (Fig. 3.9C), and are more agreeable with biostratigraphy. Given the strong increase of syndepositional DZ in the Clearwater Formation (Fig. 3.9), other MDA estimates (YSG/YGC1σ/Y3Zo/YGC2σ) from both individual and grouped DZ samples are interpreted to be negatively biased (i.e., too young; Coutts et al., 2019; Vermeesch, 2020). Additionally, even MLAs calculated from individual DZ samples are potentially negatively biased, whereas MLAs calculated from grouped DZ samples are more conservative (e.g., Fig. 3.9C; lower Clearwater Formation: 111.5 ± 0.9 Ma *vs.* grouped DZ sample: 114.1 ± 0.9 Ma).

The utility of gMDA analysis is still fundamentally limited by the availability of syndepositional DZ. While providing a step forward in resolving the age of depositional units, gMDAs remain estimations of maximum depositional age and should not be treated as TDAs. For example, both gMDAs and multi-grain MDAs for the CB Interval of the McMurray Formation are older than its TDA because they are older than the absolute age established for the end of Lower McMurray deposition. As well, DZ samples from the upper Clearwater Formation should yield an age that is younger than that of the lower Clearwater Formation (Fig. 3.9B); however, both MDAs and gMDAs from the upper Clearwater Formation return ages older than those from the lower Clearwater Formation. I hypothesize this is either a function of a) the isolated geographical area and low number of DZ samples (n=2) from the upper Clearwater Formation with limited incorporation of sediment from local tributaries (Figs. 3.6I, J), and/or b) a statistical effect associated with analytical uncertainty of individual grains, resulting in MDAs that are too young for the lower Clearwater Formation (Coutts et al., 2019). Additional modeling is required to determine the most effective sampling pattern for capturing uncertainty in the heterogeneous distribution of zircon in a 3D sediment volume.

I suggest that gMDAs be used as a part of a larger group of emerging strategies aimed at improving the accuracy of MDAs as estimations of TDAs. Other recently published strategies include multiple dates of the youngest zircon with CA-TIMS (Herriott et al., 2019), high-n DZ samples (e.g., Pullen et al., 2014; Coutts et al., 2019), and statistical approaches (Johnstone et al., 2019; Vermeesch, 2020). In contrast to these new strategies, I deem the greatest value of grouped DZ analysis, besides a more comprehensive analysis of provenance, is two-fold: (1) In large basins located far from an

active volcanic arcs, gMDAs increase the probability of sampling enough syndepositional DZ that calculated gMDAs provide reliable estimates of TDAs, and (2): In basins with plentiful syndepositional DZ, gMDAs limit the potential of negative bias in calculated MDAs (especially, in combination with the MLA method). Combining DZ samples from multiple depositional units will undoubtedly incorporate samples deposited at different TDAs, and I note the necessity of a well-developed allostratigraphic framework. However, given both dimensions of analytical uncertainty of DZ ages and the accessory nature of syndepositional DZ in many sedimentary basins (Cawood et al., 2012), gMDAs provide a refinement of geochronological constraints as I have demonstrated herein.

3.7. Conclusions

Stratigraphic correlation is used to assign 43 DZ samples into 5 stratigraphic intervals of the McMurray-Clearwater succession. For each stratigraphic interval, I combine individual moderate-n (~100) DZ samples to create a single high-n (up to >1000) grouped DZ sample. Analysis and comparison of individual and grouped DZ samples was done with two objectives: (1) understand provenance heterogeneity in the McMurray Depocenter across time and space, and (2) determine whether robust chronostratigraphic subdivision of the McMurray-Clearwater succession is possible with MDAs.

I show that grouped DZ samples permit a more comprehensive assessment of provenance by averaging DZ heterogeneity inherent to individually sampled strata through time and space. Within the McMurray Formation, grouped DZ samples become increasingly dissimilar to their constituent DZ samples with increased spatial separation of DZ samples along the major drainage axis; I attribute this to areally restricted sediment input from smaller tributaries along the length of the drainage.

Similar to conventional MDAs, gMDAs remain maximum age estimations and are most effective when integrated with existing chronostratigraphic constraints. However, this study demonstrates that in the McMurray Formation, and in basins where syndepositional DZ are accessory (<5% of the total DZ sample), calculating gMDAs from grouped DZ samples produces more accurate (i.e., gMDAs often younger than MDAs) estimations of TDAs. In the Clearwater Formation where syndepositional zircon are plentiful (>5% of the total DZ sample), calculated MLAs from grouped DZ samples are more conservative than

those calculated using other methods, which decreases the potential for calculating negatively biased (i.e., too young) depositional ages.

Chapter 4.

Resolving the Stratigraphic Architecture of McMurray Formation Deposits in the Firebag Tributary

A version of this chapter is currently in review as: L. Rinke-Hardekopf, S. E. Dashtgard, J. A. MacEachern, and Murray K. Gingras, *in review*: Resolving stratigraphic architecture and constraining ages of paralic strata in low-accommodation settings, Firebag Tributary, McMurray Formation, Canada: The Depositional Record.

4.1. Abstract

The McMurray Formation in the Athabasca Oil Sands region, Alberta Foreland Basin, Canada, is presently subdivided into stratal units on the basis of the distribution of regionally mappable mudstones, the bases of which are interpreted as flooding surfaces. However, the McMurray Fm comprises a complex array of paleoenvironments, and in the Firebag Tributary in the northeastern McMurray Depocenter, contains significant delta plain and coastal plain deposits. In this study, I use detailed facies observations of 60 logged cores (supplemented by 348 photographed core intervals), and 4763 geophysical well logs to resolve the stratigraphic architecture in the Firebag Tributary. A new ash-derived age near the top of the McMurray Fm provides only the second absolute age date for the McMurray Fm and enables a discussion of deposition rates.

Of the identified 14 facies (subdivided into 5 facies associations), I distinguish 3 types of paralic deposits occurring on delta plains and coastal plains: 1) eluviated, deeply rooted paleosols, interpreted as semi-permanent shrub- and woodlands that formed during base-level drop; and 2) gleyed paleosols with fibrous rhizoliths, interpreted as the deposits of tidal marshes, and 3) coals accumulated in coastal mires, both formed during transgression. While eluviated paleosols are found below the coal seam at the top of the Lower McMurray, potentially indicating valley incision (i.e., a maximum regressive surface), gleyed paleosols underlie the coal seam at the top of the B1 DU and do not necessitate a relative sea-level fall (i.e., representing a major flooding surface where not overlain by a coal). Coals overlying both paleosols form through paludification, and their wetting-upward characters indicate major flooding events. In the B1 DU, coals and gleyed

paleosols are commonly overlain by FA4 or are eroded by wave ravinement during transgression. Therefore, the tops of coals or gleyed paleosols can be correlated to the bases of regionally extensive marine mudstones found elsewhere in the McMurray Depocenter.

Stratigraphic cross-sections define the paleoshoreline trajectory and suggest that the McMurray Formation in the Firebag Tributary underwent 2 progradational and 2 retrogradational phases. During the Lower McMurray, the paleoshoreline resided west of Firebag Tributary. Transgression resulted in migration of paleoshorelines associated with the C2 to B2 DUs towards the Alberta – Saskatchewan border. During the B1 DU, the paleoshoreline in the Firebag Tributary underwent regression, with tidal marshes and mires only established during the latest stages of base-level rise. Finally, transgression and repeated paleoshoreline retreat occurred during the A2 and A1 DUs, as well as the Wabiskaw Member of the Clearwater Fm.

Together with a previously dated ash from the Lower McMurray, the new absolute age derived from an ash in the B1 coal seam (115.09 ± 0.16 Ma) allows an estimation of DU duration. Individual depositional units in the McMurray Fm are interpreted to represent ~1.6 Ma for the C2-B1 DUs, ~0.8 Ma for the A2 DU, and ~0.4 for the A1 DU.

4.2. Introduction

The stratigraphic architecture of the McMurray Formation (Fm) in the Athabasca Oil Sands region, Alberta Foreland Basin, Canada (referred to herein as the McMurray Depocenter (MDC)), has been revised and debated considerably over the past decades (Fig. 4.1; Carrigy, 1959; Nelson and Glaister, 1978; Mossop and Flach, 1983; Ranger and Pemberton, 1997; Alberta Energy and Utilities Board, 2003; Hein and Cotterill, 2006; Hein et al., 2013; Horner et al., 2018; Château et al., 2019, 2020). Presently, the McMurray Fm is subdivided into stratal units, based on the distribution of regionally mappable mudstones interpreted to mark marine flooding surfaces. However, the McMurray Fm comprises a complex array of terrestrial to marine paleoenvironments (Pemberton et al., 1982; Flach and Mossop, 1985; Gingras et al., 2016). In particular, the Firebag Tributary in the northeastern MDC (Fig. 4.1B) hosts a disproportionate volume of delta and coastal plain deposits (Hein et al., 2007). Herein, I place particular focus on those sedimentary strata that accumulated in paralic depositional environments, which are defined as environments

that are situated landward of the paleoshoreline, and are mainly freshwater but experience rare marine inundations. In low-accommodation depositional systems, such as the McMurray Fm in the MDC, vertical amalgamation of stratigraphic intervals is common owing to channel migration and cannibalization (e.g., Ranger, 1994; Ainsworth et al., 2017; Château et al., 2019; Van Yperen et al., 2019), and this makes it difficult to correlate paralic units laterally. Additionally, coastal mires have a high preservation potential for ash beds (e.g., Bohor and Triplehorn, 1993; Schmitz and Kuiper, 2013; Dai et al., 2017), and recently, ash beds recovered in coals at the top of the Lower McMurray provided the first absolute age in the McMurray Fm (Rinke-Hardekopf et al., 2019).

In this study, I use a dataset of 60 logged cores, photographs of an additional 348 cored intervals, and 4763 geophysical well logs to correlate McMurray Fm strata throughout the Firebag Tributary, and to assess the relation between paralic strata in the MDC and other strata elsewhere in the MDC. Detailed facies analysis using sedimentology and ichnology is employed to determine the distribution of paleo-depositional environments. Well logs are used to produce isopach maps for the McMurray Fm throughout the study area, and to extend stratigraphic correlations between cores. Stratigraphic cross-sections are used to showcase shoreline trajectories and discuss the stratigraphic architecture of the McMurray Fm. Lastly, a high-certainty maximum depositional age (i.e., an absolute age) from an ash-bed preserved in coal towards the top of the McMurray Fm provides a second chronologic age constraint on the McMurray Fm and enables a discussion of deposition rates.

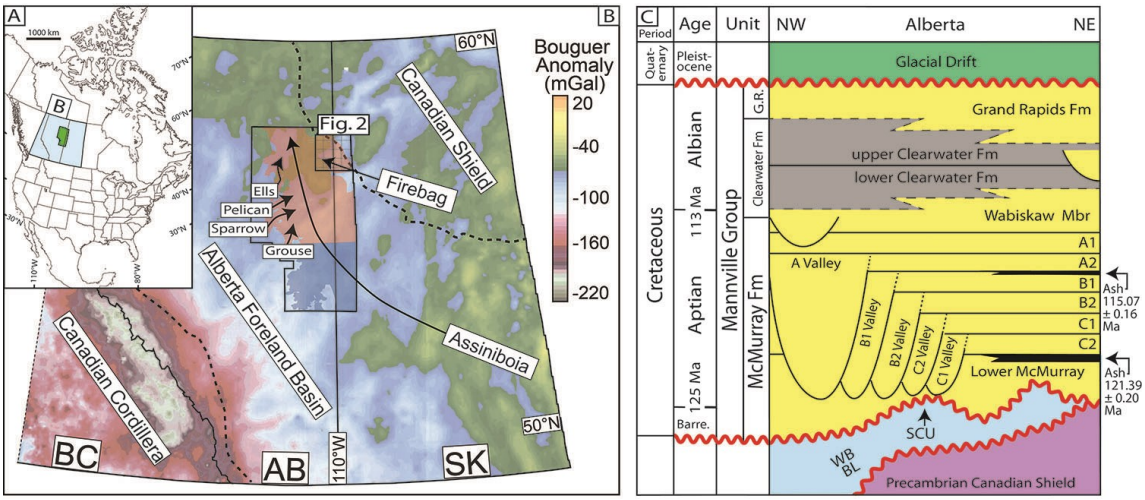

Figure 4.1. Overview of study area and the stratigraphy of the Mannville Group

(A) Location of the McMurray Depocenter (green) in western Canada. The blue overlay gives the location of the Bouger gravity map (B) of British Columbia (BC), Alberta (AB) and Saskatchewan (SK). **(B)** Bouger gravity map depicting the locations of the Athabasca (red overlay) and Cold Lake (blue overlay) oil sands regions in the Alberta Foreland Basin (adapted from Rinke-Hardekopf et al., 2021). The dashed lines demarcate the boundaries of the Alberta Foreland Basin with the Canadian Cordillera and Canadian Shield. Also included are the interpreted positions of the major paleo-drainages (black arrows), including the Assiniboia (Main) Valley, Firebag Tributary, and the Ells, Pelican, Sparrow and Grouse Paleovalleys (Christopher, 1997; valley positions derived from Broughton, 2013a; Horner et al., 2019; Rinke-Hardekopf et al., 2019; Château et al., 2020).The location of Fig. 2 is also shown. **(C)** Allostratigraphic framework of the Lower Cretaceous Mannville Group in the Firebag Tributary. Clastic sedimentary rocks (sandstone (yellow), mudstone (grey), and coal (black)) unconformably overlie Devonian carbonates of the Woodbend (WB) and Beaverhill Lake (BL) groups (blue) and the Precambrian Canadian Shield (purple). Also included are the ages derived from ash layers found within coal seams near the top of the Lower McMurray (Rinke-Hardekopf et al., 2019) and the B1 depositional unit (new data presented herein).

Sequence stratigraphy was originally developed by identifying coeval depositional environments in the shallow-marine realm and interpreting observed shoreline trajectories as a result of relative sea-level fluctuations (Posamentier and Vail, 1988; Van Wagoner et al., 1988). These concepts were expanded into the paralic realm by correlating delta- and coastal-plain environments (e.g., coastal mires, interfluve areas) with coeval shallow-marine environments, and the boundary between them, which defines the shift in the position of the paleoshoreline (Shanley and McCabe, 1991, 1994; Wright and Marriott, 1993; Plint et al., 2001; Gani et al., 2015; Amorosi et al., 2017). Delta- and coastal-coastal plain environments accumulate or erode sediment to a hypothetical “base-level”. In the paralic realm, base-level is driven by the groundwater table, which is hydrologically connected to sea-level (Diessel, 1992; Bohacs and Suter, 1997). Base-level change, therefore, approximates relative sea-level change, and hence is used in this study as its proxy (Posamentier et al., 1988). Base-level changes can be preserved in coals and paleosols that form in coastal mires or interfluve areas (Clymo, 1984; Leckie et al., 1989; Shanley and McCabe, 1991; Diessel, 1992; Banerjee et al., 1996; Bohacs and Suter, 1997; Holz et al., 2002; Wadsworth et al., 2002; Diessel, 2007; Jerrett et al., 2011b; Tabor et al., 2017; Rinke-Hardekopf et al., 2019). In the McMurray Fm, delta and coastal plain strata are common in the informally named basal lower McMurray member (herein referred to as Lower McMurray), and also occur intermittently at multiple stratigraphic levels throughout the McMurray Fm (e.g., Flach and Mossop, 1985; Ranger and Pemberton, 1997). Correlation of strata across the fresh-to-salt water interface at various stratigraphic levels of the McMurray Fm provides crucial data for understanding the depositional history of the interval.

4.2.1. Geological Overview of the Mannville Group

Within the MDC, the McMurray Fm is the basal unit of the Lower Cretaceous Mannville Group, and it unconformably overlies Devonian carbonates of the Beaverhill Lake Group (Fig. 4.1C; Carrigy, 1959; Williams, 1963). The contact between them has been designated as the Sub-Cretaceous Unconformity (SCU; Jardine, 1974). The McMurray Fm was deposited during a 3rd order transgression of the Boreal Sea (Hein et al., 2013), and is capped by the Wabiskaw Member of the Clearwater Fm (Fig. 4.1C; Carrigy, 1959). Sedimentologically, the McMurray Fm comprises a wide array of sedimentary deposits, including cross-stratified sandstones, pedogenically altered mudstones and coals, and a variety of heterolithic facies (Carrigy, 1959; Mossop and Flach, 1983; Keith et al., 1988; Rinke-Hardekopf et al., 2019). From the bottom to the top of the stratigraphic succession of the McMurray Formation, heterolithic deposits preferentially exhibit sedimentary structures characteristic of fluvial, tidal, and wave influence (e.g., Hein and Cotterill, 2006; Timmer et al., 2016; Hayes et al., 2017; Weleschuk and Dashtgard, 2019; Château et al., 2021). The ichnology and palynology of McMurray Fm strata also indicates deposition under freshwater through to brackish-water depositional conditions (e.g., Pemberton et al., 1982; Mossop and Flach, 1983; Ranger and Pemberton, 1997; Hubbard et al., 2011; Czarnecki et al., 2014; La Croix and Dashtgard, 2015; La Croix et al., 2015; Harris et al., 2016; Gingras et al., 2016; Hein and Dolby, 2018).

Regionally mappable marine mudstones, interpreted to record transgression, are used to subdivide the McMurray Fm into a series of vertically stacked and regionally extensive depositional units (DU), designated the Lower McMurray, C2, C1, B2, B1, A2, and A1 (Fig. 4.1C). Depositional units were partially removed by channel-belt migration and/or valley incision, some of which have been attributed to major base-level falls (Ranger and Pemberton, 1997; Alberta Energy and Utilities Board, 2003; Hein and Cotterill, 2006; Hein et al., 2013; Horner et al., 2018, 2019; Château et al., 2019, 2020). Recent research suggests at least some of these channels/valleys are more akin to contemporaneous fluvial or fluvio-tidal channel belts that actively fed regional depositional units (e.g., Baniak and Kingsmith, 2018; Château et al., 2019). While stratigraphic relations are partially obscured by syndepositional subsidence associated with salt dissolution in the Devonian Prairie Evaporite Fm (e.g., Broughton, 2013; Barton et al., 2017), Rinke-Hardekopf et al. (2019) interpreted the paralic coals of the Lower McMurray

to be the result of the earliest Cretaceous base-level rise, driven by southward transgression of the Boreal Sea.

4.2.2. Stratigraphic Concepts on Delta and Coastal plains

Coals

Peat-forming mires are paralic sedimentary environments in which coal accumulates, and these mires require a rising water table to maintain organic matter production (Ingram, 1978; Clymo, 1984). In delta and coastal plains, the water table is hydrologically linked to relative sea-level (Diessel, 1992; Törnqvist, 1993). Diessel et al. (2000) established that extensive mire formation occurs when the rate of base-level rise tracks closely the rate of peat accumulation, and that base-level change in coal successions is commonly expressed by the accommodation rate / peat production rate ratio (Fig. 4.2A). Accumulated peats can show various internal lithotype successions (Fig. 4.2A), including successions indicative of increasing rates of base-level rise during the transgressive systems tract (i.e., wetting-upward coals; e.g., Jerrett, et al., 2011b; Shiers et al., 2017; Rinke-Hardekopf et al., 2019) or successions indicative of decreasing rates of base-level rise during the lowstand and highstand systems tracts (i.e., drying-upward coals; e.g., Holz et al., 2002; Davies et al., 2006; Jerrett et al., 2011a; Chalmers et al., 2013).

When interpreting coals with respect to their stratigraphic significance, autogenic processes such as peat compaction must also be considered. Peats commonly lose ≥50% volume due to autocompaction at rates of up to ~10s $cm \cdot yr^{-1}$ (more commonly, several $mm \cdot yr^{-1}$) and during shallow burial (Pizzuto and Schwendt, 1997; Long et al., 2006; Törnqvist et al., 2008; van Asselen et al., 2009; Sahoo and Gani, 2016).

Paleosols

On delta and coastal plains, soils can form in interfluve areas or in marshes (Fig. 4.2B-C; Gore, 1982). Fossilized soils (i.e., paleosols) typically record phases of lowered water tables during base-level falls, or phases of elevated water tables and water saturation during base-level rises (e.g., Wright and Marriott, 1993; Aitken and Flint, 1996; McCarthy and Plint, 1998; Kraus, 1999; Plint et al., 2001). Wright and Marriott (1993) noted that well-developed (i.e., mature, well-drained; Fig. 4.2B) paleosols form during phases of

prolonged exposure during the lowstand and/or late highstand systems tracts. By contrast, hydromorphic and weakly developed paleosols form on delta and coastal plains during the transgressive and/or early highstand systems tracts (Fig. 4.2C; Aitken and Flint, 1996). Gleying (i.e., water logging and reduction) of hydromorphic soils can occur during both initial soil formation or post-depositionally during ensuing transgression. By extension, paleosols can either form during the temporal duration of subaerial unconformities, and/or in close stratigraphic proximity of marine flooding surfaces.

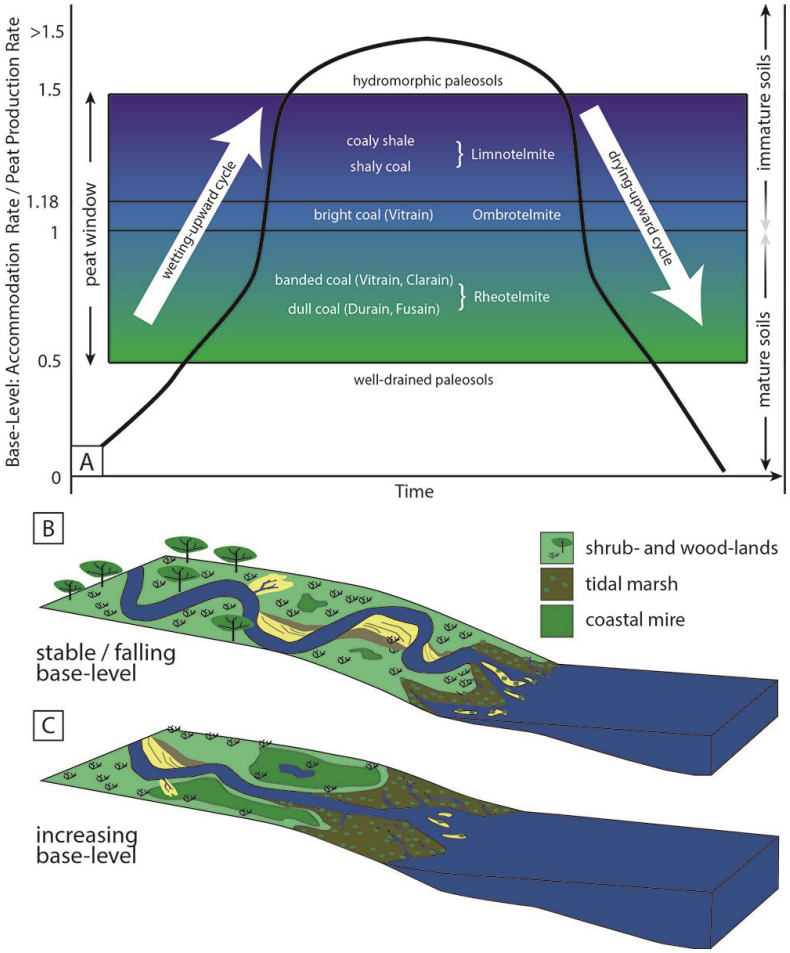

Figure 4.2. Stratigraphic concepts on delta and coastal plains
(A) Schematic overview of the relation between base-level (expressed through the accommodation rate / peat production rate ratio) and resultant coal lithotypes and paleosols. Note the peat window extends between ratios of 0.5 and 1.5, while the base-level window for mature and hydromorphic soils has a more poorly defined boundary (indicated by faded arrows on the right-hand y-axis). This diagram shows schematically how coals and paleosols form either wetting-upward or drying-upward successions based on changes in base-level and / or organic productivity (adaptred from: Rinke-Hardekopf et al., 2019). **(B)** Schematic representation of depositional environments on a delta-plain during stable or falling base-level, including more widely developed shrub- and wood-lands. **(C)** Schematic representation of depositional environments on a delta-plain when the base-level is rising. Note the widespread development of mires and marshes.

4.3. Study Area, Methods and Data

4.3.1. Core and Well Log Database

Sedimentological and ichnological features, including lithology, primary physical and biogenic sedimentary structures, grain size, bioturbation index (BI; Taylor and Goldring, 1993), and lithological accessories were described from 60 cored successions (Fig. 4.3) and recorded using AppleCORE logging software (donated to SFU by Dr. Mike Ranger). Cored successions were logged at the Core Research Center in Calgary, Alberta, Canada. These 60 logged core intervals are supplemented by photographic files of an additional 348 cored sections (Fig. 4.3; donated by Cenovus Energy, Husky Energy, and Synenco Energy Inc).

Stratigraphic surfaces are correlated throughout the study area using all logged cores and supplemented where necessary with geophysical well logs (Fig. 4.3). Well logs are accessed through GeoScout (donated to Simon Fraser University by geoLOGIC). Well log suites include most or all of the following curves per well: gamma-ray, caliper, neutron and density porosity, photo-electric log, and resistivity.

Stratigraphically significant surfaces include the bases of regional mudstones (e.g., Ranger and Pemberton, 1997; Hein and Cotterill, 2006; Hein et al., 2013; Horner et al., 2018, 2019; Château et al., 2019, 2020), and the tops of coal seams, and paleosols (Hein et al., 2007; Barton et al., 2017; Rinke-Hardekopf et al., 2019). On well logs, regional mudstones are identified based on criteria provided by Château et al. (2019), which includes a gamma ray reading >100 API and density-porosity values <18%. Coals are identified based on very high neutron and density porosity readings >50%. Paleosols are identified by resistivity values <1 Ωm and a high separation of neutron porosity (45-50%) and density porosity (20-30%) readings. Stratigraphic relations are shown in 4 cross-sections (3 along depositional-dip, 1 along depositional-strike), containing 7 individual core-logs each and augmented by well-logs to infill gaps between cored locations.

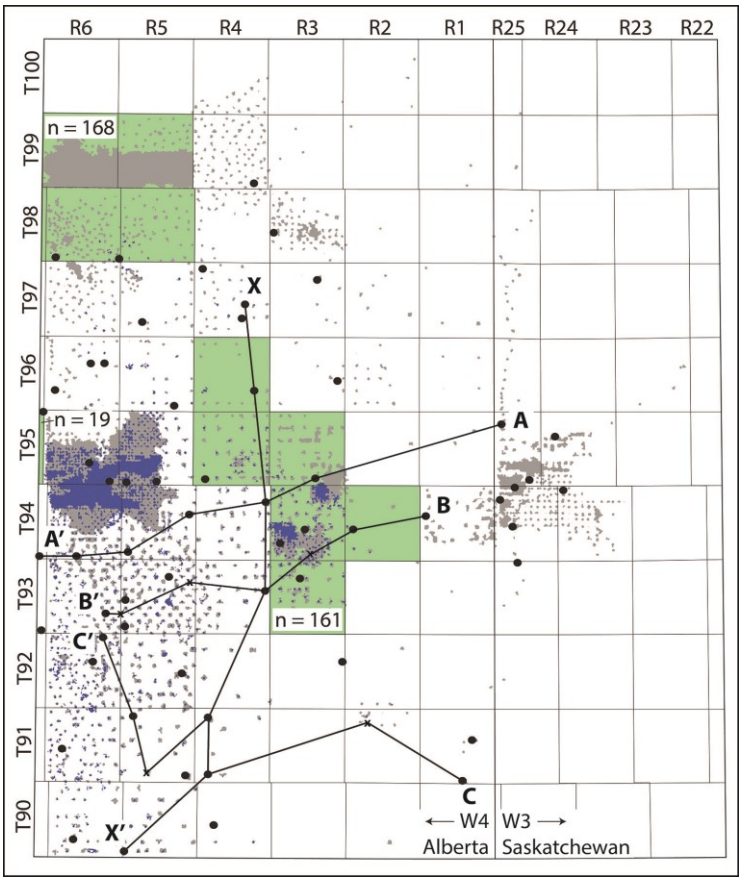

Figure 4.3. Outline of the study area, including all available data.
The grey grid is the dominion land survey (DLS), which subdivides western Canada into 6 x 6 mile (~10 x 10 km) (T)ownships and (R)anges. The border between Alberta and Saskatchewan also demarcates the boundary between ((W)est of) the 3rd and W4th Meridian. The location of the study area is shown in Fig. 1. Black circles represent cores logged at the Core Research Center in Calgary, Canada. Grey small dots represent available well-logs, and blue dots represent well-logs that preserve the top of the McMurray Formation, and 1865 of these were used in this study. Green polygons define areas with photographed core intervals (n: number of photographed cores). Also included are the locations of along-dip cross-sections A'-A, B'-B, and C'-C (Fig. 4.12), and the along-strike cross-section X'-X (Fig. 4.13).

4.3.2. Three-Dimensional Modelling

The isopach thickness of McMurray Fm strata within the Firebag Tributary is mapped using all available well logs. On well logs, the base of the McMurray Fm is readily identified directly overlying Devonian carbonates, based on an upward shift of photo-electric log signal from ~2.5–4.5 to values typically <2.3. The top of the McMurray Fm is identified on the basis of the first appearance of glauconitic sandstones, marking the Wabiskaw Member of the Clearwater Fm. On well logs, glauconitic sandstones (few meters) appear as a spike of the photo-electric log reading to ~2.3–2.5, overlying McMurray strata showing values of ~2.0–2.3.

For well logs that encompass the entire McMurray Fm (Fig. 4.3), the locations of the top and the base of the formation were imported into Petrel 2018 (donated to Simon Fraser University by Schlumberger). In total, 1865 (of 4763 total) wells were imported. In Petrel 2018, these wells were used to create isochore points and model isopach thicknesses using the convergent interpolation algorithm. The isochore points algorithm adds values every 50m between wells, thereby guiding the convergent interpolation algorithm in creating a thickness map for the McMurray Fm. Based on thicknesses of the McMurray Fm, I were also able to interpret the paleo-topography of the SCU at the end of McMurray deposition, wherein thicker strata correspond to paleotopographic lows and thinner intervals mark paleotopographic highs. Thickness maps for individual depositional units (e.g., B2, A1) throughout the Firebag Tributary were not created, as common amalgamation of depositional units due to erosion by channels renders the resultant isopachs created by the convergent interpolation algorithm futile.

4.3.3. Chemical Abrasion Thermal Ionization Mass-Spectrometry (CA-TIMS)

In the coal seam capping the B1 DU, an ash layer was identified in well 1AA/02-03-095-03W4 at a depth of 165.0 m and sampled for zircon. Uranium-Lead (U-Pb) isotope ratios were obtained from 6 individual zircon grains using chemical abrasion thermal ionization mass-spectrometry (CA-TIMS; after Mattinson, 2005) at the Isotope Geology Laboratory of Boise State University, Idaho, USA. CA-TIMS U-Pb dates and uncertainties were calculated using standard algorithms (Schmitz and Schoene, 2007; Crowley et al., 2007), EARTHTIME ET535 tracer solution (Condon et al., 2015), and standard U-decay constants (Jaffey et al., 1971). $^{206}Pb/^{238}U$ ratios and dates were corrected for initial ^{230}Th disequilibrium, using $D_{Th/U} = 0.20 \pm 0.05$ (1σ) (Crowley et al., 2007). A weighted mean age of the 2 youngest zircon grains was calculated using IsoplotR (Vermeesch, 2018b). The other four grains were detrital and exhibited a pre-Cretaceous age.

4.4. Results

4.4.1. Facies and Facies Associations

The sedimentary strata of the McMurray Fm and Wabiskaw Member of the Clearwater Fm comprise 14 facies (Table 4.1). Based on facies successions observed in

cored intervals and their spatial distribution, 14 facies into 5 facies associations are proposed that define the regional depositional system (Table 4.2; Figs. 4.4–4.5). The 5 facies associations (FA) include: FA1 - Fluvial and fluvio-tidal channel deposits; FA2 - Delta and coastal plain deposits; FA3 - Bay deposits; FA4 - Delta-front and prodelta deposits; and FA5 - Lower shoreface to offshore deposits. Whereas FA1–4 are found in the McMurray Fm, the Wabiskaw Member of the Clearwater Fm is dominated by FA5 with only rare occurrences of FA1 and FA4.

Table 4.1. Summary of all facies observed in the McMurray Formation and Wabiskaw Member of the Clearwater Formation in the study area.

Facies are then grouped into facies associations (FA1-5), which are detailed in Table 4.2, and figure numbers (Fig.) refer to photographs of individual facies. Acronyms used , include: Arenicolites (*Ar*), Asterosoma (*As*), Chondrites (*Ch*), Cylindrichnus (*Cy*), Diplocraterion (*Di*), fibrous roots (fr), fugichnia (fu), Gyrolithes (*Gy*), Naktodemasis (*Nk*), Palaeophycus (*Pa*), Phycosiphon (*Ph*), Planolites (*Pl*), Rosselia (*Ro*), Schaubcylindrichnus freyi (*Sf*), Skolithos (*Sk*), Taenidium (*Ta*), Teichichnus (*Te*), Thalassinoides (*Th*), woody roots (wr), Zoophycos (*Zo*).

Facies	Name	Sedimentology (sediment, grain-size, physical structures, accessories)	Ichnology (trace fossils, BI, description)	Facies contacts	Interpretation	FA
F1	Structureless to cross-stratified sandstone [Fig.6A]	sediment: sandstone with rare mudstone laminae (<1cm) thickness: 10s cm – 10s of meters grain size: fL to vcU; rare granules structures: structureless, cross-stratification, current ripples accessories: pyrite, carbonaceous debris, pebbles, mud-clasts	BI: 0-1 traces: *Pl* description: bioturbation is only observed in mud laminae	Sharp or erosional basal contacts with all facies; overlain by F3, F4, F5, F6, or F10	Channel thalweg dunes. Facies is interpreted as channel deposits deposited under mainly (fluvial) unidirectional flow. Rare mud beds may represent low flow conditions as a result of reduced river discharge, or flow retardation associated with the tidal backwater. Low flow conditions allow rare colonization by infauna.	FA1
F2	Mud-clast breccia in sandstone [Fig.6B]	sediment: structureless sandstone, with irregular, elongate and/or angular mud clasts (0.5 - 20cm in length) thickness: 10cm – meters grain size: sand is vf – mU, rarely cU structures: mud-clasts show imbrication, soft-sediment deformation, lamination, and syneresis cracks accessories: organic detritus	BI: 0-1 traces: n/a (except for PI in mud clasts)	Erosive basal contact with all facies; overlain by F1, F5, F11, and F12	Mud-rich sediment from channel migration and bank collapse or wave ravinement. Thicker deposits (meters) are found in association with other channelized deposits (FA1) and result from cut-bank collapse related to channel migration and cannibalization. Thinner deposits (~10cm) of F2 show imbrication and are found in association with FA4. These thinner deposits are interpreted to represent wave ravinement in shallow-marine environments during transgression.	FA1, FA4
F3	Chaotic heterolithic sediment with abundant soft-sediment deformation [Fig.6C]	sediment: variable proportions of sandstone and mudstone (approximately 50:50 ratio) thickness: 10cm - 10m grain size: sand is vf to fU sand structures: chaotic bedding, micro-fractures, soft-sediment deformation, convolute bedding, current ripples accessories: carbonaceous debris, frequent mud clasts	BI: 0 traces: n/a description: n/a	Sharp basal contact with F1, F2, F6, and F7; overlain sharply by F1	Slump or levee collapse. Facies is interpreted to represent rapid deposition of non-lithified sediment, either by collapsing levees onto a floodplain, or as a result of rapid basement subsidence (sinkholes) and local creation of accommodation.	FA1, FA2

Facies	Name	Sedimentology (sediment, grain-size, physical structures, accessories)	Ichnology (trace fossils, BI, description)	Facies contacts	Interpretation	FA
F4	Finely laminated light and dark grey mudstone with rare sandstone beds [Fig.6D-E]	sediment: laminae of grey, clay-rich mudstone (1-5mm) interbedded with light-grey, silt-rich mudstone (1-5mm); rare sandstone layers (0.5-3cm) thickness: 10s cm - 7m grain size: sands ≤vfU structures: parallel lamination, current ripples, soft-sediment deformation, erosional surfaces accessories: pyrite	BI: 0-3 traces: *Cy, Pa, Pl, Te* description: trace fossils are diminutive, sporadically distributed and only observed in lighter mudstone and sandstone beds; darker mudstone laminae are unbioturbated	Gradational basal contact with F5; erosionally overlain by F1, F5, and F7	Abandoned channel. Laminated fine-grained sediment indicates low depositional energy, and color variation is interpreted to result from variable oxygenation (darker sediment results from reduction in oxygen and more organic preservation) in either an oxbow lake or in the sediment. Erosionally based, coarser grained bioturbated sediment with soft-sediment deformation and current ripples is interpreted as periodic rapid influx of sediment and brackish waters. Opportunistic infaunal colonization relates to influx of brackish-water larvae and oxygenated water.	FA1
F5	Sparsely to sporadically bioturbated sandstone- to mudstone-dominated, muddying upward inclined heterolithic stratification [Fig.6F-H]	sediment: sandstone (layers: 0.1cm - meters) to mudstone (layers: 0.1cm - 20cm); sand to mud ratio gradually shifting upwards from 80:20 to 20:80 thickness: 10s cm - 10s m grain size: mud, sand ≤mU structures: inclined (high- and low-angle) heterolithic bedding, double mud-drapes, wavy to flaser bedding, tidal bundles, biogenically churned; sand: cross-stratification, current ripples; mud: syneresis cracks, soft-sediment deformation, micro-fractures accessories: carbonaceous debris, mud clasts	BI: 1-5 traces: *Ar, Cy, Gy, Pa, Pl, Sk, Te* description: bioturbation typically higher (BI 3-5) in mudstone beds, and lower in sandstone beds (1-3); low-diversity suite with diminutive burrows; moderate to higher mudstone content is associated with higher diversity of trace fossils and bioturbation intensity; *Gy* largely occurs in monogeneric associations	Gradational basal contact with F1, F2, and sharp basal contacts with F4, F6, F7, F8, F9; overlain gradationally by F8, F9, F10 and sharply by F1, F2, F10, F11	Fluvio-tidal point bars (lateral-, down-stream accretion, counter point bars): Heterolithic sediment indicates variable depositional energy, and unidirectional current flow structures in sand suggests that channels were fluvially dominated. Tidal influence and (at least intermittently) brackish water are interpreted from bioturbation, double mud-drapes, and varying thicknesses of tidal bundles. Mud-content can be driven by bar migration and possibly proximity to the turbidity maximum zone. A low-diversity, diminutive trace-fossil suite suggests high degrees of faunal stress (high mortality) owing to reduced and/or fluctuating salinity, and rapid sedimentation.	FA1
F6	Light to dark grey sandstone with woody roots [Fig.7A-C]	sediment: 50-80% sandstone thickness: ≤1m grain size: vf - fU structures: rarely mottled from peds (angular blocky texture) accessories: prominent carbonaceous detritus, and possibly woody branches	BI: 0-2 traces: fr, *Nk, Pl,* wr description: bioturbation is rare and only observed in the vicinity of rhizoliths	Gradational basal contact with F1, F5, and F9; gradationally overlain by F7	Semi-permanent shrub- and woodlands. Thick woody roots (up to 5cm width, 30cm depth) and common fibrous roots suggest presence of higher land plants and, potentially, more permanently vegetated areas. Peds and mottled texture, as well as illuviated sediment suggests a water table that resided significantly below the delta or coastal plain during soil formation.	FA2

Facies	Name	Sedimentology (sediment, grain-size, physical structures, accessories)	Ichnology (trace fossils, BI, description)	Facies contacts	Interpretation	FA
F7	Coal and organic-rich mudstone [Fig.7D-E]	sediment: dull durain, banded clarain, rare shiny vitrain, fusain, and carbonaceous mudstone thickness: 5cm - 11m, locally up to 35m grain size: n/a structures: coal interbedded with sand, inclined bedding, rare micro-fractures, pedoturbation (ped formation) accessories: pyrite, woody branches, rare volcanic ash	BI: 0-3 traces: fr, *Nk*, wr description: bioturbation is only observed in clastic-rich intervals of the facies	Gradational basal contact with F6 and F8; overlain sharply by F1, F2, F11, F12	Coastal mires and swamps. Various coal types represent different mire stages on a coastal or delta plain: vitrain - ombotrophic mires; durain and clarain - rheotrophic mires; fusain -oxidized mires. Changes in lithotypes are interpreted to record variability in water table position related to base-level changes. Deformation structures reflect subsidence due to underlying salt-dissolution during mire accumulation; swamp (clastic-rich lithotypes) conditions may allow for faunal activity, or pedoturbation.	FA2
F8	Light to dark colored mudstone with fibrous roots [Fig.7F]	sediment: >70% mudstone thickness: 10cm - 7m grain size: <vfL structures: local interbedding of thick lighter (5cm - >1m) and thin (1 - 20cm) darker horizons accessories: pyritized roots, rare carbonaceous detritus	BI: 1-4 traces: fr, *Pl, Cy, Sk, Te* description: rhizoturbation is largely ubiquitous; *Cy* and *Te* only appear where facies is interbedded with other heterolithic and bioturbated facies	Gradational to sharp basal contact with F1, F4, F7, F8; overlain gradationally by F7, and sharply by F1, F5, F11, F12	Tidal marsh. Gleyed rooted sediment suggests a continuously elevated water table, and color changes within the soil horizon may record periodic increases in base-level (darker, organic-rich sediment is interpreted as base-level increase). Sporadically distributed bioturbation with diminutive trace fossils suggests a tidal marsh environment in the shallow supratidal or upper intertidal zones, where brackish-water larvae can periodically colonize the sediment.	FA2
F9	Abundantly bioturbated heterolithic deposits [Fig.8A-B]	sediment: Sandstone to mudstone ratio ranging between 90:10 and 10:90 thickness: 10cm - few meters grainsize: <fL structures: commonly biogenically churned, rare wavy to lenticular bedding accessories: rare carbonaceous detritus	BI: 3-6 traces: *Ar, Pa, Pl, Sk, Te, Th* description: bioturbation is ubiquitous and thorough, with the exception of the muddiest deposits.	Gradational basal contact with F1, F5, F11, and F12; overlain gradationally by F8, and sharply by F1, F2, F5, F11, F12	Sandy and muddy tidal flats. High BI values and churned sedimentary strata reflect low energy deposition with reduced sedimentation rates. Lower BI values in the muddiest parts of the facies are interpreted to reflect soupground conditions, which limited colonization by infauna.	FA3

Facies	Name	Sedimentology (sediment, grain-size, physical structures, accessories)	Ichnology (trace fossils, BI, description)	Facies contacts	Interpretation	FA
F10	Thoroughly bioturbated silty mudstone [Fig.8C-D]	sediment: silty mudstone thickness: 5cm - 3.5m grain size: <vfL structures: mostly biogenically churned, rare parallel lamination and oscillation ripples accessories: carbonaceous detritus	BI: 4-6 traces: *Ar, As, Ch, Pa, Pl, Ro, Te, Th, Sf*	Gradual basal contact with F9, sharp basal contact with F1, F5; overlain sharply by F1, F6, F11, F12	Sheltered bay. Fine grain-size, coupled with ubiquitous bioturbation suggest low depositional energy and low sedimentation rates. Lack of sedimentary structures (possibly also churned) suggests a sheltered environment, with rare ripples indicating a more open depositional environment. This facies contains the most diverse trace fossil assemblage observed in the McMurray Formation suggests strong marine influence, interpreted to result from transgression.	FA3
F11	Cross-stratified sandstone with combined flow ripples and common escape structures [Fig.9A]	sediment: 90% sandstone interbedded with 10% mudstone thickness: ≤5m grain size: <fU structures: cross-stratification, combined-flow ripples, current ripples, oscillation ripples, micro-HCS, aggradational oscillation ripples accessories: mud clasts	BI: 0-3 traces: *Ar, fu, Pl, Sk*	Gradational or sharp basal contact with F1, F5, F7, and F8; overlain gradationally by F12	Storm-influenced, fluvial-dominated delta front. Sand-rich sediment with cross-stratification and trace fossils recording filter-feeding and deposit feeding behaviour (and fugichnia) indicate overall high-energy depositional environments and storm events (fluvial discharge: cross-stratified sands; storm waves: micro-HCS) with large quantities of sediment.	FA4
F12	Variably bioturbated heterolithic sediment with oscillation ripples, and erosively-based mudstones [Fig.9B-D]	sediment: sandstone-to-mudstone ratios ranging from 20:80 to 80:20 thickness: ≤10m, rarely up to 15m grain size: ≤fL structures: oscillatory ripples, combined-flow ripples, current ripples, flaser bedding; mud beds: erosional bases, parallel lamination, graded bedding, soft-sediment deformation, load casts, syneresis cracks accessories: organic detritus, mud clasts	BI: 1-5 traces: *Ar, As, Cy, fr, fu, Pa, Pl, Ro, Sk, Te* description: most bioturbation is restricted to mud-rich (>40%) heterolithic sediments and only rarely in sandstone beds; however, erosionally based mud beds with internal lamination are typically unbioturbated	Gradational basal contact with F1, F2, and F11; sharp basal contact with F7 and F8; overlain sharply by F13, or gradationally overlain by F10	Storm-influenced, fluvial-dominated prodelta. Variability in grain size and bioturbation is interpreted to represent variable depositional energy and sedimentation rates. Common oscillatory structures indicate a strong wave influence. Erosively based mud beds (showing normal and inverse grading, and internal laminae) are interpreted as flood-induced hyperpycnites generated due to heightened precipitation during storms. Unburrowed beds are attributed to salinity fluctuations (mud beds, syneresis cracks) and elevated sedimentation rates. More thoroughly bioturbated heterolithic sediment is interpreted as distal positions in the prodelta or positions off active channels.	FA4

Facies	Name	Sedimentology (sediment, grain-size, physical structures, accessories)	Ichnology (trace fossils, BI, description)	Facies contacts	Interpretation	FA
F13	Bioturbated, sanding-upward blue grey mudstone and sand [Fig. 11A-B]	sediment: steel-grey mudstone (0.5-15cm) interbedded sandstone (≤5cm), sanding-upward from sandstone-to-mudstone ratios of 30:70 to 90:10 thickness: ≤5m grain size: ≤fL (basal lag up to mU) structures: flaser bedding, wavy bedding, lenticular bedding, locally biogenically churned; sandstone: oscillation ripples accessories: basal lag, rare carbonaceous debris, rare glauconite in sandstone	BI: 1-5 traces: *As, Cy, Di, Pa, Pl, Sk, Te, Th* description: Trace fossils are significantly more robust relative to those of other facies. Trace fossil suite generally displays low diversity. Lower BI values are found in association with units containing greater proportions of sandstone beds.	Sharp basal contact (locally demarcated by *Glossifungites* Ichnofacies) with F1, F9, F10, and F11; overlain sharply by F14)	Storm-influenced upper offshore. Heterolithic sediment suggests variable depositional energy. Oscillatory structures suggest a wave-dominated environment. Significantly more robust trace fossils suggests decreased environmental stress. However, lack of diversity may suggest brackish water conditions. A sharp basal contact demarcated by omission suites of the *Glossifungites* Ichnofacies is interpreted to result from wave ravinement during transgression.	FA5
F14	Bioturbated dark grey fissile shale with sand beds [Fig. 11C-E]	sediment: dark grey to black shale (0.5cm - >1m) interbedded with (<0.5cm - 5cm) sandstone layers. Sand-to-mud ratios vary from 10:90 to 50:50. thickness: 15m - 20m grain size: ≤vfU structures: lenticular bedding, wavy bedding, flaser bedding; in sands: oscillatory and combined-flow ripples, rare syneresis cracks; mudstone: internal laminae, graded bedding accessories: glauconite, pyrite nodules, rare carbonaceous detritus, mud clasts	BI: 2-5 traces: *As, Ch, Cy, Di, Pa, Ph, Pl, Sf, Sk, Ta, Te, Th, Zo* description: trace fossil suite is the most diverse found in the observed strata. Lower and more sporadically distributed BI values are found in association with intervals containing a greater proportion of sandstone beds.	Gradational basal contact with F13 (surface commonly demarcated by the *Glossifungites* Ichnofacies; traces are typically filled with glauconitic sand)	Storm-influenced distal offshore with prodeltaic overprint. Overall fine grain sizes and the most diverse trace fossil assemblages indicate low depositional energy and sedimentation rates. Traces are also positively correlated to marine conditions (*As, Ch, Ph, Zo*); rare storm influence (both waves and river outflows) is indicated by non-bioturbated sandstone beds containing oscillatory ripples, syneresis cracks and graded bedding. Distal expressions of the facies are more mud dominated, whereas proximal expressions are sandstone dominated with more sporadically distributed and reduced bioturbation. Basal erosion surfaces demarcated by glauconitic sand-filled omission suites of the *Glossifungites* Ichnofacies are interpreted to record wave ravinement during transgression.	FA5

Table 4.2. Facies associations interpreted in the McMurray Fm and the Wabiskaw Member of the Clearwater Fm in the study area

Facies Associations	Name
FA1	Fluvial and fluvio-tidal channel deposits
FA2	Deltaic and coastal plain deposits
FA3	Sheltered bay deposits
FA4	Delta-front and prodelta deposits
FA5	Lower shoreface and offshore deposits

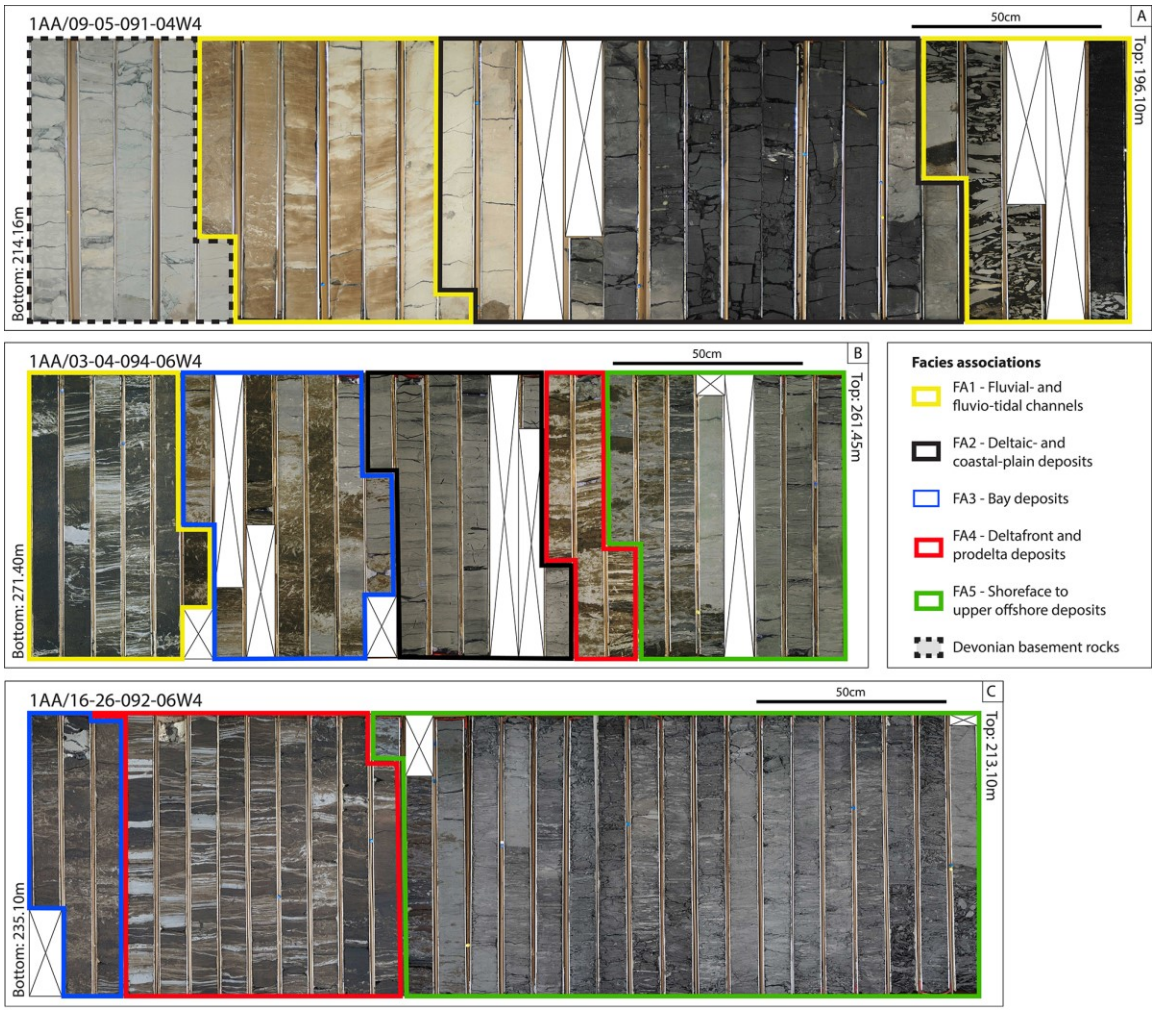

Figure 4.4. Three core successions displaying the five facies associations. Core successions are also shown as lithologs in Fig. *4.5*.

(A) Core 1AA/09-05-091-04W4 shows FA2 overlying FA1, and FA2 is erosively overlain by F2 of FA1. **(B)** Core 1AA/03-04-094-06W4 exhibits FA3 overlying FA1, and FA3 grades upwards into FA2. FA2 is overlain by FA4, and in turn, FA4 is overlain by FA5; the contact between FA2 and FA4 is sharp and the contact between FA4 and FA5 is erosive. **(C)** Core 1AA/16-26-092-06W4 exhibits FA3 sharply overlain by FA4, which itself is sharply overlain by FA5.

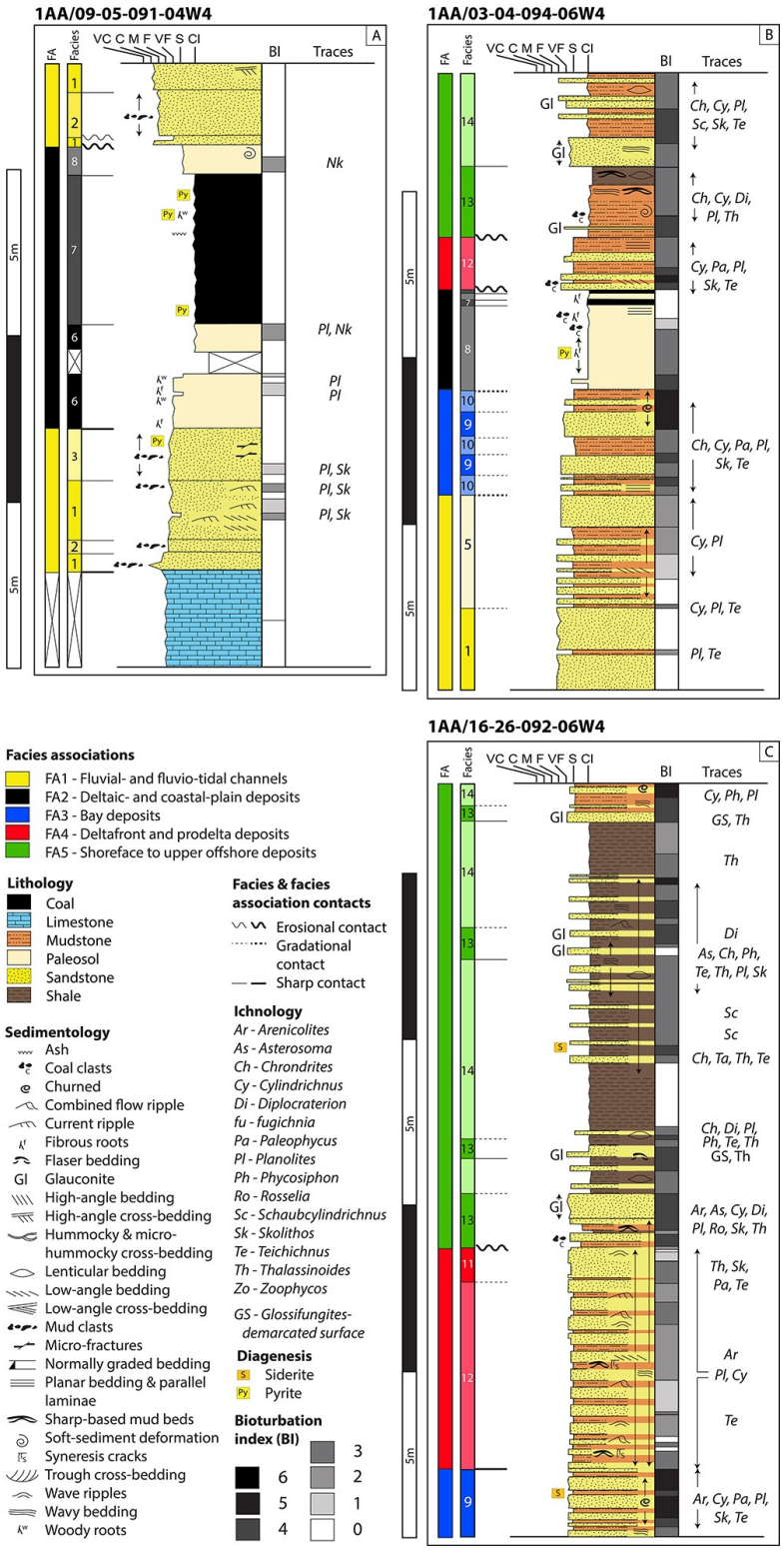

Figure 4.5. Facies and facies associations displayed on litholog representations of the cores in Fig. *4.4*

(A) 1AA/09-05-091-04W4, **(B)** 1AA/03-04-094-06W4**,** and **(C)** 1AA/16-26-092-06W4**.**

Facies Association 1: Fluvial and Fluvio-Tidal Channels

Facies association 1 (FA1) consists of facies F1–F5 (Fig. 4.6; Table 4.1), and is dominated primarily by dune-scale cross-stratified sand of F2 (Fig. 4.6A) and inclined interstratified sandstone and mudstone of F5 (Fig. 4.6F - H; commonly referred to as IHS; Thomas et al., 1987). FA1 typically displays an erosional basal contact (typically demarcated by F2; Fig. 4.6B), and comprises a vertical succession of F2 overlain by F5 (Figs. 4.4–4.5).

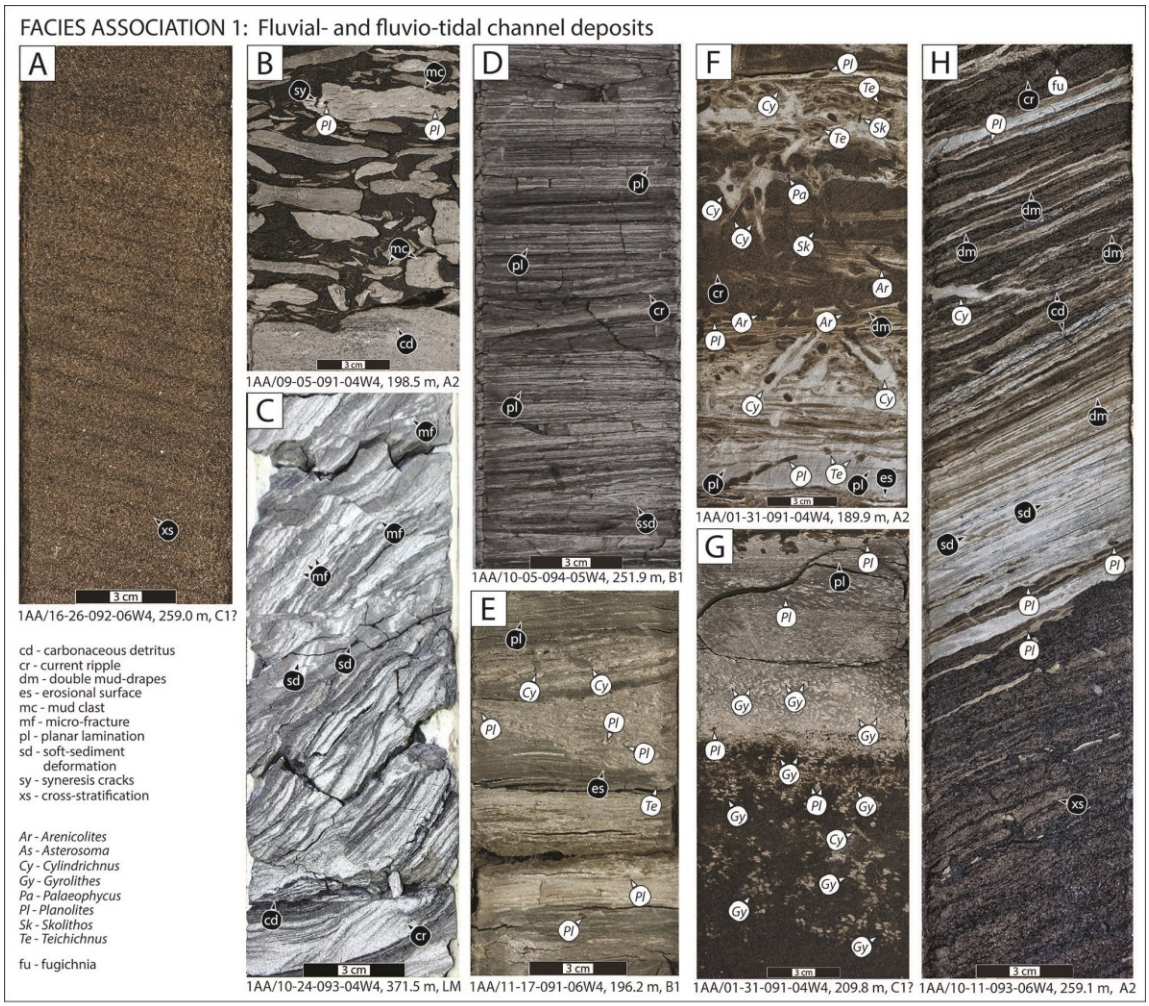

Figure 4.6. Core photographs of Facies Association 1: Fluvial and fluvio-tidal channel deposits.

White circles indicate trace fossils, and black circles indicate physical sedimentary features. Each photograph includes a UWI, depth in core, and stratigraphic position. **(A)** Facies 1 includes structureless and cross-stratified sandstones. **(B)** Facies 2 includes mud-clast breccias . **(C)** Facies 3 includes heterolithic deposits exhibiting soft-sediment deformation and micro-fractures. **(D)** Facies 4 includes finely laminated dark and light mudstones, as well as **(E)** mudstones interbedded with sharply based, bioturbated heterolithic sediments. **(F)** Facies 5 includes inclined sporadically

bioturbated IHS, **(G)** monogenerically bioturbated IHS, and **(H)** IHS that displays cross-stratification and double mud drapes.

FA1 is interpreted to represent fluvial and fluvio-tidal channel complexes. Structureless and cross-stratified sands (F1) are interpreted as channel thalweg dunes or dunes that formed on the lower parts of point bars. IHS (F5) deposits are interpreted as tidally influenced point bars and include those that lateral accrete, migrate downstream and develop as counter point bars. Within the channel complexes, deposition of channel abandonment facies (F4; Fig. 4.6D) can result from chute cut-off or avulsion (F3; Fig. 4.6C).

Facies Association 2: Delta and Coastal Plains

Facies association 2 (FA2) consists of facies F6–F8, with rare occurrences of F3 (Fig. 4.7; Table 4.1). FA2 is dominated by coal beds (F7; Fig. 4.7D) and two distinct rooted and organic-rich paleosols (F6, F8; Fig. 4.7A–C, E–F). FA2 typically displays a facies succession of F6 or F8 overlain by F7, and is most commonly observed at the tops of the Lower McMurray and the B1 DU (Fig. 4.4A–B, and Fig. 4.5A–B). In the Lower McMurray, eluviated paleosols (F6) typically occurs below F7. Gleyed paleosols (F8), locally overlain by F7, is the dominant expression of FA2 at the top of the B1 DU. FA2 commonly overlies channelized deposits (FA1) or bay deposits (FA3), and is in turn overlain by channelized FA1 or prodelta deposits (FA4) (Fig. 4.4A–B, 4.5A–B). While rhizoturbation is common, infaunal bioturbation is only rarely observed, characterized by occurrences of *Planolites* and *Naktodemasis* (Fig. 4.7E). Exceptions are noted where F8 deposits have a gradational contact with FA3. Such occurrences display the highest BI values and a more diverse trace-fossil suite (Fig. 4.4B).

FA2 is interpreted to represent various depositional environments that occur on delta and coastal plains. Facies 6 (e.g., Figs. 4.7A–C) is found largely in the Lower McMurray and contains both fibrous and woody rhizoliths, (e.g., Fig. 4.7A-B) and is interpreted as shrub- and woodlands associated with a well-drained paleosol resulting from longer-term base-level fall. Base-level enabled colonization by higher land-plants on the proximal portion of the delta or coastal plain. Prior to peat formation, longer-term base-level fall required higher land plants to develop deeper roots to reach groundwater. Furthermore, higher land plants require salinity not to inhibit plant growth and survival (Barrett-Lennard, 2003). In contrast, F8 (Fig. 4.7C) exhibits a gleyed appearance, typically

associated with a perennially high water table. While gleying has been attributed to both syn- and post-depositional reducing pore waters (e.g., Aitken and Flint, 1996), I interpret interbedding of tidal marshes (F8) with bay deposits (e.g., F9; Fig. 4.4B) to indicate that gleying was syn-depositional, as the groundwater table would have resided in close proximity to the surface. Additionally, interfingering of F8 with F9 is interpreted to suggest that tidal marshes served as the most distal (seaward) paleoenvironment of FA2, and fibrous rhizoliths stem from halophile plants.

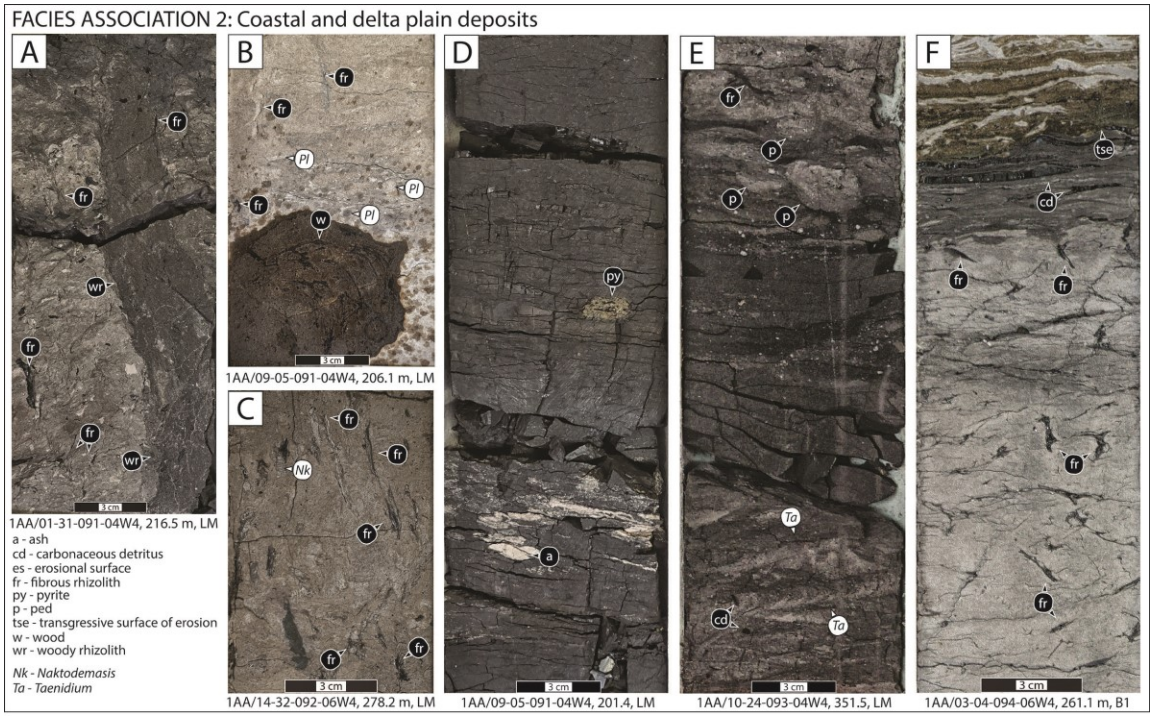

Figure 4.7. Core photographs of Facies Association 2: Deltaic- and coastal plain-deposits.

White circles indicate trace fossils, and black circles indicate physical sedimentary features. Each photograph includes a UWI, depth in core, and stratigraphic position. Facies 6 includes **(A)** deeply rooted and **(B-C)** eluviated paleosols. Facies 7 includes **(D)** coals and **(E)** organic-rich mudstones. Facies 8 includes **(F)** gleyed mudstones with frequent fibrous rhizoliths.

Coals (F7) form in coastal mires and swamps over both types of paleosols. Therefore, the mires in which peats were formed resulted from paludification (Diessel, 1992), and developed during base-level rise. However, while F7 overlying F8 displays a direct genetic relationship, F7 overlying F6 indicates a potential base-level fall prior to peat accumulation. Where FA2 is erosionally overlain by FA4, that surface is interpreted as a flooding surface.

Facies Association 3: Sheltered Bay

Facies association 3 (FA3) consists of F9 and F10 (Fig. 4.8; Table 4.1), and is typified by heterolithic deposits with consistently high intensities of bioturbation (BI > 4). FA3 typically displays a gradational contact with other facies associations (Fig. 4.4B, 4.5B), and only rarely exhibits a sharp basal contact. While trace fossils are commonly diminutive, the ichnological suites in FA3 exhibit the most diverse range of ethologies observed in the McMurray Fm. Regularly occurring trace fossils include *Asterosoma, Chondrites, Cylindrichnus, Planolites, Rosselia, Schaubcylindrichnus freyi*, *Skolithos,* and *Teichichnus* (Fig. 4.8).

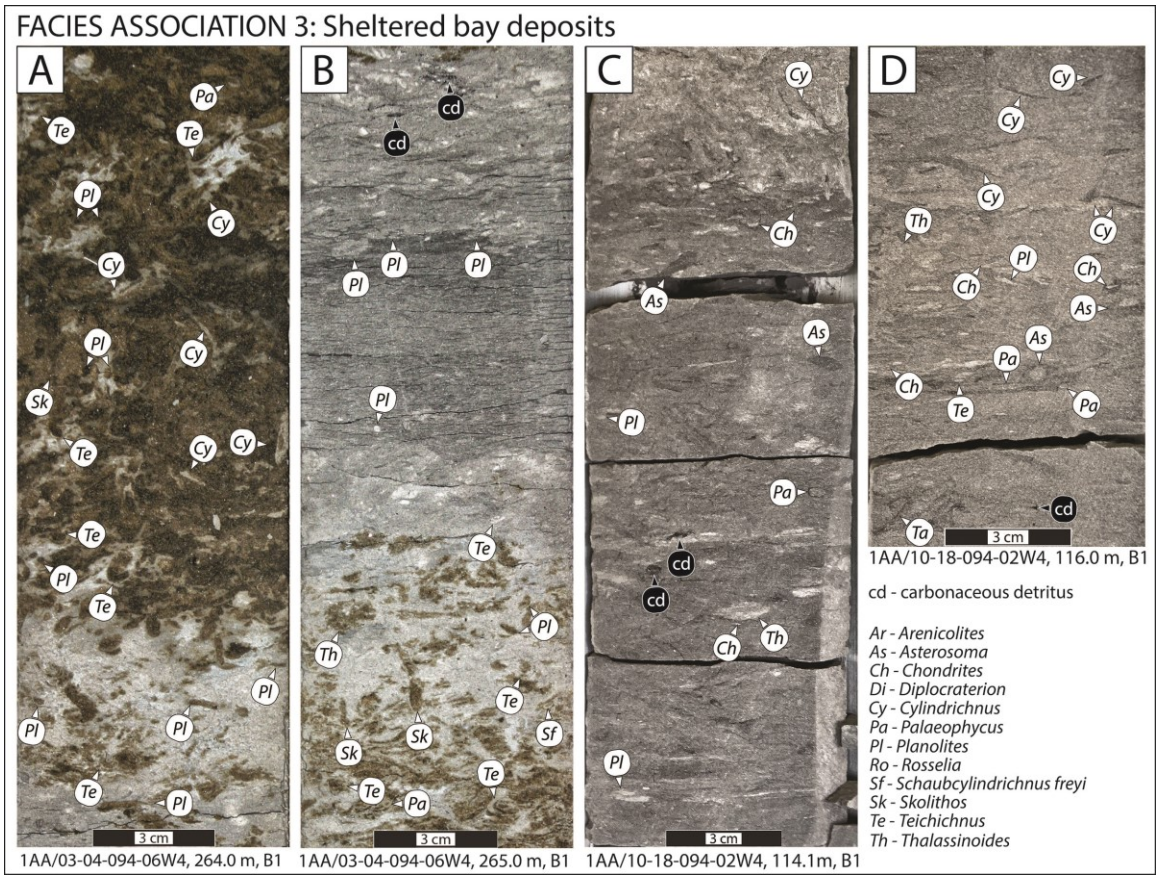

Figure 4.8. Core photographs of Facies Association 3: Sheltered bay deposits. White circles indicate trace fossils, and black circles indicate physical sedimentary features. Each photograph includes a UWI, depth in core, and stratigraphic position. **(A-B)** Facies 9 includes thoroughly bioturbared heterolithic deposits. **(C-D)** Facies 10 includes thoroughly bioturbated silty mudstones.

FA3 is interpreted to include both proximal tidal flat deposits (F9) and distal portions of bay environments with minimal fluvial input (F10). The minimal fluvial influence

on deposits resulted in low deposition rates, which is reflected by the high BI values, as well as less variable and more normal marine salinities favoring diverse trace-fossil assemblages. FA3 is therefore interpreted to have been deposited in coastal margin environments during transgression of the Firebag Tributary. In some cases, proximal tidal flat (F9) deposits of FA3 grade upwards into coastal-plain facies of FA2, and this is interpreted to represent gradual filling of bays. By contrast, F10 is interpreted to be more prevalent during later stages of transgression.

Facies Association 4: Wave-influenced to Wave-dominated Delta-Front and Prodelta

Facies association 4 (FA4) consists of cross-stratified sandstone with combined flow ripples and common escape structures of F11, (Fig. 4.9A) and variably bioturbated heterolithic sediment with oscillation ripples and non-bioturbated mud beds of F12 (Fig. 4.9B-C). Both facies are typified by sporadically bioturbated heterolithic strata exhibiting abundant oscillation-generated structures and erosionally based mudstone beds (Table 4.1). In rare instances, FA4 is floored by a mud-clast breccia (F2; Fig. 4.4A). FA4 is commonly dominated by F12 (Fig. 4.4C, 4.5C), but in uncommon occurrences, it comprises F12 overlain by F11.

FA4 is interpreted to represent prodelta to delta-front complexes. Deposition is interpreted to be driven by both high-energy (storm) waves (e.g., oscillation ripples, micro-HCS) and high-output fluvial discharge (erosionally-based non-bioturbated mud beds exhibiting syneresis cracks, interpreted as deposits of hyperpycnal mudflows; aggradational oscillation ripples, interpreted to result from elevated sediment discharge) resulting from heightened precipitation during storms (MacEachern James A. et al., 2005; Bhattacharya and MacEachern, 2009; Collins et al., 2017). High fluvial flow produced various physico-chemical stresses on infaunal communities including high sedimentation rates, as well as variation and general reduction of salinity. Where FA4 displays an erosive contact with an underlying interval of FA1 (Fig. 4.10A) or FA2 (Fig. 4.10B), locally demarcated by an imbricated mud-clast breccia, the contact is interpreted to represent a transgressive ravinement surface.

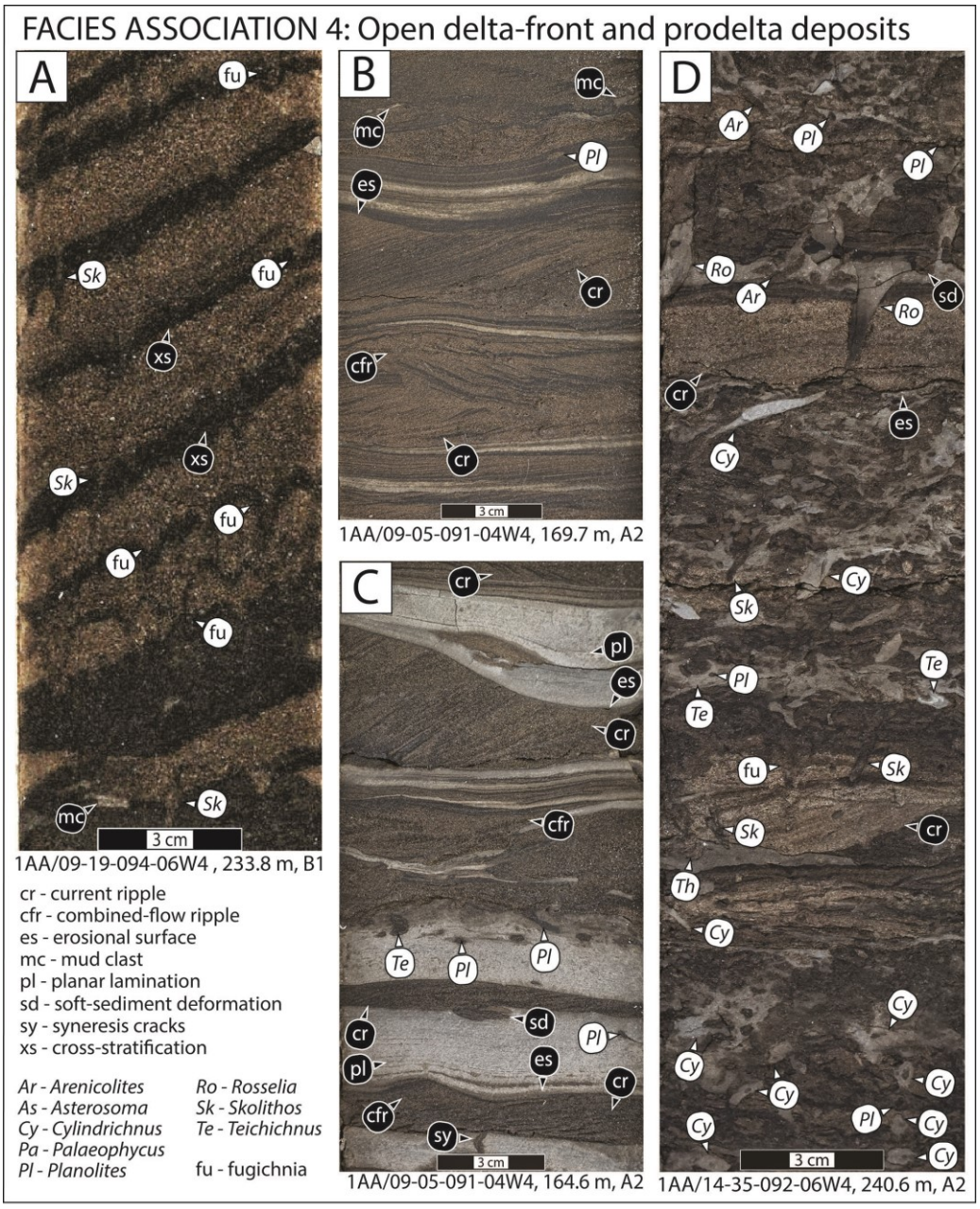

Figure 4.9. Core photographs of Facies Association 4: Delta-front and prodelta deposits.

White circles indicate trace fossils, and black circles indicate physical sedimentary features. Each photograph includes a UWI, depth in core, and stratigraphic position. **(A)** Facies 11 includes sandstones with uni-directional and oscillatory flow structures, as well as frequent escape structures. Facies 12 includes heterolithic deposits with **(B)** combined flow structures, **(C)** interpreted rapidly deposited fluid muds, and with **(D)** uncommon bioturbated intervals.

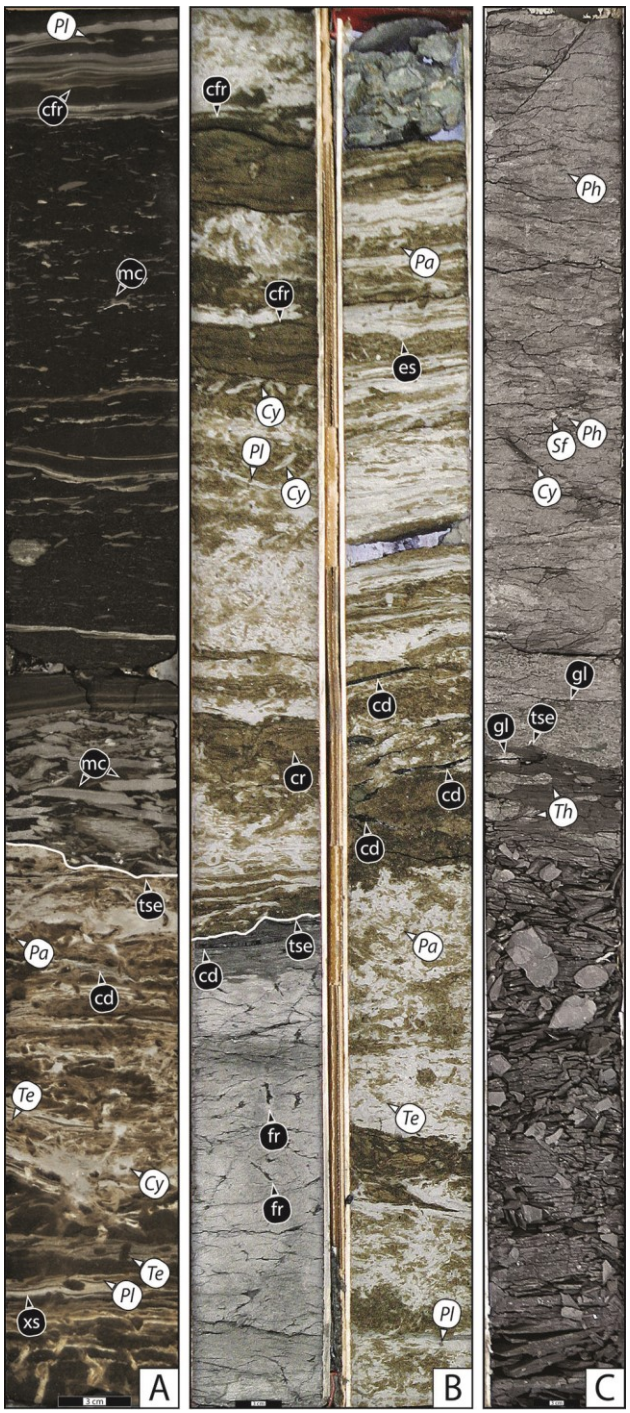

Figure 4.10. Three expressions of interpreted transgressive surface of erosion (tse) at the top of the B1 DU (A, B), and within the Wabiskaw Member of the Clearwater Fm (C).

(A) TSE between F4 (FA1) and F12 (FA4), demarcated by a ~10cm thick, imbricated mud-clast breccia (F2), in well 1AA/01-31-091-04W4 at a depth of 185.5 m. **(B)** TSE between F8 (FA2) and F12 (FA4) demarcated by a erosional surface of tidal marsh deposits. **(C)** TSE within stacked successions of FA5 showing a glauconite-filled *Thalassinoides* burrow, which demarcates this surface by the *Glossifungites* ichnofacies. Abbreviations can be found in figs. 4, 5 7, and 11.

Facies Association 5: Offshore to Lower Shoreface

Facies association 5 (FA5) consists of bioturbated, sanding-upward, blue-grey mudstone and sand of F13 and bioturbated dark grey fissile shale with sand beds of F14. Both facies are characterized by mud-rich heterolithic deposits and relatively robust trace fossils. FA5 is only observed from the Wabiskaw Member of the Clearwater Fm (Fig. 4.11; Table 4.1), and commonly comprises multiple stacked successions of F13 overlain by F14 (Figs. 4.4C, 4.5C). In addition, F13 commonly exhibits a basal *Glossifungites* Ichnofacies-demarcated surface (Fig. 4.11B), wherein sharp-walled, firmground ichnogenera such as *Thalassinoides* are filled with glauconitic sand.

Fluvial influence is inferred through the presence of graded beds and current ripples with carbonaceous detritus and non-bioturbated sand beds. Overall, however, FA5 exhibits the most distal appearance of all observed FAs. FA5 is interpreted as a vertical succession of lower shoreface sands grading up into offshore deposits, recording the widespread stepwise transgression of the Boreal Sea. Basal *Glossifungites* Ichnofacies-demarcated surfaces are interpreted to represent wave ravinement surfaces generated during transgression.

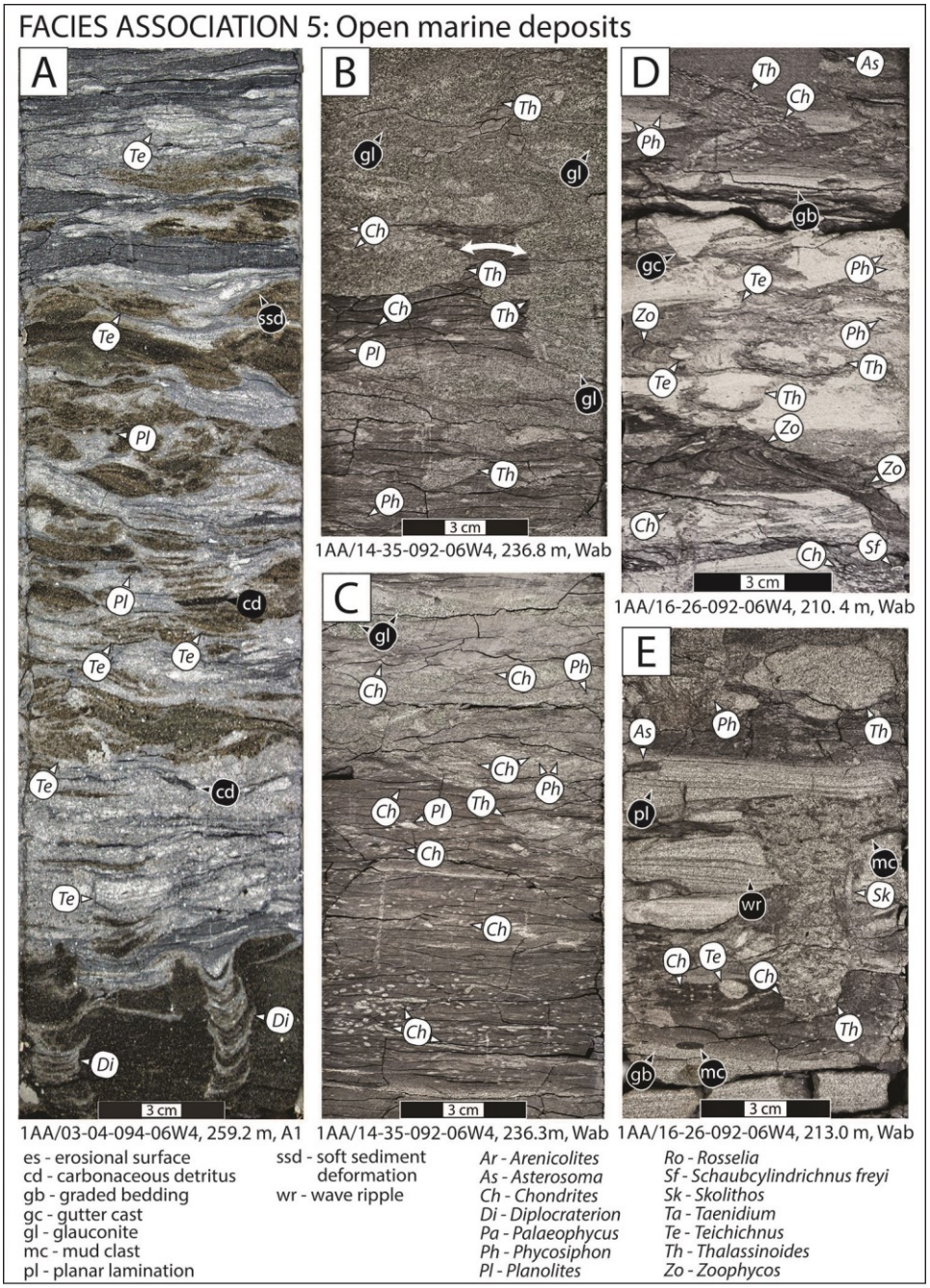

Figure 4.11. Core photographs of Facies Association 5: Lower shoreface and offshore deposits.

White circles indicate trace fossils, and black circles indicate physical sedimentary features. Each photograph includes a UWI, depth in core, and stratigraphic position. **(A)** Facies 13 includes bioturbated blue grey mudstones interbedded with sand beds, and **(B)** frequent sharp basal surfaces demarcated by the *Glossifungites* ichnofacies exhibiting glauconite infill (white arrow). **(C–E)** Facies 14 includes bioturbated fissile shales interbedded with unbioturbated sand beds.

4.4.2. Stratigraphic Correlations and Depositional History

Three west-to-east cross-sections (Fig. 4.12) that run approximately parallel to depositional dip in the Firebag Tributary, and stacking patterns of DUs and FAs within DUs allow for the identification of systems tracts and correlation of stratigraphic breaks. An additional south-to-north cross-section (Fig. 4.13) runs approximately along depositional strike. For correlation of McMurray Fm strata across the Firebag Tributary, I use the top of the McMurray Fm (top of the A1 DU; Figs. 4.12 and 4.13) as the datum. While this datum is not optimal, owing to evidence of local erosion across the study area (Fig. 4.4), the thickness of the overlying Wabiskaw Member of the Clearwater Fm is relatively uniform (LCW; Fig. 4.12), suggesting that removal of strata was not pronounced and distortion of stratigraphic architecture likely to be minimal. In addition, the top of the A1 DU is readily identified in both core and on well logs (e.g., Figs. 4.5B–C).

In the Firebag Tributary, individual DUs in the McMurray Fm comprise thick regressive packages separated by thin transgressive packages. Regressive packages within DUs largely consist of thick (up to ~50 m) channelized successions of FA1 (mostly F1 and F5) and/or are overlain by ~3-10m thick successions of delta-associated FA4 (e.g., 4.12A). Successions of FA1 commonly show erosive basal contacts that have cut through and removed underlying stratigraphic contacts (e.g., 1AA/02-01-094-07W4; Fig. 4.12A). Transgressive packages are expressed as ~0.5–10 m successions of coals (F7) and gleyed paleosols (F8) of FA2 (e.g., regionally at top of Lower McMurray and B1 DU; Fig. 4.12A), and as rare, thin (<1 m) occurrences of FA3 (e.g., locally at the top of B1 DU, 100/10-18-094-02W4; Fig. 4.12B).

Deposition of the Lower McMurray is dominated by thick channel deposits of FA1. Channel successions consist largely of cross-stratified sands (F1) and mud-clast breccias (F2) (e.g., Fig. 4.12C). In the Lower McMurray, FA1 is typically overlain by delta and coastal plain packages of FA2, commonly expressed as shrub- and woodland facies (F6; Figs. 4.7A-C) overlain by coastal mires (F7; Figs. 4.7D-E, 4.12A). In rare instances, and coinciding with paleo-topographic lows on the SCU, the coal seam at the top of the Lower McMurray comprises multiple sub-seams (e.g., 1AA/10-24-093-04W4; Fig. 4.13).

Individual stratigraphic intervals are challenging to distinguish during deposition of the C2-B2 DUs in the Firebag Tributary. Widespread erosion of stratigraphic surfaces

results from both contemporaneous and post-depositional channels (Figs. 4.12, 4.13), as well as progressive Pleistocene glacial erosion and removal of stratigraphic datums towards the eastern extent of the study area (marked by a sharp contact with overlying diamict). Consequently, stratigraphic correlations of DUs C2–B2 must be treated with caution. Deposits of the C2-B2 DUs largely comprise thick successions of FA1 (most commonly F1 overlain by F5), which are rarely overlain by thin intervals of FA3 and FA4 in the western portions of the study area (e.g., 1AA/14-32-091-05W4, 1AA/01-31-091-04W4; Fig. 4.12C, and 1AA/09-06-090-05W4; Fig. 4.13). Interestingly, while the top of the McMurray Fm is not preserved in well 131/15-28-095-25W3 (Fig. 4.12A), multiple intervals of paralic strata occur in the vertical succession. These paralic strata probably correspond to DUs that resided further to the west, although the exact correlation of paralic strata to DUs is uncertain.

Deposition of the B1 DU is commonly characterized by thick successions of FA1 overlain by delta- and coastal-plain deposits of FA2. FA1 deposits are dominated by channel thalweg facies (F1) overlain by thick fluvio-tidal pointbars (F5). These channelized deposits are overlain by a <7 m thick succession of FA2, consisting of tidal marsh deposits (F8) overlain by coastal mires (F7). Coals found at the top of the B1 DU are significantly thinner (rarely exceed 2 m in thickness) than those at the top of the Lower McMurray. In rare instances, there is a thin interval of thoroughly bioturbated distal bay facies (F10) overlying coals and underlying deltaic strata of FA4 (e.g., 100/10-18-094-02W4; Fig. 4.12B). The top of the B1 DU is also locally demarcated by an abandoned channel, which transitions into a shaly coal (F7) upwards (e.g., 1AA/14-35-092-06W4; Fig. 4.12C).

DUs A2 and A1, as well as facies of the Wabiskaw Member of the Clearwater Fm largely comprise deltaic (FA4) and shallow-marine (FA5) strata, crosscut by channel facies of FA1. Where the DUs are not removed by channels, basal contacts commonly are scoured. In core, this scoured contact is overlain by a thin (<0.5 m) mud-clast breccia (F2) with clasts showing imbrication (Fig. 4.10A). Elsewhere, the surface is overlain by deposits of FA4 or FA5 with common organic detritus and pebbles (Fig. 4.10B). In the Wabiskaw Member of the Clearwater Fm and where the scoured surface is overlain by FA5, it is commonly demarcated by firmground *Diplocraterion* and *Thalassinoides* filled with glauconite, corresponding to an omission suite of the *Glossifungites* Ichnofacies (Fig. 4.10C).


A' (NW)
A (NE)
LCW
A1
A2
B1
B2
C1
C2
LM
datum
Pleistocene
NDP (%)
Grainsize
A
B' (SW)
B (NE)
B
C' (SW)
C (SE)
C
Well-drained paleosol (F6)
Coal (F7)
Gleyed paleosol (F8)
Datum
TSE
Channel

Figure 4.12. Three dip-oriented cross-sections through Firebag Tributary, which show correlations (and probable correlations) of regional DUs.

Many surface picks (e.g., Top C1) through Firebag Tributary are low confidence due to extensive removal of strata by subsequent channel incision. Where strata is removed or correlations are uncertain, surfaces are shown as dashed lines. The position of the 3 cross sections is shown on Figure 3, and include one in the northern study area (**A**; A'-A), one in the central study area (**B**; B'-B), and one in the southern study area (**C**; C'-C). Each cross-section includes 7 wells. Individual core-logs show lithology, BI, and neutron- and density-porosity logs. Where only well-logs exist, both the gamma-ray log, and neutron- and density-porosity logs are shown. Cross-sections include all depositional units of the McMurray Formation and the Wabiskaw Member of the Clearwater Formation. The top of the A1 DU is the datum. All three cross-sections highlight the positions of well-drained paleosols (F6), coals (F7), and gleyed paleosols (F8). Two yellow stars show the position of ash beds sampled for zircon in the coal seam situated towards the top of the B1 depositional unit (A'-A; 1AA/02-03-095-03W4), and the ash bed towards the top of the Lower McMurray (C'-C; 1AA/09-05-091-04W4; Rinke-Hardekopf et al., 2019).

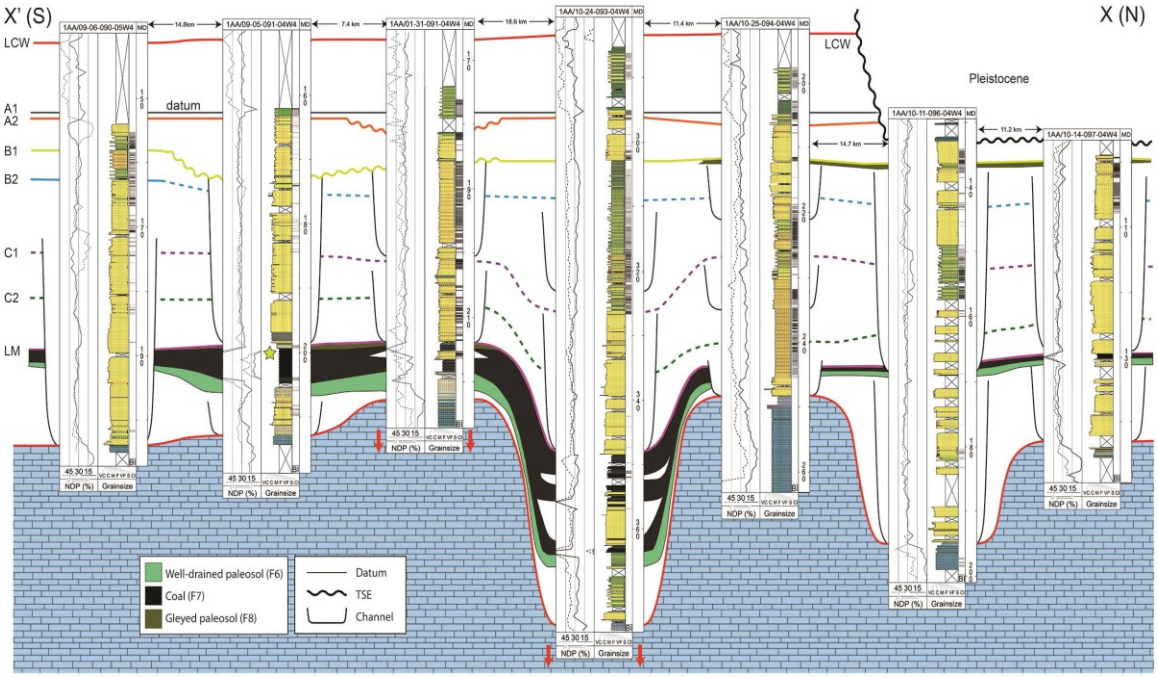

Figure 4.13. Along-strike cross-section through Firebag Tributary that runs approximately south to north.

The cross-section shows the correlations (and probable correlations) of regional DUs. Many surface picks (e.g., Top C1) through Firebag Tributary are low confidence due to extensive removal of strata by subsequent channel incision. Where strata is removed or correlations are uncertain, surfaces are shown as dashed lines. . The position of the cross section is shown on Figure 3. Individual core-logs show lithology, BI, and neutron- and density-porosity logs. Cross-sections include all depositional units of the McMurray Formation, and the Wabiskaw Member of the Clearwater Formation (LCW). The top of the A1 depositional unit is the datum. Tops of certain depositional units are removed by channels or by transgressive surfaces of erosion (TSE). The cross-section also highlights the positions of well-drained paleosols (F6), coals (F7), and gleyed paleosols (F8).

4.4.3. Isopach Mapping

The McMurray Fm isopach map of the Firebag Tributary reveals strata that range in thickness from 30–110 m (Fig. 4.14). Isopachs were created in Petrel using the convergent interpolation algorithm. However, isopachs were excluded where no wells within a 10km radius included both the SCU and the top of the McMurray Fm (i.e., northeastern and southeastern study area; Fig. 4.3), as unchecked results of the convergent interpolation algorithm are not deemed meaningful (Fig. 4.14).

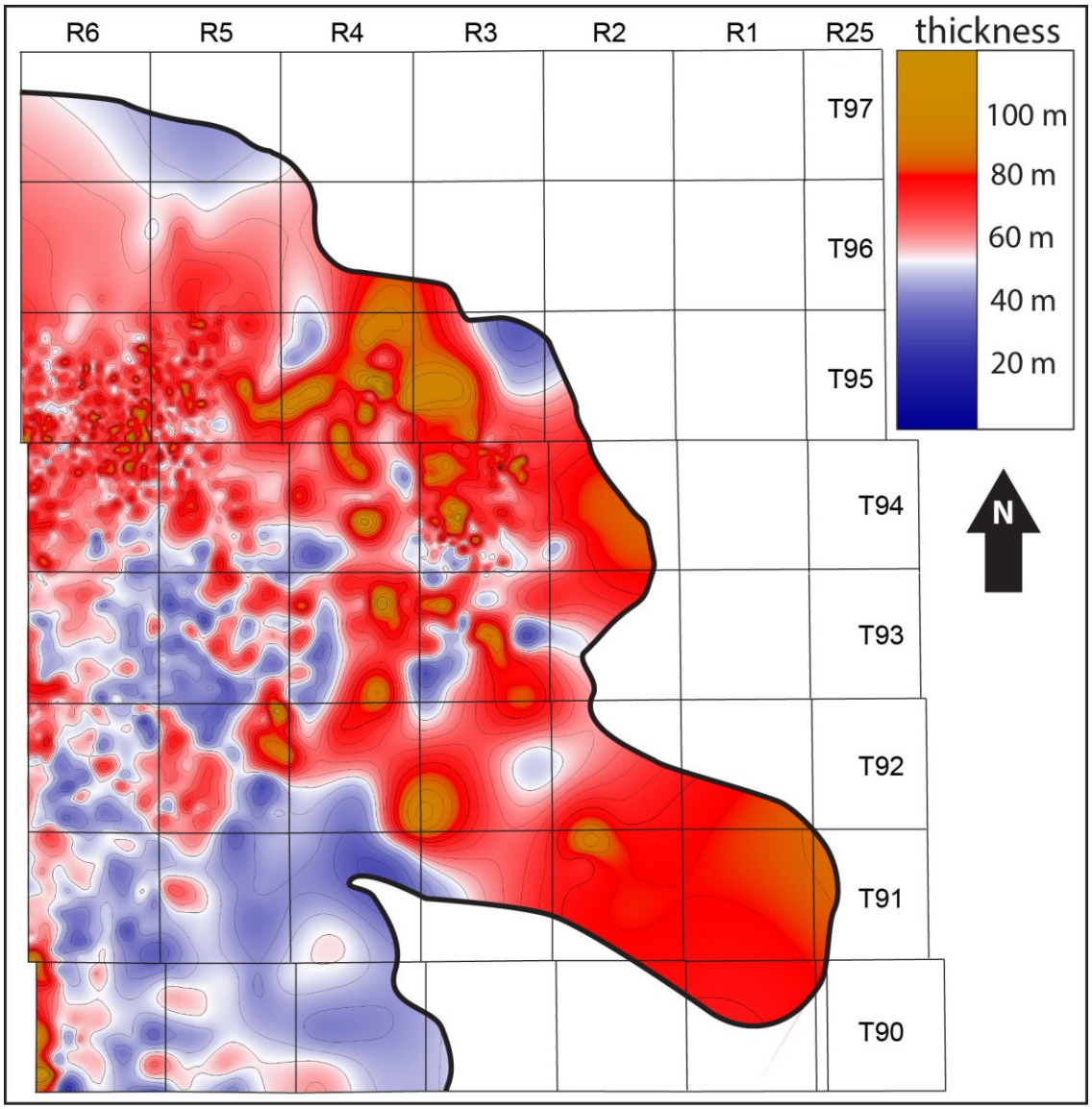

Figure 4.14. McMurray Formation isopach map in Firebag Tributary.
Blues depict thin McMurray strata and reds and browns depict thick strata. The grey outline is the DLS grid. The thick black outline provides a 10km radius around well logs that preserve the top of the McMurray Formation. McMurray Formation strata extend beyond the contoured area, but are

of an unknown thickness. Data points for this figure are derived from all wells used in this study (n = 1865) that preserve the top of the McMurray Formation (Fig. 4.2).

The McMurray Fm is thinnest in the southern portion of Firebag Tributary (e.g., T91-R6, T91-R5; Fig. 4.14), and thickest in the eastern to northern reaches (e.g., T92-R3, T95-R3; Fig. 4.14. Laterally restricted (thin) “ribbons” of thick strata crosscut regions of relatively thin strata in the southern part of Firebag Tributary (e.g., T92-R5, T93-R3; Fig. 4.14). Exceptionally thick packages of McMurray Fm strata (i.e., light browns; Fig. 4.14) are commonly found in areas with thick successions of FA1 (e.g., 1AA/03-03-091-01W4; Fig. 4.12C), and/or in areas where split coal seams have been observed and attributed to syn-depositional basement subsidence (e.g., 1AA/10-24-093-04W4; Fig. 4.12B, see Rinke-Hardekopf et al., 2019).

4.4.4. CA-TIMS

Thirteen zircon grains were recovered from an ash layer encased in a coal seam at the top of the B1 DU in well 1AA/02-03-095-03W4 (Figs. 4.12A, 4.15A). Seven of these grains were chosen for thermal annealing and chemical abrasion, and 6 were dated using CA-TIMS (1 zircon dissolved during chemical abrasion). The zircon grains ranged from approximately 50–150 μm long and 10–60 μm wide, and included both rounded and prismatic (euhedral) morphologies (*Supplementary Materials A*). Four of the 6 dated grains yield ages between 167 Ma and 1711 Ma, and are clearly detrital in origin. Two of the grains, however, returned overlapping ages of 115.05 ± 0.20 Ma and 115.11 ± 0.26 Ma (Fig. 4.15B). Although the sample size is small, 2 of 6 grains represents approximately 33% of the sample, and this is significantly higher than the regional occurrence of young zircon in the McMurray Fm, which is less than 0.4% (Rinke-Hardekopf et al., 2021). A weighted mean average of the 2 youngest grains yields an age of 115.07 ± 0.16 Ma (mean standard weighted deviation: 0.045, probability of fit: 0.83).

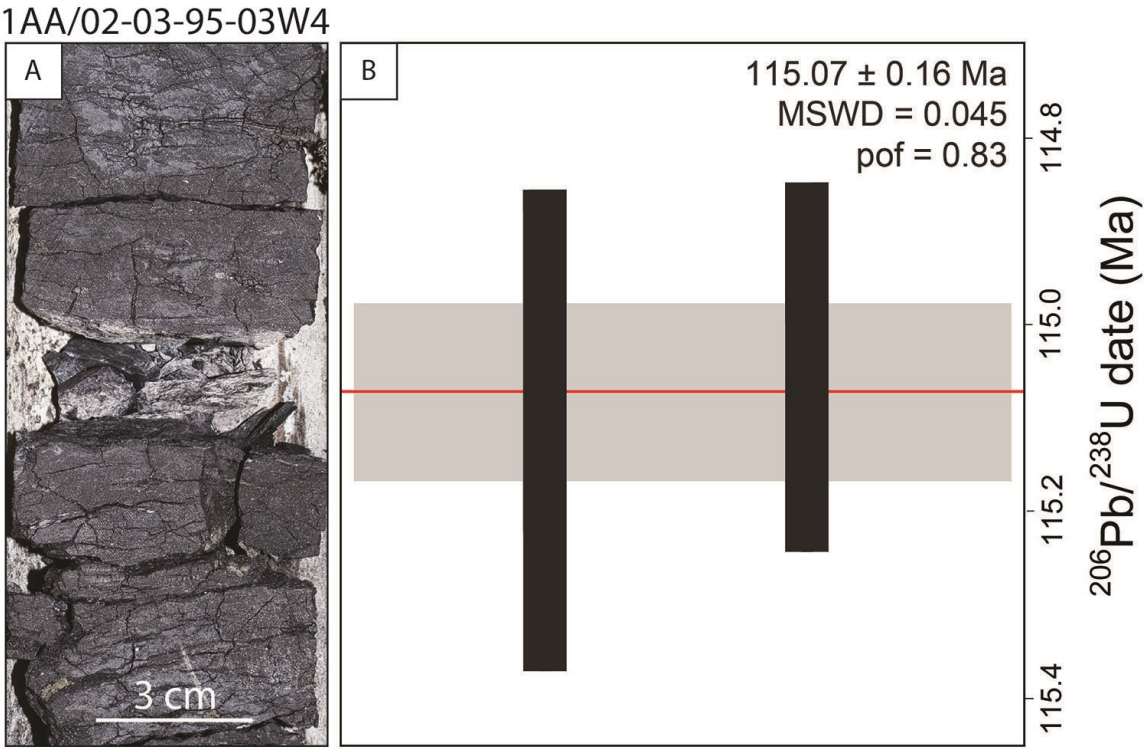

Figure 4.15. New high precision maximum depositional age for the B1 DU.
(A) White betonitic ash bed situated in a coal seam at the top of the B1 depositional unit in core 1AA/02-03-095-03W4 at 165.0m depth. The location of the ash bed within the core succession can be found in Fig. 4.12A (1AA/02-03-095-03W4. **(B)** CA-TIMS derived ages of the youngest single zircon grains (black boxes give 2σ error around the determined CA-TIMS age) found within the ash bed and show a tight age cluster. IsoplotR (Vermeesch, 2018b) was used to calculate a weighted mean average age these grains: 115.07 ± 0.16 Ma (red line, and grey box), with a mean standard weight derivation (MSWD) of 0.045 Ma, and a probability of fit (pof) of 0.83.

4.5. Discussion

4.5.1. Stratigraphic Breaks Expressed in Paralic Strata of the McMurray Fm in Firebag Tributary

Paralic sedimentary facies in the McMurray Fm in Firebag Tributary define 3 distinct depositional environments: permanent shrub- and woodlands (F6), coastal and delta mires (F7), and tidal marshes (F8). Paralic sedimentary strata are particularly dominant at the top of 2 depositional units in the Firebag Tributary: Lower McMurray and B1 DU (Figs. 4.12, 4.13). At the tops of these DUs, F6 formed during base-level fall and represent major regressive surfaces. Both F7 and F8 formed during base-level rise and demarcate transgression of the Firebag Tributary. As they are overlain by deltaic FA4 or channelized FA1, both the top of F7 and F8 can both demarcate major flooding surfaces. However, F8 only constitutes the major flooding surface when not overlain by F7. By

extension, the tops of F7 and F8 can correlate to the bases of regional marine mudstones found elsewhere in the basin, where they are used to subdivide the regional stratigraphy of the McMurray Fm (e.g., Ranger and Pemberton, 1997; Hein et al., 2013; Château et al., 2020). During deposition of DUs C2–B2, paleosols and coals are only found at the tops of DUs towards the eastern margin of the study area (e.g., well 131/15-28-095-24W3; Fig. 4.12A). I note, however, that the correlation of these strata to regional DUs is highly interpretative because: 1) channels locally erode these regional surfaces throughout Firebag Tributary (Figs. 4.12, 4.13); 2) the datum towards the eastern edge of the study area has been removed by Pleistocene glacial erosion (Fig. 4.3); and 3) there is soft-sediment deformation potentially associated with local syndepositional subsidence (e.g., well 131/15-28-095-24W3). Distinguishing between distinct types of non-coal paleosols (i.e., F6 or F8) is imperative for determining whether they define valley margins and are associated with a subaerial unconformity formed during valley incision (Zaitlin et al., 1994), or are paralic depositional environments that are not associated with sediment bypass (Pattison, 2019b).

Coal seams (F7) found at the top of the Lower McMurray and B1 DUs both exhibit a wetting-upward character (Fig. 4.2A), and largely formed through paludification over a paleosol (Fig. 4.7; Diessel et al., 2000; Plint and Wadsworth, 2003; Rinke-Hardekopf et al., 2019). Similar to other coals in the eastern Alberta Foreland Basin, peat formation on coastal plains of low-accommodation settings distal to the Canadian Cordillera appear to more commonly result in wetting-upward coal seams (Chalmers et al., 2013). The two prominent coal-bearing intervals in the McMurray Fm differ in the paleosol facies, which they overlie. Whereas the coal seam at the top of the Lower McMurray is underlain by the mature paleosol facies (F6), the coal seam at the top of the B1 DU is largely underlain by the hydromorphic paleosol facies (F8) (Figs. 4.4A–B, 4.7, 4.12).

Paleosols found below the coal seam at the top of the Lower McMurray are dominantly well-drained (F6), and indicate a longer duration of non-deposition prior to peat formation (Wright and Marriott, 1993; Kraus, 1999). The mature and eluviated character of F6 (large woody rhizoliths, mottled texture associated with peds, coarser sediment; Figs. 4.7A–C) is interpreted to suggest pronounced base-level drop and valley incision during paleosol formation, wherein plant roots were required to access deep groundwater (Wright and Marriott, 1993; Plint et al., 2001; Kraus and Hasiotis, 2006; Tabor et al., 2017). While F6 could have formed in a significantly more proximal position than F7 and F8, many

of the fibrous rhizoliths found in F6 are similar to those found in F8 (Figs. 4.7A, C and F), suggesting that these could have formed closer to the paleoshoreline prior to base-level fall and mature soil formation. In addition, reconstructions of early Cretaceous climate for moderate to high latitudes do not appear to suggest a shift from arid to humid conditions in the Aptian (Leckie et al., 1989; Hay and Floegel, 2012). Therefore, I interpret the top of F6 in the Lower McMurray to represent a maximum regressive surface, and the top of the overlying coal to represent a major flooding surface.

Paleosols underlying the coal seam near the top of the B1 DU are dominated by the tidal marsh paleosol facies (F8; Figs. 4.4B, 4.7F, 4.12A), and these characteristics suggest that there was no major base-level fall prior to peat formation. Towards the top of the B1 DU, F8 displays abundant fibrous rhizoliths, sporadically distributed bioturbation, a grey matrix, and a gradational and/or interbedded relationship with FA3 (Figs. 4.4B, 4.5B). Gleying and interbedding with shallow-marine strata are interpreted to represent paleosol formation during a high or rising base-level, with grey discoloration related to pore-water chemistry during deposition rather than to post-depositional gleying (Retallack, 1991). These hydromorphic and weakly developed paleosols are commonly observed on delta and coastal plains undergoing aggradation as base level rises during the TST, or potentially the late LST / early HST (Wright and Marriott, 1993; Kraus, 1999; Gani et al., 2015; Amorosi et al., 2017). While coals in the Lower McMurray likely formed throughout the TST, hydromorphic soils and thinner coals of the B1 DU overly fluvio-tidal channels of FA1 and likely only formed in the latest TST as bank margins began to stabilize, however prior to progradation of the channel systems. Similar to recent observations of shallow-marine strata in the McMurray Fm, I interpret F8 as delta and coastal plain deposits that formed contemporaneously with parasequences actively fed by channel belts (Baniak and Kingsmith, 2018; Château et al., 2019, 2020; Weleschuk and Dashtgard, 2019). The depositional system within the Firebag Tributary was probably more akin to a series of deltas that formed in an overall transgressive system, such as is envisioned for Campanian strata in the Book Cliffs in Utah and Colorado, USA (Pattison, 2018, 2019a, 2019b). The paucity of evidence supporting sediment bypass in the B1 DU strengthens the interpretation that 4th order relative sea-level fluctuations (i.e., base-level falls) did not necessarily result in deeply incised valleys that formed post-depositionally (e.g., Ranger and Pemberton, 1997; Alberta Energy and Utilities Board, 2003; Hein and Cotterill, 2006; Hein et al., 2013; Horner et al., 2018).

Finally, F7 (coal) and F8 (gleyed paleosol) are found laterally adjacent to one other at the top of the B1 DU in Firebag Tributary, and the tops of both facies are interpreted to demarcate the same major flooding surface, with one exception. Where shaly coals form over an abandoned channel (F4, Fig. 4.6D; 1AA/02-01-094-07W4, Fig. 4.12A), they should be considered part of the early HST (Plint et al., 2001) and the top of F4 interpreted as the major flooding surface.

4.5.2. Understanding Paleoshoreline Trends by correlating between Paralic and Shallow-Marine Strata

Correlation between regional marine flooding surfaces and the tops of paralic deposits in Firebag Tributary allows for critical assessment of trends pertaining to the position of the paleoshoreline. McMurray Fm strata in Firebag Tributary are dominated by fluvial- and fluvio-tidal channels (FA1; Fig. 4.6), and removal of regional stratigraphic surfaces is common (Figs. 4.12 and 4.13). No individual cores or wells preserve all deposits at the tops of all DUs (Lower McMurray to B1; Fig. 4.12), although preservation of paralic strata is more common on paleo-topographic highs where channelized deposits of FA1 are less prevalent (Fig. 4.13).

In the McMurray Fm isopach map (Fig. 4.14), the thickest strata are interpreted to represent the positions of major or persistent channel belts. Cross-sections in Figs. 4.12 and 4.13 exhibit thick channelized facies in certain locations, whereas other wells appear to showcase thinner channels. I interpret consistency of thick channelized *versus* non-/ or thin channelized strata to result from channels only migrating within their larger nested channel belt system, which commonly follows paleotopographic lows on the SCU (Fig. 4.16). The orientation of paleotopographic lows, and by extension the interpreted orientation of channel belts, aligns well with the isopach of channel complexes interpreted by Hein et al. (2007) and with dip-meter data (Gray, 2019). In all cases, channels are interpreted to have a southeast to northwest orientation in southern Firebag Tributary, and an east-west orientation in central Firebag Tributary (Fig. 4.16). All channels drain towards the Bitumont Trough (e.g., Ranger, 1994; Broughton, 2014). Where paralic strata are preserved, these areas generally correspond to paleotopographic highs (e.g., T92-91, R5-4; Figs. 4.13 and 4.16), and widespread vegetation is interpreted to have stabilized bank margins (van Asselen et al., 2009; Ielpi and Lapôtre, 2020). Based on the presence or absence of paralic strata, I subdivide McMurray Fm in Firebag Tributary into 4 phases of

deposition: 1) progradational phase 1 (PP1), which comprises the Lower McMurray; 2) retrogradational phase 1 (RP1), which comprises the C2–B2 DUs; 3) progradational phase 2 (PP2), which comprises the B1 DU; and 4) retrogradational phase 2 (RP2), which comprises the A2 and A1 DUs (Fig. 4.17).

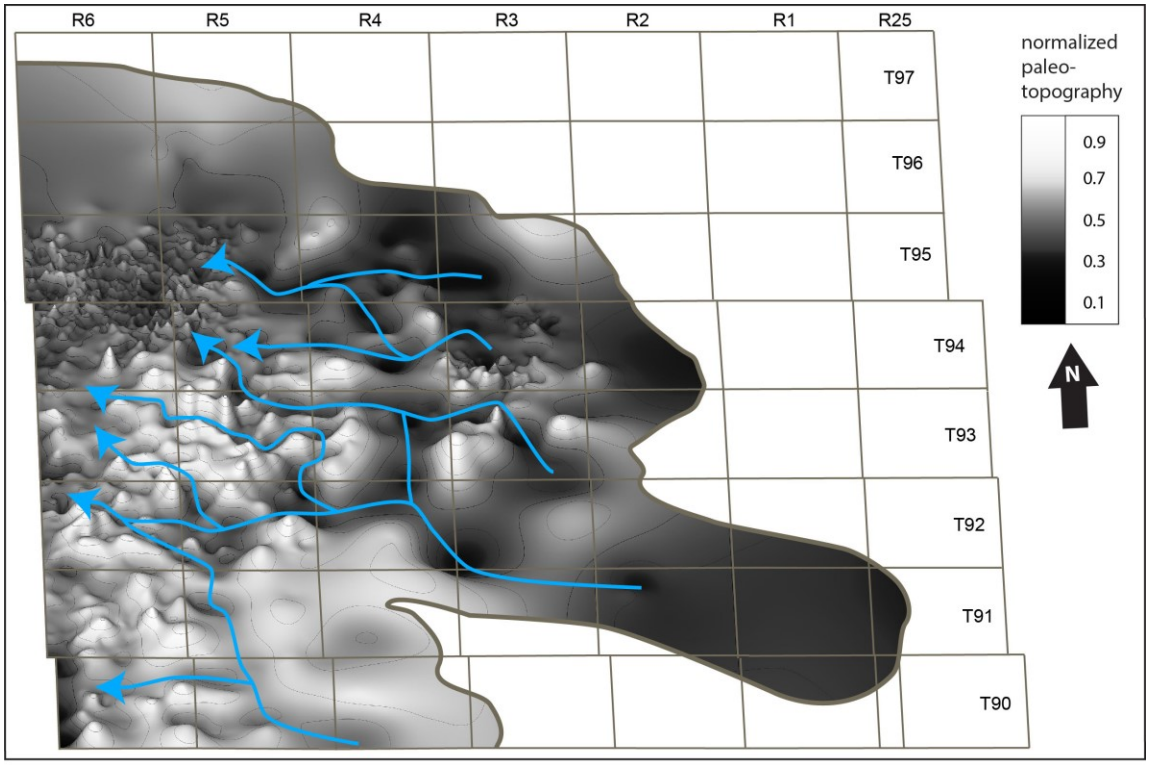

Figure 4.16. Oblique view of the reconstructed paleo-topography of the SCU at the end of McMurray Fm deposition.

Normalized values are created for each well that preserves the entire McMurray Formation (Fig. 4.2; n = 1865), by dividing the minimum thickness of the McMurray Formation by the thickness of the McMurray Fm in the respective well (i.e., the thickest McMurray Fm strata produce the smallest values, and by extension appear as paleo-topographic lows; view is 500fold exaggerated). The outline of the map is the same as in Fig. 14. The darkest values in the plot represent the smallest values of the normalized paleo-topography and are interpreted to represent the most likely locations of major channel belt systems (displayed as blue arrows).

The Lower McMurray defines PP1, and paleosols indicating a more pronounced base-level fall (F6) under the widely observed coal seam suggests a period of major shoreline progradation during Lower McMurray times (Figs. 4.11). The paleoshoreline was likely located at the western edge of the Firebag Tributary (Fig. 4.17A). The coal seam overlying the well drained paleosol records the earliest major southward transgression of the Boreal Sea during McMurray time, and has been shown to demarcate an arcuate-shaped proximal shoreline in the Firebag Tributary as far east as R5-3 (Fig. 4.14; Rinke-

Hardekopf et al., 2019). As well, locally thick coals also created accommodation through autocompaction on the order of 0.1-10s of mm/yr (Törnqvist et al., 2008; van Asselen et al., 2009; Sahoo and Gani, 2016; Mulhern and Johnson, 2017), which may explain why nearly all occurrences of thick Lower McMurray coals are overlain by fluvial and fluvio-tidal channels (FA1) that down-cut from overlying DUs (Fig. 4.12). For example, Sahoo and Gani (2016) showcase how differential compaction of precursor mires in the Cretaceous Blackhawk Fm in Utah autogenically modulated the positions of incised valleys, and/or was the driving force of accommodation space creation.

Depositional units C2, C1, and B2 define RP1. Therein, paralic strata are only found towards the eastern edge of the study area, which is interpreted to reflect major retrogradation of the paleoshoreline in the Firebag Tributary (Fig. 4.17B), likely close to the Alberta-Saskatchewan border (Fig. 4.12A). Paleoshorelines are challenging to attribute to specific depositional units due to prevalence of Pleistocene glacial erosion and resultant deformation (Figs. 4.12A-B, 4.13); however, several paleosol (F6 and F8) and coal successions can be found in well 131/15-26-095-25W3 (Fig. 4.12A) and likely approximate the position of the shoreline during this time. While strata of these DUs are most commonly dominated by channelized FA1 (similar to the Lower McMurray), FA1 in the C2-B2 DUs are more commonly dominated by the tidally modulated point bars of F5, which typically encompass a brackish-water trace fossil assemblage (e.g., Pemberton et al., 1982; Gingras et al., 2016). I interpret that major transgression in the Firebag Tributary inhibited bank stabilization and paralic environments as fluvial and delta systems rapidly prograded towards the basin (Fig. 4.17B). Similar retrogradation has also been observed for the C2 and C1 DUs in shallow-marine deposits of the Sparrow Paleovalley in the southern McMurray Depocenter (Château et al., 2020).

The B1 DU defines PP2, during which major progradation of the paleoshoreline took place towards the western edge of the study area. Progradation is demarcated by wide-spread coal and tidal marsh development (Figs. 4.12, 4.13 and 4.17C), that likely formed in the late transgressive systems tract as bank margins stabilized. In contrast to the widespread development in the Lower McMurray, paralic strata sitting at the top of the B1 DU are dominated by tidal marshes overlain by a thin coal seam (mostly <1.5 m). In other cases, this paralic succession is partially or completely removed and replaced by an imbricated mud-clast breccia lying between FA1 and FA4, which is interpreted to represent

a transgressive wave ravinement surface (e.g., 1AA/03-04-094-06W4, Fig. 4.12A; or 1AA/01-31-091-04W4, Fig. 4.12C).

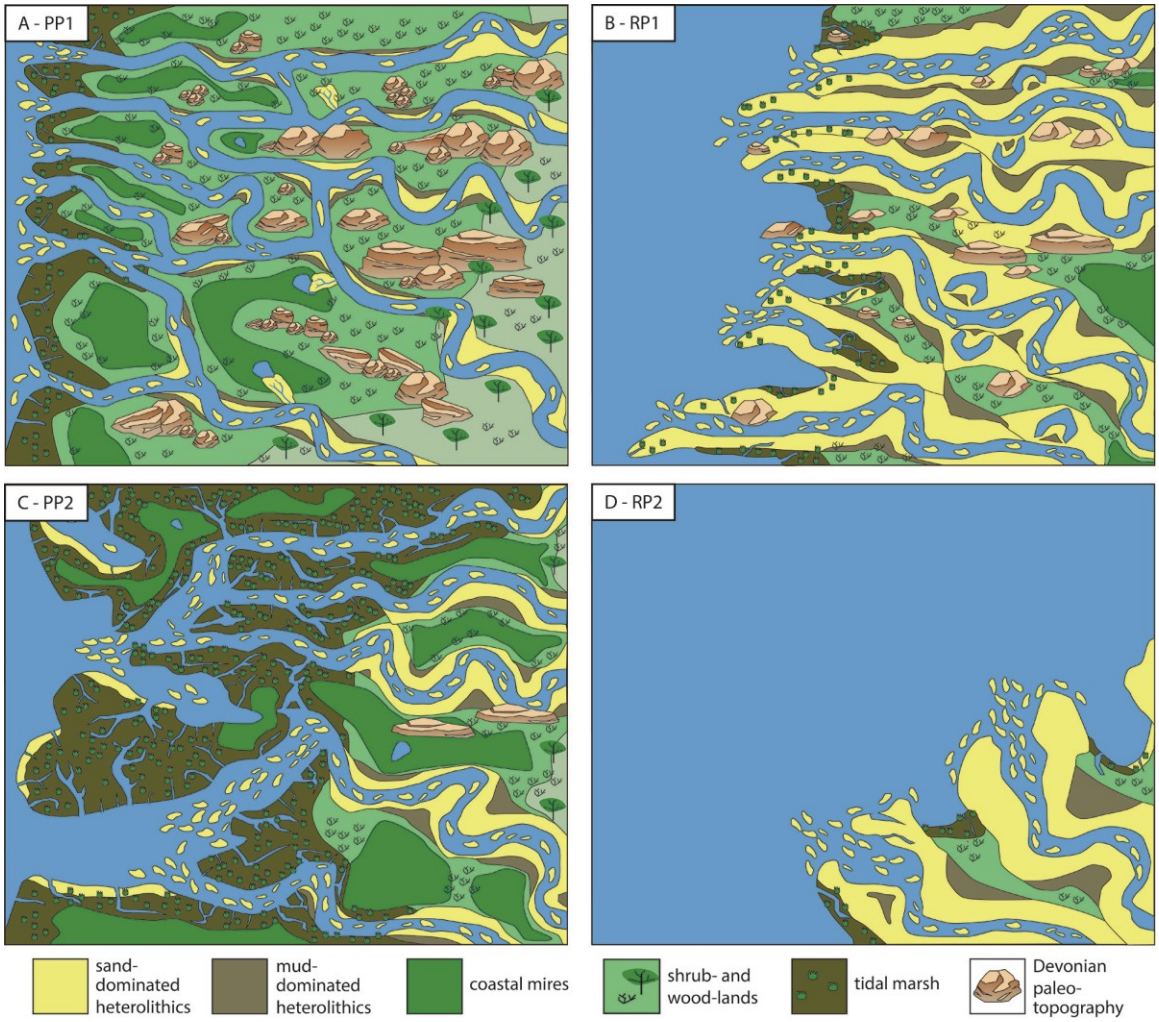

Figure 4.17. Artistic rendition depicting the depositional environments during the history of the McMurray Formation in the Firebag Tributary.

The position of the major channel-belts are derived from figs. 4.14 and 4.16, however will have likely switched position. **(A)** Conceptual paleo-geography map of the Firebag Tributary at the end of Lower McMurray deposition (progradational phase 1; PP1). Note the extensive mires and shrub- and wood-lands. **(B)** Conceptual paleo-geography of the Firebag Tributary during the C2, C1, and B2 DUs (retrogradational phase 1; RP1). Note retrogradation and displacement of paleo-shorelines towards the basin margin (right) of the Firebag Tributary. **(C)** Conceptual paleo-geography map of the Firebag Tributary at the end of B1 DU (progradational phase 2; PP2). Note the extensive mires and tidal marsh formation. **(D)** Conceptual paleo-geography map of the Firebag Tributary at the A2, A1 DUs (retrogradational phase 2; RP2). Note a second displacement of the paleo-shoreline towards the basin margin (right).

Deposition of the A2 and A1 DUs defines RP2, during which major shoreline retrogradation once again ensued. The location of the paleoshoreline has not been resolved within the Firebag Tributary as it would have resided further towards the east,

where it was eroded by Pleistocene glaciers (Fig. 4.17D). I infer potential vicinity to the paleoshoreline in the southeastern corner of the study area where prominent deltaic strata occur in RP2 (e.g., 1AA/03-03-091-01W4; Fig. 4.12C), and the A2 and A1 DUs are dominated by pro-delta deposits of FA4. Above this, wave ravinement surfaces demarcated by the omission suites of the *Glossifungites* Ichnofacies (Fig. 4.11B) and overlain by lower shoreface or offshore deposits of FA5 mark the Wabiskaw Member of the Clearwater Fm, and suggest progressive retreat of the paleoshoreline.

4.5.3. Ash Beds in Paralic Coals: Towards improving Chronostratigraphic Subdivisions

Ash beds found in the coal seams sitting at the top of the Lower McMurray (121.39 ± 0.20 Ma; Rinke-Hardekopf et al., 2019) and at the top of the B1 DU (115.09 ± 0.16 Ma; Fig. 4.15) remain the only absolute ages determined in the McMurray Fm. Dating and correlation of ash beds in coal seams in various formations around the globe have been used to understand their geochronology and chronostratigraphy (e.g., Gore, 1982; Bohor and Triplehorn, 1993; Burchart et al., 1998; Daniels et al., 2018). As I provide correlations between paralic coals and coeval shallow-marine deposits, these ash-derived ages become a powerful tool for understanding the chronostratigraphy and evolution of the McMurray Fm.

In the McMurray Fm, ash-derived ages for 2 depositional units allow for estimation of the duration of individual depositional units, and to estimate the timing of McMurray deposition. Volcanic ages are consistent with or younger than detrital zircon maximum depositional ages determined in the McMurray Fm (Rinke-Hardekopf et al., 2021), as well as with biostratigraphy (Hein and Dolby, 2018), and become younger up-section. They are, therefore, considered reliable sources of depositional age (Rossignol et al., 2019). The McMurray Fm contains 7 individual depositional units, of which I have the age of the Lower McMurray and the B1 DU (Fig. 4.1C). Approximately 6.3 Ma passed during deposition of the C2, C1, B2, and B1 DUs, and this equates to ~1.6 Ma per depositional unit. If this depositional duration per depositional unit is extrapolated to the base (Lower McMurray) and top (A1 DU) of McMurray Fm, I hypothesize that the McMurray Fm was deposited between ~123 Ma and 112 Ma, extending from the early Aptian into the early Albian. Termination of McMurray deposition therefore appears roughly coincide with oil migration into the formation at 112 Ma (Selby and Creaser, 2005), and has been

hypothesized to be a contributing factor that prevented McMurray strata from lithification. Chateau et al. (2021) note decreased average DU thicknesses for the A2 (~50 % decrease) and A1 (~73 % decrease) intervals, relative to the C2-B1 DUs, and interpret a decreased duration of relative sea-level still-stands. If thickness decreases correspond to proportional decreases in depositional duration of the A2 and A1 DUs, I speculate that these DUs might represent ~0.8 Ma and ~0.4 Ma of deposition, respectively, and McMurray Deposition would terminate at 113 Ma.

4.6. Conclusions

Paralic depositional environments associated with delta and coastal plains (e.g., interfluves and mires) and their deposits (e.g., paleosols and coals, respectively) are particularly prominent at the top of the Lower McMurray and the B1 depositional units of the McMurray Formation in the Firebag Tributary, northeastern McMurray Depocenter. Based on facies analysis of 60 cored intervals, supplemented by over 300 photographed cored intervals, I distinguish 3 different types of paralic deposits, including: 1) coarse, eluviated, deeply rooted paleosols, interpreted as semi-permanent shrub- and woodlands that formed during periods of base-level drop and major regression; 2) gleyed paleosols with fibrous rhizoliths, interpreted as the deposits of widespread tidal marshes formed during transgression; and 3) coals interpreted to have formed in coastal mires and swamps during transgression. While eluviated paleosols are found below the coal seam sitting at the top of the Lower McMurray and potentially indicate valley incision (i.e., represent a maximum regressive surface), gleyed paleosols underlie the coal seam sitting at the top of the B1 DU, and do not necessitate a relative sea-level fall (i.e., represents a major flooding surface where not overlain by a coal). The coals overlying both paleosol types have a wetting-upward character and indicate major flooding events. In the B1 DU, coals and gleyed paleosols are commonly overlain by regressive prodelta and delta-front deposits or are eroded by wave ravinement during transgression, as shown by imbricated mud-clast breccias or erosive surfaces. Therefore, the tops of coals or gleyed paleosols can be correlated to the bases of regional marine mudstones found elsewhere in the McMurray Depocenter.

On 4 cross-sections (3 along depositional dip, 1 along depositional strike), I show how coals and paleosols reveal trends in the position of the paleoshoreline during deposition of the McMurray Fm in Firebag Tributary. Of 4763 total wells, 1865 preserve

both the base and top of the McMurray Fm and are used to show the positions, and mainly east-west orientation of major channel belts. During deposition of the Lower McMurray, the paleoshoreline resided west of Firebag Tributary. Progressive transgression resulted in deposition of the C2 to B2 DUs, where the paleoshoreline exhibited a major landward retreat and likely resided closer to the Alberta – Saskatchewan border. During deposition of the B1 DU, the paleoshoreline in the Firebag Tributary underwent a phase of major regression, where widespread tidal marshes and mires only formed during the later stages of base-level rise. Finally, transgression and repeated paleoshoreline retreat occurred during the deposition of the A2 and A1 DUs, as well as the Wabiskaw Member of the Clearwater Fm.

Paralic coals are an ideal depositional environment to preserve ash beds and improve chronostratigraphic subdivision. Together with a previously dated ash in the Lower McMurray, the new age derived from an ash in the B1 coal seam (115.09 ± 0.16 Ma) allows an estimation of DU duration, based on absolute age data. I showcase that individual depositional units in the McMurray Fm may represent ~1.6 Ma (C2-B1 DUs), ~0.8 Ma (A2 DU), and ~0.4 (A1 DU) of deposition and the formation as a whole was probably deposited between 123 and 113 Ma.

Chapter 5.

Concluding Remarks

In this thesis, a combined sedimentological and geochronological approach is employed to reconstruct the depositional history of the Lower Cretaceous McMurray Formation (Fig. 5.1) in the McMurray Depocenter (MDC), Canada, with focus on the Firebag Tributary. The Firebag Tributary is situated in the northeastern MDC and extends from townships (T) 90 – 99, and ranges (R) 23 west of the 3rd meridian to range 6 west of the 4th meridian (23W3 – 06W4); an area that exceeds 10 000 km^2 (Fig. 5.2). In comparison to McMurray Formation (Fm) strata elsewhere in the MDC, deposits in the Firebag Tributary comprise an anomalously high volume of delta- and coastal-plain deposits, and channel belts (Hein et al., 2007).

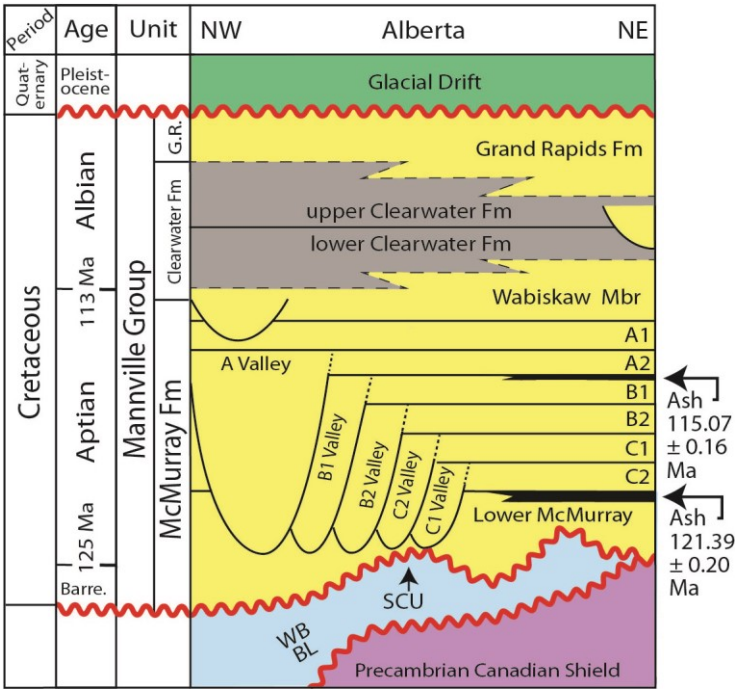

Figure 5.1. Allostratigraphic framework for the Lower Cretaceous Mannville Group in the Firebag Tributary.

Clastic sedimentary rocks (sandstone (yellow), mudstone (grey), and coal (black)), unconformably overlie slightly tilted Devonian carbonates of the Woodbend (WB) and Beaverhill Lake (BL) groups (blue), as well as the Precambrian Canadian Shield (purple). Also included are ages derived from ash layers found within coal seams near the top of the Lower McMurray (Rinke-Hardekopf et al., 2019) and B1 depositional unit (Rinke-Hardekopf et al., *in review*).

A dataset comprising 60 logged cores, 348 photographed core intervals, and 4 763 well logs are used for facies analysis and stratigraphic correlations. Core- and well-log analysis showcases the positions and trajectories of 2 progradational and 2 retrogradational paleo-shoreline positions in the Firebag Tributary. Four petrographic and two geochemical (sulphur and ash content) profiles through coal successions outlines how base-level was influenced by both local basement subsidence and incremental relative sea-level rise. Geochronology of detrital zircon (DZ) samples (4 new, 39 literature-derived; Fig. 5.2) and volcanic zircon (2 new ash-derived absolute ages; Figs. 5.1 – 2) are used to refine and constrain the chronostratigraphy of depositional units that comprise the McMurray Fm. Detrital zircon are also used to assess variations in provenance both spatially and temporally. The main findings of this thesis are listed below.

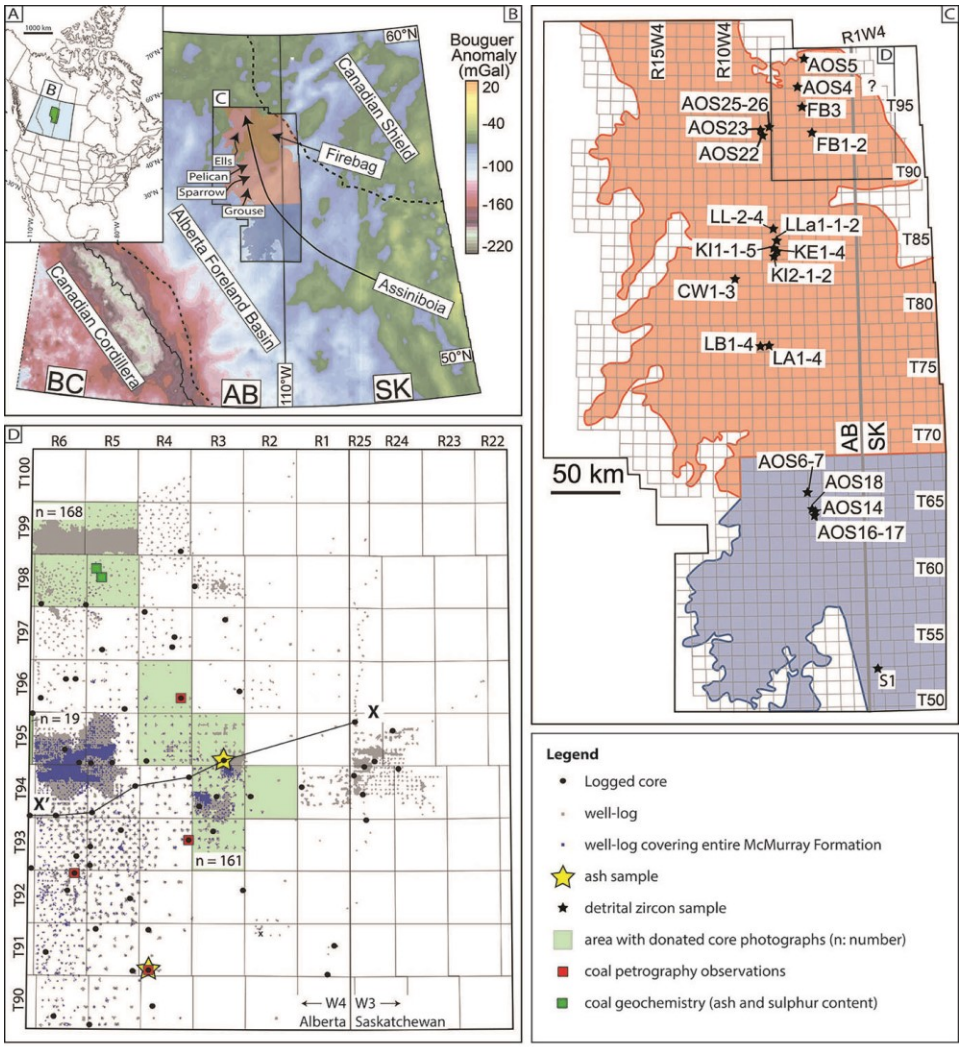

Figure 5.2. Summary of the study area and data used in this thesis (adapted from Rinke-Hardekopf et al., 2019, 2021, in review).

(A) Map of Canada, with the position of **(B)** shown in the blue polygon and the McMurray Depocenter (MDC) in the green polygon. **(B)** Bouger anomaly map of part of British Columbia (BC), and all of Alberta (AB) and Saskatchewan (SK) with the positions of the Athabasca (red overlay) and Cold Lake (blue overlay) oil sands regions in the MDC. Also included are paleotopographic lows on the underlying Sub-Cretaceous Unconformity (SCU), which are interpreted as paleovalleys (arrows indicate probable discharge directions). These paleovalleys include the main Assiniboia Valley (Christopher, 1974), the Grouse, Sparrow, Pelican, and Ells paleovalleys in the western Athabasca Oil Sands region, and the Firebag Tributary in the northeast MDC (Broughton, 2013a; Château et al., 2019; Rinke-Hardekopf et al., 2019). **(C)** Location of the Firebag Tributary in the northeastern MDC and the locations of wells from which detrital zircon (DZ) samples were extracted (see Chapter 3). **(D)** All data in the Firebag Tributary used in this thesis (all chapters), including logged cores, well logs, cores from which volcanic zircon were derived (ash sample), and regions with high-density core photograph coverage. Wells with detailed coal petrography and coal geochemistry used in Chapter 2 are also shown, as is the position of an approximately along-dip cross-section shown in Fig. 5.7A. The grey grid is the Dominion Land Survey (DLS) system, which subdivides western Canada into 6 mile by 6 mile (~10 km by 10 km) township blocks.

5.1. Local and regional base-level history of early McMurray deposition

In Chapter 2, detailed observations of coal petrography, coal geochemistry, sedimentary facies analysis, and stratigraphic correlations are used to investigate the significance of the coal seam (up to >20 m thick) situated at the top of the Lower McMurray (LM) in the Firebag Tributary (Figs. 5.1, 5.3A–B). As well, an ash bed situated toward the top of the Lower McMurray coal seam was dated using chemical abrasion thermal ionization mass-spectrometry (CA-TIMS) and provides the first absolute age in the McMurray Formation (Fig. 5.3C). A version of this chapter is published as Rinke-Hardekopf et al. (2019).

Petrographic and geochemical data reveal several wetting-upward and drying-upward cycles in coal seams, as well as stratigraphically significant surfaces, which relate to both the local and regional base-level history. Wetting-upward character coal seams form through paludification and record up to 4 successive wetting-upward cycles (Fig. 5.3A), which resulted from the initial transgression of the Boreal Sea over Milankovitch time scales. Cycles are interpreted to have occurred during late lowstand or early transgression. The presence of multiple wetting-upward cycles displaying progressively higher rates of accommodation increase, as well as drowning of peat-forming mires towards the top of the LM are interpreted to record punctuated transgression of the Boreal Sea (Fig. 5.3A). Some coal seams display drying-upward character in association with terrestrialization or accommodation reversal surfaces, and/or are split into sub-seams (Fig. 5.3B). Split coal seams commonly occur in paleo-topographic lows on the SCU, and their

characteristics support the interpretation that peat-accumulation in mires was locally influenced by short-term syndepositional subsidence associated with dissolution of the underlying Devonian Prairie Evaporite Formation and/or epikarst collapse (Figs. 5.3B, 5.4B).

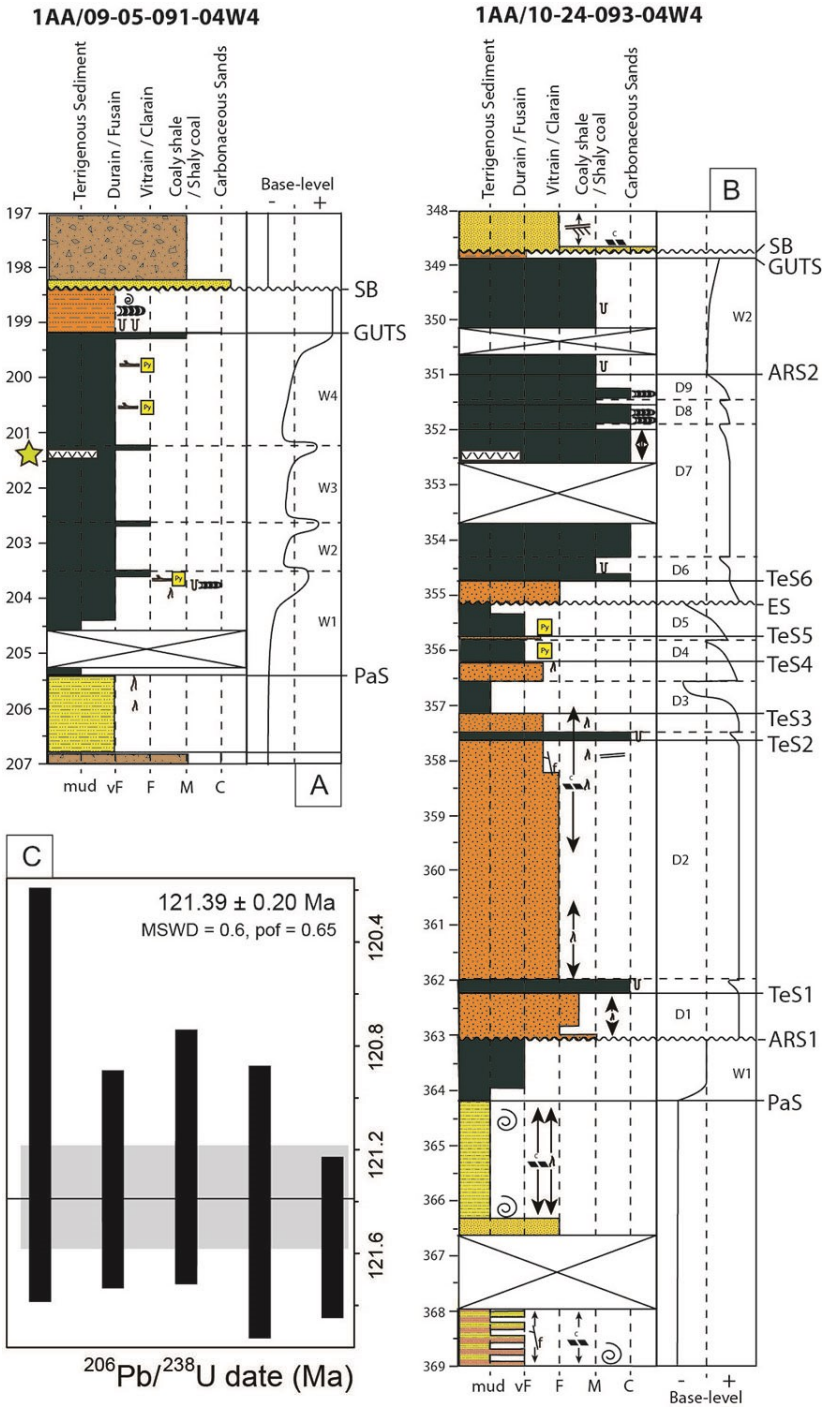

Figure 5.3. Coal petrographic data and the absolute age derived from an ash bed in well 1AA/09-05-091-04W4.

(A–B) Detailed sedimentological and coal petrographic logs of two coal successions that are part of the Lower McMurray coal seam. An interpretation of base-level changes based on changes in facies and coal petrography is provided next to each log and includes wetting-upward (W) and drying-upward (D) cycles. Also included are several significant surfaces, including: paludification surfaces (PaS), give-up transgressive surfaces (GUTS), a sequence boundary at the top of the LM (SB), accommodation reversal surfaces (ARS), terrestrialization surfaces (TeS), and an erosional surface (ES). Whereas (A) reveals 4 wetting-upward cycles and the position of the ash bed (yellow star), which is dated in (C), the coal in (B) displays varying drying-upward and wetting-upward characteristics, and is split into several sub-seams. **(C)** CA-TIMS derived ^{206}Pb / ^{238}U ages of 5 zircon grains recovered from the ash bed in (A), displaying a tight age cluster. The weighted mean age is 121.39 ± 0.20 Ma (mean standard weighted derivation, MSWD = 0.6; probability of fit, pof = 0.65). Figure adapted from Rinke-Hardekopf et al., (2019).

The LM coal seam forms a discrete arcuate shape that is interpreted to preserve the shape and position of the paleo-shoreline in the Firebag Tributary towards the end of LM deposition (Fig. 5.4A). Wetting-upward coal seams are interpreted to record transgression of the Boreal Sea. Using the thickness of the coal, the accumulation rates of temperate, peat-forming environments, and peat-to-coal compaction-rates, the rate of Early Cretaceous base level rise is estimated at between 0.5 and 3 mm*a^{-1} (Fig. 5.4B).

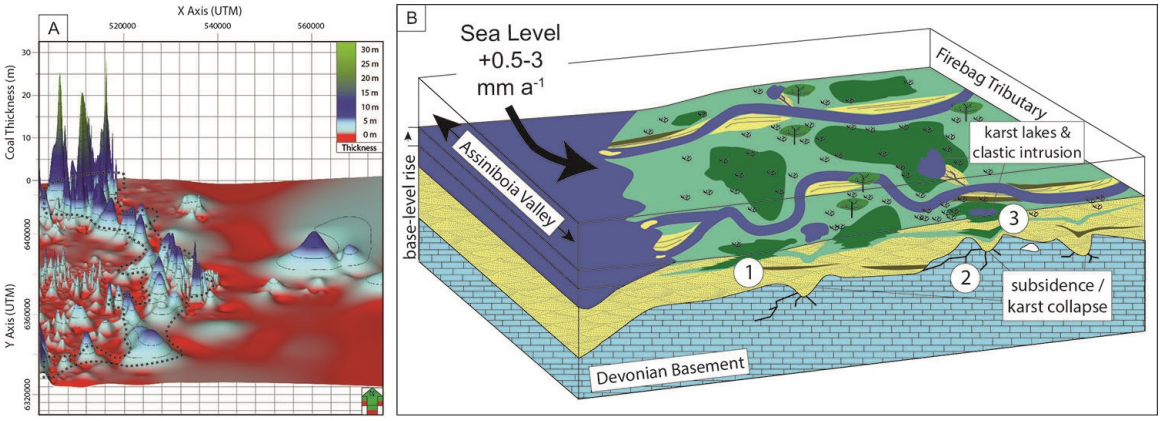

Figure 5.4. Arcuate-shaped distribution of LM coals
(A) Oblique, 3D view of the thickness of the LM coal seam in the Firebag Tributary, displaying an arcuate shape, which is interpreted to preserve the paleo-shoreline at the end of LM deposition (1000x vertically exaggerated). This arcuate-shaped zone of thick coal also exhibits a north to south decrease in thickness. **(B)** Schematic block diagram of the Firebag Tributary depicting paleo-environments at the end of LM deposition. The diagram shows meandering channels that flowed towards the Assiniboia Valley, and a zone of widespread peat-forming mires (dark green (1)). Light green areas indicate coastal plain. Mires are affected by syndepositional subsidence and/or karst collapse (2), where channel-margin or levee collapse leads to clastic sediment outflows onto the floodplain (3). Increasing relative sea level rate is estimated from the thickness of wetting-upward coal seams. Figure adapted from Rinke-Hardekopf et al., (2019).

Lastly, an ash-bed in a coal seam at the top of the LM coal in well 1AA/09-05-091-04W4 was sampled, and 5 sharply faceted zircon grains were recovered and dated using chemical abrasion thermal ionization mass-spectrometry (CA-TIMS; Fig. 5.3C). CA-TIMS

ages of these 5 zircon exhibit a tight ^{206}Pb / ^{238}U age cluster, and a weighted mean age of these grains provides the first absolute geochronological age (121.39 ± 0.20 Ma) in the McMurray Formation.

5.2. Provenance variability and geochronology of the Mannville Group

In Chapter 3, the age of the ash-bed found in a coal seam near the top of the LM (Section 1.1 and Chapter 2) is used as a chronological reference point, and chronostratigraphic subdivision as well as provenance variability of the McMurray and Clearwater formations are investigated using 43 DZ samples from 20 cored well locations (Figs. 1C and 5). A version of this work is published as Rinke-Hardekopf et al. (2021).

Stratigraphic correlation is used to subdivide 43 DZ samples (4 new samples, 39 literature-derived samples; Benyon et al., 2014, 2016; Blum and Pecha, 2014) into five stratigraphic intervals. For each of the five stratigraphic intervals, all associated DZ samples are combined to create 5 grouped DZ samples for the: 1) Lower McMurray Interval (10 samples, total (grouped) zircon (g.n.) = 1227); 2) the CB Interval, which includes all channels and parasequences associated with the C2, C1, B2 and B1 DUs (13 samples, g.n. = 1249); 3) the A Interval, which includes all channels and parasequences associated with the A2 and A1 DUs (14 samples, g.n. = 1335); 4) the lower Clearwater Formation containing the Wabiskaw Member (4 samples, g.n. = 379); and 5) the upper Clearwater Formation (2 samples, g.n. = 194; Fig. 5.5).

To understand provenance variability in the Mannville Group along the main paleo-drainage axis, grouped DZ samples and individual DZ samples are compared by means of their DZ population proportions, and their pairwise dissimilarity based on the Kuiper V_{max} statistic, which is visually displayed as multi-dimensional scaling plots (e.g., Fig. 5.6F). Individual DZ samples (typically n ~ 100) within the same stratigraphic interval show up to 40% variation in individual DZ age-population proportions (Fig. 5.6A). Furthermore, age-population proportions of individual DZ samples have standard deviations of up to 31% (Fig. 5.6D) relative to their respective grouped DZ sample (McMurray Fm samples: n > 1000).

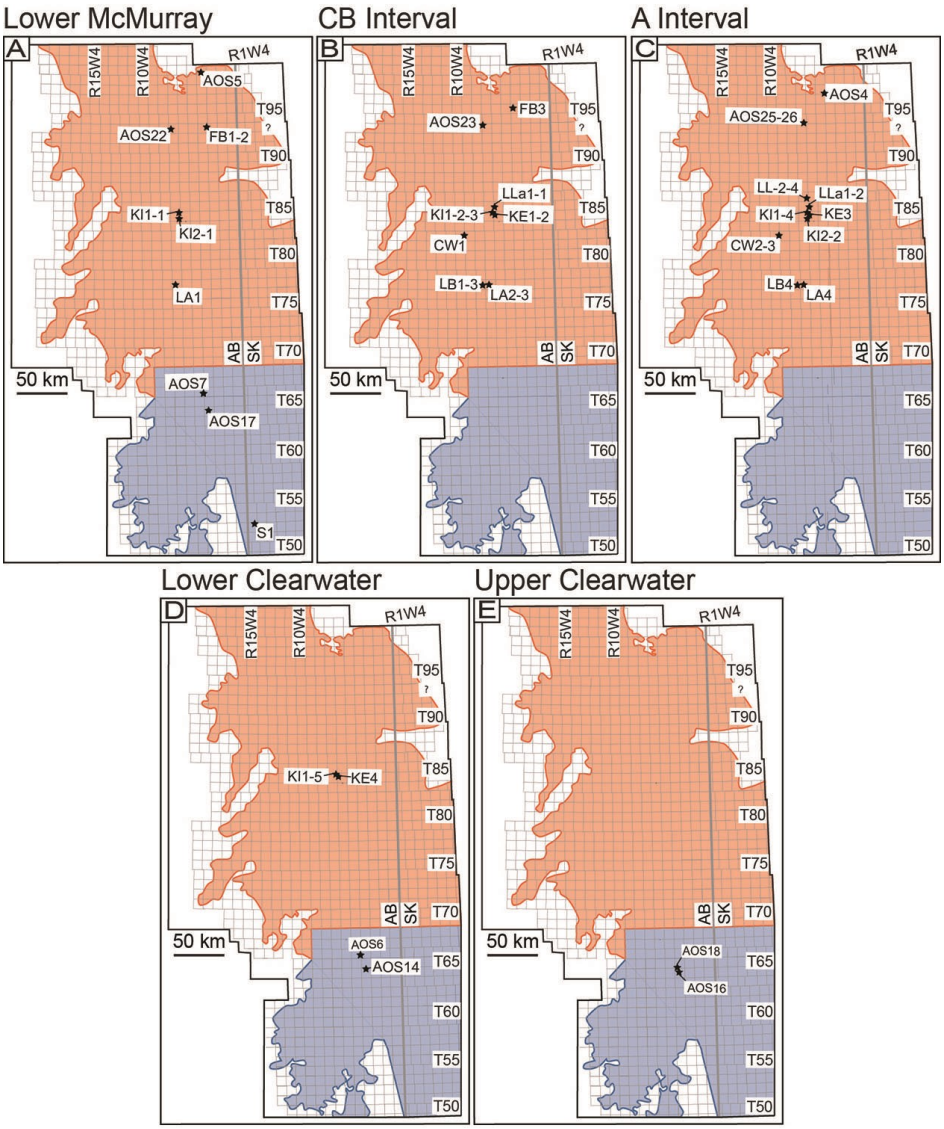

Figure 5.5. (A–E) Well locations from which DZ samples were acquired in each of the five stratigraphic intervals.

Comparing dissimilarity (Kuiper V_{max} statistics) between DZ samples and grouped DZ samples from the same stratigraphic interval and between stratigraphic intervals reveals that average dissimilarity between individual and grouped DZ samples increases with increasing geographic distance between samples. For example, individual DZ samples in the LM were taken from cores along a 459 km north-to-south transect (Fig. 5.5A) and exhibit the largest average Kuiper V_{max} statistic or dissimilarity (K_{av}: 0.25) to the associated grouped DZ sample (Fig. 5.6F). By contrast, individual DZ samples in the CB Interval were taken from cores along a 178 km north-to-south transect (Fig. 5.5B) and exhibit the lowest K_{av} (0.18; Fig. 5.6F). When visualized through MDS, grouped DZ

samples of the McMurray Formation plot significantly closer to one another than individual DZ samples from within any stratigraphic interval (Fig. 5.6F). These data suggest that grouped DZ analysis leads to a more comprehensive assessment of provenance.

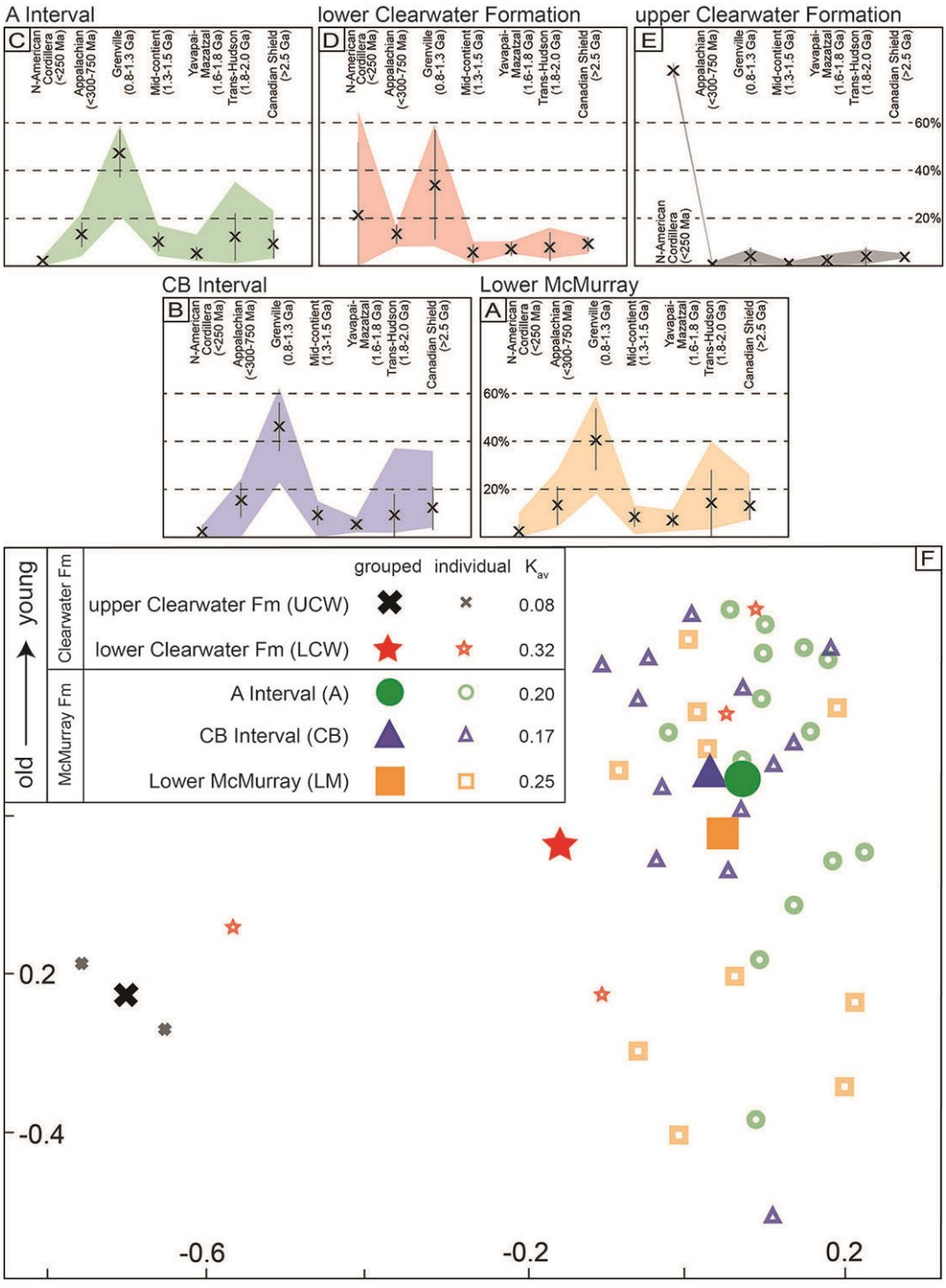

Figure 5.6. Comparing individual and grouped DZ samples in the McMurray and Clearwater formations.

(**A-E)** Plots highlighting the DZ age-population proportions in each stratigraphic interval. Age populations represent source terranes from across North America (Benyon et al. 2014, 2016; Blum and Pecha, 2014). X's in each column of each plot mark the DZ age-population's proportions in the grouped DZ sample. Grey bars give the standard deviation of a DZ age-population between individual DZ samples and their respective grouped DZ sample. Shaded areas give the range in age-population proportions in individual DZ populations of each stratigraphic interval. **(F)** Multi-dimensional scaling plot showing dissimilarity between individual and grouped DZ samples from the 5 intervals defined in the McMurray and Clearwater formations, and the average Kuiper V_{max} statistic / dissimilarity (K_{av}) between individual DZ samples and their respective grouped DZ sample. A higher Kuiper V_{max} statistic indicates more dissimilarity between DZ samples. Figure adapted from Rinke-Hardekopf et al. (2021).

Maximum depositional ages (MDA) are calculated for individual DZ samples (Fig. 5.5F) and for grouped DZ samples using multiple published MDA calculation methods. Grouped DZ sample MDAs are introduced in this work and are referred to as gMDAs (Fig. 5.7A). In basins or formations where young zircon are plentiful (e.g., the Clearwater Formation; Figs. 6D-E), gMDAs commonly yield older (i.e., more conservative) depositional ages than the biostratigraphically defined depositional age of a unit (Fig. 5.7). In basins where syn-depositional DZ are accessory components of DZ samples (i.e., <5%), gMDAs enable transformation of low-confidence MDAs (e.g., youngest single grains) into high-confidence (multi-grain) gMDAs, which more closely resemble true depositional age (Fig. 5.7B). The gMDA method can be used in any basin with multiple DZ samples and well-defined stratigraphic intervals for estimating the ages of depositional systems.

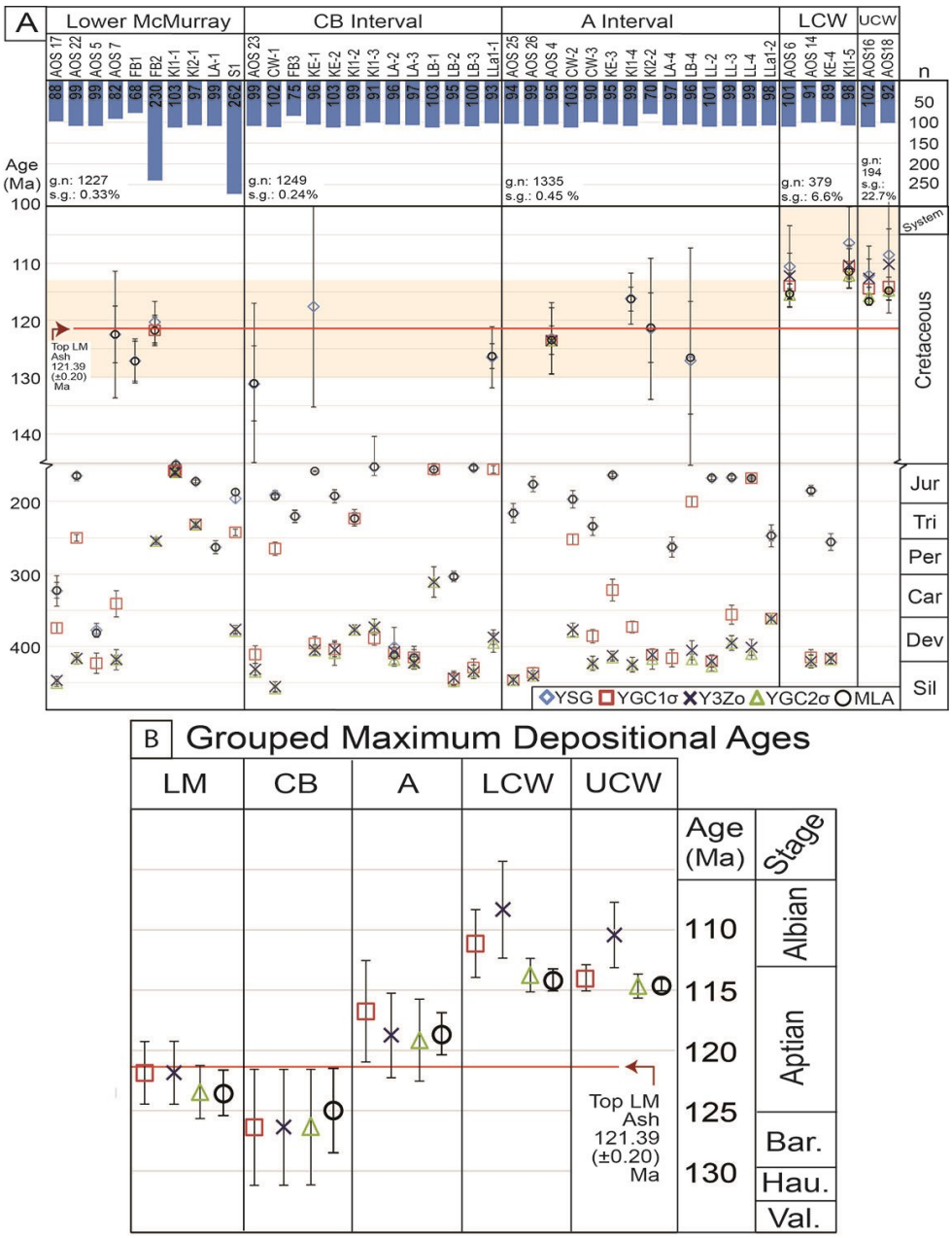

Figure 5.7. MDAs calculated with individual and grouped DZ samples for the McMurray and Clearwater formations.

(A) Calculated MDAs for individual DZ samples using multiple calculation methods, including: youngest single grain (YSG); youngest grain cluster (2 or more grains) whose ages overlap within 1σ standard deviation (YGC1σ); youngest 3 zircon (Y3Zo); youngest grain cluster (3 or more grains) whose ages overlap within at 2σ standard deviation (YGC2σ),; and maximum likelihood age (MLA) (Dickinson and Gehrels, 2009; Ross et al., 2017; Vermeesch, 2020). Sample names are given in row 2. Row 3 includes the number of concordant zircon per sample and per stratigraphic interval (g.n.), as well as the percentage of syndepositional grains (s.g.). Biostratigraphic constraints for formations are given as orange shaded areas. Figure adapted from Rinke-Hardekopf et al. (2021). **(B)** Results of gMDA calculation for the stratigraphic intervals (LM: Lower McMurray, CB: CB Interval, A: A Interval, LCW: lower Clearwater Formation, UCW: upper Clearwater Formation). Figure adapted from Rinke-Hardekopf et al. (2021).

5.3. Paleo-Shoreline Trajectory during McMurray Formation deposition in the Firebag Tributary

In Chapter 4, a detailed facies analysis (sedimentology, ichnology) is used to: 1) resolve depositional environments in delta- and coastal-plain settings; 2) develop stratigraphic relationships between paralic and shallow-marine strata within Firebag Tributary; and 3) reconstruct the trajectory of the paleo-shoreline. A second ash-based zircon age is also presented for the top of the B1 DU, and is used to predict deposition rates of DUs, based on absolute ages and average DU thickness. A version of this work is currently in review in *The Depositional Record* as Rinke-Hardekopf et al. (*in review*).

Paralic paleoenvironments associated with delta and coastal plains (e.g., interfluves and mires) and their deposits (e.g., paleosols and coals, respectively) are particularly prominent at the tops of the LM and the B1 depositional units of the McMurray Formation in the Firebag Tributary (Fig. 5.8). Based on detailed facies analysis, a total of 14 facies are recognized in the McMurray Fm in the Firebag Tributary and are grouped into 5 facies associations (FA) that define the regional depositional system, including: fluvial and fluvio-tidal channels (FA1); delta- and coastal-plains (FA2); sheltered bays (FA3); wave-influenced to wave-dominated delta-front and prodelta (FA4); and offshore to lower shoreface (FA5). The delta- and coastal-plains facies association (FA2) comprises 3 facies, including: 1) coarse, eluviated, deeply rooted (mature) paleosols interpreted as semi-permanent shrublands and woodlands (F6); 2) coals interpreted to have formed in coastal mires (F7); and 3) gleyed (immature) paleosols with fibrous rhizoliths interpreted as the deposits of tidal marshes (F8; Fig. 5.8A). Mature paleosols are found below the coal seam that is situated at the top of the LM and potentially record a period of valley incision (i.e., top of the paleosol represents a maximum regressive surface). This interpretation is based on the eluviated (coarse-grained) appearance of the paleosol, as well as the thick roots. These thick roots indicate that plants needed to reach a deeply positioned groundwater table, which on delta and coastal plains is hydrologically linked to sea-level. Deep groundwater in the coastal plain suggests the paleosol developed during the falling stage and/or lowstand systems tract. By contrast, immature paleosols underlying the coal seam situated at the top of the B1 DU did not require relative sea-level fall for their development (i.e., top represents a major flooding surface where not overlain by a coal). This interpretation is based on interbedding of F8 with the bay facies association FA3 suggesting that the groundwater table near the land surface, and that

gleying as a result of reducing pore waters was syndepositional. Coals overlying the paleosols at the top of the B1 DU have a wetting-upward character and demarcate major flooding events. In the B1 DU, coals and gleyed paleosols are commonly overlain by regressive prodelta and delta-front deposits, or are eroded by wave ravinement during transgression, as shown by imbricated mud-clast breccias or erosive surfaces in paralic strata (Fig. 5.8A). Consequently, the tops of coals or gleyed paleosols can be correlated to the bases of regional marine mudstone units found elsewhere in the McMurray Depocenter.

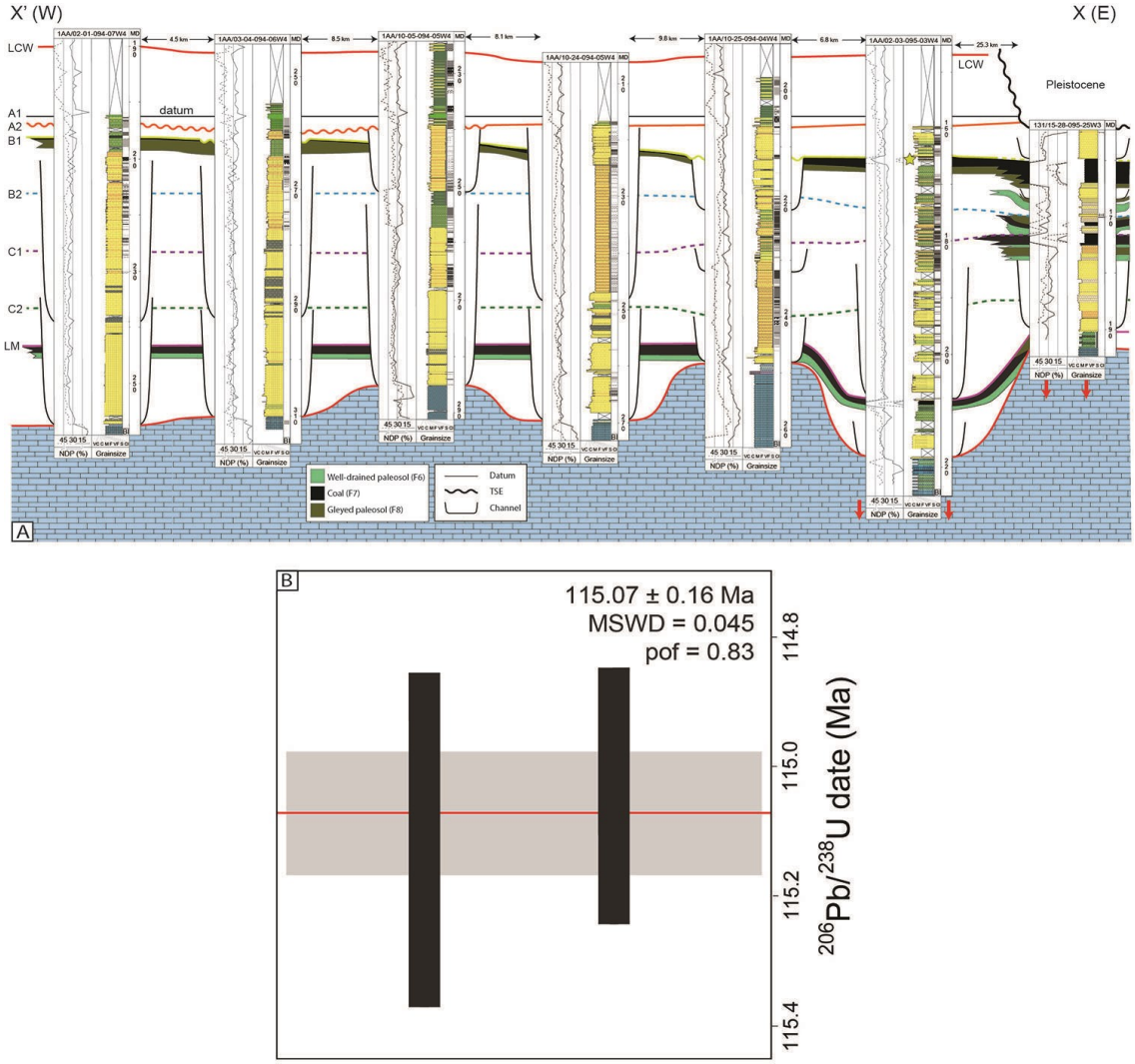

Figure 5.8. Correlation of paralic strata throughout the Firebag Tributary and new age derived from an ash bed at the top of the B1 DU.

(A) Dip-oriented cross-section through Firebag Tributary showing high- (bold line) and low-confidence (dashed-line) correlations of regional DUs. Many surface picks (e.g., Top C1) are of low confidence, due to extensive removal of strata by subsequent channel incision. Probable surfaces are shown as dashed lines. The position of the cross-section is given in Figure 1D. Individual core-

logs show lithology, BI, and neutron- and density-porosity logs. The cross-section includes all depositional units of the McMurray Formation and the Wabiskaw Member of the Clearwater Formation. The top of the A1 DU is the datum. The cross-section also highlights the positions of well-drained paleosols (F6), coal seams (F7), and gleyed paleosols (F8). The yellow star shows the position of an ash bed sampled for zircon in the coal seam situated towards the top of the B1 DU (1AA/02-03-095-03W4). **(B)** CA-TIMS-derived ages of the youngest single zircon grains (black boxes give 2σ error around the determined CA-TIMS age) found within the ash bed. These show a tight age cluster, the average of which gives an age of 115.07 ± 0.16 Ma (red line, and grey box) with a mean standard weight derivation (MSWD) of 0.045 Ma and a probability of fit (pof) of 0.83 (adapted from Rinke-Hardekopf et al., in review).

Based on the predominance of paralic strata, stratigraphic cross-sections (e.g., Fig. 5.8A) are used to define the paleo-shoreline trajectory, and suggest that the McMurray Formation in the Firebag Tributary underwent 2 major progradational phases (PP) - during deposition of the LM DU (PP1) and during the B1 DU (PP2). The McMurray also experienced 2 major retrogradational phases (RP) - during deposition of the C2-B2 DUs (RP1) and during the A2-A1 DUs (RP2; Fig. 5.9). During PP1, the paleo-shoreline resided west of the Firebag Tributary (Fig. 5.9A). Subsequent transgression resulted in deposition of RP1. The paleo-shoreline exhibited a major landward retreat that placed it near the Alberta – Saskatchewan border at maximum transgression (Fig. 5.9B). During PP2, the Firebag Tributary experienced major regression, which is expressed as widespread tidal marsh and mire formation (Fig. 5.9C). These tidal marshes and mires likely only formed at the end of the transgressive systems tract, where bank margins established prior to progradation of the river systems. Finally, transgression and paleo-shoreline retreat ensued, resulting in deposition of RP2 (Fig. 5.9D), expressed as the A2 and A1 DUs, and continued during Wabiskaw Member of the Clearwater Formation.

Lastly, paralic coals are excellent low-energy depositional environments that promote preservation of ash beds from which volcanic zircon can be extracted and dated to precisely constrain the timing of deposition. Six zircon grains were extracted from an ash bed situated in the B1 coal seam and were dated using CA-TIMS. Of the six zircon, two returned consistent ages that overlap with the biostratigraphic age of the McMurray Fm. These two grains yield a MDA of 115.09 ± 0.16 Ma, which is considered to be an accurate representation of the true depositional age of the ash bed (Fig. 5.8B; Rinke-Hardekopf et al., in review).

Using the previously dated ash bed in the Lower McMurray and recently published average thicknesses of DUs (Château et al., 2021), the new age constraint is used to estimate deposition rates for the McMurray Formation. Individual DUs in the McMurray

Formation are estimated to represent ~1.6 Ma for each of the C2-B2 DUs, 0.8 Ma for the A2 DU and 0.4 Ma for the A1 DU, assuming DU thicknesses scale to depositional duration. The formation as a whole was likely deposited between 123 and 113 Ma, and concurs with previously published biostratigraphic constraints and DZ-derived MDAs (Hein and Dolby, 2018; Rinke-Hardekopf et al., 2021).

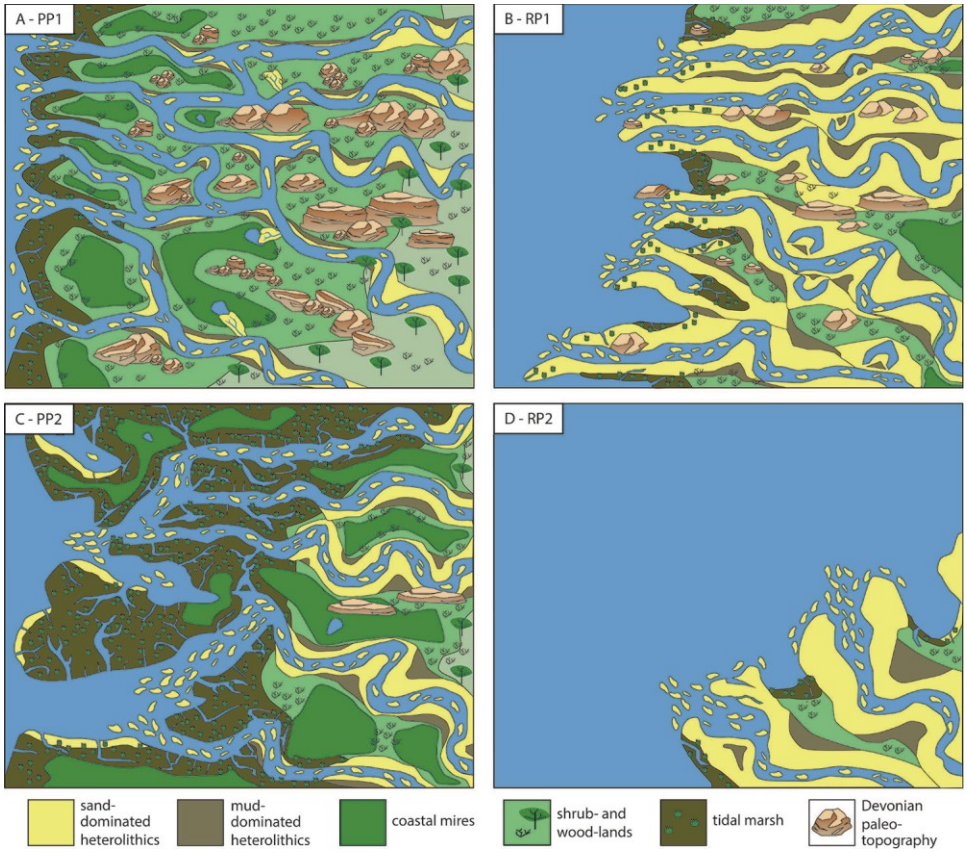

Figure 5.9. Schmeatic model of depositional environments during the 4 phases of deposition of the McMurray Formation in Firebag Tributary.
(A) At the end of Lower McMurray deposition (progradational phase 1; PP1), mires with shrubland and woodland extended over most of Firebag Tributary. **(B)** During deposition of the C2, C1, and B2 DUs (retrogradational phase 1; RP1), the paleo-shoreline was situated towards the eastern margin of Firebag Tributary. **(C)** At the end of B1 DU deposition (progradational phase 2; PP2), extensive mires and tidal marsh formation once again extended throughout Firebag Tributary. **(D)** Deposition of the A2, A1 DUs (retrogradational phase 2; RP2) resulted in a second displacement of the paleo-shoreline towards the southeastern margin of the Firebag Tributary. The basin was subsequently drowned. (Figure from Rinke-Hardekopf et al., in review).

5.4. Relevant Applications and Future Research Directions

The papers produced from this PhD and presented in modified form as chapters 2-4 in this thesis provide a step towards unravelling the depositional history of complex

sedimentary successions, particularly in low-accommodation settings. Research presented herein includes detailed observations of paralic sedimentary systems, their correlation to coeval shallow-marine depositional systems, and novel approaches to detrital and volcanic zircon geochronology. Correspondingly, the results of this work have multiple local and global implications.

For the McMurray Formation and the Mannville Group in the MDC of the Alberta Foreland Basin, several interesting avenues of research arise from the presented work. Post-depositional erosion of McMurray Formation (and younger) strata by Pleistocene glaciers increases eastward and northward in the Athabasca oil sands region. In the Firebag Tributary, glacial erosion has removed evidence of the position of regressive paleo-shorelines associated with the C2-B2 DUs, as well as those overlying the B1 DU. However, an interesting opportunity exists to study Upper Mannville (i.e., Clearwater Fm and Grand Rapids Fm) paralic strata of the Cold Lake oil sands region in the south (Fig. 5.1). In the Cold Lake area, coal and paralic strata are common in the Albian Grand Rapids Formation in Alberta (e.g., Beynon et al., 1988) and its equivalents in Saskatchewan (e.g., Morshedian et al., 2012), a period of time known for increased volcanic activity in the Canadian Cordillera (e.g., Gehrels et al., 2009). Future work could make detailed observations of paralic facies and their correlation with coeval shallow-marine strata to more precisely constrain base-level fluctuations, and to reconstruct positions of the paleo-shoreline. As well, volcanic activity in the Canadian Cordillera likely would have deposited ash beds within these paralic strata, providing an opportunity to expand our understanding of chronostratigraphy of the Mannville Group in the MDC.

The global implications of the work presented in this thesis relate to analyses of paralic strata and geochronology. For example, detailed facies analysis of paralic strata is used to understand when coals and paleosols form and how they relate to base-level during falling (i.e., valley incision) or rising (i.e., conformable stratigraphic succession) relative sea-level. Recently, the incised valley paradigm (see Zaitlin et al., 1994) and its implication(s) in stratigraphic successions have undergone some scrutiny and reassessment (e.g., Pattison, 2018). While some (mature) paleosols are suggestive of major base-level falls and valley incision, other (immature) paleosols are indicative of a conformable succession and reflect ongoing normal regression. Similar to revisited strata of the Book Cliffs in the USA (e.g., Pattison, 2019b), re-evaluating interpreted incised valleys with a particular focus on their associated paralic strata can provide potential

alternative interpretations of the depositional history of stratigraphically complex formations, specifically in low-accommodation settings.

Where paralic strata are well preserved in stratigraphic successions, peat-forming mires are excellent low-energy depositional environments in which ash beds can be preserved. When accurately correlated and dated (e.g., CA-TIMS), ages derived from volcanic zircon in ash-beds provide a powerful tool for temporally constraining stratigraphy. Where paralic strata are poorly preserved in stratigraphic successions, age constraints of formations can also be supplemented by novel use of stratigraphically grouped DZ samples and gMDAs calculated from them, especially in basins with accessory syndepositional DZ populations. When used in conjunction with other statistical methods (i.e., DZ population proportions, MDS analysis), these grouped DZ samples also provide a method to understand geographical discrepancies in provenance evolution. With increasing acceptance of the importance of high-n DZ samples (n > 300; e.g., Pullen et al., 2014), confirming geographical provenance differences in the MDC with high-n DZ samples should be considered as a valuable avenue of future research.

References

Ainsworth, R.B., Vakarelov, B.K., MacEachern, J.A., Rarity, F., Lane, T.I., and Nanson, R.A., 2017, Anatomy of a shoreline regression: Implications for the high-resolution stratigraphic architecture of deltas: Journal of Sedimentary Research, v. 87, p. 425–459, doi: 10.2110/jsr.2017.26.

Aitken, J.F., and Flint, S.S., 1996, Variable expressions of interfluvial sequence boundaries in the Breathitt Group (Pennsylvanian), eastern Kentucky, USA, in Howell, J.A. and Aitken, J.F. (eds., High Resolution Sequence Stratigraphy: Innovations and Applications, Geological Society Special Publication No.104, p. 193–206, doi: 10.1144/GSL.SP.1996.104.01.12.

Alberta Energy and Utilities Board, 2003, Athabasca Wabiskaw-McMurray regional geological study: Alberta Energy and Utilities Board, Report 2003-A, 195 p.

Amorosi, A., Bruno, L., Cleveland, D.M., Morelli, A., and Hong, W., 2017, Paleosols and associated channel-belt sand bodies from a continuously subsiding late quaternary system (Po basin, Italy): New insights into continental sequence stratigraphy: Bulletin of the Geological Society of America, v. 129, p. 449–463, doi: 10.1130/B31575.1.

Andersen, T., 2005, Detrital zircons as tracers of sedimentary provenance: Limiting conditions from statistics and numerical simulation: Chemical Geology, v. 216, p. 249–270, doi: 10.1016/j.chemgeo.2004.11.013.

Andriashek, L.D., and Atkinson, N., 2007, Buried channels and glacial-drift aquifers in the Fort McMurray region, northeast Alberta: Alberta Energy and Utilities Board, EUB/AGS Earth Sciences Report 2007-01, p. 1–170, ISBN: 0-7785-3837– 0.

van Asselen, S., Stouthamer, E., and van Asch, T.W.J., 2009, Effects of peat compaction on delta evolution: A review on processes, responses, measuring and modeling: Earth-Science Reviews, v. 92, p. 35–51, doi: 10.1016/j.earscirev.2008.11.001.

van Asselen, S., Stouthamer, E., and Smith, N.D., 2010, Factors controlling peat compaction in alluvial floodplains: A case study in the cold-temperate Cumberland Marshes, Canada: Journal of Sedimentary Research, v. 80, p. 155–166, doi: 10.2110/jsr.2010.015.

Banerjee, I., Kalkreuth, W., and Davies, E.H., 1996, Coal seam splits and transgressive-regressive coal couplets: A key to stratigraphy of high-frequency sequences: Geology, v. 24, p. 1001–1004, doi: 10.1130/0091-7613(1996)024<1001:CSSATR>2.3.CO;2.

Baniak, G.M., and Kingsmith, K.G., 2018, Sedimentological and stratigraphic characterization of Cretaceous upper McMurray deposits in the southern Athabasca Oil Sands, Alberta, Canada: AAPG Bulletin, v. 102, p. 309–332, doi: 10.1306/0502171619317010.

Barbeau, D.L., Olivero, E.B., Swanson-hysell, N.L., Zahid, K.M., Murray, K.E., and Gehrels, G.E., 2009, Detrital-zircon geochronology of the eastern Magallanes foreland basin: Implications for Eocene kinematics of the northern Scotia Arc and Drake Passage: Earth and Planetary Science Letters, v. 284, p. 489–503, doi: 10.1016/j.epsl.2009.05.014.

Barrett-Lennard, E.G., 2003, The interaction between waterlogging and salinity in higher plants: Causes, consequences and implications: Plant and Soil, v. 253, p. 35–54, doi: 10.1023/A:1024574622669.

Barton, M.D., Porter, I., O'Byrne, C., and Mahood, R., 2017, Impact of the Prairie Evaporite dissolution collapse on McMurray stratigraphy and depositional patterns, Shell Albian Sands Lease 13, northeast Alberta: Bulletin of Canadian Petroleum Geology, v. 65, p. 175–199, doi: 10.2113/gscpgbull.65.1.175.

Beaumont, C., 1981, Foreland basins: Geophysical Journal of the Royal Astronomical Society, v. 65, p. 291–329, doi: 10.4135/9781446247501.n1534.

Benyon, C., Leier, A., Leckie, D., Webb, A., Hubbard, S.M., and Gehrels, G., 2014, Provenance of the Cretaceous Athabasca oil sands, Canada: Implications for continental-scale sediment transport: Journal of Sedimentary Research, v. 84, p. 136–143, doi: 10.2110/jsr.2014.16.

Benyon, C., Leier, A.L., Leckie, D., Hubbard, S.M., and Gehrels, G.E., 2016, Sandstone provenance and insights into the paleogeography of the McMurray Formation from detrital zircon geochronology, Athabasca Oil Sands, Canada: AAPG Bulletin, v. 100, p. 269–287, doi: 10.1306/10191515029.

Beynon, B.M., Pemberton, S.G., Bell, D.D., and Logan, C.A., 1988, Environmental implications of ichnofossils from the Lower Cretaceous Grand Rapids Formation, Cold Lake Oil Sands deposit, in James, D.P. and Leckie, D.A. eds., Sequences, stratigraphy, sedimentology; surface and subsurface. Memoir - Canadian Society of Petroleum Geologists, v. 15, p. 275–289.

Bhattacharya, J.P., Copeland, P., Lawton, T.F., and Holbrook, J., 2016, Estimation of source area, river paleo-discharge, paleoslope, and sediment budgets of linked deep-time depositional systems and implications for hydrocarbon potential: Earth-Science Reviews, v. 153, doi: 10.1016/j.earscirev.2015.10.013.

Bhattacharya, J.P., and MacEachern, J.A., 2009, Hyperpycnal rivers and prodeltaic shelves in the cretaceous seaway of North America: Journal of Sedimentary Research, v. 79, p. 184–209, doi: 10.2110/jsr.2009.026.

Blum, M., and Pecha, M., 2014, Mid-cretaceous to paleocene North American drainage reorganization from detrital zircons: Geology, v. 42, p. 607–610, doi: 10.1130/G35513.1.

Bohacs, K., and Suter, J., 1997, Sequence stratigraphic distribution of coaly rocks: Fundamental controls and paralic examples: AAPG Bulletin, v. 81, p. 1612–1639, doi: 10.1306/3B05C3FC-172A-11D7-8645000102C1865D.

Bohor, B.F., and Triplehorn, D.M., 1993, Tonsteins: Altered volcanic-ash layers in coal-bearing sequences: Geological Society of America Special Paper 285, p. 44, doi: 10.1130/SPE285.

Broughton, P.L., 1977, Origin of coal basins by salt solution: Nature, v. 270, p. 420–423, doi: 10.1038/270420a0.

Broughton, P.L., 2013a, Depositional setting and oil sands reservoir characterization of giant longitudinal sandbars at Ells River: Marginal marine facies of the McMurray Formation, northern Alberta Basin, Canada, in Hein, F.J., Leckie, D.A., Larter, S., and Suter, S.R. eds., Heavy-oil and oil-sand petroleum systems in Alberta and beyond: AAPG Studies in Geology 64, v. 64, p. 313–357, doi: 10.1306/13371584St643556.

Broughton, P.L., 2013b, Devonian salt dissolution-collapse breccias flooring the Cretaceous Athabasca oil sands deposit and development of lower McMurray Formation sinkholes, northern Alberta Basin, Western Canada: Sedimentary Geology, v. 283, p. 57–82, doi: 10.1016/j.sedgeo.2012.11.004.

Broughton, P.L., 2014, Syndepositional architecture of the northern Athabasca Oil Sands Deposit, northeastern Alberta: Canadian Journal of Earth Sciences, v. 52, p. 21–50, doi: 10.1139/cjes-2014-0021.

Broughton, P.L., 2016, Collapse-induced fluidization structures in the Lower Cretaceous Athabasca Oil Sands Deposit, Western Canada: Basin Research, v. 28, p. 507–535, doi: 10.1111/bre.12120.

von Bubnoff, S., 1937, Kohlebildung in Raum und Zeit: Glück Auf, v. 73, p. 641–652.

Burchart, J., Kasza, L., and Lorenc, S., 1998, Fission-track zircon dating of tuffitic intercalations (Tonstein) in the Brown - Coal Mine “Bełchatów”: Bull. Pol. Acad. Sci. Earth Sci., v. 36, p. 281–286.

Bush, A.B.G., 1997, Numerical simulation of the Cretaceous Tethys circumglobal current: Science, v. 275, p. 807–810, doi: 10.1126/science.275.5301.807.

Canadian Geochronology Database, 2013, Geological Survey of Canada, Earth Science Sector, Natural Resources Canada.

Cant, D.J., and Stockmal, G.S., 1989, The Alberta foreland basin: Relationship between stratigraphy and Cordilleran terrane-accretion events: Canadian Journal of Earth Sciences, v. 26, p. 1964–1975, doi: 10.1139/e89-166.

Carrigy, M.A., 1959, Geology of the McMurray Formation, part III: General geology of the McMurray area: Geological Division Memoir 1, Research Council of Alberta, p. 1–130.

Cawood, P.A., Hawkesworth, C.J., and Dhuime, B., 2012, Detrital zircon record and tectonic setting: Geology, v. 40, p. 875–878, doi: 10.1130/G32945.1.

Chalmers, G.R.L., Boyd, R., and Diessel, C.F.K., 2013, Accommodation-based coal cycles and significant surface correlation of low-accommodation Lower Cretaceous coal seams, Lloydminster heavy oilfield, Alberta, Canada: Implications for coal quality distribution: AAPG Bulletin, v. 97, p. 1347–1369, doi: 10.1306/12181211187.

Château, C.C.F., Dashtgard, S.E., Maceachern, J.A., and Hauck, T.E., 2019, Parasequence architecture in a low-accommodation setting, impact of syndepositional carbonate epikarstification, McMurray Formation, Alberta, Canada: Marine and Petroleum Geology, v. 104, p. 168–179, doi: 10.1016/j.marpetgeo.2019.03.021.

Château, C.C.F., Dashtgard, S.E., and Maceachern, J.A., 2020, Refinement of the stratigraphic framework for the Regional C depositional unit of the Mcmurray Formation and implications for the early transgression of the Alberta Foreland Basin, Canada: Journal of Sedimentary Research, v. 90, p. 1322–1345, doi: 10.2110/JSR.2020.62.

Château, C.C.F., Dashtgard, S.E., and MacEachern, J.A., 2021, Changes in the rate of the Boreal Sea transgression recorded in the Lower Cretaceous McMurray Formation, Canada: Marine and Petroleum Geology.

Chen, W.-S., Huang, Y.-C., Liu, C.-H., Feng, H.-T., Chung, S.-L., and Lee, Y.-H., 2016, U-Pb zircon geochronology constraints on the ages of the Tananao Schist Belt and timing of orogenic events in Taiwan: Implications for a new tectonic evolution of the South China Block during the Mesozoic: Tectonophysics, v. 686, p. 68–81, doi: 10.1016/j.tecto.2016.07.021.

Christiansen, E.H., Kowallis, B.J., and Barton, M.D., 1994, Temporal and spatial distribution of volcanic ash in Mesozoic sedimentary rocks of the Western Interior: An alternative record of Mesozoic magmatism, in Caputo, M. V., Peterson, J.A., and Franczyk, K.J. eds., Mesozoic systems of the Rocky Mountain Region, USA, Rocky Mountain Section SEPM, p. 73–94.

Christopher, J.E., 1997, Evolution of the Lower Cretaceous Mannville Sedimentary Basin in Saskatchewan, in Pemberton, S.G. and James, D.P. eds., Petroleum geology of the Cretaceous Mannville Group, western Canada, Canadian Society of Petroleum Geologists Memoir 18, p. 191–210.

Christopher, J.E., 1974, The Upper Jurrasic Vangard and Lower Cretaceous Mannville Groups: Saskatchewan Geological Survey, Department of Mineral Resources, p. 323.

Clymo, R.S., 1984, The limits to peat bog growth: Philosophical Transactions of the Royal Society of London, Series B, v. 303, p. 605–654, doi: jstor.org/stable/2396128.

Cohen, K.M., Finney, S.C., Gibbard, P.L., and Fan, J.-X., 2013, The ICS International Chronostratigraphic Chart: Episode 36, p. 199–204.

Collins, D.S., Johnson, H.D., Allison, P.A., Guilpain, P., and Damit, A.R., 2017, Coupled 'storm-flood' depositional model: Application to the Miocene–Modern Baram Delta Province, north-west Borneo: Sedimentology, v. 64, p. 1203–1235, doi: 10.1111/sed.12316.

Condon, D.J., Schoene, B., McLean, N.M., Bowring, S.A., and Parrish, R.R., 2015, Metrology and traceability of U-Pb isotope dilution geochronology (EARTHTIME Tracer Calibration Part I): Geochimica et Cosmochimica Acta, v. 164, p. 464–480, doi: 10.1016/j.gca.2015.05.026.

Copeland, P., 2020, On the use of geochronology of detrital grains in determining the time of deposition of clastic sedimentary strata: Basin Research, p. 40, doi: 10.1111/bre.12441.

Coutts, D.S., Matthews, W.A., and Hubbard, S.M., 2019, Assessment of widely used methods to derive depositional ages from detrital zircon populations: Geoscience Frontiers, v. 10, p. 1421–1435, doi: 10.1016/j.gsf.2018.11.002.

Coutts, D.S., Matthews, W.A., Englert, R.G., Brooks, M.D., Boivin, M.P., and Hubbard, S.M., 2020, Along-strike variations in sediment provenance within the Nanaimo basin reveal mechanisms of forearc basin sediment influx events: Lithosphere, v. 12, p. 180–197, doi: 10.1130/L1138.1.

Crerar, E.E., and Arnott, R.W.C., 2007, Facies distribution and stratigraphic architecture of the Lower Cretaceous McMurray Formation, Lewis Property, northeastern Alberta: Bulletin of Canadian Petroleum Geology, v. 55, p. 99–124, doi: 10.2113/gscpgbull.55.2.99.

La Croix, A.D., and Dashtgard, S.E., 2015, A synthesis of depositional trends in intertidal and upper subtidal sediments across the tidal–fluvial transition in the Fraser River, Canada: Journal of Sedimentary Research, v. 85, p. 683–698, doi: 10.2110/jsr.2015.47.

La Croix, A.D., Dashtgard, S.E., Gingras, M.K., Hauck, T.E., and MacEachern James A., 2015, Bioturbation trends across the freshwater to brackish-water transition in rivers: Palaeogeography, Palaeoclimatology, Palaeoecology, v. 440, p. 66–77, doi: 10.1016/j.palaeo.2015.08.030.

La Croix, A.D., Dashtgard, S.E., and MacEachern, J.A., 2019, Using a modern analogue to interpret depositional position in ancient fluvial-tidal channels: Example from the McMurray Formation, Canada: Geoscience Frontiers, doi: 10.1016/j.gsf.2019.03.008.

Crowley, J.L., Schoene, B., and Bowring, S.A., 2007, U-Pb dating of zircon in the Bishop Tuff at the millennial scale: Geology, v. 35, p. 1123–1126, doi: 10.1130/G24017A.1.

Czarnecki, J.M., Dashtgard, S.E., Pospelova, V., Mathewes, R.W., and MacEachern, J.A., 2014, Palynology and geochemistry of channel-margin sediments across the tidal-fluvial transition, lower Fraser River, Canada: Implications for the rock record: Marine and Petroleum Geology, v. 51, p. 152–166, doi: 10.1016/j.marpetgeo.2013.12.008.

Dai, S., Ward, C.R., Graham, I.T., French, D., Hower, J.C., Zhao, L., and Wang, X., 2017, Altered volcanic ashes in coal and coal-bearing sequences: A review of their nature and significance: Earth-Science Reviews, v. 175, p. 44–74, doi: 10.1016/j.earscirev.2017.10.005.

Daniels, B.G., Auchter, N.C., Hubbard, S.M., Romans, B.W., Matthews, W.A., and Stright, L., 2018, Timing of deep-water slope evolution constrained by large-n detrital and volcanic ash zircon geochronology, Cretaceous Magallanes Basin, Chile: GSA Bulletin, v. 130, p. 438–454, doi: 10.1130/B31757.1.

Davies, R., Howell, J., Boyd, R., Flint, S., and Diessel, C., 2006, High-resolution sequence-stratigraphic correlation between shallow-marine and terrestrial strata: Examples from the Sunnyside Member of the Cretaceous Blackhawk Formation, Book Cliffs, eastern Utah: AAPG Bulletin, v. 90, p. 1121–1140, doi: 10.1306/02210604077.

DeCelles, P.G., 2004, Late Jurassic to Eocene evolution of the Cordilleran thrust belt and foreland basin system, western U.S.A: American Journal of Science, v. 304, p. 105–168, doi: 10.2475/ajs.304.2.105.

Decelles, P.G., Ducea, M.N., Kapp, P., and Zandt, G., 2009, Cyclicity in Cordilleran orogenic systems: Nature Geoscience, v. 2, p. 251–257, doi: 10.1038/ngeo469.

Deschamps, R., Omodeo-Salé, S., Chauveau, B., Fierens, R., and Euzen, T., 2017, The coal-bearing strata of the Lower Cretaceous Mannville Group (Western Canadian Sedimentary Basin, South Central Alberta). Part 1: Stratigraphic architecture and coal distribution controlling factors: International Journal of Coal Geology, v. 179, p. 113–129, doi: 10.1016/j.coal.2017.05.019.

Dickinson, W.R., and Gehrels, G.E., 2009, Use of U-Pb ages of detrital zircons to infer maximum depositional ages of strata: A test against a Colorado Plateau Mesozoic database: Earth and Planetary Science Letters, v. 288, p. 115–125, doi: 10.1016/j.epsl.2009.09.013.

Diessel, C.F.K., 1992, Coal-Bearing Depositional Systems: Berlin, Springer-Verlag, 727 p., doi: 10.1007/978-3-642-75668-9.

Diessel, C.F.K., 2007, Utility of coal petrology for sequence-stratigraphic analysis: International Journal of Coal Geology, v. 70, p. 3–34, doi: 10.1016/j.coal.2006.01.008.

Diessel, C., Boyd, R., Wadsworth, J., Leckie, D., and Chalmers, G., 2000, On balanced and unbalanced accommodation/peat accumulation ratios in the Cretaceous coals from Gates Formation, Western Canada, and their sequence-stratigraphic significance: International Journal of Coal Geology, v. 43, p. 143–186, doi: 10.1016/S0166-5162(99)00058-0.

Dodson, M.H., Compston, W., Williams, I.S., and Wilson, J.F., 1988, A search for ancient detrital zircons in Zimbabwean sediments: Journal of the Geological Society, v. 145, p. 977–983, doi: 10.1144/gsjgs.145.6.0977.

Elder, W.P., 1988, Geometry of Upper Cretaceous bentonite beds: Implications about volcanic source areas and paleowind patterns, western interior, United States: Geology, v. 16, p. 835–838, doi: 10.1130/0091-7613(1988)016<0835:GOUCBB>2.3.CO;2.

Englert, R.G., Hubbard, S.M., Coutts, D.S., and Matthews, W.A., 2018, Tectonically controlled initiation of contemporaneous deep-water channel systems along a Late Cretaceous continental margin, western British Columbia, Canada: Sedimentology, v. 65, p. 2404–2438, doi: 10.1111/sed.12472.

Feldman, H.R., McCrimmon, G.G., and De Freitas, T.A., 2008, Fluvial to estuarine valley-fill models without age-equivalent sandy shoreline deposits, based on the Clearwater Formation (Cretaceous) at Cold Lake, Alberta, Canada, in Hampson, G., Steel, R.J., Burgess, P.M., and Dalrymple, R.W. eds., Recent advances in models of siliciclastic shallow-marine stratigraphy, Tulsa, Oklahoma, p. 443–472, doi: 10.2110 /pec.08.90.0443.

Finzel, E.S., 2014, Detrital zircons from Cretaceous midcontinent strata reveal an Appalachian Mountains-Cordilleran foreland basin connection: Lithosphere, v. 6, p. 378–382, doi: 10.1130/L400.1.

Flach, P.D., and Mossop, G.D., 1985, Depositional environments of the Lower Cretaceous McMurray Formation, Athabasca Oil Sands, Alberta: AAPG Bulletin, v. 69, p. 1195–1207, doi: 10.1306/AD462BAF-16F7-11D7-8645000102C1865D.

Flint, S., Aitken, J., and Hampson, G., 1995, Application of sequence stratigraphy to coal-bearing coastal plain successions: implications for the UK Coal Measures, in Whateley, M.K.G. and Spears, D.A. eds., European Coal Geology, Geological Society Special Publication No. 82, p. 1–16, doi: 10.1144/GSL.SP.1995.082.01.01.

Friedman, R., and Armstrong, R.L., 1995, Jurassic and Cretaceous geochronology of the southern Coast Belt, British Columbia, 49° to 51°N, in Miller, D.M. and Busby, C. eds., Jurassic Magmatism and Tectonics of the North American Cordillera: Boulder, Colorado, Geological Society Special Paper 299, p. 95–139.

Galbraith, R.F., 2005, Statistics for fission track analysis: Chapman & Hall/CRC, 240 p., doi: 10.1201/9781420034929.

Galbraith, R.F., and Laslett, G.M., 1993, Statistical models for mixed fission track ages: Nucl. Tracks. Radiats. Meas., v. 21, p. 459–470, doi: 10.1016/1359-0189(93)90185-C.

Gani, R.M., Ranson, A., Cross, D.B., Hampson, G.J., Gani, N.D., and Sahoo, H., 2015, Along-strike sequence stratigraphy across the Cretaceous shallow marine to coastal-plain transition, Wasatch Plateau, Utah, U.S.A.: Sedimentary Geology, v. 325, p. 59–70, doi: 10.1016/j.sedgeo.2015.05.003.

Gastil, G., Morgan, G.J., and Krummenacher, D., 1978, Mesozoic history of Peninsular California and related areas east of the Gulf of California, in Pacific Coast Paleogeography Symposium 2: Mesozoic Paleogeography of the Western United States, Pacific Section SEPM, p. 107–115.

Gehrels, G., 2014, Detrital zircon U-Pb geochronology applied to tectonics: Annual Review of Earth and Planetary Sciences, v. 42, p. 127–149, doi: 10.1146/annurev-earth-050212-124012.

Gehrels, G.E., 2000, Introduction to detrital zircon studies of Paleozoic and Triassic strata in western Nevada and northern California, in Soreghan, M.J. and Gehrels, G.E. eds., Paleozoic and Triassic paleogeography and tectonics of western Nevada and northern California, Boulder, Colorada, U.S.A, Geological Society of America Special Paper 347, p. 1–17, doi: 10.1130/0-8137-2347-7.1.

Gehrels, G., and Pecha, M., 2014, Detrital zircon U-Pb geochronology and Hf isotope geochemistry of Paleozoic and Triassic passive margin strata of western North America: Geosphere, v. 10, p. 49–65, doi: 10.1130/GES00889.1.

Gehrels, G.E., Rusmore, M., Woodsworth, G., Crawford, M., Andronicos, C., Hollister, L., Patchett, J., Ducea, M., Butler, R., Klepeis, K., Davidson, C., Friedman, R., Haggarf, J., Mahoney, B., et al., 2009, U-Th-Pb geochronology of the Coast Mountains batholith in north-coastal British Columbia: Constraints on age and tectonic evolution: GSA Bulletin, v. 121, p. 1341–1361, doi: 10.1130/B26404.1.

Gehrels, G.E., Valencia, V.A., and Ruiz, J., 2008, Enhanced precision, accuracy, efficiency, and spatial resolution of U-Pb ages by laser ablation–multicollector–inductively coupled plasma–mass spectrometry: Geochemistry, Geophysics, Geosystems, v. 9, p. 1–13, doi: 10.1029/2007GC001805.

Gingras, M.K., MacEachern, J.A., Dashtgard, S.E., Ranger, M.J., and Pemberton, S.G., 2016, The significance of trace fossils in the McMurray formation, Alberta, Canada: Bulletin of Canadian Petroleum Geology, v. 64, p. 233–250, doi: 10.2113/gscpgbull.64.2.233.

Gore, A.J.P., 1982, Introduction, in Gore, A.J.P. ed., Mires: Swamp, Bog, Fen and Moor, Elsevier, p. 1–34.

Gray, H.A., 2019, Depositional Architecture of the middle McMurray Formation: Suncor Firebag SAGD Asset: GeoConvention, May 13–17, Calgary, Alberta, Canada, p. 3–5.

Greb, S.F., Eble, C.F., and Hower, J.C., 1999, Depositional history of the Fire Clay coal bed (Late Duckmantian), Eastern Kentucky, USA: International Journal of Coal Geology, v. 40, p. 255–280, doi: 10.1016/S0166-5162(99)00004-X.

Harris, B.S., Timmer, E.R., Ranger, M.J., and Gingras, M.K., 2016, Continental ichnology of the Lower McMurray Formation inclined heterolithic strata at Daphne Island, Athabasca River, north-eastern Alberta, Canada: Bulletin of Canadian Petroleum Geology, v. 64, p. 218–232, doi: 10.2113/gscpgbull.64.2.218.

Hauck, T.E., MacCormack, K.E., and Babakhani, M., 2018, Regional stratigraphic mapping and 3D modelling of the Paleozoic succession in Northeastern Alberta (Townships 59–104, Ranges 1– 19, West of the Fourth Meridian): AER/AGS Report 95, p. 1–38, ISBN: 978-1-4601-1675–3.

Hay, W., and Floegel, S., 2012b, New thoughts about the Cretaceous climate and oceans: Earth-Science Reviews, v. 115, p. 262–272, doi: 10.1016/j.earscirev.2012.09.008.

Hayes, D.A., Timmer, E.R., Deutsch, J.L., Ranger, M.J., and Gingras, M.K., 2017, Analyzing dune foreset cyclicity in outcrop with photogrammetry: Journal of Sedimentary Research, v. 87, p. 66–74, doi: 10.2110/jsr.2016.93.

Heimhofer, U., Hochuli, P.A., Burla, S., and Weissert, H., 2007, New records of Early Cretaceous angiosperm pollen from Portuguese coastal deposits: Implications for the timing of the early angiosperm radiation: Review of Palaeobotany and Palynology, v. 144, p. 39–76, doi: 10.1016/j.revpalbo.2005.09.006.

Hein, F.J., 2000, Historical Overview of the Fort McMurray Area and Oil Sands Industry in Northeast Alberta: Alberta Energy and Utilities Board, p. 1–37.

Hein, F.J., and Cotterill, D.K., 2006, The Athabasca Oil Sands - A regional geological perspective, Fort McMurray area, Alberta, Canada: Natural Resources Research, v. 15, p. 85–102, doi: 10.1007/s11053-006-9015-4.

Hein, F.J., Cotterill, D.K., and Rice, R., 2006, Subsurface geology of the Athabasca Wabiskaw-McMurray succession: Lewis-Fort McMurray Area, northeastern Alberta (NTS 74D / 74E): EUB/AGE Earth Sciences Report, p. 1–67.

Hein, F.J., Cotterill, D.K., Weiss, J., and Berhane, H., 2007, Subsurface geology and facies characterization of the Athabasca Wabiskaw-McMurray succession: Firebag-Sunrise area, northeastern Alberta (NTS 74D/74E): EUB/AGS Earth Sciences Report 2006-08, p. 1–66, ISBN: 0-7785-3833–8.

Hein, F.J., Fairgrieve, B., and Dolby, G., 2013, A regional geologic gramework for the Athabasca Oil Sands, northeastern Alberta, Canada, in Hein, F.J., Leckie, D., and Suter, J.R. eds., Heavy-oil and oil-sand petroleum systems in Alberta and beyond, AAPG Studies in Geology, v. 64, p. 207–250, doi: 10.1306/13371581St643550.

Hein, F.J., and Dolby, G., 2018, Lithostratigraphy, Palynology, and Biostratigraphy of the Athabasca Oil Sands Deposit, Northeastern Alberta: AER/AGS Open File Report 2017-08, p. 1–105, ISBN: 978-1-4601-2219–8.

Herriott, T.M., Crowley, J.L., Schmitz, M.D., Wartes, M.A., and Gillis, R.J., 2019, Exploring the law of detrital zircon: LA-ICP-MS and CA-TIMS geochronology of Jurassic forearc strata, Cook Inlet, Alaska, USA: Geology, v. 47, p. 1044–1048, doi: 10.1130/G46312.1.

Holz, M., Kalkreuth, W., and Banerjee, I., 2002, Sequence stratigraphy of paralic coal-bearing strata: an overview: International Journal of Coal Geology, v. 48, p. 147–179, doi: 10.1016/S0166-5162(01)00056-8.

Horner, S.C., Hubbard, S.M., Martin, H.K., and Hagstrom, C.A., 2019, Reconstructing basin-scale drainage dynamics with regional subsurface mapping and channel-bar scaling, Aptian, Western Canada Foreland Basin: Sedimentary Geology, v. 385, p. 26–44, doi: 10.1016/j.sedgeo.2019.03.012.

Horner, S.C., Hubbard, S.M., Martin, H.K., Hagstrom, C.A., and Leckie, D.A., 2018, The impact of Aptian glacio-eustasy on the stratigraphic architecture of the Athabasca Oil Sands, Alberta, Canada: Sedimentology, v. 66, p. 1600–1642, doi: 10.1111/sed.12545.

Horstwood, M.S.A., Ko, J., Gehrels, G., Jackson, S.E., Mclean, N.M., Paton, C., Pearson, N.J., Sircombe, K., Sylvester, P., Vermeesch, P., Bowring, J.F., Condon, D.J., and Schoene, B., 2016, Community-derived standards for LA-ICP-MS U-(Th-)Pb geochronology – Uncertainty propagation, age interpretation and data reporting: Geostandards and Geoanalytical Research, v. 40, p. 311–332, doi: 10.1111/j.1751-908X.2016.00379.x.

Huang, C., Dashtgard, S.E., Kent, B.A.P., Gibson, H.D., and Matthews, W.A., 2019, Resolving the architecture and early evolution of a forearc basin (Georgia Basin, Canada) using detrital zircon: Scientific Reports, v. 9, p. 1–12, doi: 10.1111/bre.12378.

Hubbard, S.M., Smith, D.G., Nielsen, H., Leckie, D., Fustic, M., Spencer, R.J., and Bloom, L., 2011, Seismic geomorphology and sedimentology of a tidally influenced river deposit, Lower Cretaceous Athabasca oil sands, Alberta, Canada: AAPG Bulletin, v. 95, p. 1123–1145, doi: 10.1306/12131010111.

Hughes, P.D.M., and Barber, K.E., 2003, Mire development across the fen – bog transition on the Teifi floodplain at Tregaron Bog, Ceredigion, Wales, and a comparison with 13 other raised bogs: Journal of Ecology, v. 91, p. 253–264, doi: 10.1046/j.1365-2745.2003.00762.x.

Ielpi, A., and Lapôtre, M.G.A., 2020, A tenfold slowdown in river meander migration driven by plant life: Nature Geoscience, v. 13, doi: 10.1038/s41561-019-0491-7.

Ingram, H.A.P., 1978, Soil layers in mires: Function and terminology: Journal of Soil Science, v. 29, p. 224–227, doi: 10.1111/j.1365-2389.1978.tb02053.x.

Jacobson, C.E., Grove, M., Pedrick, J.N., Barth, A.P., Marsaglia, K.M., Gehrels, G.E., and Nourse, J.A., 2011, Late Cretaceous-early Cenozoic tectonic evolution of the southern California margin inferred from provenance of trench and forearc sediments: GSA Bulletin, v. 123, p. 485–506, doi: 10.1130/B30238.1.

Jaffey, A.H., Flynn, K.F., Glendenin, L.E., Bentley, W.C., and Essling, A.M., 1971, Precision measurement of half-lives and specific activities of U235 and U238: Physical Review C, v. 4, p. 1889–1906, doi: 10.1103/PhysRevC.4.1889.

Jardine, D., 1974, Cretaceous oil sands of western Canada, in Hills, L. V. eds., Oil Sands, Fuel of the Future: Canadian Society of Petroleum Geologists, Memoir 3, p. 50–67.

Jerrett, R.M., Davies, R.C., Hodgson, D.M., Flint, S.S., and Chiverrell, R.C., 2011a, The significance of hiatal surfaces in coal seams: Journal of the Geological Society, v. 168, p. 629–632, doi: 10.1144/0016-76492010-178.

Jerrett, R.M., Flint, S.S., Davies, R.C., and Hodgson, D.M., 2011b, Sequence stratigraphic interpretation of a Pennsylvanian (Upper Carboniferous) coal from the central Appalachian Basin, USA: Sedimentology, v. 58, p. 1180–1207, doi: 10.1111/j.1365-3091.2010.01200.x.

Jerrett, R.M., Hodgson, D.M., Flint, S.S., and Davies, R.C., 2011c, Control of relative sea level and climate on coal character in the Westphalian C (Atokan) Four Corners Formation, Central Appalachian Basin, U.S.A.: Journal of Sedimentary Research, v. 81, p. 420–445, doi: 10.2110/jsr.2011.37.

Johnstone, S.A., Schwartz, T.M., and Holm-Denoma, C.S., 2019, A stratigraphic approach to inferring depositional ages from detrital geochronology data: Frontiers in Earth Science, v. 7, p. 1–19, doi: 10.3389/feart.2019.00057.

Keith, D.A.W., Wightman, D.M., Pemberton, S.G., MacGillivray, J.R., Berezniuk, T., and Berhane, H., 1988, Sedimentology of the McMurray Formation and Wabiskaw Member (Clearwater Formation), Lower Cretaceous, in the central region of the Athabasca Oil Sands area, northeastern Alberta, in James, D.P. and Leckie, D.A. eds., Sequences, Stratigraphy, Sedimentology: Surface and Subsurface, Canadian Society of Petroleum Geologists, Memoir 15, p. 309–324.

Kent, B.A.P., Dashtgard, S.E., Huang, C., Maceachern, J.A., Gibson, H.D., and Cathyl-Huhn, G., 2019, Initiation and early evolution of a forearc basin: Georgia Basin, Canada: Basin Research, p. 1–23, doi: 10.1111/bre.12378.

Košler, J., Sláma, J., Belousova, E., Corfu, F., Gehrels, G.E., Gerdes, A., Horstwood, M.S.A., Sircombe, K., Sylvester, P., Tiepolo, M., Whitehouse, M.J., and Woodhead, J.D., 2013, U-Pb detrital zircon analysis – Results of an inter-laboratory comparison: Geostandards and Geoanalytical Research, v. 37, p. 243–259, doi: 10.1111/j.1751-908X.2013.00245.x.

Kraus, M.J., 1999, Paleosols in clastic sedimentary rocks: Their geologic applications: Earth Science Reviews, v. 47, p. 41–70, doi: 10.1016/S0012-8252(99)00026-4.

Kraus, M.J., and Hasiotis, S.T., 2006, Significance of different modes of rhizolith preservation to interpreting paleoenvironmental and paleohydrologic settings: Examples from paleogene paleosols, Bighorn Basin, Wyoming, U.S.A: Journal of Sedimentary Research, v. 76, p. 633–646, doi: 10.2110/jsr.2006.052.

Labrecque, P.A., Jensen, J.L., Hubbard, S.M., and Nielsen, H., 2011, Sedimentology and stratigraphic architecture of a point bar deposit, Lower Cretaceous McMurray Formation, Alberta, Canada: Bulletin of Canadian Petroleum Geology, v. 59, p. 147–171, doi: 10.2113/gscpgbull.59.2.147.

Laskowski, A.K., Decelles, P.G., and Gehrels, G.E., 2013, Detrital zircon geochronology of Cordilleran retroarc foreland basin strata, western North America: Tectonics, v. 32, p. 1027–1048, doi: 10.1002/tect.20065.

Leckie, D.A., Fox, C., and Tarnocai, C., 1989, Multiple paleosols of the late Albian Boulder Creek Formation, British Columbia, Canada: Sedimentology, v. 36, p. 307–323, doi: 10.1111/j.1365-3091.1989.tb00609.x.

Leckie, D.A., and Smith, D.G., 1992, Regional setting, evolution, and depositional cycles of the Western Canada Foreland Basin: Chapter 1, in MacQueen, R.W. and Leckie, D.A. eds., Foreland basins and fold belts, AAPG Memoir 55, p. 9–46.

Leckie, D.A., Wallace-Dudley, K.E., Vanbeselaere, N.A., and James, D.P., 2004, Sedimentation in a low-accommodation setting: Nonmarine (Cretaceous) Mannville and marine (Jurassic) Ellis groups, Manyberries field, southeastern Alberta: AAPG Bulletin, v. 18, p. 1391–1418, doi: 10.1306/05120403131.

Long, A.J., Waller, M.P., and Stupples, P., 2006, Driving mechanisms of coastal change: Peat compaction and the destruction of late Holocene coastal wetlands: Marine Geology, v. 225, p. 63–84, doi: 10.1016/j.margeo.2005.09.004.

Ludwig, K.R., 2012, Isoplot 3.75, a geochronological toolkit for Microsoft Excel: Berkeley Geochronology Center Special Publication No. 5, p. 1–72.

Ludwig, K.R., and Mundil, R., 2002, Extracting reliable U-Pb ages and errors from complex populations of zircons from Phanerozoic tuffs: Geochemica et Comschimica Acta 66, p. 461.

MacEachern James A., Bann, K.L., Bhattacharya, J.P., and Howell Jr., C.D., 2005, Ichnology of deltas; organism responses to the dynamic interplay of rivers, waves, storms, and tides: v. 83, 49–85 p.

Martin, H.K., Hubbard, S.M., Hagstrom, C.A., Horner, S.C., and Durkin, P.R., 2019, Planform recognition and implications of a Cretaceous-age continental-scale river avulsion node in the Western Interior Basin, Alberta, Canada: Journal of Sedimentary Research, v. 89, p. 610–628, doi: 10.2110/jsr.2019.37.

Matthews, W.A., and Guest, B., 2016, A practical approach for collecting large-n detrital zircon U-Pb data sets by Quadrupole LA-ICP-MS: Geostandards and Geoanalytical Research, v. 41, p. 161–180, doi: 10.1111/ggr.12146.

Matthews, W.A., Guest, B., Coutts, D., Bain, H., and Hubbard, S., 2017, Detrital zircons from the Nanaimo basin, Vancouver Island, British Columbia: An independent test of Late Cretaceous to Cenozoic northward translation: Tectonics, v. 36, p. 854–876, doi: 10.1002/2017TC004531.

Mattinson, J.M., 2005, Zircon U-Pb chemical abrasion (“CA-TIMS”) method: Combined annealing and multi-step partial dissolution analysis for improved precision and accuracy of zircon ages: Chemical Geology, v. 220, p. 47–66, doi: 10.1016/j.chemgeo.2005.03.011.

McCarthy, P.J., and Plint, A.G., 1998, Recognition of interfluve sequence boundaries: integrating paleopedology and sequence stratigraphy: Geology, v. 26, p. 387–390, doi: 10.1130/0091-7613(1998)026<0387:ROISBI>2.3.CO;2.

McCrimmon, G.G., and Arnott, R.W.C., 2002, The Clearwater Formation, Cold Lake, Alberta: A worldclass hydrocarbon reservoir hosted in a complex succession of tide-dominated deltaic deposits: Bulletin of Canadian Petroleum Geology, v. 50, p. 370–392, doi: 10.2113/50.3.370.

Moecher, D.P., and Samson, S.D., 2006, Differential zircon fertility of source terranes and natural bias in the detrital zircon record: Implications for sedimentary provenance analysis: Earth and Planetary Science Letters, v. 247, p. 252–266, doi: 10.1016/j.epsl.2006.04.035.

Monger, J., and Price, R., 2002, The Canadian Cordillera: Geology and tectonic evolution: CSEG Recorder, v. 27, p. 17–36, doi: 10.13140/2.1.4483.1520.

Monger, J.W.H., Price, R.A., and Tempelman-Kluit, D.J., 1982, Tectonic accretion and the origin of the two major metamorphic and plutonic welts in the Canadian Cordillera.: Geology, v. 10, p. 70–75, doi: 10.1130/0091-7613(1982)10<70:TAATOO>2.0.CO;2.

Morshedian, A., MacEachern, J.A., and Dashtgard, S.E., 2012, Integrated ichnology, sedimentology and stratigraphy of the Lower Cretaceous Sparky Alloformation (Mannville Group), Lloydminster Area, west-central Saskatchewan, Canada: Bulletin of Canadian Petroleum Geology, v. 60, p. 69–91, doi: 10.2113/gscpgbull.60.2.69.

Mossop, G.D., and Flach, P.D., 1983, Deep channel sedimentation in the Lower Cretaceous McMurray Formation, Athabasca Oil Sands, Alberta: Sedimentology, v. 30, p. 493–509, doi: 10.1111/j.1365-3091.1983.tb00688.x.

Mulhern, J.S., and Johnson, C.L., 2017, Time-space variability of paralic strata deposited in a high accommodation, high sediment supply setting: Example from the Cretaceous of Utah, in Hampson, G.J., Kostic, B., and Wells, M.R. eds., Sedimentology of Paralic Reservoirs: Recent Advances, Geological Society Special Publication, 444, p. 349–392, doi: 10.1144/SP444.7.

Nadon, G.C., 1998, Magnitude and timing of peat-to-coal compaction: Geology, v. 26, p. 727–730, doi: 10.1130/0091-7613(1998)026<0727:MATOPT>2.3.CO;2.

Nelson, H.W., and Glaister, R.P., 1978, Subsurface environmental facies and reservoir relationships of the McMurray oil sands, northeastern Alberta: Bulletin of Canadian Petroleum Geology, v. 26, p. 177–207, doi: 10.35767/gscpgbull.26.2.177.

Omodeo-Salé, S., Deschamps, R., Michel, P., Chauveau, B., and Suárez-Ruiz, I., 2017, The coal-bearing strata of the Lower Cretaceous Mannville Group (Western Canadian Sedimentary Basin, South Central Alberta). Part 2: Factors controlling the composition of organic matter accumulations: International Journal of Coal Geology, v. 179, p. 219–241, doi: 10.1016/j.coal.2017.05.020.

Pattison, S.A.J., 2018, Rethinking the incised-valley fill paradigm for Campanian Book Cliffs strata, Utah-Colorado, U.S.A.: Evidence for discrete parasequence-scale, shoreface-incised channel fills: Journal of Sedimentary Reseach, v. 88, p. 1381–1412, doi: 10.2110/jsr.2018.72.

Pattison, S.A.J., 2019a, Re-evaluating the sedimentology and sequence stratigraphy of classic Book Cliffs outcrops at Tusher and Thompson canyons, eastern Utah, USA: Applications to correlation, modelling, and prediction in similar nearshore terrestrial to shallow marine subsurf: Marine and Petroleum Geology, v. 102, p. 202–230, doi: 10.1016/j.marpetgeo.2018.12.043.

Pattison, S.A.J., 2019b, Using classic outcrops to revise sequence stratigraphic models: Reevaluating the Campanian Desert Member (Blackhawk Formation) to lower Castlegate Sandstone interval, Book Cliffs, Utah and Colorado , USA: Geology, v. 47, p. 11–14, doi: 10.1130/G45592.1.

Pemberton, S.G., Flach, P.D., and Mossop, G.D., 1982, Trace Fossils from the Athabasca Oil Sands, Alberta, Canada: Science, v. 217, p. 825–827, doi: 10.1126/science.217.4562.825.

Pizzuto, J.E., and Schwendt, A.E., 1997, Mathematical modeling of autocompaction of a Holocene transgressive valley-fill deposit, Wolfe Glade, Delaware: Geology, v. 25, p. 57–60, doi: 10.1130/0091-7613(1997)025<0057:MMOAOA>2.3.CO;2.

Plint, A.G., Hart, B.S., and Donaldson, W.S., 1993, Lithospheric flexure as a control on stratal geometry and fades distribution in Upper Cretaceous rocks of the Alberta foreland basin: Basin Research, v. 5, p. 69–77, doi: 10.1111/j.1365-2117.1993.tb00058.x.

Plint, A.G., McCarthy, P.J., and Faccini, U.F., 2001, Nonmarine sequence stratigraphy: Updid expression of sequence boundaries and systems tracts in a high-resolution framework, Cenomanian Dunvegan Formation, Alberta Foreland Basin, Canada: AAPG Bulletin, v. 85, p. 1967–2001, doi: 10.1306/8626d0c7-173b-11d7-8645000102c1865d.

Plint, A.G., and Wadsworth, J.A., 2003, Sedimentology and palaeogeomorphology of four large valley systems incising delta plains, western Canada Foreland Basin: implications for mid-Cretaceous sea-level changes: Sedimentology, v. 50, p. 11: Sedimentology, v. 50, p. 1147–1186, doi: 10.1046/j.1365-3091.2003.00599.x.

Porter, J.W., Price, R.A., and McCrossan, R.G., 1982, The Western Canada Sedimentary Basin: Philosophical Transactions of the Royal Society of London, v. 305, p. 169–192.

Posamentier, H.W., Jervey, M.T., and Vail, P.R., 1988, Eustatic controls on clastic deposition I - Conceptual framework, in Wilgus, C.K., Hastings, B.S.., C.G.St.C., K., H.W., P., C.A., R., and J.C., V.W. eds., Sea-Level Changes: An Integrated Approach, p. 109–124, doi: 10.2110/pec.88.01.0109.

Posamentier, H.W., and Vail, P.R., 1988, Eustatic controls on elastic deposition II - Sequence and systems tracts models, in Wilgus, C.K., Hastings, B.S., Kendall, C.G.S.C., Posamentier, H.W., Ross, C.A., and Van Wagoner, J.C. eds., Sea-level Research: An Integrated Approach, SEPM Special Publication 42, p. 125–154, doi: 10.2110/pec.88.01.0125.

Poulton, T.P., Christopher, J.E., Hayes, B.J.R., Losert, J., Tittemore, J., and Gilchrist, R.D., 1994, Jurassic and lowermost Cretaceous Strata of the Western Canada Sedimentary Basin, in Mossop, G. and Shetsen, I. eds., Geological Atlas of the Western Canada Sedimentary Basin: Calgary, Alberta, Canadian Society of Petroleum Geologists and Alberta Research Council, p. 297–316.

Price, R.A., 1981, The Cordilleran foreland thrust and fold belt in the southern Canadian Rocky Mountains, in McClay, K.R. and Price, N.J. eds., Thrust and Nappe Tectonics, Geological Society of London, Special Publication 9, p. 427–448.

Pullen, A., Ibáñez-Mejía, M., Gehrels, G.E., Ibáñez-Mejía, J.C., and Pecha, M., 2014, What happens when n=1000? Creating large-n geochronological datasets with LA-ICP-MS for geologic investigations, in Journal of Analytical Atomic Spectrometry, doi: 10.1039/c4ja00024b.

Quinn, G.M., Hubbard, S.M., van Drecht, R., Guest, B., Matthews, W.A., and Hadlari, T., 2016, Record of orogenic cyclicity in the Alberta Foreland Basin, Canadian Cordillera: Lithosphere, v. 8, p. 317–332, doi: 10.1130/L531.1.

Rahnama, F., Marsh, R.A., and Philp, L., 2013, The Alberta Oil Sands: Reserves and long-term supply outlook: Heavy-oil and Oil-sand Petroleum Systems in Alberta and Beyond, v. 64, p. 133–144, doi: 10.1306/13371577St643551.

Ranger, M.J., 1994, A basin study of the southern Athabasca Oil Sands deposit: University of Alberta, 289 p.

Ranger, M.J., 2006, The northeastern sector of the Lower Cretaceous oil-sands basin: Facies and fluids, in Gilboy, C.F. and Whittaker, S.G. eds., Saskatchewan and Northern Plains Oil & Gas Symposium 2006, Saskatchewan Geological Society Special Publications 19, p. 249–256.

Ranger, M.J., and Pemberton, S.G., 1997, Elements of a stratigraphic framework for the McMurray Formation in south Athabasca area, Alberta, in Pemberton, S.G. and James, D.P. eds., Petroleum Geology of the Cretaceous Mannville Group, Western Canada, Canadian Society of Petroleum Geologists, Memoir 18, p. 263–291.

Retallack, G.J., 1991, Untangling the effects of burial alteration and ancient soil formation: Annual Review of Earth and Planetary sciences, v. 19, p. 183–206, doi: 10.1146/annurev.earth.19.1.183.

Rinke-Hardekopf, L., Dashtgard, S.E., Huang, C., and Gibson, H.D., 2021, Application of grouped detrital zircon analyses to determine provenance and closely approximate true depositional age: Early Cretaceous McMurray-Clearwater succession, Canada: Geoscience Frontiers, v. 12, p. 877–892, doi: 10.1016/j.gsf.2020.11.016.

Rinke-Hardekopf, L., Dashtgard, S.E., and Maceachern, J.A., 2019, Earliest Cretaceous Transgression of North America Recorded in Thick Coals: McMurray Sub-Basin, Canada: International Journal of Coal Geology, v. 204, p. 18–33, doi: 10.1016/j.coal.2019.01.011.

Rinke-Hardekopf, L., Dashtgard, S.E., MacEachern, J.A., and Gingras, M.K. Resolving stratigraphic architecture and constraining ages of paralic strata in a low-accommodation setting, Firebag Tributary, McMurray Formation, Canada: The Depositional Record.

Ross, G.M., Broome, J., and Miles, W., 1994, Chapter 4 - Potential fields and basement structure - Western Canada Sedimentary Basin, in Mossop, G.D. and Shetsen, I. eds., Geological Atlas of the Western Canada Sedimentary Basin, Canadian Society of Petroleum Geologists, p. 41–48.

Ross, J.B., Ludvigson, G.A., Möller, A., Gonzalez, L.A., and Walker, J.D., 2017, Stable isotope paleohydrology and chemostratigraphy of the Albian Wayan Formation from the wedge-top depozone, North American Western Interior Basin: Science China Earth Sciences, v. 60, p. 44–57, doi: 10.1007/s11430-016-0087-5.

Ross, G.M., Patchett, P.J., Hamilton, M., Heaman, L., DeCelles, P.G., Rosenberg, E., and Giovanni, M.K., 2005, Evolution of the Cordilleran orogen (southwestern Alberta, Canada) inferred from detrital mineral geochronology, geochemistry, and Nd isotopes in the foreland basin: GSA Bulletin, v. 117, p. 747–763, doi: 10.1130/B25564.1.

Rossignol, C., Hallot, E., Bourquin, S., Poujol, M., Jolivet, M., Pellenard, P., Ducassou, C., Nalpas, T., Heilbronn, G., Yu, J., and Dabard, M.P., 2019, Using volcaniclastic rocks to constrain sedimentation ages: To what extent are volcanism and sedimentation synchronous? Sedimentary Geology, v. 381, p. 46–64, doi: 10.1016/j.sedgeo.2018.12.010.

Ryer, T.A., and Langer, A.W., 1980, Thickness change involved in the peat-to-coal transformation for a bituminous coal of Cretaceous age in central Utah: Journal of Sedimentary Petrology, v. 50, p. 987–992, doi: 10.1306/212F7B44-2B24-11D7-8648000102C1865D.

Sahoo, H., and Gani, M.R., 2016, Autogenic modulation of fluvial channel fills in allogenically formed incised valleys: Cretaceous Blackhawk Formation, U.S.A.: SEPM Special Publication, p. 1–13, doi: 10.2110/sepmsp.106.08.

Saylor, J.E., Stockli, D.F., Horton, B.K., Nie, J., and Mora, A., 2012, Discriminating rapid exhumation from syndepositional volcanism using detrital zircon double dating: Implications for the tectonic history of the Eastern Cordillera, Colombia: Bulletin of the Geological Society of America, v. 124, p. 762–779, doi: 10.1130/B30534.1.

Saylor, J.E., and Sundell, K.E., 2016, Quantifying comparison of large detrital geochronology data sets: Geosphere, v. 12, p. 203–220, doi: 10.1130/GES01237.1.

Schmitz, M.D., and Kuiper, K.F., 2013, High-precision geochronology: Elements, v. 9, p. 25–30, doi: 10.2113/gselements.9.1.25.

Schmitz, M.D., and Schoene, B., 2007, Derivation of isotope ratios, errors, and error correlations for U-Pb geochronology using 205Pb-235U-(233U)-spiked isotope dilution thermal ionization mass spectrometric data: Geochemistry, Geophysics, Geosystems, v. 8, p. 1–20, doi: 10.1029/2006GC001492.

Schneider, C.L., Hauck, T.E., and Grobe, M., 2013, Sequence stratigraphic architecture and evolution of platform margin to basin sedimentation: 178–210 p., doi: 10.2110/sepmsp.105.15.

Schwartz, T.M., Schwartz, R.K., and Weislogel, A.L., 2019, Orogenic recycling of detrital zircons characterizes age distributions of North American Cordilleran strata: Tectonics, doi: 10.1029/2019TC005810.

Selby, D., and Creaser, R.A., 2005, Direct radiometric dating of hydrocarbon deposits using Rhenium-Osmium isotopes: Science, v. 308, p. 1293–1295, doi: 10.1126/science.1111081.

Shanley, K.W., and McCabe, P.J., 1994, Perspectives on the sequence stratigraphy of continental strata: AAPG Bulletin, v. 78, p. 544–568, doi: 10.1306/bdff9258-1718-11d7-8645000102c1865d.

Shanley, K.W., and McCabe, P.J., 1991, Predicting facies architecture through sequence stratigraphy -- An example form the Kaiparowits Palteau, Utah: Geology, v. 19, p. 742–745, doi: 10.1130/0091-7613(1991)019<0742:PFATSS>2.3.CO;2.

Sharman, G.R., Graham, S.A., Grove, M., Kimbrough, D.L., Wright, J.E., Sciences, G., Diego, S., and Diego, S., 2015, Detrital zircon provenance of the Late Cretaceous – Eocene California forearc: Influence of Laramide low-angle subduction on sediment dispersal and paleogeography: GSA Bulletin, p. 38–60, doi: 10.1130/B31065.1.

Sharman, G.R., and Malkowski, M.A., 2020, Needles in a haystack: Detrital zircon U-Pb ages and the maximum depositional age of modern global sediment: Earth-Science Reviews, v. 203, p. 103109, doi: 10.1016/j.earscirev.2020.103109.

Sharman, G.R., Sharman, J.P., and Sylvester, Z., 2018, detritalPy: A Python-based toolset for visualizing and analysing detrital geo-thermochronologic data: The Depositional Record, v. 4, p. 202–215, doi: 10.1002/dep2.45.

Shiers, M.N., Hodgson, D.M., and Mountney, N.P., 2017, Response of a coal-bearing coastal-plain succession to marine transgression: Campanian Neslen Formation, Utah, U.S.A.: Journal of Sedimentary Research, v. 87, p. 168–187, doi: 10.2110/jsr.2017.7.

Sickmann, Z.T., Paull, C.K., and Graham, S.A., 2016, Detrital-zircon mixing and partitioning in fluvial to deep marine systems, central California, U.S.A.: Journal of Sedimentary Research, v. 86, p. 1298–1307, doi: 1527-1404/16/086-1298/$03.00.

Spencer, C.J., Kirkland, C.L., and Taylor, R.J.M., 2016, Strategies towards statistically robust interpretations of in situ U-Pb zircon geochronology: Geoscience Frontiers, v. 7, p. 581–589, doi: 10.1016/j.gsf.2015.11.006.

Stovert, L.E., Brinkhuis, H., Damassa, S.P., Verteuil, L. De, Helby, R.J., Monteil, E., Partridge, A.D., Powell, A.J., Riding, J.B., Smelror, M., and Williams, G.L., 1996, Chapter 19. Mesozoic-Tertiary Dinoflagellates, Arcitarchs and Prasinophytes, in Jansonius, J. and McGregor, D.C. eds., Palynology: Principles and applications, Association of Stratigraphic Palynologists Foundations, p. 641–750, ISBN: 9-931871- 03–04.

Sundell, K.E., and Saylor, J.E., 2017, Unmixing detrital geochronology age distributions: Geochemistry, Geophysics, Geosystems, v. 18, p. 2872–2886, doi: 10.1002/2016GC006774.

Tabor, N.J., Myers, T.S., and Michel, L.A., 2017, Sedimentologist's guide for recognition, description, and classification of paleosols, in Zeigler, K. E., Parker, W. G. eds: Terrestrial Depositional Systems: Deciphering Complexities through Multiple Stratigraphic Methods, Elsevier, 165–208 p., doi: 10.1016/B978-0-12-803243-5.00004-2.

Taylor, A.M., and Goldring, R., 1993, Description and analysis of bioturbation and ichnofabric: Journal of the Geological Society, v. 150, p. 141–148, doi: 10.1144/gsjgs.150.1.0141.

Thomas, R.G., Smith, D.G., Wood, J.M., Visser, J., Calverley-Range, E.A., and Koster, E.H., 1987, Inclined heterolithic stratification - Terminology, description, interpretation and significance: Sedimentary Geology, v. 53, p. 123–179, doi: 10.1016/S0037-0738(87)80006-4.

Timmer, E.R., Gingras, M.K., Morin, M.L., Ranger, M.J., and Zonneveld, J.P., 2016, Laminae-scale rhythmicity of inclined heterolithic stratification, Lower Cretaceous McMurray Formation, NE Alberta, Canada: Bulletin of Canadian Petroleum Geology, v. 64, p. 199–217, doi: 10.2113/gscpgbull.64.2.199.

Törnqvist, T.E., 1993, Holocene alternation of meandering and anastomosing fluvial systems in the Rhine-Meuse Delta (Central Netherlands) controlled by sea-level rise and subsoil erodibility: Journal of Sedimentary Petrology, v. 63, p. 683–693, doi: 10.1306/D4267BB8-2B26-11D7-8648000102C1865D.

Törnqvist, T.E., Wallace, D.J., Storms, J.E.A., Wallinga, J., Dam, R.L.V.A.N., Blaauw, M., Derksen, M.S., Klerks, C.J.W., Meijneken, C., and Snijders, E.M.A., 2008, Mississippi Delta subsidence primarily caused by compaction of Holocene strata: Nature Geoscience, v. 1, p. 173–176, doi: 10.1038/ngeo129.

Vermeesch, P., 2004, How many grains are needed for a provenance study? Earth and Planetary Science Letters, v. 224, p. 441–451, doi: 10.1016/j.epsl.2004.05.037.

Vermeesch, P., 2013, Multi-sample comparison of detrital age distributions: Chemical Geology, v. 341, p. 140–146, doi: 10.1016/j.chemgeo.2013.01.010.

Vermeesch, P., 2018a, Dissimilarity measures in detrital geochronology: Earth-Science Reviews, v. 178, p. 310–321, doi: 10.1016/j.earscirev.2017.11.027.

Vermeesch, P., 2018b, IsoplotR: A free and open toolbox for geochronology: Geoscience Frontiers, v. 9, p. 1479–1493, doi: 10.1016/j.gsf.2018.04.001.

Vermeesch, P., 2020, Maximum depositional age estimation revisited: Geoscience Frontiers, v. 12, p. 843–850, doi: j.gsf.2020.08.008.

Wadsworth, J., Boyd, R., Diessel, C., Leckie, D., and Zaitlin, B.A., 2002, Stratigraphic style of coal and non-marine strata in a tectonically influenced intermediate accommodation setting: the Mannville Group of the Western Canadian Sedimentary Basin, south-central Alberta: Bulletin of Canadian Petroleum Geology, v. 50, p. 507–541, doi: 10.2113/50.4.507.

Wadsworth, J., Boyd, R., Diessel, C., and Leckie, D., 2003, Stratigraphic style of coal and non-marine strata in a high accommodation setting: Falher Member and Gates Formation (Lower Cretaceous), western Canada: Bulletin of Canadian Petroleum Geology, v. 51, p. 275–303, doi: 10.2113/51.3.275.

Van Wagoner, J.C., Posamentier, H.W., Mitchum, R.M., Vail, P.R., Sarg, J.F., Loutit, T.S., and Hardenbol, J., 1988, An overview of the fundamentals of sequence stratigraphy and key definitions: SEPM Special Publication, p. 39–45, doi: 10.2110/pec.88.01.0039.

Weleschuk, Z.P., and Dashtgard, S.E., 2019, Evolution of an ancient (Lower Cretaceous) marginal-marine system from tide-dominated to wave-dominated deposition, McMurray Formation: Sedimentology, p. 1–38, doi: 10.1111/sed.12601.

Wellner, R.W., Varban, B.L., Roca, X., Flaum, J.A., Stewart, E.K., and Blum, M.D., 2018, Simple is better when it comes to sequence stratigraphy: The Clearwater Formation of the Mannville Group reinterpreted using a genetic body approach: AAPG Bulletin, v. 102, p. 447–482, doi: 10.1306/0503171607717150.

Wightman, D.M., and Pemberton, S.G., 1997, The Lower Cretaceous (Aptian) McMurray Formation: An overview of the Fort McMurray area, northeastern Alberta, in Pemberton, S.G. and James, D.P. eds., Petroleum Geology of the Cretaceous Mannville Group, Western Canada, Canadian Society of Petroleum Geologists Memoir 18, p. 312–344.

Williams, G.D., 1963, The Mannville Group (Lower Cretaceous) of central Alberta: Bulletin of Canadian Petroleum Geology, v. 11, p. 350–368.

Winston, R.B., 1994, Models of the geomorphology, hydrology, and development of domed peat bodies: Geological Society of America Bulletin, v. 106, p. 1594–1604, doi: 10.1130/0016-7606(1994)106<1594:MOTGHA>2.3.CO;2.

Wright, P. V., and Marriott, S.B., 1993, The sequence stratigraphy of fluvial depositional systems: the role of floodplain sediment storage: Sedimentary Geology, v. 86, p. 203–210, doi: 10.1016/0037-0738(93)90022-W.

van Yperen, A.E., Holbrook, J.M., Poyatos-Moré, M., and Midtkandal, I., 2019, Coalesced delta-front sheet-like sandstone bodies from highly avulsive distributary channels: The low-accommodation mesa rica sandstone (Dakota Group, New Mexico, USA): Journal of Sedimentary Research, v. 89, p. 654–678, doi: 10.2110/jsr.2019.27.

Zaitlin, B.A., Dalrymple, R.W., and Boyd, R., 1994, The stratigraphic organization of incised-valley systems associated with relative sea-level change: SEPM Special Publication, p. 45–60.

Zhang, X., Pease, V., Skogseid, J., and Wohlgemuth-Ueberwasser, C., 2016, Reconstruction of tectonic events on the northern Eurasia margin of the Arctic, from U-Pb detrital zircon provenance investigations of late Paleozoic to Mesozoic sandstones in southern Taimyr Peninsula: GSA Bulletin, p. 29–46, doi: 10.1130/B31241.1.

Appendix A.

Core logs from the Firebag Tributary

Digital strip logs for cores logged in the Firebag Tributary in the northeastern McMurray Depocenter, Alberta and Saskatchewan, Canada. Cores were logged at the Core Research Center (CRC), Calgary, using the AppleCORE software (donated to SFU by Dr. Mike Ranger). Core logs were adapted to suit the requirements of each individual chapter.

Filename: App_A_Core_logs.pdf

Appendix B.

Coal geochemical data

Coal geochemical analyses for the Lower McMurray coal seam found in cores 1AA/12-20-098-05W4, and 1AA/05-29-098-05W4. Individual data includes the following: ash content, sulphur content, caloric value (in BTU/lb), as well as descriptions.

Filename: App_B_Coal_data.csv

Appendix C.

CA-TIMS age for B1 depositional unit ash

Results of an ash bed sampled in core 1AA/02-03-095-03W4 at a depth of 165.0m, for single grain CA-TIMS analysis. Samples were processed at the Isotope Geology Laboratory at Boise State University, Idaho, USA. A total of 6 individual zircon were dated.

Filename: App_C_ASH_2-3-95-3W4_B1_CA-TIMS_U-Pb_data_table.csv

Appendix D.

CA-TIMS age for Lower McMurray ash

Results of an ash bed sampled in core 1AA/09-05-091-04W4 at a depth of 201.5m, for single grain CA-TIMS analysis. Results of an ash bed sampled in core 1AA/02-03-095-03W4 at a depth of 201.4m, for single grain CA-TIMS analysis. Samples were processed at the Isotope Geology Laboratory at Boise State University, Idaho, USA. A total of 7 individual zircon were dated.

Filename: App_D_ASH_9-5-91-4W4_LM_CA-TIMS_U-Pb_data_table.csv

Appendix E.

DZ U-Pb geochronology samples

Results of 4 DZ samples collected samples in cores: 1AA/13-01-052-27W3 at a depth of 580.3-578.5m (sample S1), 1AA/10-24-93-04W4 at depths of 344.3-346.6m (sample FB1) and 358.2-361.1m (sample FB2), as well as 1AA/10-17-095-04W4 at a depth of 259.2–262.3m (sample FB3). U-Th-Pb dating of DZ samples was conducted at the Centre for Applied Basin Studies, at the University of Calgary, Canada.

Filename: App_E_DZ_Samples.csv